The Dissertation Committee for Brette Morgan Chapin Certifies that this is the approved version of the following dissertation:

ortho-Aminomethylphenylboronic Acids and *ortho*-Iminophenylboronic Acids: Structural and Optical Studies and Synthetic Applications

Committee:

Eric V. Anslyn, Supervisor

Christopher Ellison

Richard Crooks

Jonathan Sessler

Adrian Keatinge-Clay

ortho-Aminomethylphenylboronic Acids and *ortho*-Iminophenylboronic Acids: Structural and Optical Studies and Synthetic Applications

by

Brette Morgan Chapin, B.S.

Dissertation

Presented to the Faculty of the Graduate School of

The University of Texas at Austin

in Partial Fulfillment

of the Requirements

for the Degree of

Doctor of Philosophy

The University of Texas at Austin

August 2016

Dedication

This dissertation is dedicated to Mr. Stuart, my first chemistry teacher, who, on the first day of my first chemistry course, said that those of us sitting in the back row would most likely get Fs.

Acknowledgements

The short version:

Thank you to everyone who has supported me, encouraged me, listened to me complain, listened to and sometimes shared in my insecurities, and told me repeatedly that I didn't suck at chemistry and/or life at any time during the past five years.

The long version:

Eric Anslyn: Thank you for putting up with me when I am headstrong, opinionated, and grumpy, and for encouraging me when I am insecure and pessimistic. (I use the present tense because, let's face it – we both know there's plenty more where that came from.) Thank you for supporting me as I worked towards becoming the scientist *I* am supposed to be, and not expecting me to be a carbon copy of you. I like to think I am quite a lot like you, but you have always accepted and nurtured my individuality as a scientist too. Thank you for encouraging me to pursue my hypotheses ("I won't talk you out of an experiment"), whether or not you thought they would turn out to be correct. Thank you for engaging in really fun conversations (and sometimes arguments) about science. And thank you for always being a humble and enthusiastic individual with a great sense of humor. I will always be grateful for the influence you have had on me as a scientist and as a person.

The Anslyn Group: Thank you to Leo Joyce and Michelle Adams Ivy for being there when I fell in love with physical organic chemistry and for introducing me to the group. Thank you for your mentorship and advice then, and your friendship (and sometimes also advice!) now. Thank you also to Reid Long, Pedro Metola, Alex Gade, Katharine Diehl, Hannah Jo, Ram Edupuganti, Amber Johnson, and Jimmy Reuther for

your mentorship and continued friendship. Thanks to all of you that came before me for leading by example and for various combinations of getting me through candidacy, telling me to stress less, teaching me things, trusting me to teach you things, and assuring me that I would get my dissertation done on time. Thank you to John Lin and Maggie Meadows, who have been there beside me the whole time, and also to Igor Kolesnichenko, Rogelio Escamilla, Logan Bachman, Brenden Herrera, and Sam Dahlhauser – thank you all for your friendship. You people keep me sane, drive me *in*sane, put up with me, motivate me, make me smarter, and (almost) always remember to say "loud noises!" before you grind coffee beans. EAST SIDE! Thank you to all members of the Anslyn group, past and present, for making this a great place to work.

John Fossey and the Fossey Group: Thank you, John, for welcoming me into your group and for giving me the opportunity to leave the U.S. for the first time. Thank you to Will Brittain and Wenlei Zhai for being wonderful to work with, whether we were on that side of the pond, this side of the pond, or across the pond. Thank you to both of you, and also to Rama Byravan, Mark Dutton, and Dan Payne for treating me like one of the group from the very beginning and for your continued friendship.

Thank you, Betsy Hamblen, for taking care of me, and all of us, as if we are all your nieces and nephews. You have kept me sane, or at least as sane as I could have been, these past five years! Thank you to Steve Sorey and Angela Spangenberg – yes, for your invaluable expertise related to NMR – but also for listening to me complain about research not working and about impostor syndrome, and for always having a story about your kids (Angela) or dogs (Steve) to make me laugh.

Thank you to Will Brittain, Pedro Metola, Maggie Meadows, Amber Johnson, and Hannah Jo for giving me feedback on various parts of my dissertation. I look smarter than I am because you fixed my typos, said I couldn't have the word "thus" appear twice

in one sentence, and asked me how on earth I had a peak at 8 ppm assigned to “unbound amine”. Thus, I thank you thusly.

Thank you to all of the chemistry professors at Harvey Mudd College for preparing me for graduate school and for making life and work a lot of fun in the process. Thank you especially to Adam Johnson – you have supported and encouraged me when I really needed it, time and time again. You were exactly the kind of advisor I needed, and you continue to give me realistic, honest, and compassionate advice… even though I stopped being your responsibility five years ago! I am forever grateful.

Those who love me unconditionally: Thank you Mom, Dad, Jaedyn, Karmen, Ethan, and Elena for always telling me that I can do anything, even though it annoys me, and for telling me over and over and *over* again, “No, really, you ARE smart.” Thanks for the cards and the “good luck” texts, and thanks for believing I could do this even though none of you understands chemistry (except Karmen, who understands it but hates it). Thank you to my grandparents, aunts, uncles, cousins, and honorary family members who I know are always cheering me on, even though you haven’t seen or heard from me in way too long (sorry!). Thank you to my closest childhood friends – Ashley Youngdale, Keisha Bowron, Raul Najera, and Lindsey Morse Najera – and my closest college friends – Marie Godla, Becky Glick, and Michelle DeBoever – who have all become my lifelong friends. Like my family, you’re always on my team, and I can’t express how much that means to me, because unlike my family, you’re not necessarily stuck with me! Thank you, Will, for making me smile every day. Despite the distance, you make my life better, and I know just how lucky I am. And last but not least, thank you, Bonnie, for all the snuggles… even though you literally just unplugged my laptop on your way to my lap as I typed those words.

To all of you, I am truly grateful. Thank you.

ortho-Aminomethylphenylboronic Acids and *ortho*-Iminophenylboronic Acids: Structural and Optical Studies and Synthetic Applications

Brette Morgan Chapin, Ph.D.

The University of Texas at Austin, 2016

Supervisor: Eric V. Anslyn

The tools and principles of physical organic chemistry have spread far and wide to many subdisciplines of organic chemistry. Chapter 1 highlights examples of physical organic chemistry being applied to studies in other arenas and details its role in this dissertation.

In 1994, Shinkai reported a saccharide sensor composed of a phenylboronic acid with a pendant anthracene. "Shinkai's Host" becomes significantly more fluorescent in the presence of saccharides, but the mechanism for this turn-on has been debated. Previous work established how binding occurs, and Chapter 2 elucidates the mechanism of fluorescence turn-on. The experiments presented show that the fluorescence modulation is largely a function of disaggregation of the fluorophore, and that binding to a saccharide does not influence the intensity of fluorescence. In other words, binding and fluorescence turn-on both occur in the presence of saccharides, but these two phenomena are only correlated; there is no causal link between the two.

Bull and James have developed a three-component assembly consisting of 2-formylphenylboronic acid, a diol, and a primary amine. The primary amine condenses onto the formyl group to form an imine, while the diol condenses onto the boronic acid to form a cyclic boronate ester. The nitrogen and boron atoms have several possibilities for

interaction, depending on the solvent. In Chapter 3, structural studies are carried out on this three-component assembly in order to assign the type of N-B interaction in protic and aprotic solvent. Further, the complex equilibrium between the three components is investigated in detail, and individual binding constants are calculated. Chapter 4 explores the Bull-James assembly in two additional contexts. In the first, a procedure is developed for use in an undergraduate teaching laboratory. In the second, the assembly is used simultaneously as a chiral auxiliary and an *in situ* enantiomeric excess determination platform for the kinetic resolution of a chiral primary amine alkyne *via* a copper-catalyzed azide-alkyne cycloaddition (CuAAC).

Chapter 5 details three mechanistic approaches to the reversibility of CuAAC. Though none of the approaches comes to fruition, this chapter brings the dissertation full circle, with much of the design of the experiments rooted in physical organic chemistry.

Table of Contents

List of Tables

List of Figures

List of Schemes

Chapter 1: Physical Organic Chemistry By Any Other Name Would Smell as Sweet[a]

1.1 INTRODUCTION

The classic field of physical organic chemistry, which was once focused on small organic molecule structure and reactivity, has been co-opted by numerous other fields, including but not limited to: sensor design, organometallics, organic materials, organocatalysis, and supramolecular chemistry. The unifying principles of each field stem from physical organic chemistry pursuits. The insights, terminology, and lessons, as well as the experimental and computational techniques of physical organic chemistry, currently permeate all fields of organic chemistry. Thus, while the number of individuals that call themselves physical organic chemists is dwindling, we should all recognize this is the inevitable outcome, revealing the strength of the discipline – it is so powerful that all areas of organic chemistry have adopted it, and therefore we are all physical organic chemists at heart. Several recent studies in fields not historically recognized as physical organic chemistry can still be described as being so. The message is upbeat; organic chemists have a common background and language that emanates from physical organic chemistry, irrespective of the titles we associate ourselves with.

Saying that one is a physical organic chemist is unfortunately out of vogue, but we believe mistakenly so. Why does the National Science Foundation have a program called Organic Dynamics rather than Physical Organic Chemistry, and why do current students commonly hear that physical organic chemistry is dead? The answer to these

[a] This chapter was adapted from a published review: Chapin, B. M.; Anslyn, E. V. Physical Organic Chemistry By Any Other Name Would Smell as Sweet. *Isr. J. Chem.* **2016**, 56, 38-45. Brette Chapin and Eric Anslyn cowrote the review.

questions is simple – the experimental and computational techniques associated with physical organic chemistry, as well as the terminology, thought processes, and chemical insights, have been adopted by fields whose specific goals are not necessarily focused on small molecule organic structure and reactivity. Because the knowledge gained and techniques developed during the height of physical organic chemistry are so powerful, they have been adopted to understand and study organometallic reactivity, supramolecular assembly, biomolecule structure and function, and material and polymer properties, and have even been used to develop analytical protocols and expand countless other sub-disciplines of the chemical sciences. Thus, the discipline has become so broad that it permeates nearly all other fields of chemistry, and chemists in these fields naturally associate themselves with descriptors more closely aligned with the specific chemical systems they study. However, in a manner of speaking, we, and they, are all physical organic chemists.

While some may argue that because the field is so diffuse it has lost its focus, or it no longer has a cadre of like-minded chemists, or that graduate students in organic chemistry no longer need to take a physical organic chemistry class, we emphatically state the opposite to each. It is the fact that physical organic chemistry now permeates all fields of organic chemical endeavors that unites us all as like-minded individuals; it gives us a common base, further emphasizing that all students must learn the tools and lessons of this field to be functional organic chemists. Irrespective of the specific projects that organic chemists are working on or the disciplines they identify themselves with, if they rationalize results or make hypotheses about substituent effects using the terms sterics, induction, resonance, or polarizability, they are using the vernacular of physical organic chemistry. If a chemist uses linear free energy relationships, isotope effects, stereochemical reasoning, or computational analysis in pursuit of structural or

mechanistic understanding, he or she is drawing on the tools of physical organic chemistry. If a chemist uses chemical reactivity to impart selectivity, or thinks within the context of the Hammond postulate, if he or she takes into account the ramifications of Curtin-Hammett principle, or even just considers the proper choice of solvent based upon polarity reasoning, then he or she is thinking as a physical organic chemist. Thus, when considering each of these statements, we have included virtually every organic chemist, meaning that we are all now a cadre of like-minded individuals, using the same terms and experiments, all with a similar educational background. Physical organic chemistry is therefore our unifying field. Chemists should recognize that while in the early twenty-first century increasingly fewer individuals call themselves physical organic chemists, this is a lasting legacy of the strength of the field. All organic chemists are now unified – we are all physical organic chemists.

Given this premise, we examine a set of recent work from the organic chemistry community, whose topics are not classically considered physical organic, but whose foundation certainly lies in this discipline.

1.2 SENSORS

Chris Chang is well known for producing some of the most useful fluorescent cellular imaging agents, using an approach generally known as activity-based probes. This terminology in the sensing field implies a working knowledge of organic reactivity and mechanistic pathways. Probably his most well-known work centers on the imaging of H_2O_2.[1,2] He designed three homologous fluorescent sensors to be specific for H_2O_2 by installing boronic esters at the 3' and 6' positions of a xanthenone derivative (Scheme 1.1). These boronic esters are readily deprotected by H_2O_2, but no other reactive oxygen species (ROS), to convert the closed, colorless, and non-fluorescent structures to the

corresponding open, colored, and fluorescent dyes. This mechanistic insight into the selectivity of oxidation of boronic acids and esters is key to the success of these probes. The set of three sensors, PR1, PF1, and PX1, make up a suite of green, red, and blue fluorescent probes for H_2O_2, respectively. Here again, understanding the photophysics of conjugated chromophores allowed Chang to control the color of emission. Due to the high quantum yield and the design of the sensors, they demonstrate dynamic ranges of 50- to 1000-fold increases in emission, as well as a selective response that is 500-fold more sensitive to H_2O_2 than other ROS, and can detect concentrations as low as 100-200 nM. This one example highlights the use of reactivity principles, mechanistic understanding, photophysics, fluorescence spectroscopy, and analytical studies; all of which are topics on their own that classically fall in the purview of physical organic chemistry.

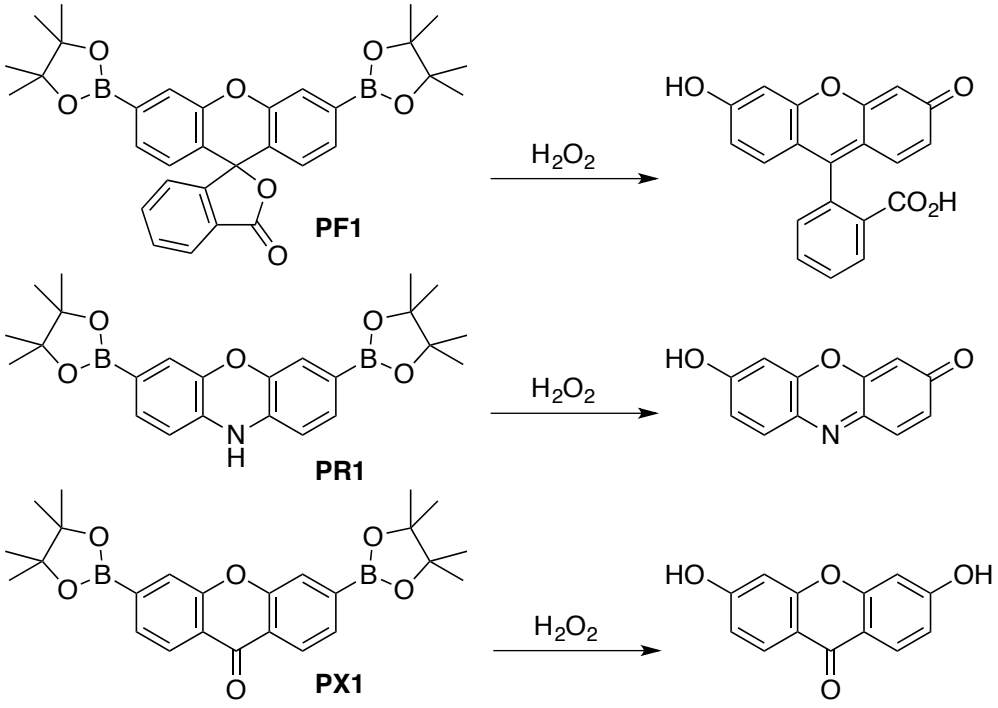

Scheme 1.1: Chang's suite of green, red, and blue fluorescent sensors.

Our own group developed a sensor for nitric oxide (NO) that shows exclusive reactivity with NO due to its unique design.[3] Typical NO probes employ *ortho*-diamino groups that add NO in the presence of oxygen to form fluorescent triazoles. A limitation is that these electron-rich probes are susceptible to attack by other ROS. This problem was solved using physical organic insights and mechanistic organic chemistry knowledge. By designing a less electron-rich probe, the Anslyn group rendered it less reactive to other oxidizing agents. Further, with the mechanistic knowledge of electrophilic aromatic substitution, the group designed a system that can only generate a fluorophore in the presence of NO (Scheme 1.2). The design of this sensor required development of a unique cascade of organic reactions, exploitation of substituent effects, and performance of kinetic studies, each of which were possible due to our educational background in physical organic chemistry.

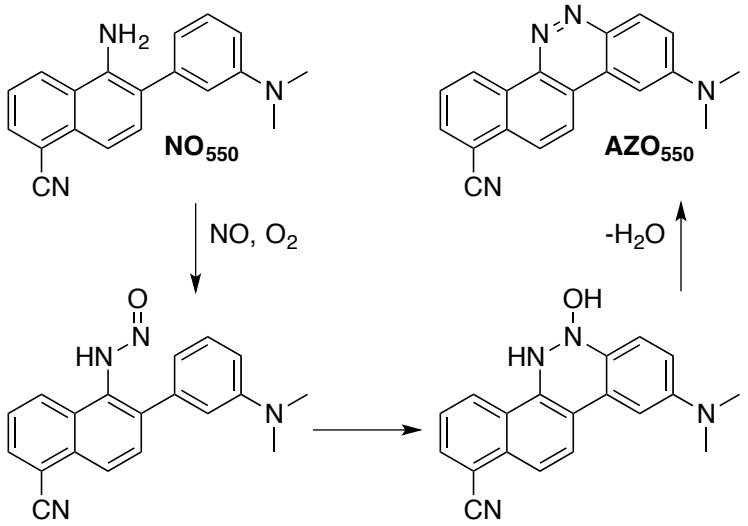

Scheme 1.2: Anslyn's NO sensor.

Peng and coworkers have developed a two-photon fluorescent probe for hydrogen sulfide to image this toxic agent in biological systems.[4] The probe includes a benzopyran

derivative and a styrene unit to extend conjugation, allowing the probe to absorb two photons in order to reach its excited state (Scheme 1.3). In the presence of H_2S, the azide is reduced to an amine and the probe exhibits a colorimetric shift from yellow to orange-red as well as emission in the near-infrared (NIR) region at 670 nm. This NIR emission is important because it is less phototoxic to cells. Phototoxicity is also reduced by using two-photon microscopy, instead of the traditional one-photon microscopy, because a lower energy excitation is involved. Additionally, high 65-fold turn-on response allows for a 5 mM concentration of probe compared to 100-200 mM for other probes. Considered together, these design features result in a sensor that is appropriate for *in vivo* studies, and indeed the Peng group shows that the sensor can image H_2S in mice. As with the previous two examples, a working knowledge of photophysics, organic mechanisms, and spectroscopic characterization were necessary for completion of this project. Hence, while the study may not appear to be a physical organic endeavor on the surface, the premise of this article shows that all such studies are modern and natural extensions of the physical organic chemistry field.

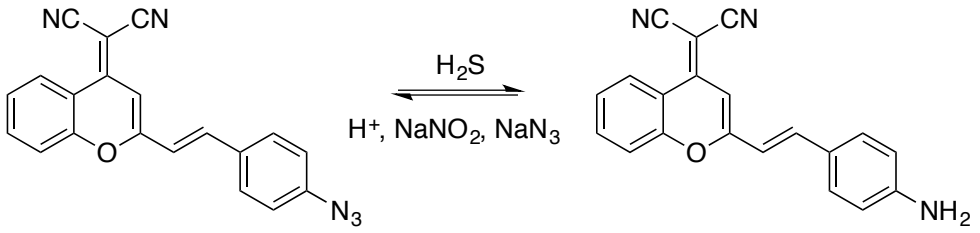

Scheme 1.3: Peng's hydrogen sulfide probe.

1.3 Synthetic Methodology

Sigman and coworkers developed analytical methods to model various reactions using steric and electronic parameters for a set of substrates and used the models to predict the outcomes of reactions with new reactants. One example was the rhodium-

catalyzed asymmetric transfer hydrogenation (ATH) of ketones,[5] where they sought to predict enantioselectivity by modeling face selection (Scheme 1.4). Because the reactants show both steric and electronic variability, classic linear free-energy relationships (LFERs) focused on just one parameter were not sufficient for good predictions. Instead, the Sigman group evaluated a set of steric and electronic parameters and used MATLAB algorithms to determine which parameters affected the enantioselectivity of the reaction. Examples of selected parameters are IR carbonyl stretching frequencies and intensities, which describe the electronics of the groups bound to the carbonyl carbon, and Sterimol parameters, which describe the minimum and maximum steric bulk of each ketone. After using these parameters to model the scope of the ketone reactivity space, the authors tested their models on new substrates and demonstrated excellent agreement with measured *ee* values. This example can be readily seen as physical organic chemistry; it is a substituent effect study correlating reactivity to chemical structure. While the goal may be asymmetric catalysis to achieve the predictive power for new reactants, Sigman relies on a combination of parameters commonly associated with the field of physical organic chemistry: IR spectroscopy to understand energy of stretches, steric interactions, reaction kinetics, and stereochemistry.

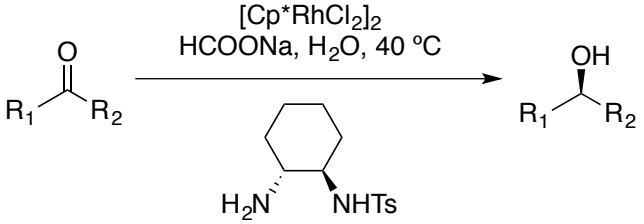

Scheme 1.4: Sigman's system for asymmetric transfer hydrogenation. Cp* = pentamethylcylcopentadienyl, Ts = 4-toluenesulfonate.

In an admittedly more obvious physical organic endeavor, Wiskur used LFERs to gain mechanistic insights on kinetic resolution *via* silylation of secondary alcohols.[6] A Hammett plot of the log of the silylation rates with various *para*-substituted triarylsilyl chlorides versus σ_{para} for enantiopure alcohols gave a steep slope ($\rho = 5.8$) that suggests significant decrease in charge in the transition state. This is consistent with a mechanism in which a nucleophilic catalyst first displaces the chloride from the triarylsilyl chloride to give a full formal charge on the nitrogen, followed by S_N2 attack of the alcohol on the silicon to give a transition state with partial positive charges (Scheme 1.5). A Swain-Lupton dual parameter approach also revealed that the substituents affect reactivity *via* both induction and resonance approximately equally. Hammett plots of the log of the selectivity factors for silylation of two racemic alcohols versus σ_{para} showed that selectivity is sensitive to the electronic variation in the triarylsilyl chlorides. Silyl chlorides that have electron-withdrawing substituents are more reactive and higher in energy, so the transition state resembles the intermediate and includes minimal participation of the alcohol, leading to lower selectivity. The interpretation of the data required insights derived from the Hammond postulate, and classic LFERs were successfully used to support one mechanism over another. Once again, while the goal is in the realm of synthetic methodology, that goal was accomplished using knowledge derived from physical organic chemistry techniques.

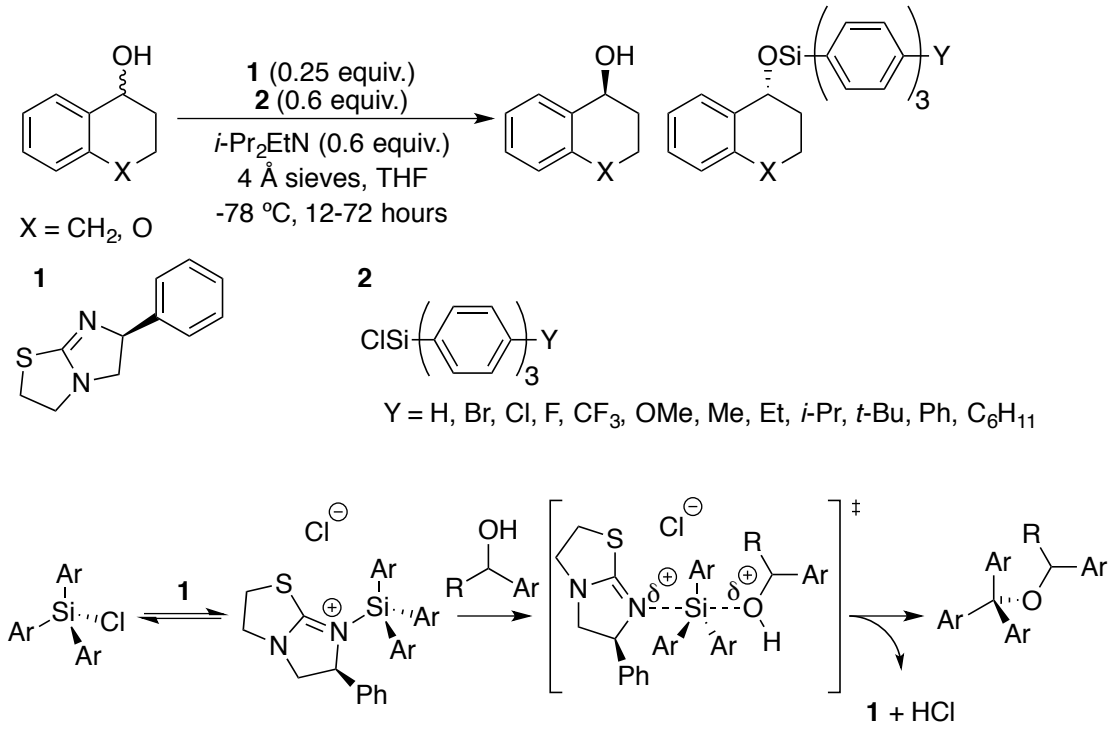

Scheme 1.5: Wiskur's kinetic resolution through silylation of secondary alcohols.

Jacobsen used experimental and computational methods to identify the mechanism by which chiral guanidinium groups catalyze and induce enantioselectivity in a Claisen rearrangement.[7] Computational studies showed that the chair-like transition state of the substrate was stabilized by hydrogen bonding with the guanidinium group, but other stabilizing interactions were also uncovered (Scheme 1.6). As the allyl fragment develops cationic charge, it is stabilized by stacking with aryl rings in the catalyst. Additionally, calculations revealed that the guanidinium NH_2 hydrogen atoms interact favorably with the faces of the pyrrole rings. These findings are consistent with experimentation, which shows that electron-rich guanidinium catalysts show higher activity and selectivity due to their stronger interactions and greater steric influence. Jacobsen's work allows for the fine-tuning of electronics to develop active and

enantioselective catalysts. While at one time computational modeling was solely the purview of computational chemists, the methods are now so user-friendly and widely available that these once dedicated physical organic methods are now used by anyone that wants to explore their mechanisms in depth and reveal reactivity insights not otherwise available.

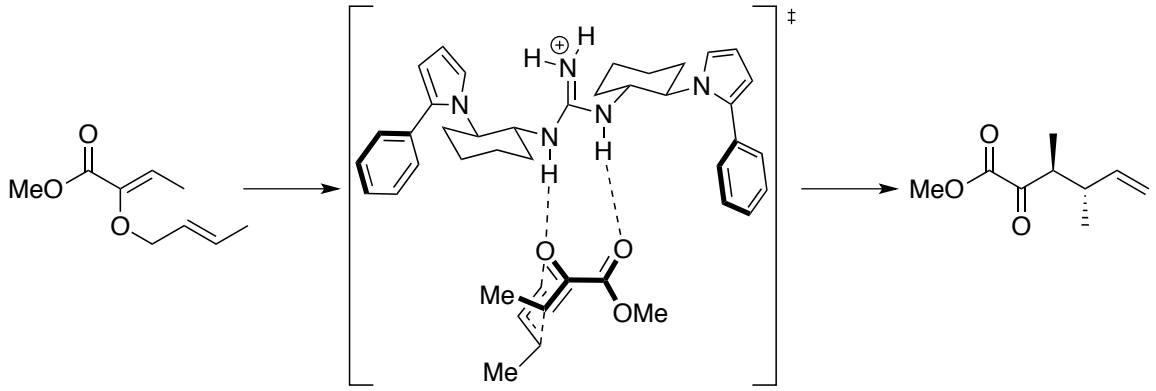

Scheme 1.6: Jacobsen's explanation of how enantioselectivity is induced in a Claisen rearrangement.

Baran and coworkers explored the C-H functionalization of electron-poor heteroarenes and determined the effects of various structural parameters.[8] They carried out these studies in order to challenge the common perception that radical reactions in general give mixed and unpredictable regioselectivity and low yields. They studied alkylation and fluoroalkylation of 4-subsituted pyridines using radicals derived from alkylsulfinate salts (Scheme 1.7). They measured the ratio of C2/C3 substitution under various conditions, including solvent, the electronic and steric nature of the C4 substituent, and the substitution and branching of the radical. These ratios provided a set of empirical guidelines for predicting regioselectivity based on the inherent reactivity of the pyridine derivative, the induced reactivity as a result of π-conjugating electron-withdrawing groups, as well as the electronic properties of the radical intermediate. In

this physical organic structure-function analysis, Baran and coworkers showed that the regioselectivity can be both predicted and controlled for future reactions.

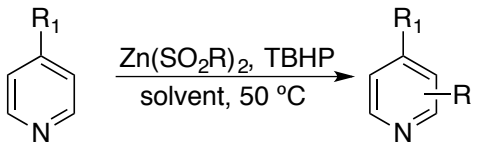

Scheme 1.7: Baran's system for C-H functionalization. TBHP = *tert*-butylhydroperoxide.

1.4 SUPRAMOLECULAR ASSEMBLY

Leigh and coworkers developed a unique ligand system for assembly of rotaxanes mediated by Cu(I).[9] Their method is an alternative to the more typical Cu(I)-$(dpp)_2$ rotaxanes and involves the assembly of a picolinaldehyde, an amine, and a bipyridine macrocycle using Cu(I) as a template (Scheme 1.8). This assembly is remarkable because of its nearly quantitative yields. The authors attribute this to the fact that the reaction is carried out under thermodynamic control and the rotaxane is the only structure with maximal site occupancy. Thus, the Leigh group's ligand system is ideal for Cu(I)-mediated rotaxane formation. Such supramolecular assemblies engineered by design are often constructed to test the limits of how much complexity chemists can achieve. To us, such studies are reminiscent of one of the earlier frontiers of physical organic chemistry, where researchers were focused upon testing the limits to which strain can be incorporated into organic compounds: i.e. cubane,[10] tetrahedrane,[11] and propellane.[12]

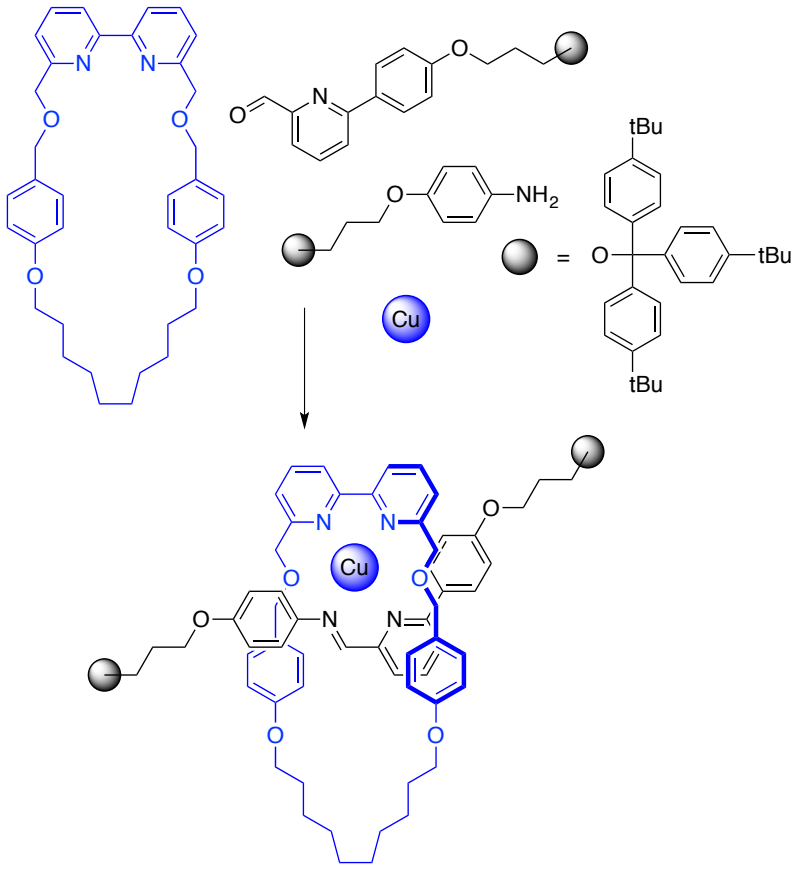

Scheme 1.8: Assembly of Leigh's rotaxane.

Bergman has studied the interior space of the supramolecular host $[Ga_4L_6]_{12}$ (where L = 1,5-bis(2,3-dihydroxybenzamido)naphthalene) using a variety of guests.[13] The host has a hydrophobic interior that has been used for catalysis of organometallic and pericyclic reactions. Bergman and coworkers studied the rotational and tumbling dynamics of benzyltrialkylphosphonium guests (Figure 1.1), both in bulk solvent and when encapsulated in the host, in order to probe the interaction between the size and shape of the guest and the size and shape of the host. They exploited the break in symmetry of the guest that occurs when it is encapsulated in the host and they used selective inversion recovery (SIR) NMR spectroscopy to measure the rate of the guests'

Ph-CH_2 bond rotation inside the host. They also measured tumbling dynamics using low-temperature NMR to break the symmetry of the host. Not surprisingly, the rotational studies showed that the barrier to rotation is higher when the guest is encapsulated. A more unexpected result was that rotation and tumbling motions were faster for larger guests. They postulate that, upon encapsulation, larger guests cause more distortion of the interior space of the host and thus facilitate these motions. Bergman's study gives us an important insight into the dynamic nature of flexible hosts in host-guest interactions. In order to do so, detailed and advanced spectroscopic methods were needed, as historically have been used for structural analysis in the physical organic chemistry field. Thus, while this study can be classified as supramolecular chemistry, the lessons derive from physical organic techniques.

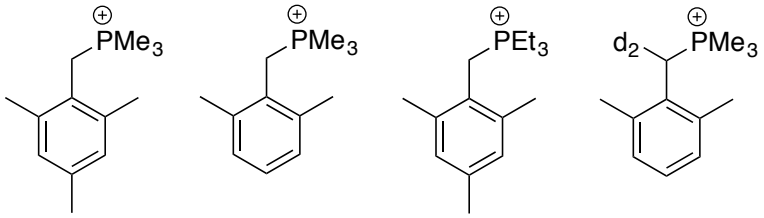

Figure 1.1: Bergman's benzyltrialkylphosphonium guests.

1.5 Organometallic Chemistry

Hartwig and coworkers achieved amination of aryl chlorides and bromides with primary aliphatic amines using a Ni(0) complex and BINAP ligands.[14] This methodology is unique because first-row metals, which are generally more electropositive than second-row metals, often exhibit one-electron redox reactions along with the desirable two-electron reaction. Kinetic studies showed that this reaction was first order with respect to catalyst and zero order in base and amine. Reactions with aryl bromides are first order in substrate and those with aryl chlorides are inverse first order in substrate. This distinction

suggests that the aryl bromide reacts directly with (BINAP)Ni(η^2-NC-Ph), whereas the aryl chloride reacts with (BINAP)Ni(0) after PhCN has dissociated (Scheme 1.9). These mechanistic studies are important for the design of the nickel catalysts, which could substitute for more expensive palladium catalysts. Thus, this physical organic study was aimed at developing a system appropriate for a first-row metal and in order to improve the practicality of a synthetic methodology by reducing the cost of the catalyst.

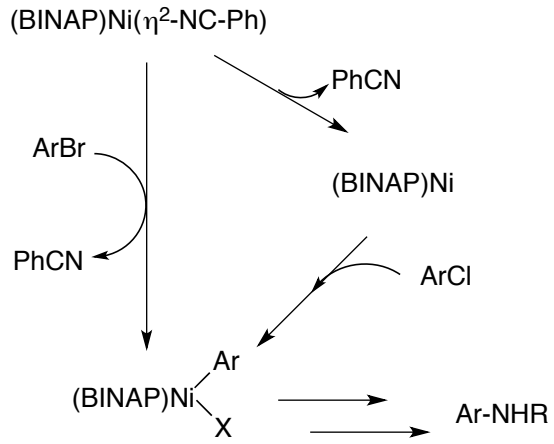

Scheme 1.9: Catalytic cycle for nickel-catalyzed amination of aryl halides elucidated by Hartwig's mechanistic studies.

By exploiting the Curtin-Hammett principle, Krische and coworkers achieved high levels of *anti*-diastereo- and enantioselectivity in the formation of quaternary centers *via tert*-(hydroxyl)prenylation (Scheme 1.10).[15] Their studies revealed that the iridium-catalyzed reaction between a primary alcohol and a vinyl epoxide gave concentration-dependent *anti*:*syn* ratios. They reasoned the (*E*)- and (*Z*)-allyliridium intermediates must interconvert rapidly and the reaction outcome is determined by their respective transition state energies as well as their thermodynamic stability. They conclude that the *anti*-diastereoselectivity improved at reduced concentrations because carbonyl addition occurs at a faster rate for the (*E*) intermediate (which leads to the *anti* diastereomer), and

reducing the concentration allows the remaining (*Z*) intermediate to convert to (*E*) before adding the carbonyl. Drawing on the classic Curtin-Hammett principle, the Krische group was able to optimize the conditions of the prenylation reaction to maximize *anti*-diastereoselectivity.

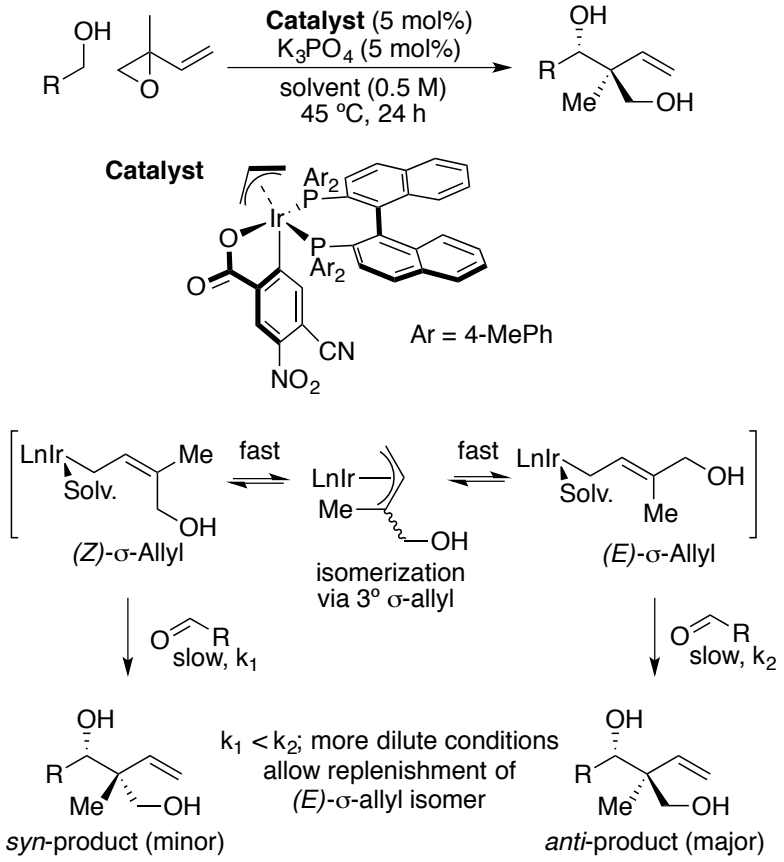

Scheme 1.10: Krische's system for *tert*-(hydroxyl)prenylation.

Bielawski and coworkers explored the electronic effects of *N*-heterocyclic carbenes (NHCs) in gold complexes to tune the ratio of bicyclic versus olefin products for 1,6-enyne cyclizations (Scheme 1.11).[16] By designing NHCs that were sterically similar, they were able to separate steric and electronic effects on the reaction outcome. They found that ^{13}C NMR resonances of the carbenoid nuclei correlated with the Tolman

electronic parameters, which are a measure of the electron-donating properties determined by the frequency of the IR C-O stretch. Notably, more electron-rich NHCs gave greater selectivity for the bicyclic product. This structure-function study showed that electronic properties had greater influence over product selectivity than sterics did.

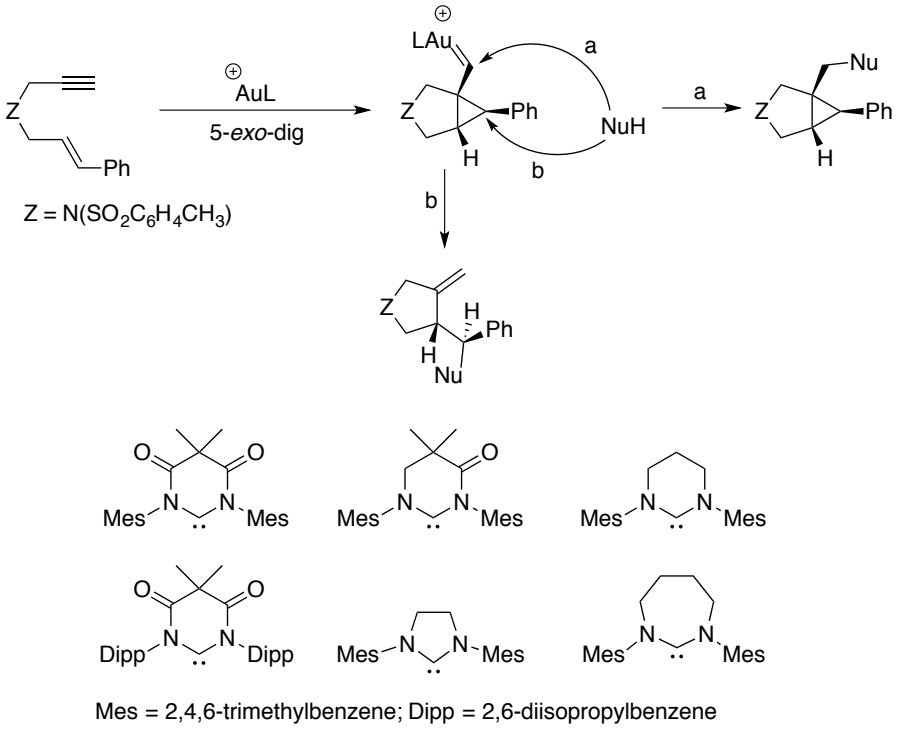

Mes = 2,4,6-trimethylbenzene; Dipp = 2,6-diisopropylbenzene

Scheme 1.11: Bielawski's 1,6-enyne cyclizations with NHCs.

1.6 MATERIALS CHEMISTRY

Phillips and coworkers described an improvement upon the previously developed method[17] of depolymerization of benzene-based carbamate polymers *via* formation of azaquinone methide.[18] These benzene-based polymers depolymerize slowly in polar conditions and even more slowly or not at all in less polar environments. Phillips and coworkers suggested that this sluggishness was due to the destruction of aromaticity during the depolymerization process. Thus, using mechanistic insights, they hypothesized

that they could increase reaction rates either by raising the HOMO of each monomer by addition of electron density to the aromatic ring, or by reducing the aromatic character of the monomer (Scheme 1.12). They found that in both cases, reaction rates increased by over 100-fold, as measured by release of UV-active *para*-nitroaniline. Phillips also demonstrated that these more reactive polymers could be depolymerized successfully even in less polar solvents, such as up to 70% dioxanes and 30% 4:1 DMSO/water. The extension of this depolymerization strategy to less polar environments could allow its use in the solid state, such as in stimuli-responsive materials. The success of the strategy relied on knowledge and insights that rest upon generations of studies of electronic substituent effects.

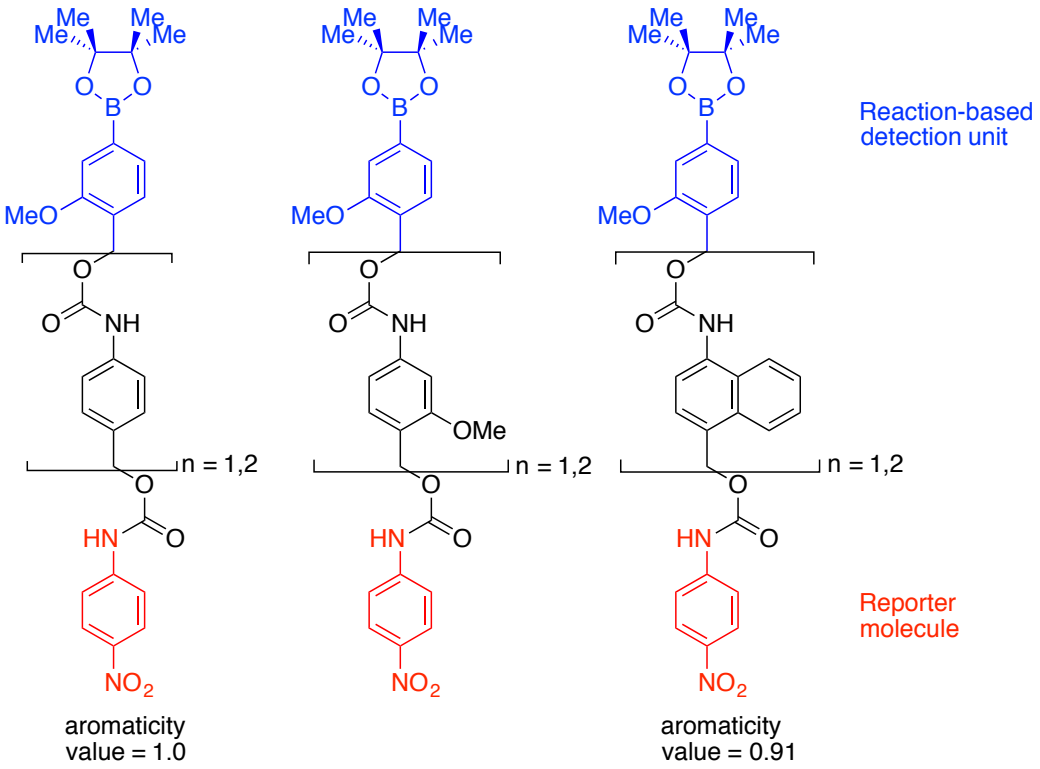

Scheme 1.12: Phillips' depolymerizable benzene-based carbamate polymers.

Shabat's group designed a series of "self-immolative" dendrimers that can be triggered to fragment into building blocks.[19] In this design, cleavage occurs under basic conditions at the core, and that causes the "adaptor" chain to undergo an intramolecular or "self-immolating" reaction to release the successive tail units one level at a time. At the end of each branch is a reporter molecule, which is released in the last cleavage step and can be quantified by HPLC or UV/Vis in order to monitor the progress of the reaction. Thus, the Shabat group designed the adaptor chains in a way that exploited their inherent reactivity in order to achieve the desired function.

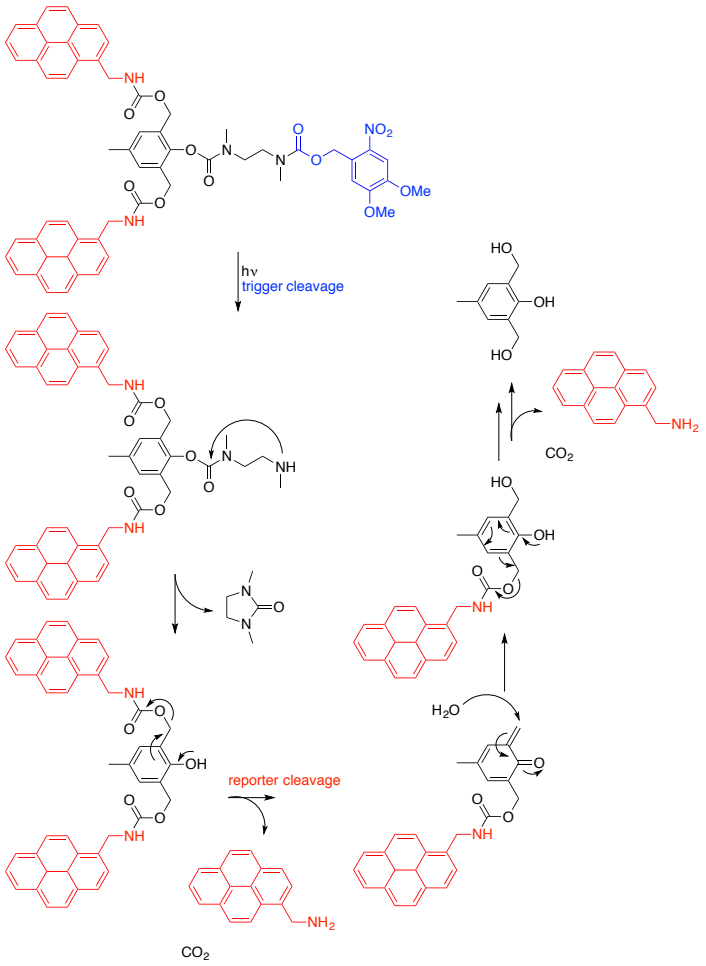

Scheme 1.13: Shabat's self-immolative dendrimer.

1.7 Physical Organic Chemistry in This Dissertation

This dissertation is also grounded in physical organic chemistry, though it contains elements of supramolecular, analytical, organometallic, and photochemistry.

Chapter 2 addresses the mechanism of fluorescence turn-on of an anthracene-appended boronic acid sensor in the presence of a saccharide. Previous work on this particular system consisted of mechanistic studies of binding – observing saturation kinetics and measuring kinetic isotope effects – as well as structural studies involving changes in pH and the nature of the nitrogen-boron interaction. The present question is how binding affects fluorescence modulation, and part of this question can be answered with physical organic concepts as simple as π-stacking and the hydrophobic effect. Fluorescence studies in this chapter are interpreted using arguments about kinetics versus thermodynamics, while binding studies point to an entropic driving force over an enthalpic one.

Chapter 3 focuses on structural and equilibrium studies of a three-component supramolecular assembly formed *via* reversible covalent bonds. Structures are assigned using ^{11}B and ^{1}H NMR spectroscopy, supported by arguments about electronegativity and pK_a values. Then the complex equilibrium between the various species is dissected into its individual binding constants using the NMR spectra and a seventh-order polynomial. Finally, these binding constants are used to support an argument for positive cooperativity of binding multiple guests.

Chapter 4 describes work done in collaboration with Dr. John Fossey's research group in Birmingham, UK. It focuses on a similar three-component assembly to that in Chapter 3, but introduces an element of chirality. The first part of the chapter introduces the assembly to a pedagogical setting, with the hope of inspiring younger chemists to delve into physical organic and supramolecular chemistry as they learn about

enantiomeric excess (*ee*). The second part of the chapter applies the assembly, as both a chiral auxiliary and as an analytical platform for determining *ee*, to the kinetic resolution of a terminal alkyne *via* copper-catalyzed azide alkyne cycloaddition (CuAAC). Factors such as sterics and solvent effects are discussed in the context of designing an auxiliary that maximizes selectivity.

Finally, Chapter 5 explores the reversibility of CuAAC. Though unsuccessful, the attempts to establish reversibility of this reaction were designed based on arguments about electronegativity, pK_a, polarizability, and microscopic reversibility.

1.8 Outlook

We hope that through these diverse and varied examples we have shown that physical organic chemistry is *not* dead. Rather, we believe it is very much alive in a new generation of chemists in every subdiscipline of organic chemistry. In a way, physical organic principles and techniques have become second nature to this generation of organic chemists, such that we no longer think of them as physical organic tools, but simply as tools. This assimilation of physical organic chemistry into a chemist's general knowledge means that it can play a role in his or her work both directly and indirectly, and this indirect use of knowledge and understanding is what really speaks to the strength and the beauty of the field. When a chemist uses physical organic principles and techniques without associating them with physical organic chemistry, it demonstrates the broad applicability and relevance of the discipline, and truly shows how ingrained physical organic chemistry is in all of us.

1.9 REFERENCES

(1) Chang, M. C. Y.; Pralle, A.; Isacoff, Ehud, Y.; Chang, C. J. A Selective, Cell-Permeable Optical Probe for Hydrogen Peroxide in Living Cells. *J. Am. Chem. Soc.* **2004**, *126* (47), 15392–15393.

(2) Miller, E. W.; Albers, A. E.; Pralle, A.; Isacoff, Ehud, Y.; Chang, C. J. Boronate-Based Fluorescent Probes for Imaging Cellular Hydrogen Peroxide. *J. Am. Chem. Soc.* **2005**, *127* (47), 16652–16659.

(3) Yang, Y.; Seidlits, S. K.; Adams, M. M.; Lynch, V. M.; Schmidt, C. E.; Anslyn, E. V.; Shear, J. B. A Highly Selective Low-Background Fluorescent Imaging Agent for Nitric Oxide. *J. Am. Chem. Soc.* **2010**, *132* (38), 13114–13116.

(4) Sun, W.; Fan, J.; Hu, C.; Cao, J.; Zhang, H.; Xiong, X.; Wang, J.; Cui, S.; Sun, S.; Peng, X. A Two-Photon Fluorescent Probe with near-Infrared Emission for Hydrogen Sulfide Imaging in Biosystems. *Chem. Commun.* **2013**, *49* (37), 3890–3892.

(5) Bess, E. N.; Bischoff, A. J.; Sigman, M. S. Designer Substrate Library for Quantitative, Predictive Modeling of Reaction Performance. *Proc. Natl. Acad. Sci.* **2014**, *111* (41), 14698–14703.

(6) Akhani, R. K.; Moore, M. I.; Pribyl, J. G.; Wiskur, S. L. Linear Free-Energy Relationship and Rate Study on a Silylation-Based Kinetic Resolution: Mechanistic Insights. *J. Org. Chem.* **2014**, *79* (6), 2384–2396.

(7) Uyeda, C.; Jacobsen, E. N. Transition-State Charge Stabilization through Multiple Non-Covalent Interactions in the Guanidinium-Catalyzed Enantioselective Claisen Rearrangement. *J. Am. Chem. Soc.* **2011**, *133* (13), 5062–5075.

(8) O'Hara, F.; Blackmond, D. G.; Baran, P. S. Radical-Based Regioselective C-H Functionalization of Electron-Deficient Heteroarenes: Scope, Tunability, and Predictability. *J. Am. Chem. Soc.* **2013**, *135* (32), 12122–12134.

(9) Campbell, C. J.; Leigh, D. A.; Vitorica-Yrezabal, I. J.; Woltering, S. L. A Simple and Highly Effective Ligand System for the Copper(I)-Mediated Assembly of Rotaxanes. *Angew. Chem. Int. Ed.* **2014**, *53* (50), 13771–13774.

(10) Eaton, P. E.; Cole, T. W. J. Cubane. *J. Am. Chem. Soc.* **1964**, *86* (15), 3157–3158.

(11) Maier, G.; Pfriem, S.; Schaefer, U.; Matusch, R. Small Rings. 25. Tetra-Tert-Butyltetrahedrane. *Angew. Chem.* **1978**, *90* (7), 552–553.

(12) Wiberg, K. B.; Walker, F. H. [1.1.1]Propellane. *J. Am. Chem. Soc.* **1982**, *104* (19), 5239–5240.

(13) Mugridge, J. S.; Szigethy, G.; Bergman, R. G.; Raymond, K. N. Encapsulated Guest-Host Dynamics: Guest Rotational Barriers and Tumbling as a Probe of Host Interior Cavity Space. *J. Am. Chem. Soc.* **2010**, *132* (45), 16256–16264.

(14) Ge, S.; Green, R. A.; Hartwig, J. F. Controlling First-Row Catalysts: Amination of Aryl and Heteroaryl Chlorides and Bromides with Primary Aliphatic Amines Catalyzed by a BINAP-Ligated Single-Component Ni(0) Complex. *J. Am. Chem. Soc.* **2014**, *136* (4), 1617–1627.

(15) Feng, J.; Garza, V. J.; Krische, M. J. Redox-Triggered C-C Coupling of Alcohols and Vinyl Epoxides: Diastereo- and Enantioselective Formation of All-Carbon Quaternary Centers via Tert-(Hydroxy)-Prenylation. *J. Am. Chem. Soc.* **2014**, *136* (25), 8911–8914.

(16) Arumugam, K.; Varghese, B.; Brantley, J. N.; Konda, S. S. M.; Lynch, V. M.; Bielawski, C. W. 1,6-Enyne Cyclizations Catalyzed by N-Heterocyclic Carbene Supported Gold Complexes: Deconvoluting Sterics and Electronics. *Eur. J. Org. Chem.* **2014**, *2014* (3), 493–497.

(17) Sagi, A.; Weinstain, R.; Karton, N.; Shabat, D. Self-Immolative Polymers. *J. Am. Chem. Soc.* **2008**, *130* (16), 5434–5435.

(18) Robbins, J. S.; Schmid, K. M.; Phillips, S. T. Effects of Electronics, Aromaticity, and Solvent Polarity on the Rate of Azaquinone-Methide-Mediated Depolymerization of Aromatic Carbamate Oligomers. *J. Org. Chem.* **2013**, *78* (7), 3159–3169.

(19) Amir, R. J.; Pessah, N.; Shamis, M.; Shabat, D. Self-Immolative Dendrimers. *Angew. Chem. Int. Ed.* **2003**, *42* (37), 4494–4499.

Chapter 2: Elucidation of the Mechanism of Fluorescence Modulation of Shinkai's Host in the Presence of Saccharides

2.1 INTRODUCTION[a]

2.1.1 Boronic Acid-Diol Binding

The high affinity of boronic acids for binding diols was first discovered in 1954.[1] Boronic acids rapidly form reversible covalent bonds with 1,2- and 1,3-diols to generate cyclic boronate esters. For this reason, boronic acids are often utilized in synthetic receptors for molecular recognition and sensing of carbohydrates, among other vicinal diol-containing compounds.[2–17] In a practical sense, carbohydrate detection is commonly applied to diagnostics for diseases such as diabetes.[18–23] In a more academic sense, carbohydrates present a challenge for molecular recognition due to their high solvation energies in water[24–26] and their great structural diversity.[27] However, boronic acids can overcome these solvation energies because their binding represents an interchange of covalent bonds, whereas in non-covalent bonding, the binding event must replace the solvent. Boronate ester formation is a unique reaction in that it is one of few rapidly reversible reactions that involves making and breaking covalent bonds (Scheme 2.1).[28–33]

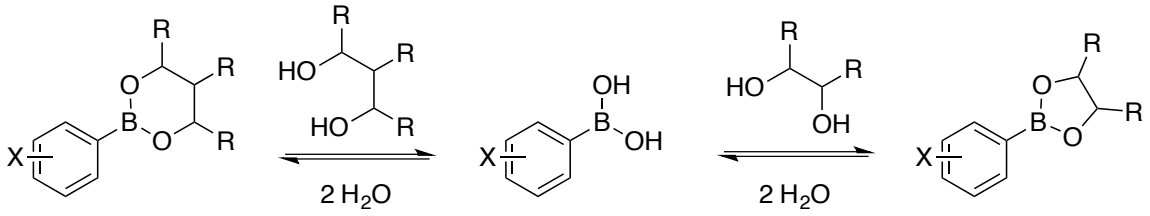

Scheme 2.1: Boronate ester formation.

[a] This section was adapted from the Ph.D. dissertation of Dr. Pedro Metola.

Since the bonds that are formed are covalent, boronic acids are able to bind diols in competitive solvents such as water and alcohols. In contrast, more conventional supramolecular binding depends on interactions such as hydrogen bonds, electrostatics, and solvophobicity in order to achieve high affinities.[34–36]

Phenylboronic acid is limited in its binding to carbohydrates and other vicinal diols because it only demonstrates significant binding several pH units above physiological pH.[37,38] Some phenylboronic acid derivatives, however, have shown much improved binding. Lorand[39] and Wulff[37,40] have delineated substituent effects for phenylboronic acids binding various diols. Most significantly, they found that installment of an aminomethyl group on the *ortho* position to the boronic acid dramatically increased the strength of diol-binding, even at neutral pH.[41] Following the inspiration of these studies, the *ortho*-aminomethyl functionality continues to be studied by other researchers.[42–44]

2.1.2 Shinkai-James Fluorescent Saccharide Sensor and the N-B Bond Hypothesis

In 1994, Shinkai and James reported their use of anthracene-based receptor **2.1** (referred to by us as Shinkai's Host) to signal the presence of various carbohydrates in neutral aqueous media *via* a fluorescence turn-on response (Scheme 2.2).[45] Addition of polyol-containing sugars led to a great fluorescent signal increase, suggesting that the *ortho*-aminomethyl group in **2.1** not only improved the thermodynamics of binding at neutral pH, but also in some manner modulated the fluorescence of the receptor in the presence and absence of sugars.

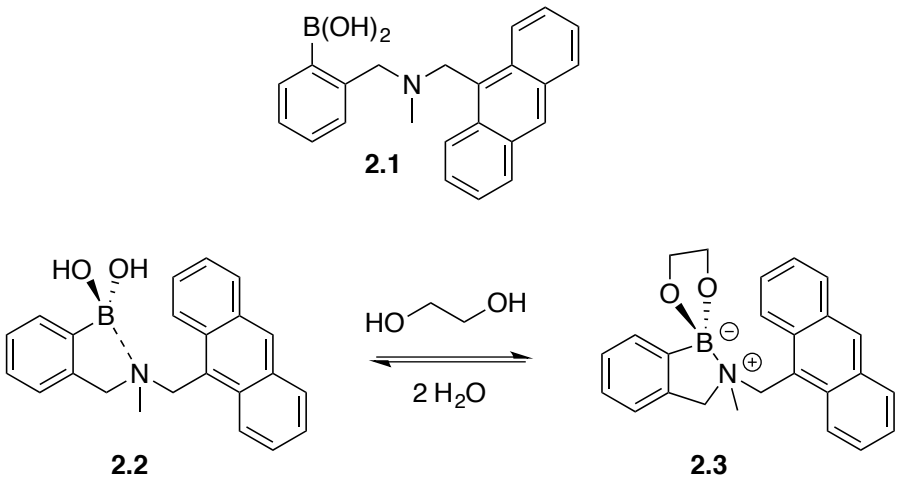

Scheme 2.2: Shinkai's Host, **2.1**, and its boronate ester condensation with formation of a N-B bond.

Shinkai and James followed their landmark 1994 work with additional studies and a hypothesis that explained the role of the *ortho*-aminomethyl group in binding and optical signaling.[4,46,47] Their postulate included a weak dative bond from the amine nitrogen atom to the boron atom, resulting in sp^3 hybridization at boron at neutral pH, represented by the dashed N-B line shown in compound **2.2**. In contrast, it had been established using ^{11}B NMR that the boron atom in phenylboronic acid is sp^2 at neutral pH.[48] Upon boronate ester formation, a five-membered ring that included the boron atom would be formed with either structure **2.2** (to form **2.3**) or phenylboronic acid. Shinkai and James reasoned that the ring would be more strained in the case of an sp^2 boron atom than it would be in an sp^3 boron atom. Thus, they postulated that pyramidalization of the boron atom *via* formation of the N-B bond would stabilize the boronate ester. In return, boronate ester formation would strengthen the N-B bond because diols are more electron-withdrawing ligands for boron than hydroxyl groups, making the boron atom more Lewis acidic.[3,49] This strengthened Lewis acid-base interaction is represented by the solid N-B line shown in **2.3**, Scheme 2.2.

The N-B bond hypothesis was also used to explain the fluorescence turn-on of compound **2.1** and its analogs.[45–47] It was postulated that photoinduced electron transfer (PET)[50,51] from the nitrogen atom's lone pair of electrons in **2.1** quenched the emission of anthracene due to its weak coordination to boron. However, upon boronate ester formation, the nitrogen lone pair would be more strongly coordinated to the boron atom, which would make it less available for PET quenching. In other words, Shinkai and James proposed that the fluorescence turn-on response was due to the absence of PET quenching when the N-B interaction was strong.

Figure 2.1 shows the fluorescence of **2.1** alone and in the presence of diols at a range of pHs. Two pH inflections are observed at pH 6 and 11.

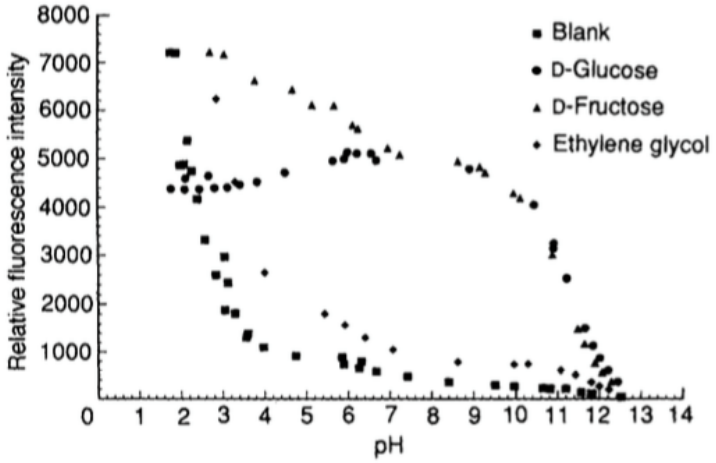

Figure 2.1[45]: Fluorescence intensity pH profile of **2.1**. 25 ºC, 12 μM solution in 2:1 water/methanol with 50 mM NaCl, [saccharide or ethylene glycol] = 50 mM; λ_{ex} = 370 nm, λ_{em} = 420 nm.

As the pH of a solution of **2.1** increases, the ammonium group is deprotonated and the boron atom is hydroxylated. Note that hydroxylation of a boronic acid is accompanied by the release of a proton, and hence is a Brønsted acid dissociation reaction that has a related pK_a value (Scheme 2.3).

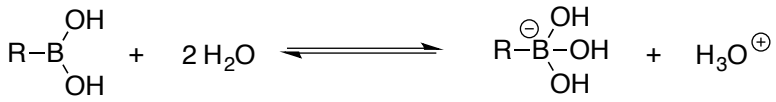

Scheme 2.3: Hydroxylation of a boronic acid.

Shinkai and James logically assigned pK_{a1} (Scheme 2.4) to the deprotonation of the ammonium ion. This value could be lowered in comparison to a standard alkyl ammonium (9-11) due to the resulting coordination with boron, since the coordination of nitrogen to boron would replace, and be in competition with, protonation. This would mean that pK_{a2} corresponded to hydroxylation of the boron with consequent breaking of the N-B bond. This pK_a is in the standard range of that for boronic acids.

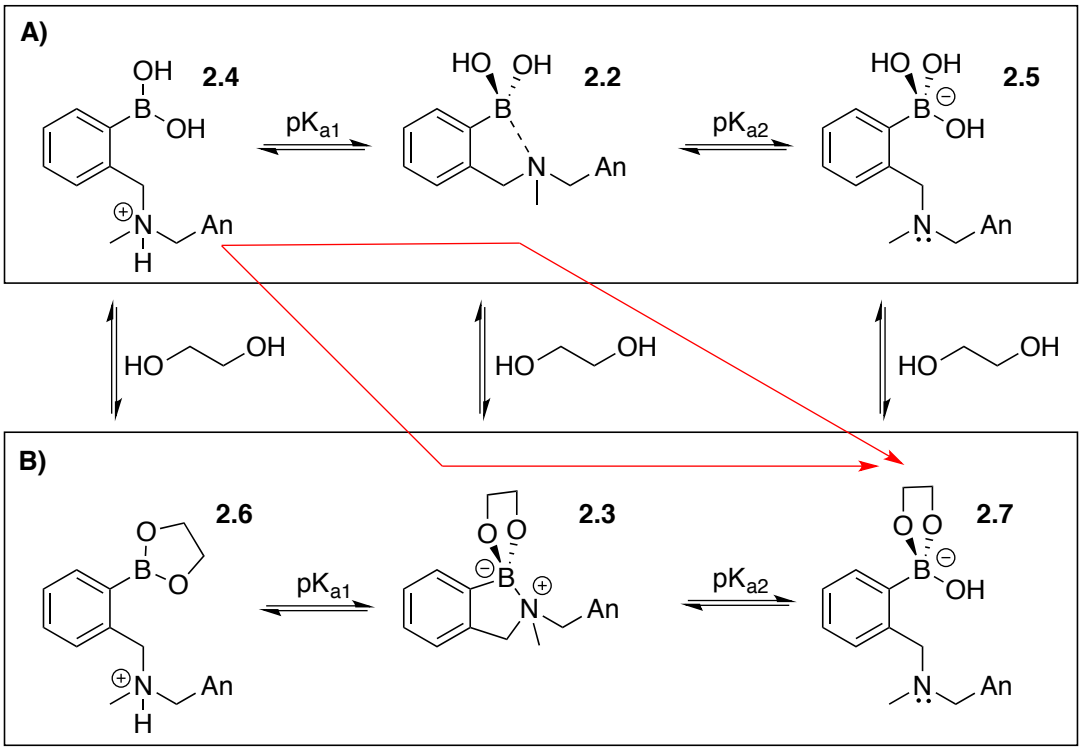

Scheme 2.4: N-B bonding scheme. The structures associated with A) the boronic acid, Shinkai's Host, and B) its corresponding boronate ester as a function of pH (low to high pH from left to right).

Scheme 2.4 summarizes the Shinkai-James interpretation of their pH titration. Following their N-B bond postulate, deprotonation of the ammonium group of **2.4** (Scheme 2.4A, pK_{a1}) would lead to liberation of the nitrogen lone pair upon formation of **2.2**. This lone pair would then be only weakly coordinated to boron, and would therefore be available to quench the anthracene fluorescence emission. The following hydroxylation of the boron atom (pK_{a2}) to form **2.5** would only slightly increase quenching, because the lone pair was largely uncoordinated and quenching already. In the case of the boronate ester (Scheme 2.4B), deprotonation of the ammonium group of **2.6** (pK_{a1}) would break a strong N-H bond and replace it with a strong dative N-B bond in **2.3**, and the degree of PET quenching would only slightly increase. Hydroxylation of the boron atom in the boronate ester (pK_{a2}) to form **2.7**, however, would leave the lone pair of electrons free to quench the anthracene's emission.

The black arrows indicate the progression of a boronic acid in (A) and a boronate ester in (B). However, in reality, structures **2.5** and **2.6** are unlikely to exist to a significant extent when both Shinkai's Host and diol are present, so the red arrows have been added to suggest a more likely pathway. We suggest that this pathway is more likely because *ortho*-(aminomethyl)phenylboronic acids have greater binding constants with sugars at higher pH. Thus, as the pH increases, binding also increases, and pK_{a1} represents not only a deprotonation, but also a binding event. The boronate ester formation is essentially complete before the hydroxylation of boron (pK_{a2}), so this pK_a would not also include a binding event.

2.1.3 Wang's Hydrolysis/Solvolysis Mechanism and the pK_a Switch Hypothesis

The Shinkai-James N-B bond hypothesis remained unchallenged until 2003, when Wang and coworkers refuted their proposed explanation.[52] Wang noted that crystal

structures show the N-B bonds in boronic acids to be shorter than those found in the corresponding boronate esters, which discounted the Shinkai-James claim that the N-B bond strengthens upon binding a diol. Additionally, density functional theory (DFT) calculations suggested that the relatively small changes in the strength of the N-B bond in the presence or absence of diol would not be significant enough to explain the large difference in PET quenching. Furthermore, the DFT results suggested that the N-B bond was not strong enough to effectively engage the lone pair electrons. Wang further argued that if the strength of the N-B bond is what dictates the fluorescence intensity of the anthracene moiety, then boronate esters, which have different pK_as depending on which sugar molecule is bound, should produce different intensities in the fluorescence of **2.1**. However, work by Wang showed that the change in fluorescence was independent of which sugar is bound.[17] Instead of a N-B bond, Wang proposed that protonation of the amine was a more likely explanation for the decreased PET quenching, pointing out that a N-H bond is far stronger than a N-B bond.

In a second paper in 2004, Wang postulated a new mechanism that further explained the role of the N-H bond.[53] In this mechanism, the first important feature was that one molecule of solvent is inserted between the nitrogen and boron atoms (Scheme 2.5). For this reason, the first part of Wang's new mechanism is referred to as the hydrolysis or solvolysis model.

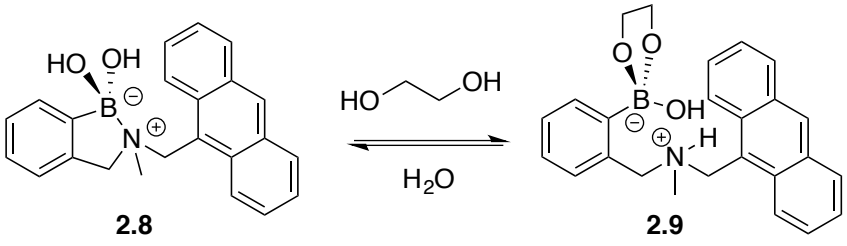

2.8 **2.9**

Scheme 2.5: Boronate ester condensation with solvent insertion.

The second important feature of the proposed mechanism was the "pK_a switch". In this postulate, pK_{a1} for the boronic acid corresponded to deprotonation of the ammonium group, and pK_{a2} represented hydroxylation of the boron atom, just as Shinkai and James had claimed. In contrast, Wang suggested that for the boronate ester, the order of pK_as was reversed, so that pK_{a1} would be associated with hydroxylation of the boron atom and pK_{a2} would correspond to deprotonation of the ammonium group. The pK_a switch hypothesis is summarized in Scheme 2.6.

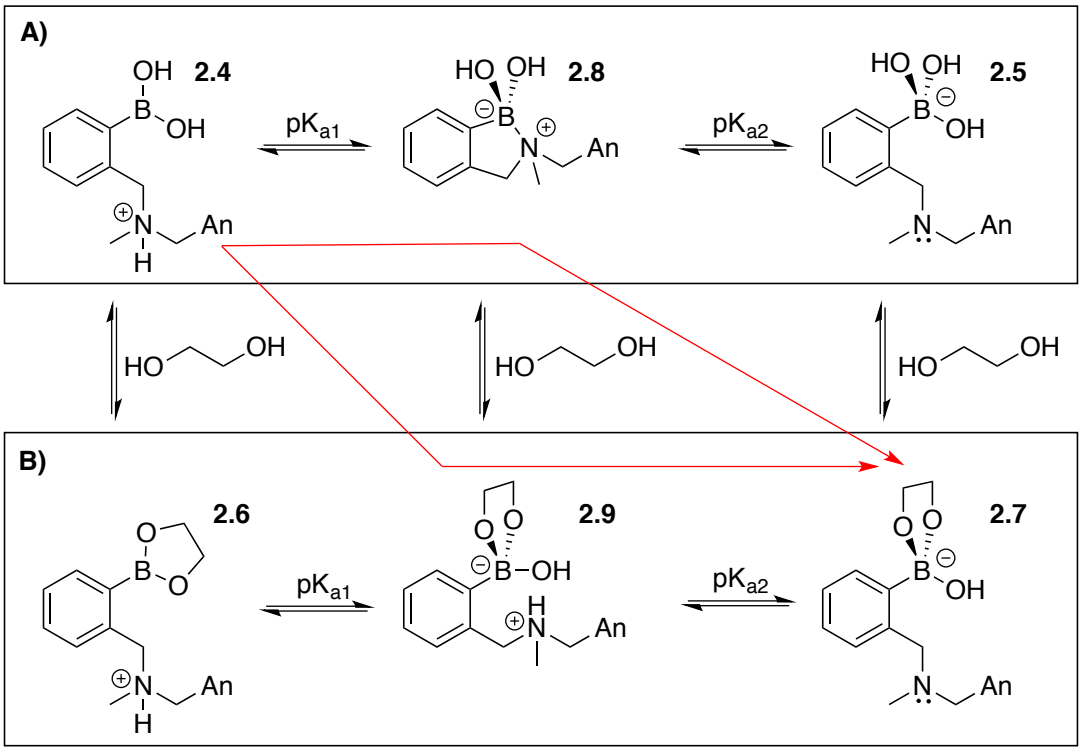

Scheme 2.6: pK_a switch mechanism scheme. The structures associated with A) the boronic acid, Shinkai's Host, and B) its corresponding boronate ester as a function of pH (low to high pH from left to right).

Following the pK_a switch hypothesis, deprotonation of the ammonium group of **2.4** (Scheme 2.6A) would liberate the nitrogen lone pair (pK_{a1}) and lead to the formation

of a full N-B bond in **2.8**. This step would only mildly affect PET quenching because the nitrogen would be engaged in the N-B bond. The following hydroxylation of the boron atom (pK_{a2}) to form **2.5** would greatly increase quenching because the nitrogen's lone pair would be newly available. So far, this was the same as the Shinkai-James interpretation presented in Scheme 2.4, except for the indicated strength and nature of the N-B bond in **2.8**, compared to that in **2.2**. In the case of the boronate ester (Scheme 2.6B), hydroxylation of the boron atom (pK_{a1}) in **2.6** would occur before deprotonation of the ammonium group (pK_{a2}) in **2.9** to form **2.7**.

Once again, red arrows have been added to indicate the most likely pathway in the presence of both Shinkai's Host and diol, as structures **2.5** and **2.6** are not likely to exist to a significant extent. In this postulate, as well as the N-B bond route, pK_{a1} of Shinkai's Host in the presence of sugars would represent both an acid-base component and a binding component. The pK_a corresponding to deprotonation of the ammonium group in the boronate ester (pK_{a2}) is high for an ammonium salt, but this can be rationalized by its proximity to the negatively charged boron center.

Wang and coworkers reproduced the pH titration reported by Shinkai and James (Figure 2.2).[53] They argued that this data could be better explained by the pK_a switch hypothesis than by the N-B bond hypothesis. The evidence in favor of this claim was that the pK_a switch mechanism predicted a large fluorescence decrease at the first pK_a for only the boronic acid, not the boronate ester, and this prediction was borne out in the data. The N-B bond hypothesis predicted large fluorescence decreases to be associated with the first pK_a for both the acid and the ester, which did not play out empirically.

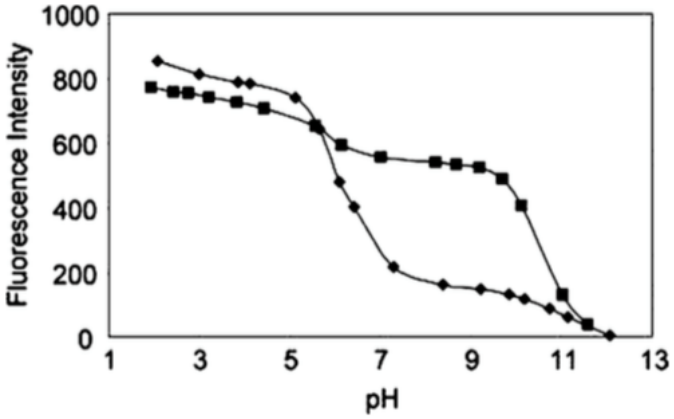

Figure 2.2[53]: Fluorescence intensity pH profile of **2.1**. 25 ºC, 2.25 μM solution in the presence (■) and absence (●) of glucose (50 mM).

One last piece of evidence that Wang presented for the pK_a switch mechanism was that some sugars (such as fructose) are known to bind to boronic acids in a trivalent coordination. He pointed out that if the N-B mechanism were active, one would not expect a trivalently binding sugar to cause a fluorescence intensity increase because the sugar would prevent an N-B bond from forming and being modulated.

2.1.4 Previous Anslyn Group Efforts Towards Reconciliation

2.1.4.1 Structural Studies

In a 2001 paper, the Anslyn group reported the pK_as of *ortho*-(aminomethyl)phenylboronic acids with both secondary and tertiary *ortho*-aminomethyl groups.[54] In both cases, pK_{a1} was approximately 5.5. Anslyn showed that trigonal boron did not exist above this first pK_a. At the time, this result was interpreted to mean that the tetrahedral boron atom was necessarily involved in a N-B bond. This is the literature precedent that Wang and coworkers cited when they proposed that the N-B bond would form in **2.8** in the absence of sugar (Scheme 2.6A). However, following Wang's solvent insertion hypothesis, the Anslyn group explored the nature of tetrahedral boron further.

In 2006, Anslyn reported a series of X-ray crystallographic and ^{11}B NMR pH titration studies of *ortho*-(pyrrolidinylmethyl)phenylboronic acid with several diols.[55] The chemical shifts of the products formed during the titrations were correlated with those found for purified boronate esters for which crystal structures were obtained. This analysis showed that N-B bonds form in aprotic solvent, but that solvolysis dominates over N-B bond formation in protic solvent. In one case, when catechol was added to the boronic acid, a small proportion of N-B bond formation was observed, meaning that N-B bonds and solvent-inserted products can coexist in equilibrium. DFT studies in the same paper confirmed that solvent insertion dominates over N-B bond formation for both boronic acids and boronate esters. More recently, advanced computation results from Larkin led to a similar conclusion.[56] Using both second-order Moller-Plesset perturbation theory and DFT, both with explicit solvation models, Larkin found that the solvent-inserted species are lower in energy than N-B dative-bonded species. It was also demonstrated that N-B bonding and solvent insertion are both lower in energy than no interaction at all between the *ortho*-aminomethyl group and the boronic acid or boronate ester in a protic solvent. Lastly, the results showed that any N-B bonding leads energetically downhill to species involving inserted solvent. A recent crystal structure of Shinkai's Host itself shows no N-B bond, even though the crystal was grown in aprotic solvent (Figure 2.3).

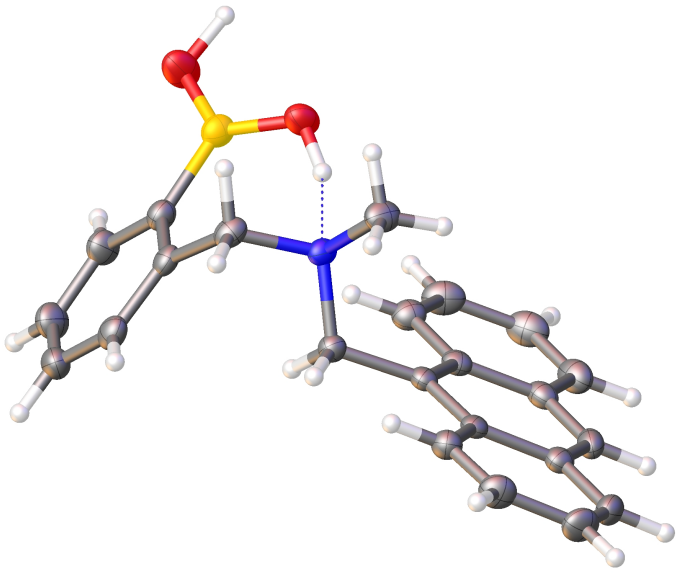

Figure 2.3[b]: Crystal structure of Shinkai's Host, indicating the absence of a N-B bond. The crystal was grown in acetonitrile.

In order to address the question of the pK_a switch, the same Anslyn 2006 report presented ^{11}B NMR pH profiles of *ortho*-(pyrrolidinylmethyl)phenylboronic acid in the presence and absence of catechol. One important observation that came from this study was that pyramidalization of boron occurs at pH 6.5, the value of pK_{a1}. When N-B bonding was presumed to be the reason for pyramidalization, this pK_a was thought to correspond to deprotonation of the ammonium group. However, the studies discussed in the previous paragraph proved that little to no N-B bonding takes place in protic solvent, so this pK_a had to be reinterpreted to signal pyramidalization *via* hydroxylation of the boron atom. The second important observation that came from these pH profiles was that pK_{a1} for the boronic acid was almost equal to pK_{a1} for the boronate ester – they differ by half a pK_a unit, at most. This would be an unlikely coincidence if the first pK_a represented

[b] Unpublished work. The crystal was grown by Dr. Pedro Metola and its structure was solved by Dr. Vincent Lynch.

two different deprotonations for the boronic acid and the boronate ester. The Anslyn group thus provided data inconsistent with the N-B bonding hypothesis as well as the pK_a switch hypothesis.

In this way, the Anslyn group established that solvent insertion was the manner by which both boronic acids and boronate esters are pyramidalized in protic solvents to form tetrahedral boronate anions. Interestingly, the same behavior is displayed by simple phenylboronic acid. At pHs near or above the pK_a, the anionic tetrahedral boronate ester is readily formed in the presence of a sugar, and the question arises as to the role that the *ortho*-aminomethyl group plays. Empirically, this functional group increases the diol-binding affinity of phenylboronic acids at neutral pH, and this is the primary reason that the group has been so widely adopted. Exactly how the group performs this function, however, remained unknown.

Phenylboronic acid itself has a pK_a of 8.8, but the first pK_a of *ortho*-(aminomethyl)phenylboronic acid compounds, which is now understood to correspond to hydroxylation at boron, is between 5 and 7, depending on the solvent. Thus, the *ortho*-aminomethyl group must lower the pK_a of the boronic acid group. It could do this by simply acting as a proximal electron-withdrawing group that shifts the phenylboronic acid's normal behavior to a lower pH range. The second pK_a must then represent deprotonation of the ammonium group. This pK_a is elevated by 1-2 units above that of a normal ammonium group, likely due to the proximity of the negatively charged boronate. Scheme 2.7 depicts the updated interpretation of the pH-dependent behavior of Shinkai's Host. This interpretation is identical to that in Scheme 2.6, except that the structure formed after hydroxylation of boron in **2.4** (pK_{a1}) is the solvent-inserted structure **2.10**, rather than the N-B bonded structure **2.8**.

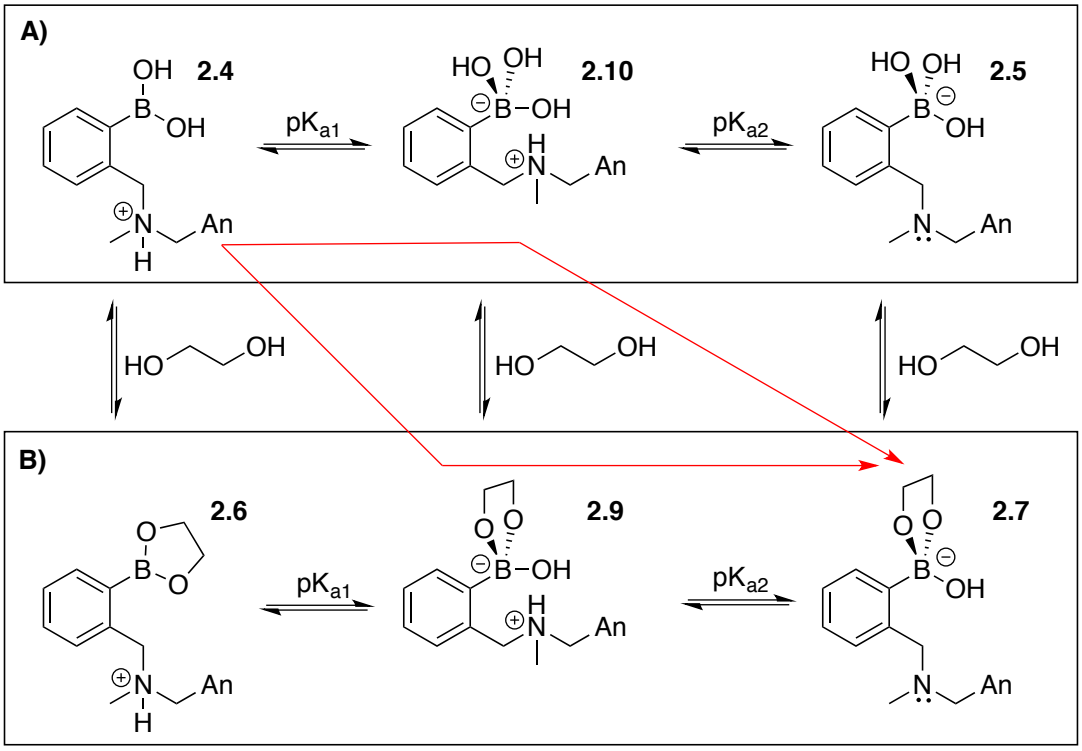

Scheme 2.7: Solvent insertion scheme. The structures associated with A) the boronic acid, Shinkai's Host, and B) its corresponding boronate ester as a function of pH (low to high pH from left to right).

2.1.4.2 The Role of the ortho-Aminomethyl Group in the Mechanism of Boronate Ester Formation

If the ammonium of the *ortho*-aminomethyl group perturbs the pK_a values of the boronic acid and boronate ester, it is logical that it could also play a key role in the mechanism of boronate ester formation. For example, consider what steps need to be involved when starting with a solvent-inserted boronic acid and transitioning to a solvent-inserted boronate ester (Scheme 2.8). The inserted solvent in **2.10** first needs to be expelled, then replaced by an alcohol of the diol or saccharide, followed by bond rotations and further stepwise replacements of inserted solvent(s), leading to a fully bound guest. Because the first replacement of the inserted solvent by the guest is intermolecular, it is likely slow relative to the subsequent steps that are intramolecular

and chelate the diol or saccharide to the boron atom. The release of an inserted solvent would lead to species **2.1** in Scheme 2.8A. This could happen in two steps: ammonium deprotonation and loss of hydroxide/alkoxide from the boron, in either order (pathway 1 *via* **2.5** or pathway 3 *via* **2.4**). In both cases, this would require loss of a very poor leaving group at neutral pH. Alternatively, the solvent could be lost in one step by simple decomplexation from the boron. This would involve producing an *ortho*-(aminomethyl)phenylboronic acid in a high-energy state (**2.1**) because it does not possess the preferred boronic acid and amine protonation states at the operating pH.

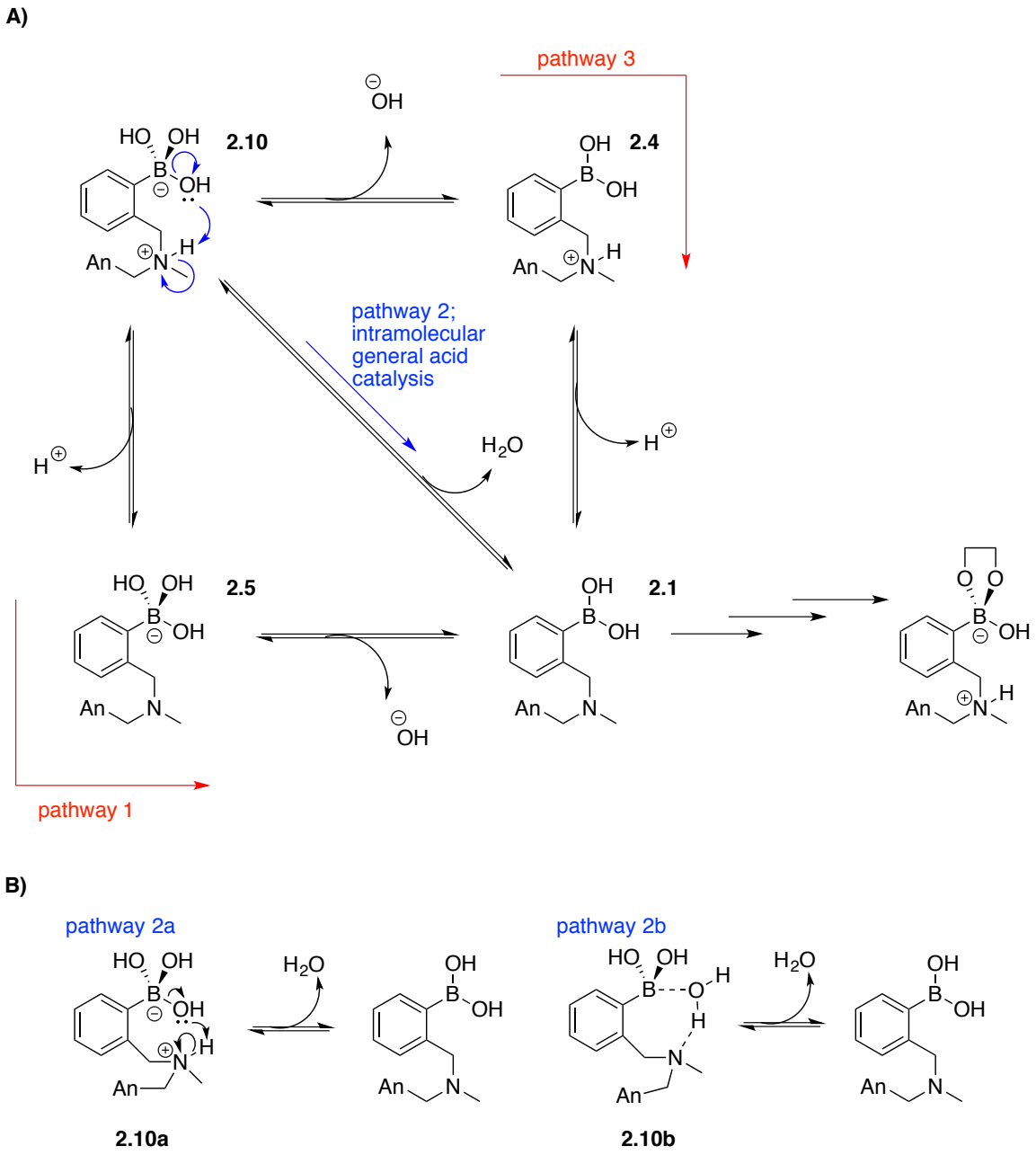

Scheme 2.8: Plausible mechanisms for boronate ester formation at a pH between the first and second pK_a values. A) Two possible two-step mechanisms and a one-step (general acid catalysis) mechanism. B) Two variations on the one-step pathway, differing in the extent of solvent ionization.

The question of stepwise versus single-step loss of the inserted solvent depends on the ionization state of the inserted solvent. The loss of the inserted solvent should have a dependence on the extent to which that solvent is deprotonated when bound between the boron and nitrogen. If the solvent is fully deprotonated when inserted (structure **2.10a** in Scheme 2.8B), thereby forming a zwitterionic boronate anion and ammonium cation, its single-step departure as a neutral species would require a proton transfer that is simultaneous with its departure (pathway 2a). If the solvent is not ionized when inserted (structure **2.10b**), it can simply depart with no proton transfer (pathway 2b). The former possibility is defined as general acid catalysis, and this sequence can be analyzed by classic experiments such as isotope effects.

All of the pathways shown in Scheme 2.8 would require the formation of high-energy intermediates, so the solvent-loss step is expected to be the rate-determining step. The next step, nucleophilic attack of a diol-containing guest, should thus demonstrate saturation kinetics. However, saturation kinetics for such systems had not been found previously.[57] Alternatively, a mechanism in which the solvent-inserted *ortho*-(aminomethyl)phenylboronic acid reacts directly with the guest would show second order kinetics – first order in both boronic acid and diol – as with an S_N2 reaction. Anslyn and coworkers studied the kinetics of the reaction of Shinkai's host with fructose at both low and high fructose concentrations.[58] At low concentrations of fructose, the kinetics appeared second order and the y-intercept of the kinetic plots revealed ratios of k_1 and k_{-1}. The reaction appeared analogous to an S_N2 mechanism, except for the fact that the y-intercept was shown to be non-zero, which is indicative of equilibrium kinetics. At high fructose concentrations, saturation kinetics were observed (Figure 2.4). At concentrations of fructose above 15 mM, the kinetics showed that a mechanism involving a rate-determining step prior to reaction with the guest was operative.

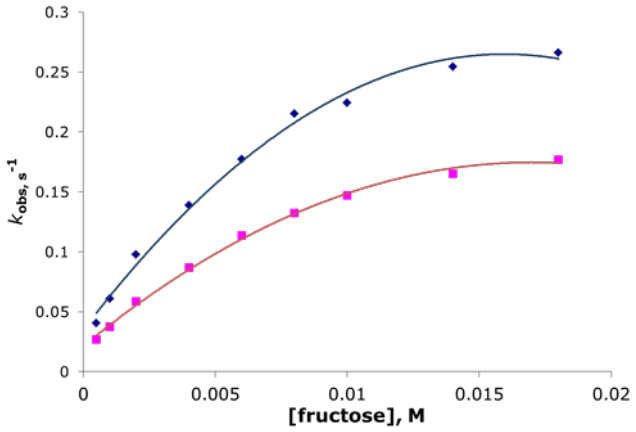

Figure 2.4[58]: Observed rate constants for the reaction of **2.1** with fructose. 10 μM solution in 2:1 H_2O/CH_3OH (◆) and in 2:1 D_2O/CD_3OD (■) at pH(D) = 8.7 with 50 mM NaCl, showing saturation of kinetics as the concentration of fructose is increased.

It was proposed that the rate-determining step was loss of the inserted solvent to form **2.1** (Scheme 2.8A). Such a mechanism is analogous to an S_N1 reaction, in which leaving group departure leads to a reactive intermediate, which is susceptible to nucleophilic attacks. Unlike S_N1 chemistry that appears first order at low concentrations of nucleophile, the boronic acid mechanism requires hundreds of equivalents (approximately 1500) of fructose to reach saturation. This makes sense, given that the reverse step that competes with the first insertion of guest (in this case, fructose) is insertion of a solvent molecule. This competing re-insertion of solvent is analogous to the common ion effect in S_N1 mechanisms,[59] but with the "common ion" being solvent.

Additionally, Anslyn investigated the extent of ionization of inserted solvent. If the general acid catalyzed mechanism in pathway 2a were operating, the solvent would be significantly ionized, so loss of solvent would involve the movement of a proton and should have an isotope effect. If the decomplexation mechanism in pathway 2b were operating, there should be little to no isotope effect. A primary isotope effect of 1.42 was

indeed observed for the reaction of Shinkai's Host with fructose. This value is smaller than a typical primary isotope effect (values of 2-6), but it is substantial enough to suggest cleavage of a weak bond to hydrogen, supporting pathway 2a in Scheme 2.8. This result is in agreement with crystallographic data published by the Anslyn group in 2009.[60] This crystal structure was of high enough quality that the hydrogen atom between the oxygen and nitrogen atoms could be located, and it was shown to be closer to the nitrogen than the oxygen of the solvent molecule, indicating at least some ionization of the inserted solvent (Figure 2.5).

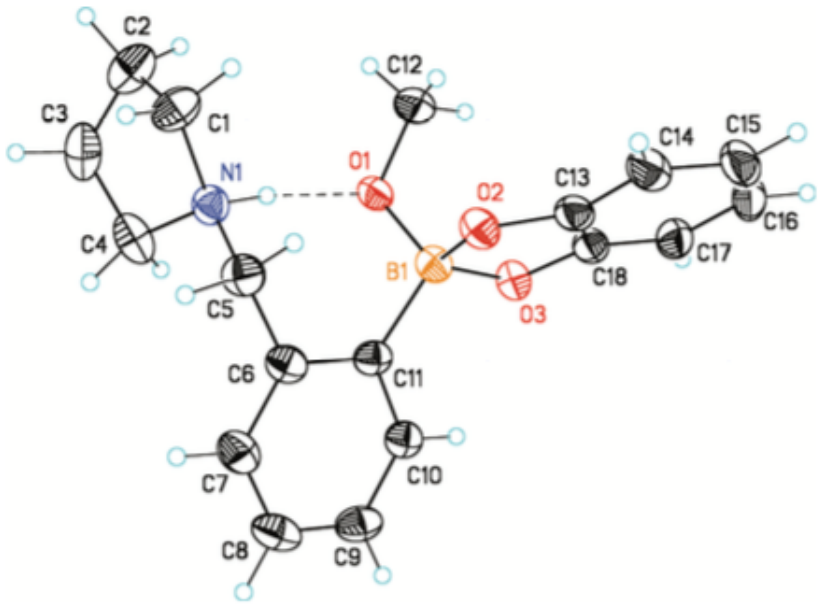

Figure 2.5[60]: Crystal structure of a methanol-inserted species with ionized solvent molecule.

The value of the kinetic isotope effect may be smaller than normal for two possible reasons. First, the isotope effect could be smaller than a standard primary kinetic isotope effect because the extent of proton transfer required to liberate the solvent is minimal due to incomplete ionization of the solvent (extent of ionization somewhere

between that of structures **2.10a** and **2.10b**). The less ionized the solvent, the lower the expected isotope effect. A second possibility is that the stepwise pathways depicted in Scheme 2.8A (pathways 1 and 3) are occurring simultaneously with the general acid catalyzed pathway. This would mean that only a fraction of the operating pathways in the departure of solvent would be expected to show an isotope effect. From this point forward, Shinkai's Host will be referred to by its isolated structural form, **2.1**, but it should be understood to be in its zwitterionic form in solution at pHs between the two pK_as.

2.1.4.3 Conclusions Regarding the Mode of Binding

Through the combined efforts of Shinkai, James, Wang, Anslyn, and Larkin, a clear view of binding – both intermolecularly, between boronic acids and diols, and intramolecularly, between the nitrogen and boron atoms in *ortho*-(aminomethyl)phenylboronic acids – has been realized. The group was able to conclude that a solvent insertion mechanism was operating, rather than the N-B bonding or pK_a switch mechanisms. Additionally, the incorporation of a diol-containing guest into a complex with **2.1** was concluded to take place *via* a general acid catalyzed mechanism.

2.2 Elucidation of the Mechanism of Fluorescence Modulation[c]

Despite the fact that previous work succeeded in drawing a clear picture of binding, it is not apparent how fluorescence of **2.1** is modulated upon binding a sugar. Developing an understanding of the mechanism for fluorescence modulation will be the focus of the rest of this chapter.

[c] All of the experiments described in this section were carried out by Brette Chapin.

2.2.1 Excimer Fluorescence of Shinkai's Host

In early fluorescence studies, an emission scan with λ_{ex} = 368 nm was carried out with a saturated solution of **2.1** in 2:1 water/methanol with 50 mM NaCl. (This was the solvent system reported in the original 1994 Shinkai-James paper.) The expected monomer fluorescence was observed, with its maximum at 417 nm. Unexpectedly, there was also a broad emission peak with its maximum at approximately 530 nm (Figure 2.6).

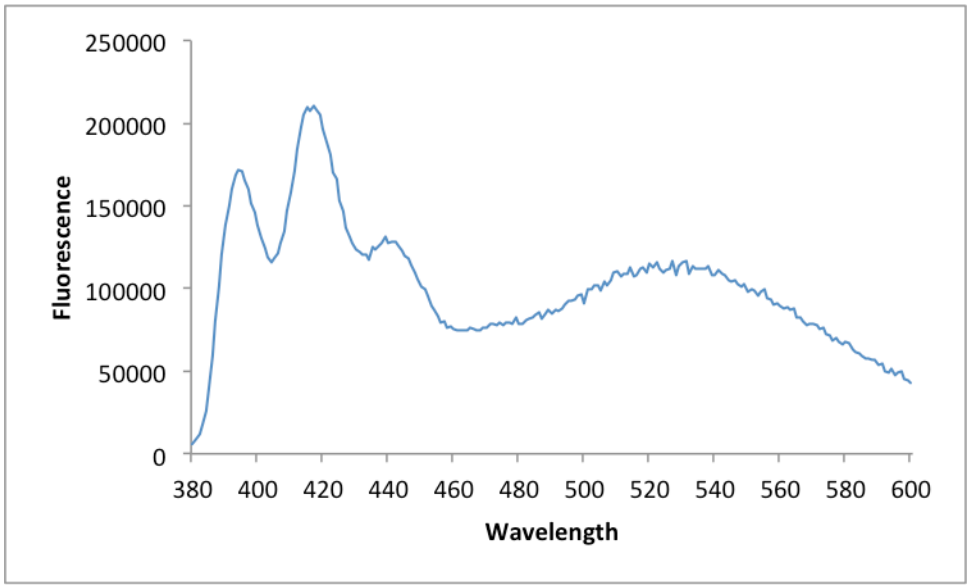

Figure 2.6: Emission scan of **2.1** with λ_{ex} = 368 nm. Saturated solution in 2:1 water/methanol with 50 mM NaCl. 1 cm path length cuvette, slit widths 4 nm, integration time 0.5 s.

This peak was initially surprising, but perusal of the literature revealed that anthracene has been known to exhibit this type of emission, called an excimer, since 1965[61,62] and that an anthracene excimer was directly observed for the first time in 1976.[63] However, excimers have never been discussed within the context of fluorescence modulation in Shinkai's Host. "Excimers", or excited dimers, form when an excited monomer collides with a ground-state monomer. An excited monomer can relax to the

ground state and release a photon with energy $h\nu_M$. If it instead forms the excited dimer, the dimer eventually relaxes to give two ground-state monomers and a photon with energy $h\nu_D$.

$$^1M + h\nu \rightarrow {}^1M^*$$

$$^1M^* \rightarrow {}^1M + h\nu_M$$

$$^1M^* + {}^1M \rightarrow {}^1D^*$$

$$^1D^* \rightarrow {}^1M + {}^1M + h\nu_D$$

Excimers have longer wavelength emission than their corresponding monomers because they experience internal conversion and an associated loss of energy. They also typically have much lower quantum yields than monomers because of internal conversion and self-quenching mechanisms. These phenomena also cause excimer fluorescence to be broad with a lot of noise.[64] Figure 2.6 displays all of these qualities, making it seem likely that the broad emission at 530 nm is indicative of an excimer of **2.1**.

Anthracene excimers are known to form when two anthracene moieties are in a slip-stack or "sandwich" conformation. Anthracenes substituted at the 9-position typically come together with their substitutions 180 degrees apart, or antiparallel, as shown in Figure 2.7.[65]

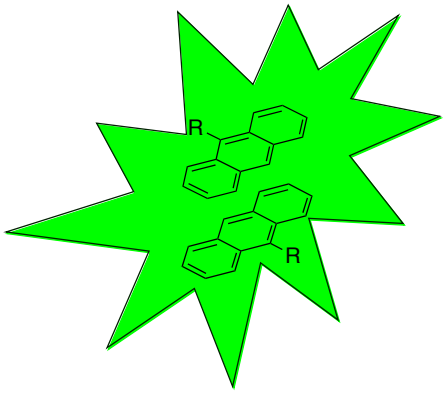

Figure 2.7: Slip-stacked anthracene moieties or "sandwich dimers" are known to form excimers.

In addition to anthracene's tendency to form ground-state aggregates, it is known that sodium chloride increases the degree of aggregation of dye molecules *via* the common ion effect.[66] Thus, it is unsurprising that an anthracene-based sensor forms aggregates in the Shinkai-James solvent system, which includes 50 mM sodium chloride. Reexamining the crystal structure from Figure 2.3, contacts can be observed between anthracene rings (Figure 2.8). Even though the crystal was grown in acetonitrile and therefore does not experience hydrophobic interactions, π-stacking interactions are clearly shown, with the distance between anthracene rings averaging 3.8 angstroms.

A)

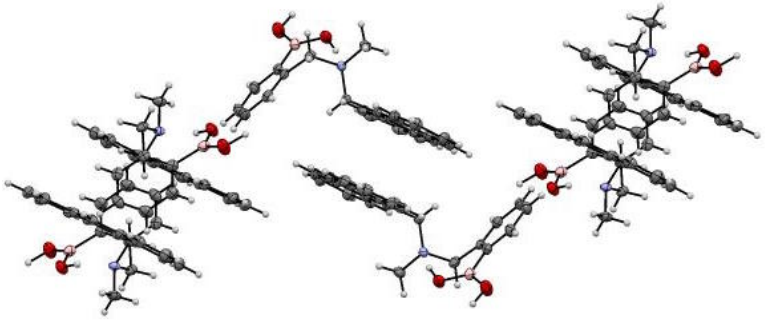

B)

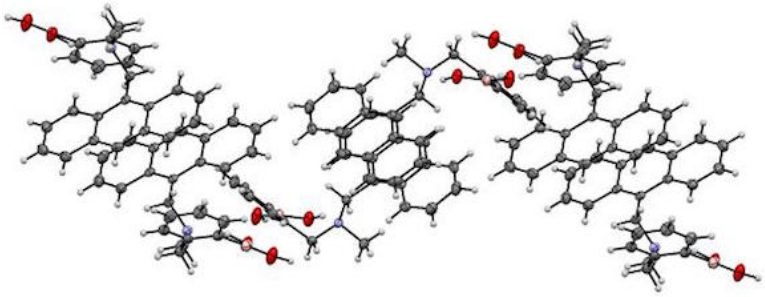

Figure 2.8: When contacts are drawn for the crystal in Figure 2.3, π-stacking is observed between anthracene rings. A) View parallel to the anthracene planes, and B) View from above the anthracene rings.

In order to provide further evidence for the formation of an excimer, additional emission and excitation scans were carried out (Figure 2.9). The blue curve shows the emission scan that results from λ_{ex} = 368 nm. Next, an excitation scan was carried out while monitoring at λ_{em} = 417 nm, the emission maximum of the monomer. This curve is colored red in Figure 2.9. The excitation profile is the mirror image of the emission scan, as expected. A second excitation scan was carried out while monitoring λ_{em} = 520 nm, emission of the putative excimer. This excitation profile, the green curve, has a completely different shape from the monomer excitation profile. This means that a different species is being excited. More importantly, there are wavelengths where the excimer can be excited in isolation, meaning that the monomer will not also be excited, and the fluorescence of the excimer can be observed alone. To achieve this, an emission scan was run at λ_{ex} = 408 nm (purple curve). At this wavelength, the red curve is at nearly zero, but the green curve is still at approximately half of its maximum fluorescence intensity. Thus, the purple curve represents fluorescence of only the excimer. This curve suggests that there is indeed an excimer present following excitation of the monomers in solution.

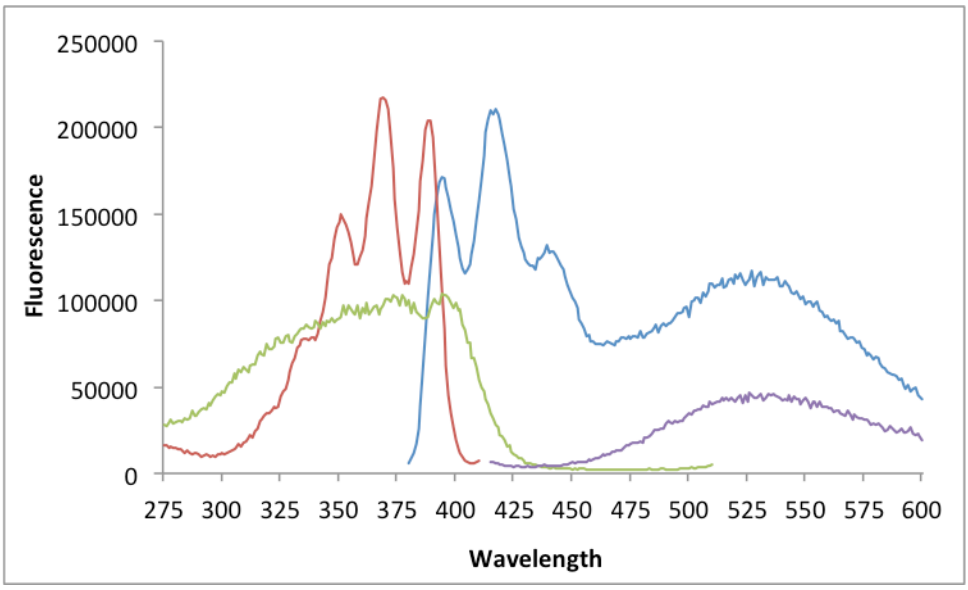

Figure 2.9: Emission and excitation scans of **2.1**. Saturated solution in 2:1 water/methanol with 50 mM NaCl, 1 cm path length cuvette, slit widths 4 nm, integration time 0.5 s. Emission scan with λ_{ex} = 368 nm (blue). Excitation scan with λ_{em} = 417 nm (red). Excitation scan with λ_{em} = 520 nm (green). Excitation scan with λ_{ex} = 408 nm (purple).

It was also noted that the fluorescence emission spectra responded to fructose (Figure 2.10). Emission scans were carried out on a 12 μM solution of **2.1** with λ_{ex} = 368 nm (dark blue curve) and λ_{ex} = 408 nm (dark purple curve). Then the scans were repeated with 12 μM **2.1** and 50 mM fructose (light blue and purple curves). The monomer fluorescence increased four-fold, while the excimer fluorescence was completely eliminated (see inset in Figure 2.10). This inverse relationship is consistent with the presence of an excimer, as are the magnitudes of the changes in fluorescence. As monomer fluorescence increases, excimer fluorescence must decrease, and to a much smaller degree, since the excimer has a lower quantum yield.[64] At this point, we hypothesized that **2.1** forms ground-state π-stacked aggregates in solution due to the hydrophobic effect, and that when these aggregates are irradiated, monomers in close

proximity with one another form the excimer that we observe. We also hypothesized that fructose assisted in breaking up these ground-state aggregates by binding to the monomers to form boronate esters.

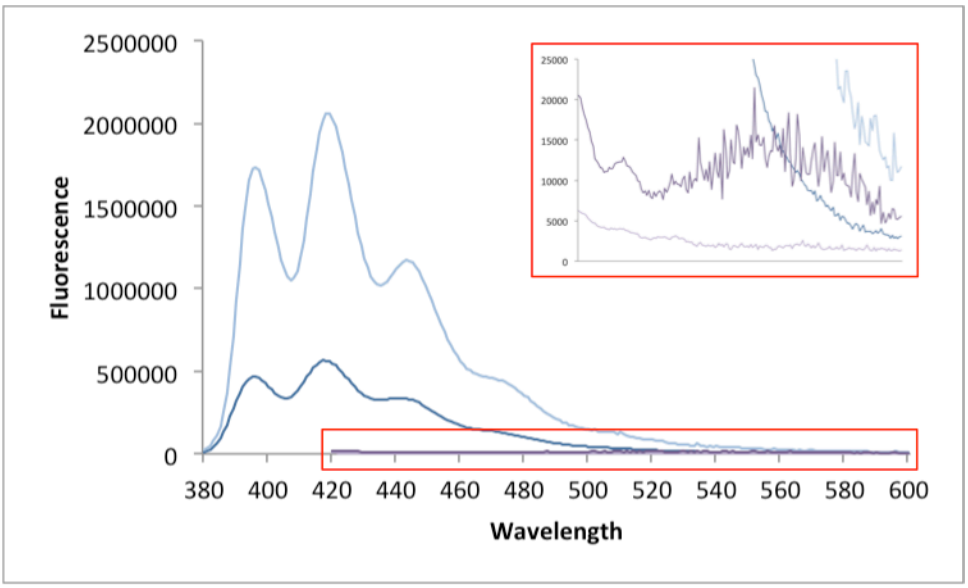

Figure 2.10: Fluorescence spectra of **2.1** in the presence and absence of fructose. 12 μM solution in 2:1 water/methanol with 50 mM NaCl, 1 cm path length cuvette, slit widths 4 nm, integration time 0.5 s. Emission scan with λ_{ex} = 368 nm (dark blue). Excitation scan with λ_{ex} = 408 nm (dark purple). Emission scan in the presence of 50 mM fructose with λ_{ex} = 368 nm (light blue). Excitation scan in the presence of 50 mM fructose with λ_{ex} = 408 nm (light purple).

A fluorescence titration in which fructose was added to a constant concentration of **2.1** was attempted. Unfortunately, the data did not demonstrate saturation of the host **2.1** (Figure 2.11). We suspected that perhaps this was due to insufficient time to reach equilibrium after each addition.

A) B)

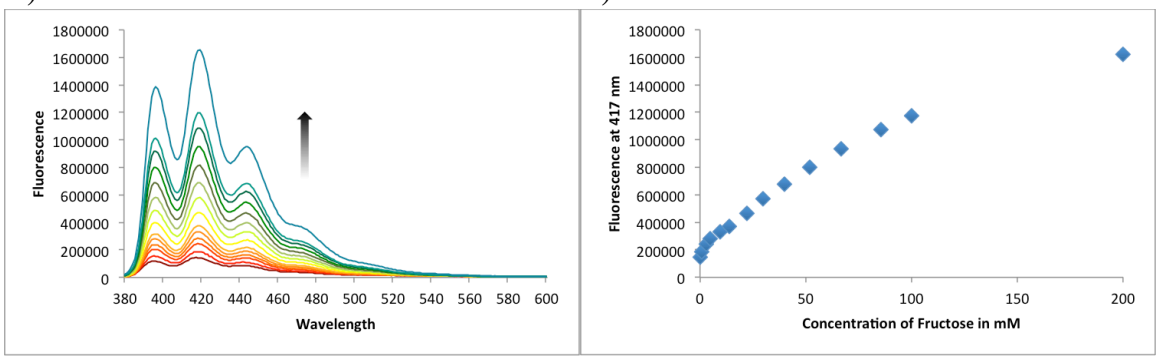

Figure 2.11: Fructose titration into **2.1**. A) Fluorescence spectra of a 12 μM solution of **2.1** in 2:1 water/methanol with 50 mM NaCl, 0-200 mM fructose, λ_{ex} = 368 nm. 1 cm path length cuvette, slit widths 4 nm, integration time 1 s. B) Fluorescence at 417 nm plotted against concentration of fructose.

This fluorescence titration was repeated, but with each sample prepared individually from stock solutions. The samples were stored at room temperature in the dark overnight, and emission spectra were obtained the next day. This time, the plot suggested that **2.1** had saturated with fructose, and the data was fit to a one-to-one binding curve with an association constant of K = 125 M^{-1} (Figure 2.12). (See Appendix for more information on fitting binding curves to calculate equilibrium constants.) This binding constant was lower than what has typically been reported for boronic acid-diol binding.[34]

A) B)

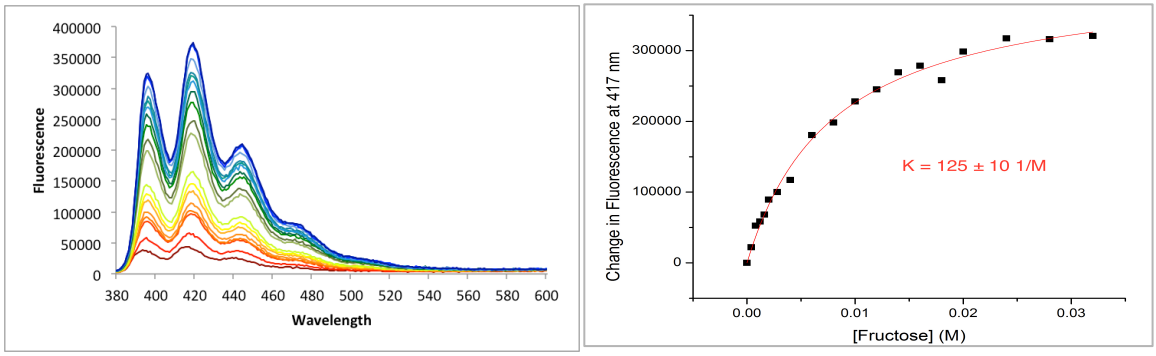

Figure 2.12: Fructose titration into **2.1** with individually prepared samples. A) Fluorescence spectra of a 12 μM solution of **2.1** in 2:1 water/methanol with 50 mM NaCl, 0-32 mM fructose, λ_{ex} = 368 nm. Semi-micro cuvette, slit widths 2 nm, integration time 1 s. B) Change in fluorescence at 417 nm plotted against concentration of fructose and fit to a one-to-one binding curve.

The time dependence of the fructose titration suggested that perhaps the fluorescence of **2.1** changed over time on its own. And in fact, this was shown to be true (Figure 2.13). Six repeat scans at λ_{ex} = 368 and λ_{ex} = 408 were carried out with 12 μM **2.1** alone, and with each pair of scans, monomer fluorescence increased and excimer fluorescence decreased (dark blue curves fading to light blue curves). The solution was stored at room temperature in the dark overnight and then scanned again the next day (red curves). We propose that the fluorescence change over time is a result of long-lived aggregates that remain intact for hours, even overnight, before dissociating. This could mean that the effects of aggregate dissociation and fructose binding could be confounded with one another, and that the binding curve in Figure 2.12B is not truly representative of binding, but a combination of binding and disaggregation.

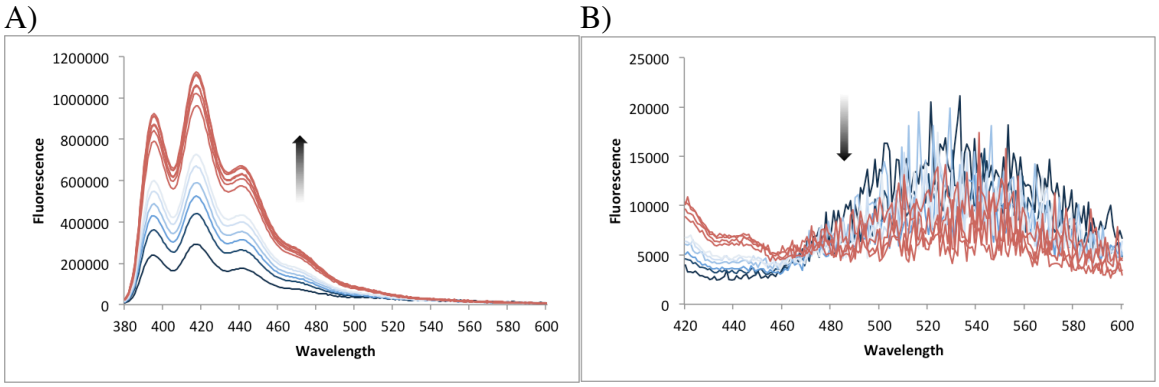

Figure 2.13: Fluorescence spectra of **2.1** over time. 12 μM solution in 2:1 water/methanol with 50 mM NaCl, λ_{ex} = 368 nm (A) and λ_{ex} = 408 nm (B). 1 cm path length cuvette, slit widths 4 nm, integration time 1 s.

In order to maximize the monomer fluorescence of **2.1** alone, a solution of 12 μM **2.1** was monitored with repeated emission scans for approximately 72 hours. Even over a span of three days, the monomer fluorescence continued to increase (Figure 2.14).

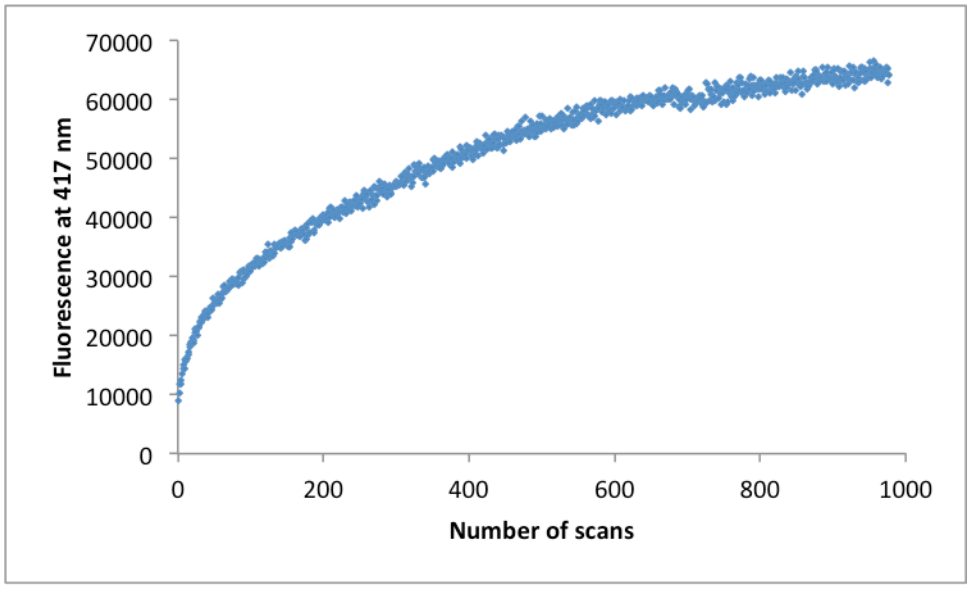

Figure 2.14: Fluorescence of **2.1** at 417 nm over 72 hours. 12 μM solution in 2:1 water/methanol with 50 mM NaCl, λ_{ex} = 368 nm. Semi-micro cuvette, slit widths 2 nm, integration time 1 s.

Another observation that came from this experiment was that a sample of **2.1** solution left in the dark became more fluorescent (at the monomer wavelength) over time, but that an aliquot of the same solution that was repeatedly subjected to excitation over the same time period increased faster. In other words, irradiation increased the rate of disaggregation. In Figure 2.15, we propose a mechanism for this phenomenon within the context of typical photophysical behavior of fluorescent compounds.

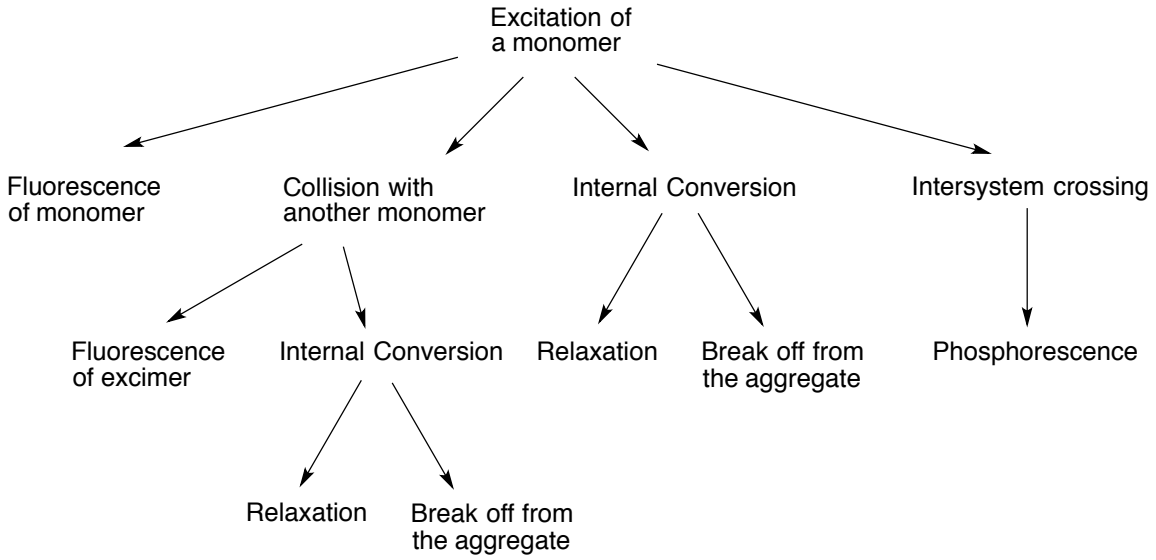

Figure 2.15: Proposed mechanism for disaggregation of **2.1** with irradiation.

As with any excited compound, **2.1** can release energy and return to its ground state *via* fluorescence, internal conversion, or intersystem crossing followed by phosphorescence. In the case of **2.1** in particular, fluorescence can be from the monomer or from the excimer, due to the dimerizable properties of anthracene. Since the excited dimers seem to be the result of aggregation in the ground state, there is also an extra possibility for internal conversion. Internal conversion is typically conceptualized as a simple relaxation, a radiationless transition that releases energy as heat. In this particular case, we believe that the released energy could simply heat up the solution, as would

normally be expected, or it could overcome the hydrophobicity and the stabilization of π-stacking and cause the monomer to break away from the rest of the ground-state aggregate. If this is the case, other methods of introducing thermal energy into the system, such as heating or sonication, should also result in accelerated aggregate break-up and a greater increase in monomer fluorescence.

In order to test this hypothesis, a solution of 12 μM **2.1** in 2:1 water/methanol with 50 mM NaCl was prepared. Initial fluorescence spectra are recorded in blue in Figure 2.16.

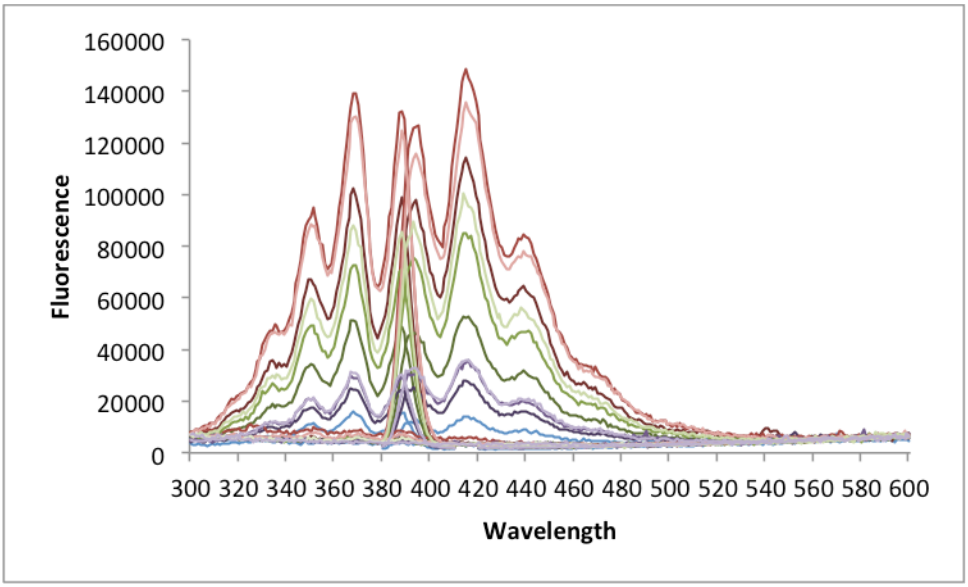

Figure 2.16: Fluorescence spectra of **2.1** with different treatment conditions. Emission scans with λ_{ex} = 368 nm, 408 nm. Excitation scans with λ_{em} = 417 nm, 520 nm. 12 μM solution in 2:1 water/methanol with 50 mM NaCl, 1 cm path length cuvette, slit widths 2 nm, integration time 1 s. Initial scans are shown in blue. The aliquot stored at room temperature in the dark is shown in purple. The aliquot warmed to 40 °C in the dark is shown in green. The aliquot that was sonicated in the dark is shown in red. For each aliquot, the curves change from dark color to light color with time.

After recording initial fluorescence spectra, three aliquots of the original solution were treated to different conditions. One aliquot was stored at room temperature in the dark, a second was warmed to 40 °C in the dark, and a third was sonicated in the dark. Each treatment lasted 90 minutes, and then the aliquots were subjected to fluorescence scans. The room temperature aliquot, shown in purple in Figure 2.16, displayed increased monomer fluorescence relative to the initial (blue) curves. Importantly, this was true despite the fact that excimer was not observed in the initial scans. This demonstrates the importance of quantum yield; even though the low quantum yield makes it impossible to observe the excimer, aggregation and self-quenching still take place. The higher quantum yield of the monomer allows observation of the increase in its fluorescence intensity, and allows one to infer that the extent of self-quenching in the aggregate is decreasing over time. The warmed aliquot, shown in green in Figure 2.16, displayed an even greater increase in fluorescence intensity over the same time period, as compared to the room temperature aliquot. The sonicated aliquot, shown in red, demonstrates the greatest increase. This is likely due to a combination of sonication and temperature, because the water bath in the sonicator warmed up significantly over the 90-minute treatment period. Two more 90-minute treatment periods were carried out for all three conditions. The fluorescence spectra are depicted in progressively lighter colors in Figure 2.16. The room temperature aliquot did not change after the second period, and the sonicated aliquot actually decreased in fluorescence intensity between the second and third measurements. The warmed aliquot continued to increase in fluorescence intensity with each measurement. These results demonstrate that an increase in thermal energy does increase the rate at which **2.1** disaggregates in the absence of diol-containing guest. The results also bring to light the surprising magnitude of the change in fluorescence intensity – more than a ten-fold increase – that is possible for **2.1** alone.

Since the fluorescence of **2.1** alone changes so dramatically over time, it was necessary to determine how much fluorescence increase was due to disaggregation alone and how much was due to the addition of fructose. To make this comparison, two portions of the same 12 μM solution of **2.1** were treated to different conditions. Portion A was scanned once, with λ_{ex} = 368 nm (Figure 2.17, maroon), then sealed in a vial and stored at room temperature in the dark overnight. Portion B was scanned repeatedly overnight (green, first scan; turquoise, last scan). Several hours after the last scan, one more scan was carried out (blue), demonstrating that the fluorescence intensity had not saturated. Then fructose was added to be 50 mM and three repeat scans were carried out (purple). This showed that once fructose was added, the fluorescence intensity did not change. Portion A was scanned once more (red), showing that while fluorescence increased overnight, it increased less than portion B, which was being scanned repeatedly all night (turquoise). Fructose was added to portion A to be 50 mM and the solution was scanned repeatedly (again, overnight) until the fluorescence intensity saturated (orange, first scan; yellow, last scan). This demonstrated that even after fructose was added, the solution did not reach its maximum fluorescence until it received more energy from irradiation. It is notable that both portions of the solution ended with nearly the same fluorescence intensity, independent of when fructose was added. This result seems to suggest that irradiation and binding to fructose both cause **2.1** to disaggregate, and that these two variables have an additive effect. However, portion B showed a greater increase in fluorescence intensity upon addition of fructose than that of portion A upon addition of the same amount of fructose; this could be interpreted to mean that portion B was already more disaggregated, that fructose thus had more monomers available to bind to, and that binding itself is what caused the fluorescence increase.

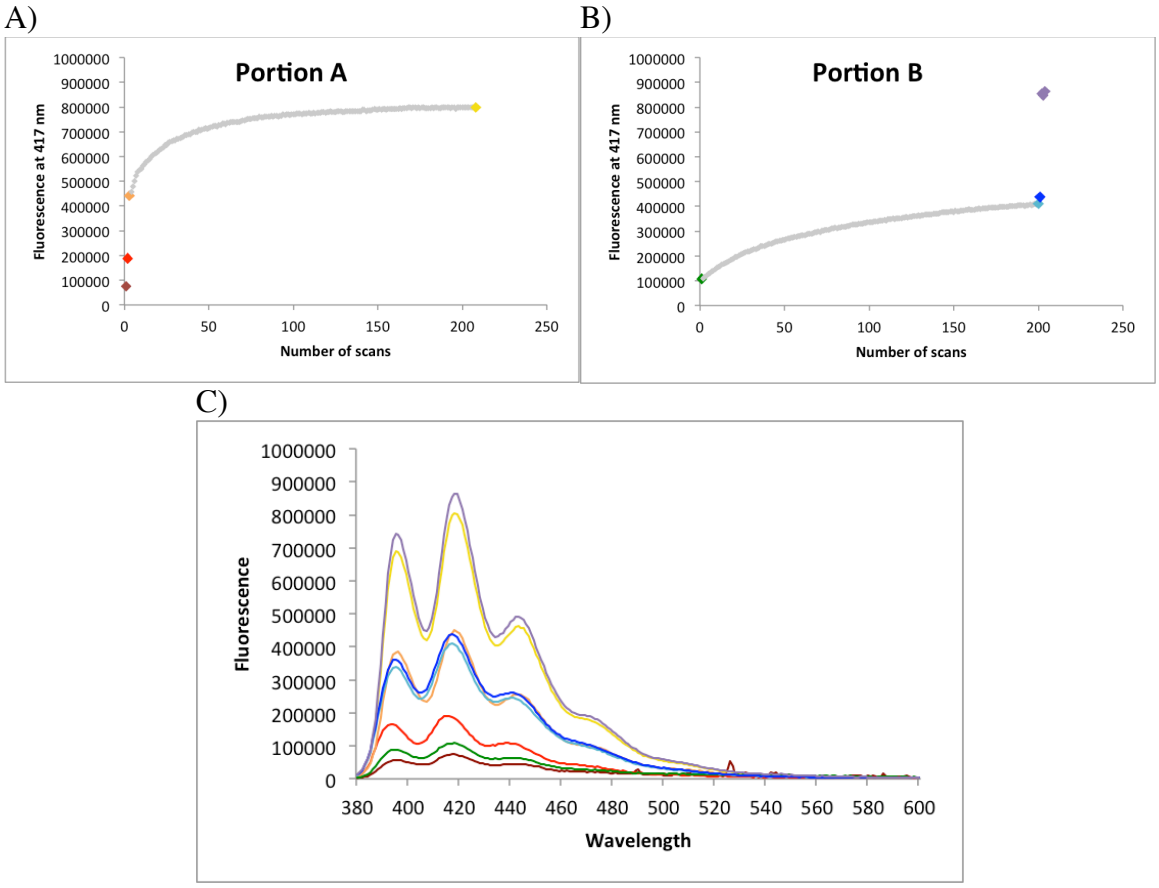

Figure 2.17: Fluorescence of **2.1** under different treatment conditions. 12 μM solution in 2:1 water/methanol with 50 mM NaCl. Emission scans with λ_{ex} = 368 nm, 1 cm path length cuvette, slit widths 4 nm, integration time 1 s. A) Fluorescence at 417 nm of portion A (maroon, initial scan; red, scan after storage in the dark overnight; orange, scan after adding fructose; yellow, after saturation of fluorescence intensity). B) Fluorescence at 417 nm of portion B (green, initial scan; turquoise, last scan after repeat scans overnight; blue, scan several hours later; purple, scans after adding fructose). C) Emission spectra with λ_{ex} = 368 nm from which the highlighted points were taken, matched by color.

In another attempt to separate the variables of disaggregation and sugar binding and their effect on fluorescence intensity, a 12 μM solution of **2.1** was sonicated in order to speed up the process of disaggregation (Figure 2.18). An emission scan with λ_{ex} = 368 nm was carried out (first blue point) and the solution was sonicated for 90 minutes, then

scanned again (red point). The solution was sonicated for a second 90-minute period, and then scanned (green point). Then scans were repeated until the fluorescence intensity remained constant, and finally fructose was added to be 50 mM (purple point). Repeat scans resulted in very small increases after the addition of fructose.

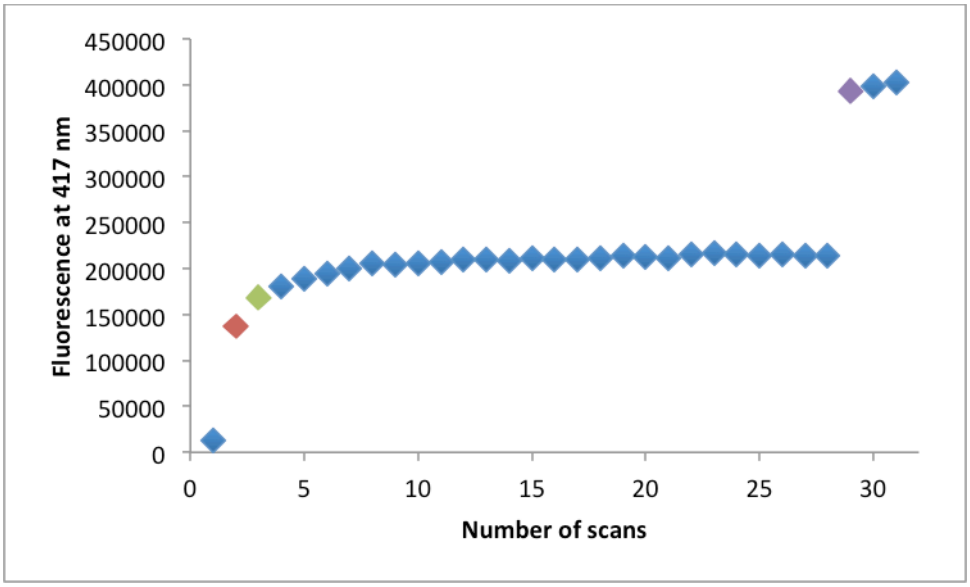

Figure 2.18: Fluorescence of **2.1** at 417 nm with sonication and repeated scans. 12 μM solution in 2:1 water/methanol with 50 mM NaCl. λ_{ex} = 368 nm, λ_{em} = 417 nm. 1 cm path length cuvette, slit widths 2 nm, integration time 1 s. Red: scan after 90 minutes of sonication. Green: scan after another 90 minutes of sonication. Purple: scan after adding fructose.

As Figure 2.18 shows, fluorescence intensity increased by more than fifteen-fold due to disaggregation, and then only increased by about two-fold upon addition of fructose. Thus, the large majority of the fluorescence turn-on occurs without binding. However, fructose did reliably effect additional turn-on over multiple repeats of this experiment. It is clear that fructose makes a difference, but it cannot be determined if fructose further disaggregates **2.1** by binding, if it disaggregates **2.1** by preventing π-stacking, or it modulates fluorescence *via* some mechanism other than disaggregation.

Similar studies to those described above were carried out in pure methanol, rather than 2:1 water/methanol and 50 mM NaCl. First, the fluorescence intensity of a 12 μM solution of **2.1** was monitored over many scans (Figure 2.19). Unlike in Figure 2.14, the fluorescence intensity did not increase dramatically over time. We propose that this is due to the much greater solubility of **2.1** in pure methanol, and serves as additional evidence that the fluorescence intensity changes in Figure 2.14 represents disaggregation. (The upper limit of solubility for **2.1** in 2:1 water/methanol with 50 mM NaCl is approximately 50 μM, compared to approximately 10 mM in pure methanol.) Instead of dramatically increasing, fluorescence intensity slowly decreases in pure methanol. This is likely due to photobleaching, which is a common occurrence for fluorophores when they are exposed to light over long periods of time.

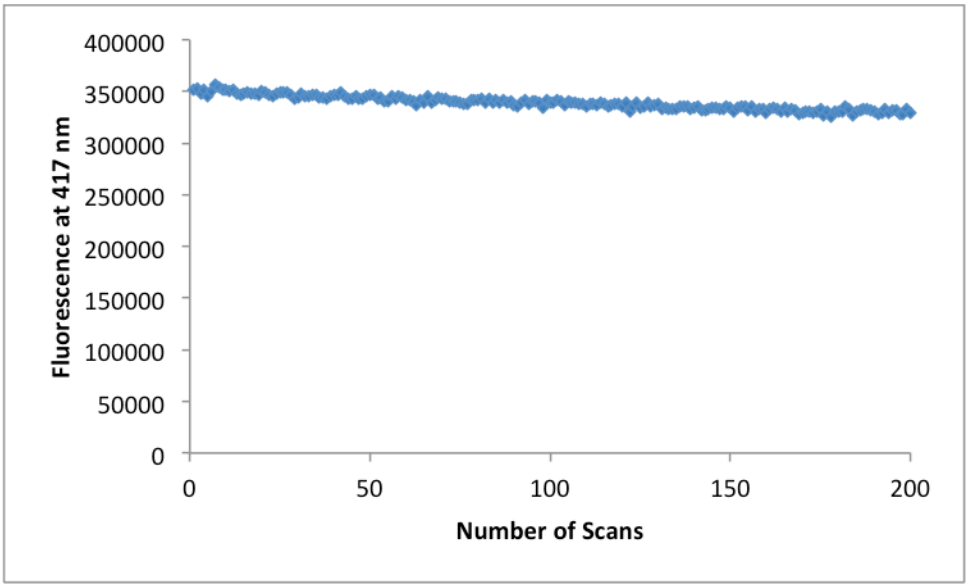

Figure 2.19: Fluorescence of **2.1** at 417 nm over time in methanol. 12 μM solution, λ_{ex} = 368 nm, λ_{em} = 417 nm. Semi-micro cuvette, slit widths 2 nm, integration time 1 s.

Finally, a titration of fructose into 12 μM **2.1** was carried out in pure methanol. As in the titration depicted in Figure 2.12A, each sample was prepared individually from stock solutions. The samples were stored at room temperature in the dark overnight, and emission spectra were obtained the next day (Figure 2.20).

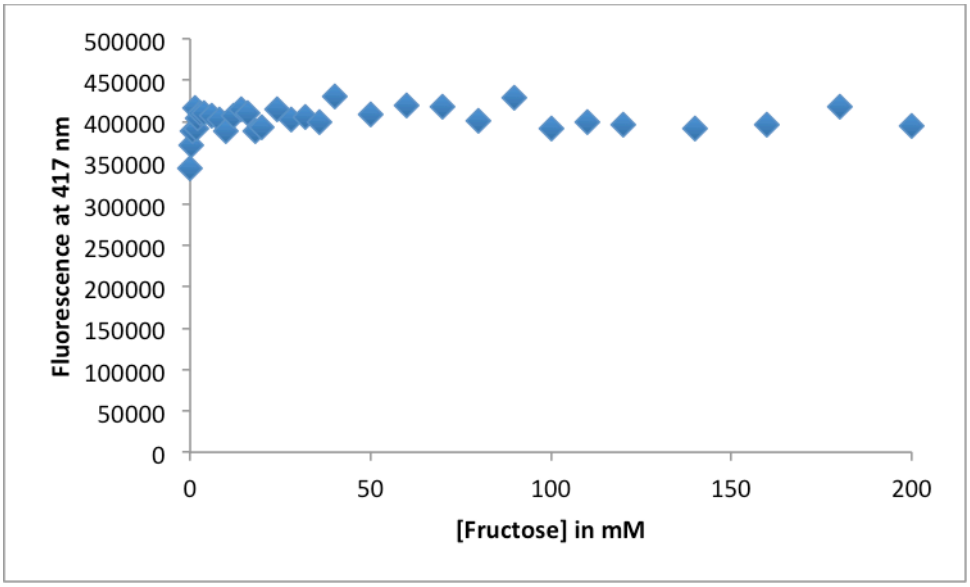

Figure 2.20: Fructose titration into **2.1** in methanol with individually prepared samples. 12 μM solution, 0-200 mM fructose, λ_{ex} = 368 nm, λ_{em} = 417 nm. Semi-micro cuvette, slit widths 2 nm, integration time 1 s.

The fructose titration shows a slight (and noisy) increase in fluorescence intensity for low concentrations of fructose, but quickly becomes independent of fructose concentration. This supports the claim that aggregation is what modulates fluorescence, rather than the binding of fructose. Since **2.1** is more soluble in pure methanol, it likely does not aggregate. Thus, fluorescence is already at its maximum intensity and cannot be further increased over time or with the addition of fructose. This suggests that the addition of fructose in Figure 2.18 likely influences fluorescence intensity indirectly,

either by shifting the monomer/aggregate equilibrium or by catalyzing disaggregation, rather than directly by simply binding.

At this juncture, our theory can be summarized as follows: **2.1** forms ground-state aggregates in 2:1 water and methanol with 50 mM NaCl, and this aggregation leads to the formation of an excimer upon irradiation. Disaggregation can be observed *via* the monomer fluorescence emission at λ_{em} = 417 nm and the excimer (excited dimer) fluorescence emission at λ_{em} = 520 nm. An increase in monomer fluorescence and/or a decrease in excimer fluorescence represents a decrease in ground-state aggregation of **2.1**. Time, heat, and the presence of fructose all shift the monomer/aggregate equilibrium and thus modulate fluorescence. The role of fructose in shifting this equilibrium could be preventing π-stacking in the aggregate, or it could be binding to monomers and releasing them from the aggregate.

2.2.2 Fluorescence Control Studies with Derivatives of Shinkai's Host

To further test our theory, the *meta* (**2.11**) and *para* (**2.12**) isomers of compound **2.1** (Figure 2.21) were synthesized and their fluorescence properties were investigated. Since these isomers cannot experience the same N-B interactions that **2.1** can due to the proximity of the boron atom and the aminomethyl substituents, we expected to see different binding behavior and predicted that the effects of binding versus disaggregation upon adding fructose could be isolated.

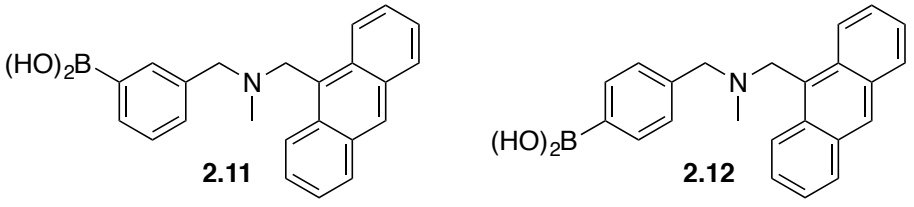

Figure 2.21: The *meta* (**2.11**) and *para* (**2.12**) isomers of compound **2.1**.

Titrations of fructose into 12 μM **2.11** and **2.12** were carried out in 2:1 water/methanol with 50 mM NaCl. Each sample was prepared individually from stock solutions. The samples were stored at room temperature in the dark overnight, and emission spectra were obtained the next day (Figures 2.22 and 2.23).

A) B)

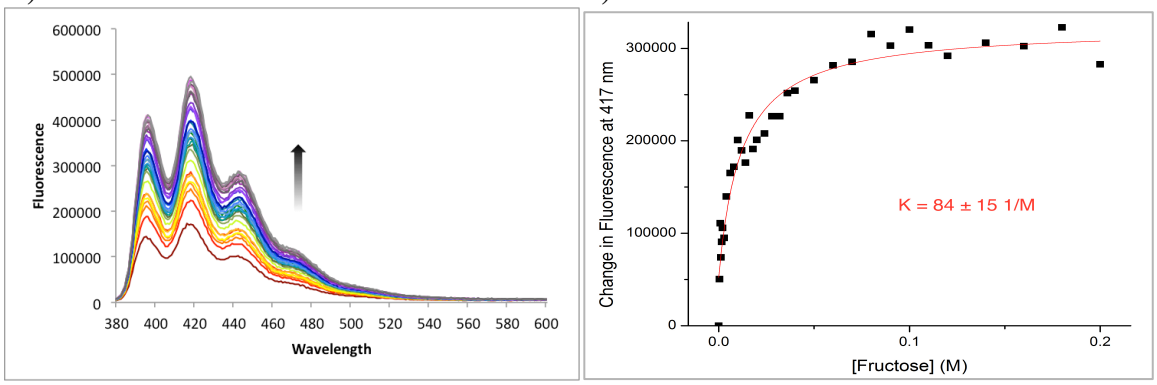

Figure 2.22: Fructose titration into **2.11** with individually prepared samples. A) Fluorescence spectra of a 12 μM solution in 2:1 water/methanol with 50 mM NaCl, 0-200 mM fructose, λ_{ex} = 368 nm. Semi-micro cuvette, slit widths 2 nm, integration time 1 s. B) Change in fluorescence at 417 nm plotted against concentration of fructose and fit to a one-to-one binding curve.

A) B)

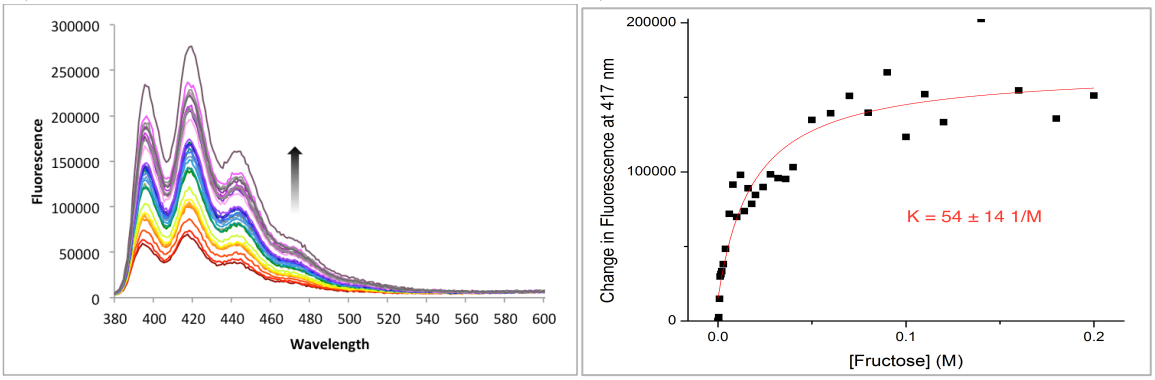

Figure 2.23: Fructose titration into **2.12** with individually prepared samples. A) Fluorescence spectra of a 12 μM solution in 2:1 water/methanol with 50 mM NaCl, 0-200 mM fructose, λ_{ex} = 368 nm. Semi-micro cuvette, slit widths 2 nm, integration time 1 s. B) Change in fluorescence at 417 nm plotted against concentration of fructose and fit to a one-to-one binding curve.

The titrations with both isomers generated plots that could be fit to one-to-one binding curves. In both cases, the binding is weaker than that of **2.1**, likely due to the lesser extent or lack of N-B interaction. However, the binding curves are still more similar to that of **2.1** than was expected, and the binding constants are only slightly lower (K_a = 84, 54 M^{-1} versus K_a = 125 M^{-1} for **2.1**).

Since compounds **2.1**, **2.11**, and **2.12** appeared to behave similarly, another way to distinguish binding versus disaggregation was desired. To remove the possibility of binding altogether, the boronic acid moiety would need to be absent. Thus, compound **2.13** (Figure 2.24) was synthesized and treated to the same titration conditions.

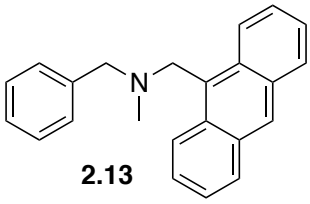

2.13

Figure 2.24: The derivative **2.13** lacks the boronic acid of compounds **2.1**, **2.11**, and **2.12** completely.

A titration of fructose into 12 μM **2.13** was carried out in 2:1 water/methanol with 50 mM NaCl. Each sample was prepared individually from stock solutions. The samples were stored at room temperature in the dark overnight, and emission spectra were obtained the next day (Figure 2.25).

A) B)

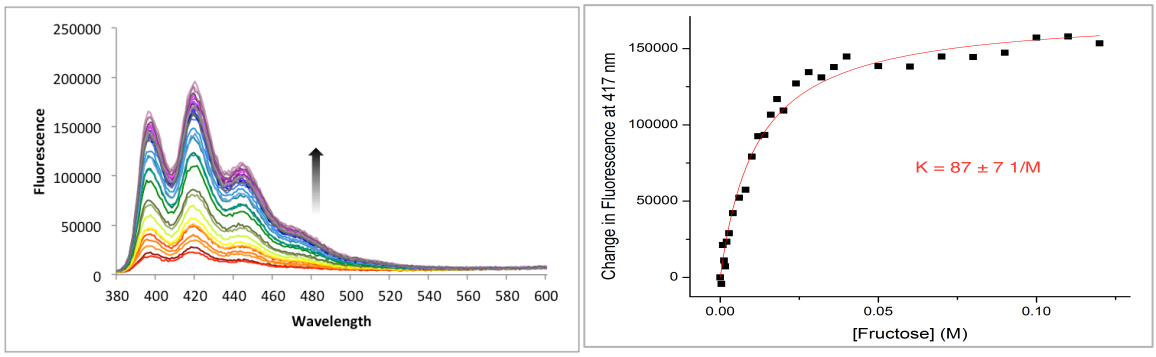

Figure 2.25: Fructose titration into **2.13** with individually prepared samples. A) Fluorescence spectra of a 12 μM solution in 2:1 water/methanol with 50 mM NaCl, 0-120 mM fructose, λ_{ex} = 368 nm. Semi-micro cuvette, slit widths 2 nm, integration time 1 s. B) Change in fluorescence at 417 nm plotted against concentration of fructose and fit to a one-to-one binding curve.

This result is extremely telling because although **2.13** does not contain a boronic acid for fructose to bind to, the titration still produces a curve that fits easily to a one-to-one binding curve. It is, of course, unreasonable to call this one-to-one binding because no binding is taking place; this curve was simply fit in order to compare the titration to

the others. However, the fact that it fits brings into question the other one-to-one binding curves – it is possible that all of them are demonstrating disaggregation in the presence of fructose and not binding.

In their original 1994 paper,[45] Shinkai and James compared the fluorescence of **2.1** in the presence of glucose and ethylene glycol to that in the presence of fructose. For this reason, we also carried out titrations of **2.1** and **2.13** with glucose (Figures 2.26 and 2.27) and ethylene glycol (Figures 2.28 and 2.29) for comparison.

A) B)

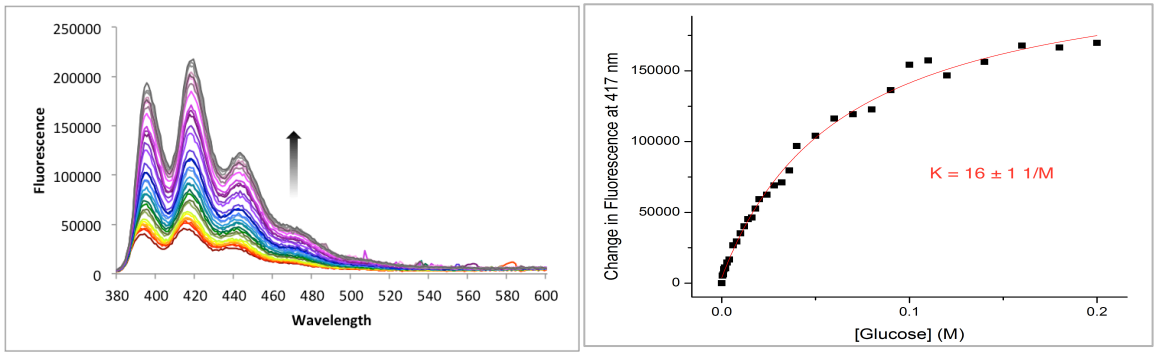

Figure 2.26: Glucose titration into **2.1** with individually prepared samples. A) Fluorescence spectra of a 12 μM solution in 2:1 water/methanol with 50 mM NaCl, 0-200 mM glucose, λ_{ex} = 368 nm. Semi-micro cuvette, slit widths 2 nm, integration time 1 s. B) Change in fluorescence at 417 nm plotted against concentration of glucose and fit to a one-to-one binding curve.

A) B)

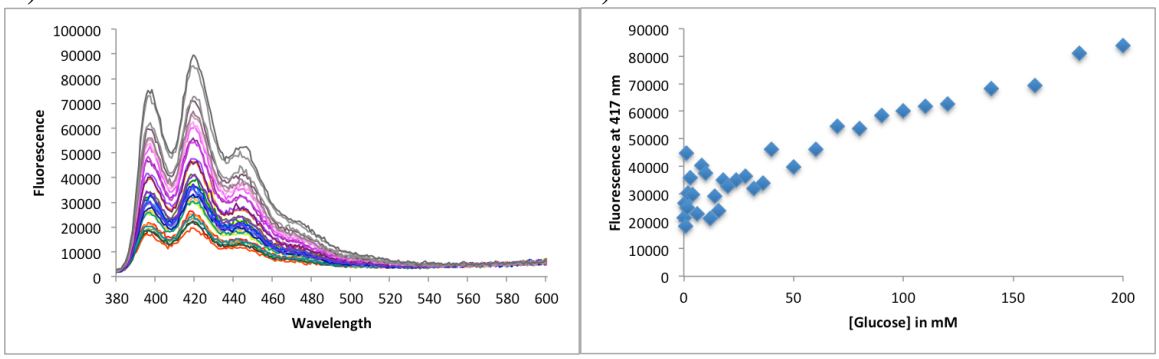

Figure 2.27: Glucose titration into **2.13** with individually prepared samples. A) Fluorescence spectra of a 12 μM solution in 2:1 water/methanol with 50 mM NaCl, 0-200 mM glucose, λ_{ex} = 368 nm. Semi-micro cuvette, slit widths 2 nm, integration time 1 s. B) Change in fluorescence at 417 nm plotted against concentration of glucose.

A) B)

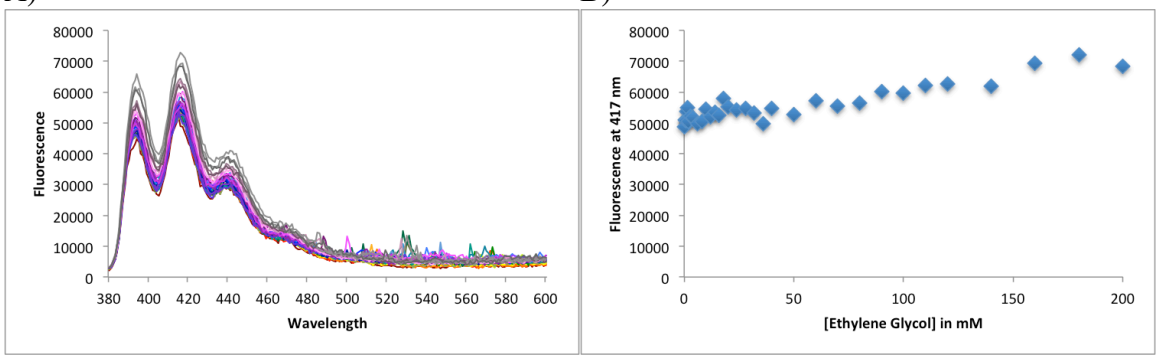

Figure 2.28: Ethylene glycol titration into **2.1** with individually prepared samples. A) Fluorescence spectra of a 12 μM solution in 2:1 water/methanol with 50 mM NaCl, 0-200 mM ethylene glycol, λ_{ex} = 368 nm. Semi-micro cuvette, slit widths 2 nm, integration time 1 s. B) Change in fluorescence at 417 nm plotted against concentration of ethylene glycol.

A) B)

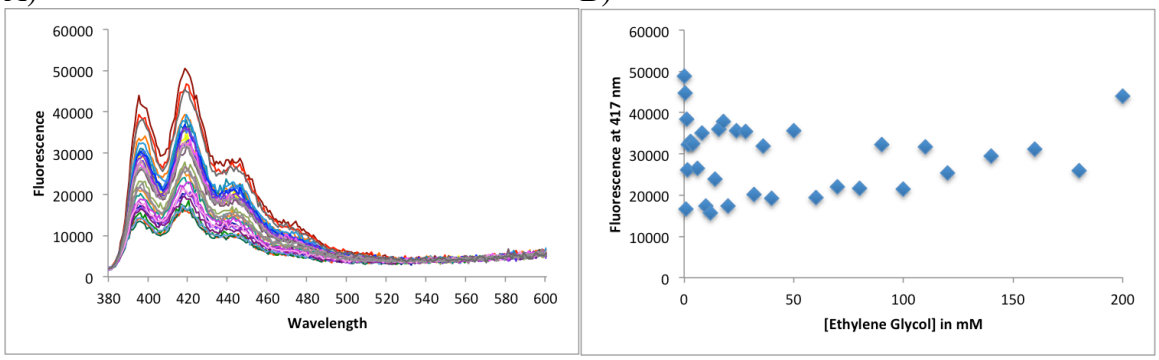

Figure 2.29: Ethylene glycol titration into **2.13** with individually prepared samples.A) Fluorescence spectra of a 12 μM solution in 2:1 water/methanol with 50 mM NaCl, 0-200 mM ethylene glycol, λ_{ex} = 368 nm. Semi-micro cuvette, slit widths 2 nm, integration time 1 s. B) Change in fluorescence at 417 nm plotted against concentration of ethylene glycol.

Compound **2.1** responded similarly to glucose as it did to fructose. However, compound **2.13** showed only a mild response, and neither compound responded to ethylene glycol. Shinkai and James observed very little fluorescence turn-on in the presence of ethylene glycol, so this result was not unexpected. Interestingly, it seems that

fructose may have some property that glucose does not have, as compound **2.13** demonstrated different responses to the two sugars.

Investigation of compound **2.13** continued with a study similar to that shown in Figure 2.18. A 12 μM solution of **2.13** in 2:1 water/methanol with 50 mM NaCl was scanned, sonicated for 90 minutes, and scanned again (red point). The solution was sonicated for another 90 minutes and scanned again (green point). Scans were repeated until fluorescence intensity remained constant, and then fructose was added to be 50 mM (purple point). Adding fructose resulted in little, if any, increase in fluorescence intensity, and repeat scans had no effect (Figure 2.30).

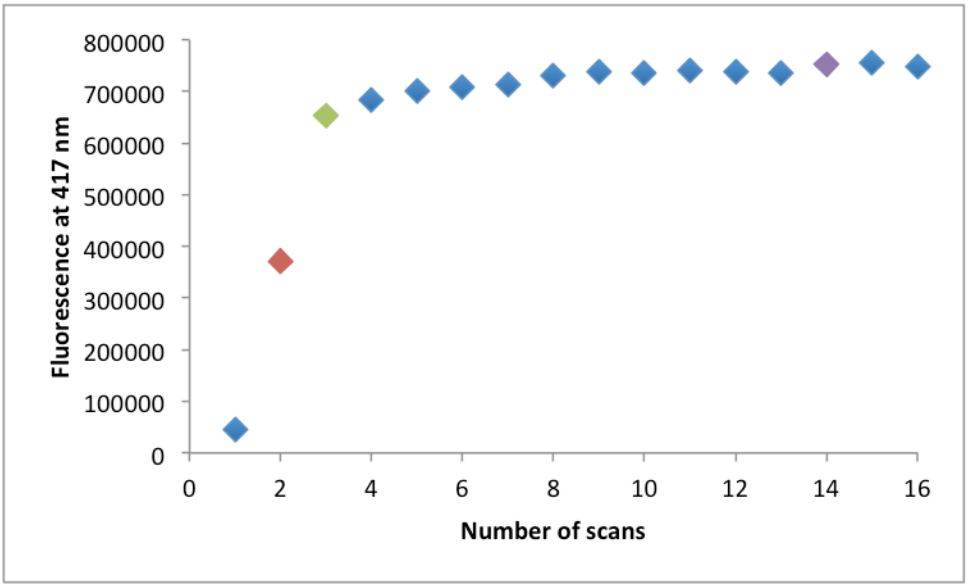

Figure 2.30: Fluorescence of **2.13** at 417 nm with sonication and repeated scans. 12 μM solution in 2:1 water/methanol with 50 mM NaCl. λ_{ex} = 368 nm, λ_{em} = 417 nm. 1 cm path length cuvette, slit widths 2 nm, integration time 1 s. Red: scan after 90 minutes of sonication. Green: scan after another 90 minutes of sonication. Purple: scan after adding fructose.

Compounds **2.1** and **2.13** were also subjected to sonication followed by addition of glucose (Figures 2.31 and 2.32).

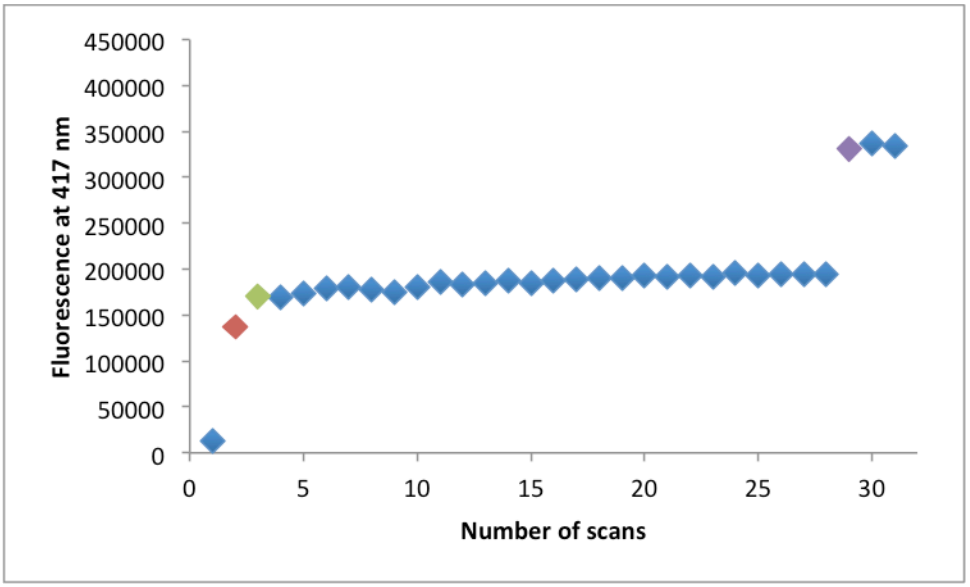

Figure 2.31: Fluorescence of **2.1** at 417 nm with sonication and repeated scans. 12 μM solution in 2:1 water/methanol with 50 mM NaCl. λ_{ex} = 368 nm, λ_{em} = 417 nm. 1 cm path length cuvette, slit widths 2 nm, integration time 1 s. Red: scan after 90 minutes of sonication. Green: scan after another 90 minutes of sonication. Purple: scan after adding glucose.

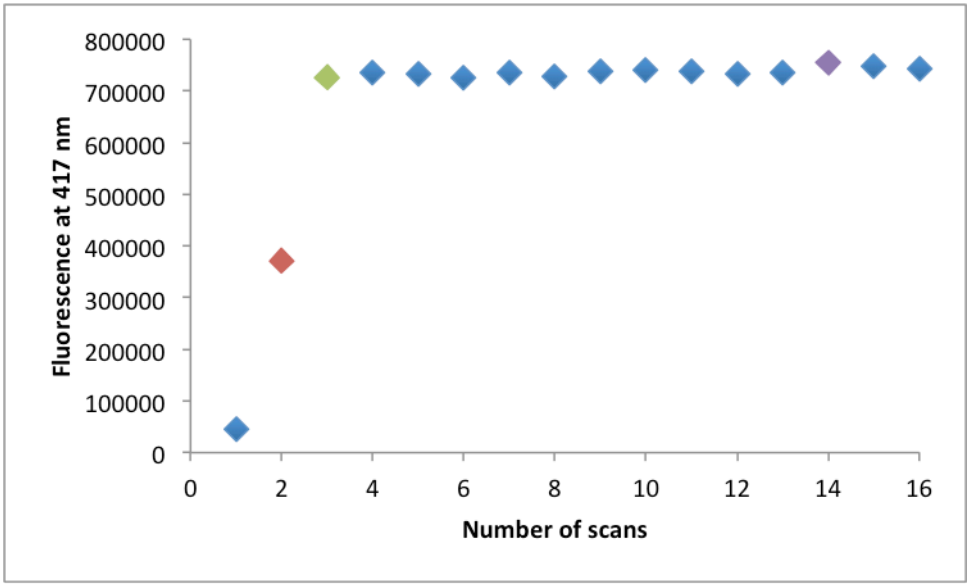

Figure 2.32: Fluorescence of **2.13** at 417 nm with sonication and repeated scans. 12 μM solution in 2:1 water/methanol with 50 mM NaCl. λ_{ex} = 368 nm, λ_{em} = 417 nm. 1 cm path length cuvette, slit widths 2 nm, integration time 1 s. Red: scan after 90 minutes of sonication. Green: scan after another 90 minutes of sonication. Purple: scan after adding glucose.

In the cases of both fructose and glucose, **2.13** responded much less to sugar than **2.1** did; the effect of adding either sugar to **2.13** is barely noticeable at all. It could be argued that the fluorescence intensity of **2.13** does not increase upon addition of sugar because it cannot bind to the sugar, but **2.13** is a positively charged species, whereas **2.1** is a zwitterion. For this reason, it would also make sense if **2.13** simply disaggregated more easily on its own due to coulombic repulsion, thus its fluorescence is already at maximum intensity and cannot be enhanced by addition of sugar. In contrast, the zwitterionic **2.1** could be still partially aggregated until adding sugar shifts the monomer/aggregate equilibrium or catalyzes disaggregation.

2.2.3 Binding of Shinkai's Host and its Derivatives to Sugars

Section 2.2.2 presents evidence that suggests that fluorescence modulation of **2.1** and its isomers in the presence of sugars may not be due to binding of sugars. However, we do not mean to suggest that binding does not occur; we claim that binding occurs but that it is not responsible for fluorescence modulation. Rather, we believe that sugars induce disaggregation and that this disaggregation is responsible for the fluorescence intensity increases. A similar argument is made by Davis and coworkers when they state that polar porphyrins "show changes in UV-visible absorption when treated with glucose, but that these are best explained by altered aggregation states, not by formation of a closely-bound complex".[67] In this section, we lay out evidence for **2.1** binding to sugars and measure the strength of that binding.

2.2.3.1 ^{11}B NMR

The first approach we took to proving binding of fructose with **2.1** was looking for a ^{11}B NMR chemical shift difference upon addition of fructose (Figure 2.33). Pure CD_3OD was used because **2.1** was not soluble enough in a mixture of D_2O and CD_3OD to get strong ^{11}B resonances.

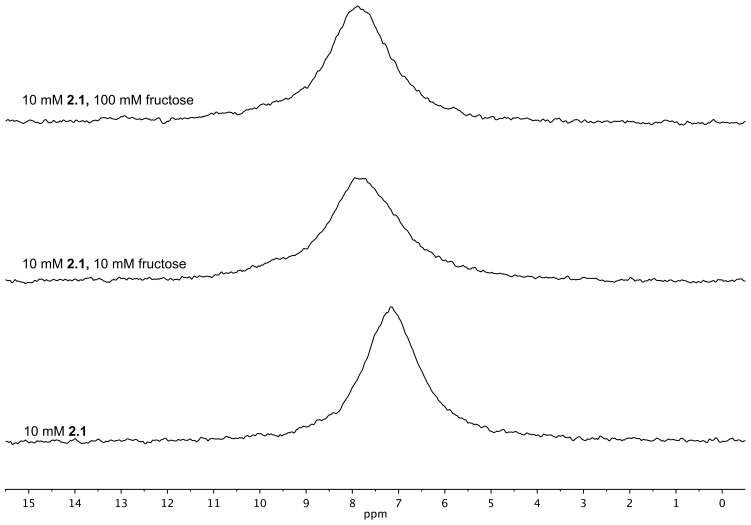

Figure 2.33: ^{11}B NMR of 10 mM **2.1** in CD_3OD with 0-100 mM fructose.

Although there is a small downfield shift after the addition of fructose, the difference is not large enough to be conclusive due to the breadth of the signal. The similarity between chemical shifts in the presence and absence of fructose was not entirely unexpected; in the absence of fructose, **2.1** is expected to contain a molecule of inserted methanol, and in the presence of fructose, **2.1** is likely bound to fructose in its tridentate form. This binding mode is not very different from solvent insertion and would likely display a similar chemical shift. This makes ^{11}B NMR unsuitable for determining binding. The ^{1}H NMR spectrum also showed no additional shifting of the boron signal with increasing concentrations of fructose.

2.2.3.2 Indicator Displacement Assay

In a second attempt to observe binding, an indicator displacement assay was performed. Once again, pure methanol had to be used rather than the Shinkai-James water/methanol mixture due to limited solubility in the mixed solvent. First, a one-to-one

binding curve had to be established for **2.1** and an indicator. Alizarin was originally chosen, but it bound too strongly to **2.1** and could not be displaced by fructose (results not shown). Then Pyrocatechol Violet was chosen because it is known to bind to boronic acids more weakly than Alizarin.[68] Figure 2.34 shows the absorbance curves (A) and one-to-one binding curve (B). Pyrocatechol Violet was kept at constant concentration so that its change in absorbance could be attributed to the increasing concentration of **2.1** throughout the titration. Fitting the data to a one-to-one binding curve produced a binding constant of 1.5 x 10^4 M^{-1}.

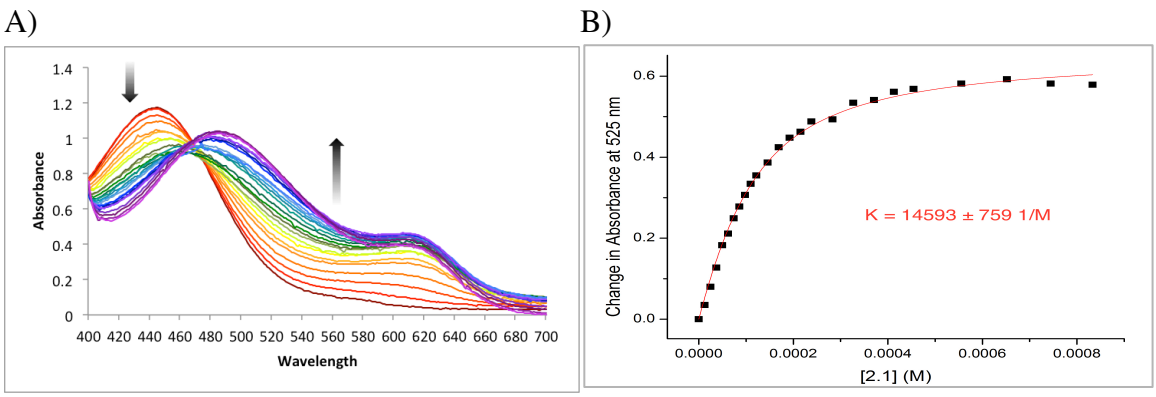

Figure 2.34: One-to-one binding of Pyrocatechol Violet and **2.1**. A) UV-Vis absorption spectra of a 80 μM solution of Pyrocatechol Violet in methanol, 0-833 μM **2.1**. 1 cm path length cuvette, 10-minute equilibration time between additions. B) Change in absorbance at 525 nm plotted against concentration of **2.1** and fit to a one-to-one binding curve.

Next, the indicator displacement experiment was performed. The concentration of Pyrocatechol Violet was kept at a constant concentration of 80 μM and the concentration of **2.1** was kept at 170 μM while fructose was titrated in. The binding of fructose to **2.1** was strong enough relative to the binding of Pyrocatechol Violet to **2.1** for fructose to displace the indicator (Figure 2.35).

A) B)

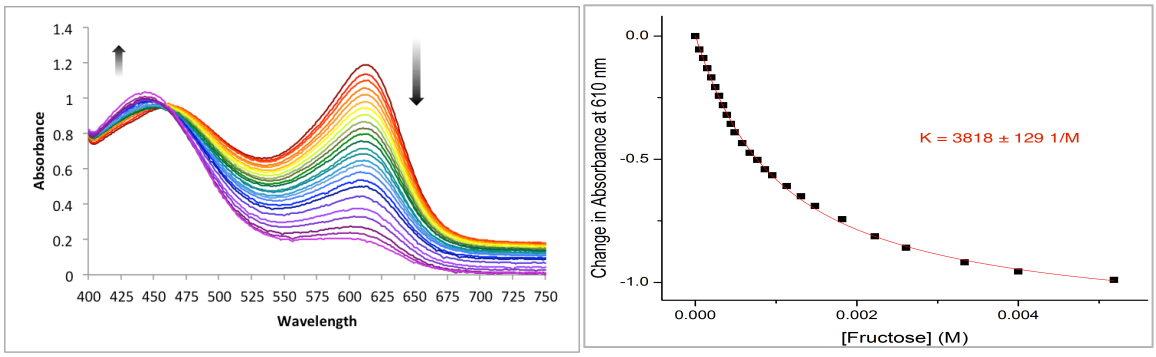

Figure 2.35: Indicator displacement assay, with fructose displacing Pyrocatechol Violet from **2.1**. A) UV-Vis absorption spectra of a solution of 80 μM Pyrocatechol Violet and 170 μM **2.1** in methanol, 0-5.2 mM fructose. 1 cm path length cuvette, 10-minute equilibration time between additions. B) Change in absorbance at 610 nm plotted against concentration of fructose and fit to an indicator displacement curve.

The curve in Figure 2.35B was fit to an indicator displacement curve using the constant concentrations and the binding constant of **2.1** binding to Pyrocatechol Violet. (See Appendix for more information on fitting data to one-to-one and indicator displacement binding curves.) The fit gave a binding constant of 4.3 x 10^3 M^{-1} for the binding of **2.1** to fructose. This value is closer to reported values than the 125 M^{-1} we found using fluorescence spectroscopy. Since the UV-Vis absorbance spectra show no evidence of aggregation (none would be expected in pure methanol), we believe this value to be much more credible than that found using fluorescence.

2.2.3.3 Isothermal Titration Calorimetry

The third method used to calculate binding constants was isothermal titration calorimetry (ITC). **2.1** was not soluble enough in 2:1 water/methanol with 50 mM NaCl, so the titration had to be carried out in pure methanol. 10 mM fructose was titrated into 1 mM **2.1** (Figure 2.36).

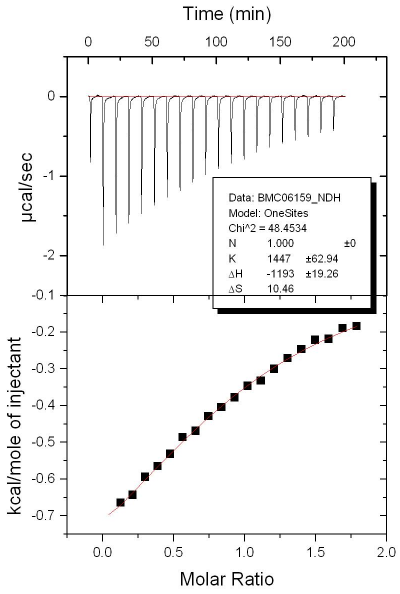

Figure 2.36: ITC of 10 mM fructose titrated into 1 mM **2.1** in methanol. 25 ºC, reference power 5 µcal/sec, stir speed 300. Initial delay 60 s, initial injection 6 µL, all following injections 12 µL with 600 s spacing.

The ΔH curve is not as steep as it should be, and it does not display an inflection point as expected. However, running a titration with higher concentrations produced an exothermic signal followed by an endothermic signal for each addition, so a binding constant could not be calculated. Although Figure 2.36 does not represent an ideal titration curve, it can still be fit to calculate a binding constant of 1.4 x 10^3 M^{-1}. This value is the same order of magnitude produced by the indicator displacement assay, so it was deemed a credible result. Since ITC measures both ΔH and K_a, ΔG and ΔS can be calculated from the equation $\Delta G = -RT\ln K_a = \Delta H - T\Delta S$. In Figure 2.36, ΔH = -1.2 kcal/mol and ΔS = 10.5 cal/(mol•K). This is a remarkable result, because 1.4 kcal/mol in ΔG corresponds to one order of magnitude difference in K.[59] This means that ΔH only contributes about one order of magnitude to the strength of the binding constant, and that

the rest is entropy-driven. This is explained by the fact that one molecule of fructose binds in a tridentate manner and releases three molecules of solvent upon binding (Scheme 2.9). Since enthalpy is dictated by bond strengths, the small ΔH indicates that the trimethoxy boronate ester and the boronate ester formed with fructose are very similar in the strength of their O-B bonds.

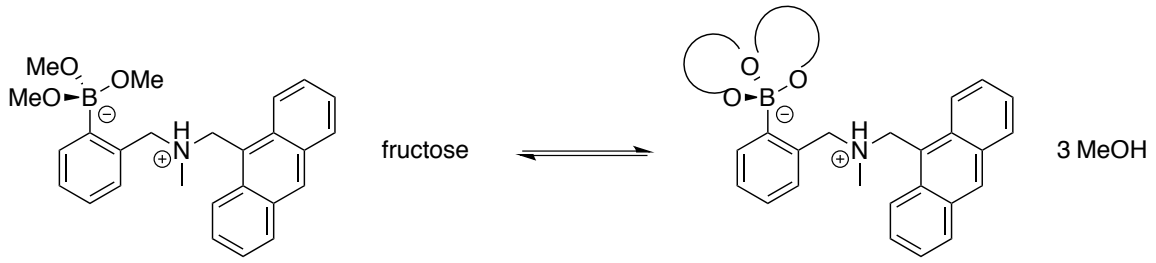

Scheme 2.9: **2.1** binds fructose and releases three equivalents of solvent, leading to an entropy-driven binding event.

In order to calculate a more accurate binding constant, the titration was repeated and a control in which fructose was titrated into pure methanol was carried out with the same fructose solution. Figure 2.37A shows the titration of fructose into **2.1** in black and the titration of fructose into methanol in red. This control allows the heat of dilution of fructose to be subtracted from the binding curve, and thus shows the binding curve in isolation. This binding curve is plotted alone in Figure 2.37B. The curve was then fit to give a binding constant of 2.9 x 10^3 M^{-1}. This value is even closer to agreement with the value calculated in the indicator displacement assay. Remarkably, the thermodynamic parameters reveal that the binding event is also even more entropy-driven than Figure 2.36 revealed. After subtracting the heat of dilution of fructose from the binding curve, ΔH = -0.2 kcal/mol and ΔS = 15.8 cal/(mol•K).

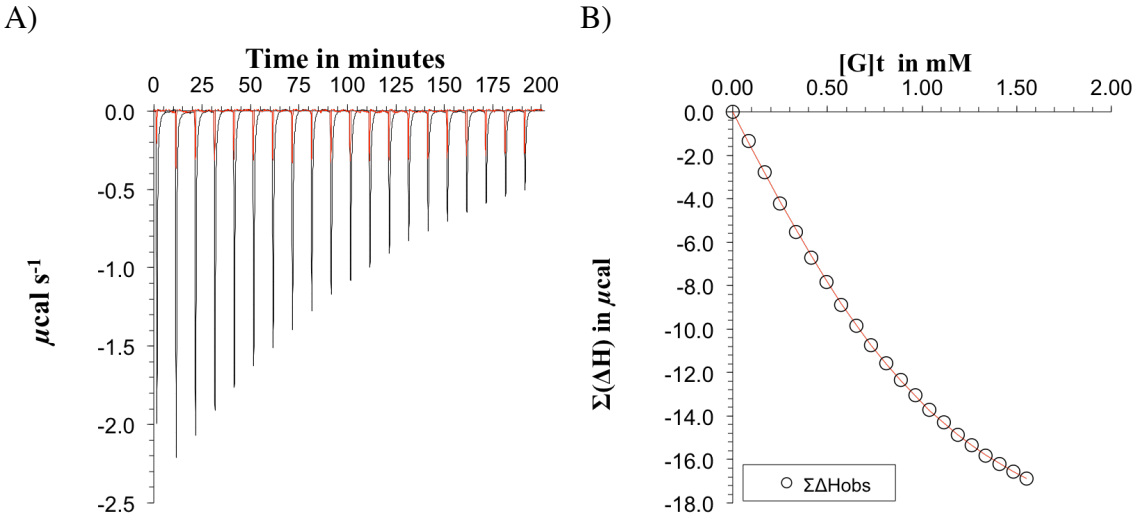

Figure 2.37: Corrected ITC of fructose titrated into **2.1**. A) ITC of 10 mM fructose titrated into 1 mM **2.1** in methanol (black), and ITC of 10 mM fructose titrated into methanol (red). 25 ºC, reference power 5 µcal/sec, stir speed 300. Initial delay 60 s, all injections 12 µL with 600 s spacing. B) Plot of the difference of the two titrations in (A).

As another control, an ITC in which fructose was titrated into **2.13** was performed. The raw ITC (Figure 2.38) was plotted on the same scale as Figure 2.36 in order to show the small magnitude of the response.

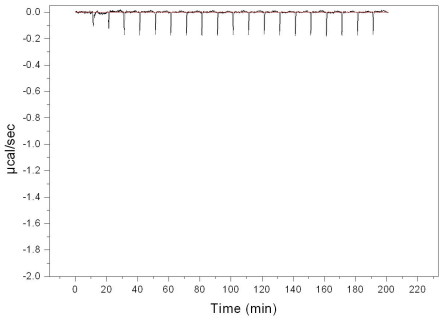

Figure 2.38: ITC of 10 mM fructose titrated into 1 mM **2.7** in methanol. 25 ºC, reference power 5 µcal/sec, stir speed 300. Initial delay 60 s, initial injection 6 µL, all following injections 12 µL with 600 s spacing.

The titration looks essentially like a blank titration, with each addition showing only the energy of dilution of fructose. This result is important because it proves that unlike fluorescence, ITC does not show any response associated with disaggregation of **2.1**. However, aggregation is not expected to take place in pure methanol, so it makes sense that there is no disaggregation. In any case, it can be trusted that the results in Figures 2.36 and 2.37 represent only binding. Since the indicator displacement data generated a binding constant very close to that calculated from the ITC data, the comparison of Figures 2.36 and 2.37 with Figure 2.38 lends further support to the theory that disaggregation, and not binding, is responsible for the fluorescence turn-on of **2.1**.

Compounds **2.11** and **2.12** were also titrated with fructose (Figures 2.39 and 2.40, respectively).

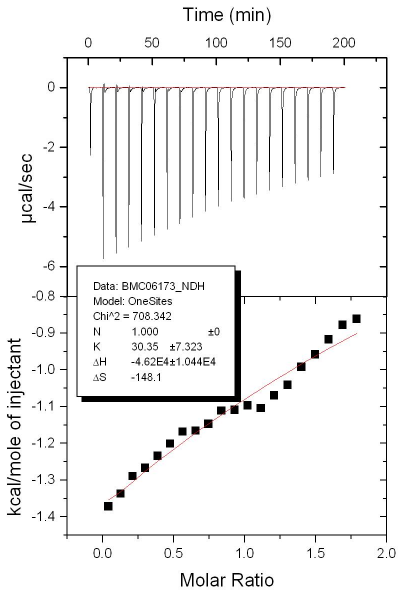

Figure 2.39: ITC of 10 mM fructose titrated into 1 mM **2.11** in methanol. 25 ºC, reference power 5 µcal/sec, stir speed 300. Initial delay 60 s, initial injection 6 µL, all following injections 12 µL with 600 s spacing.

The raw ITC in Figure 2.39 seems to show weak binding, but the ΔH curve does not fit well and the binding constant cannot be trusted.

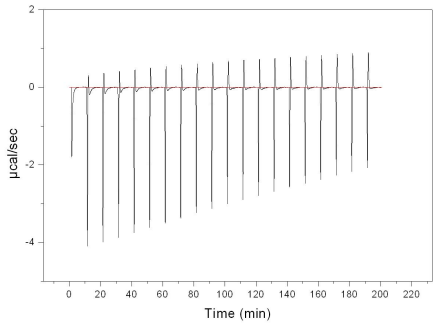

Figure 2.40: ITC of 10 mM fructose titrated into 1 mM **2.12** in methanol. 25 ºC, reference power 5 µcal/sec, stir speed 300. Initial delay 60 s, initial injection 6 µL, all following injections 12 µL with 600 s spacing.

Figure 2.40 shows a raw ITC with exothermic signals followed by endothermic signals after each addition. For this reason, a binding constant could not be calculated.

Finally, glucose and ethylene glycol were titrated into **2.1** (Figures 2.41 and 2.42, respectively). Glucose gave little to no response, and ethylene glycol gave no response, likely because it is too similar to methanol. As in the fluorescence titrations, glucose produces a smaller response than fructose. In the ITC, the difference is necessarily due to binding, whereas in the fluorescence titration it may be due to binding or a conformational difference, or perhaps both.

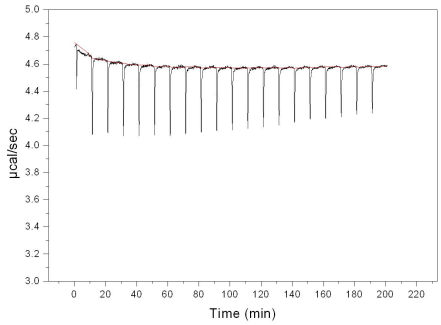

Figure 2.41: ITC of 10 mM glucose titrated into 1 mM **2.1** in methanol. 25 ºC, reference power 5 µcal/sec, stir speed 300. Initial delay 60 s, initial injection 6 µL, all following injections 12 µL with 600 s spacing.

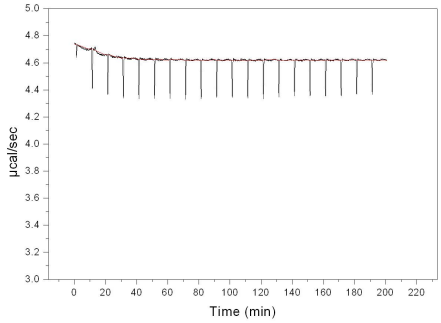

Figure 2.42: ITC of 10 mM ethylene glycol titrated into 1 mM **2.1** in methanol. 25 ºC, reference power 5 µcal/sec, stir speed 300. Initial delay 60 s, initial injection 6 µL, all following injections 12 µL with 600 s spacing.

2.2.4 Fluorescence Lifetime Studies

Figure 2.9 presents convincing evidence that an excimer is present after irradiation, but another way to prove this is with fluorescence lifetimes. If only one fluorescent species is present, the decay data will fit one exponential, $y = A + B1*e^{(-1/T1)}$, with lifetime T1. If two fluorescent species are present, the decay data will fit the sum of two exponentials, $y = A + B1*e^{(-1/T1)} + B2*e^{(-1/T2)}$, with lifetimes T1 and T2, and so on. Thus, if only the monomer is fluorescent, the decay should fit one exponential, and if an excimer is also present, the decay data will require at least two exponentials to fit.

The fluorescence lifetime studies were carried out with an excitation repetition rate of 1 MHz. The detector began counting photons 40 nanoseconds after excitation and continued counting for 200 nanoseconds. The same solutions were used for the experiments depicted in Figures 2.43-2.45. Figure 2.43 shows the data collected with λ_{ex} = 371 nm (LED diode) and λ_{em} = 417 nm (wavelength of the monomer fluorescence). Figure 2.43A shows the data collected from a solution of 12 μM **2.1**, and B shows that from a solution of 12 μM **2.1** and 50 mM fructose. C and D are collected from the same solutions as A and B, respectively, the following day.

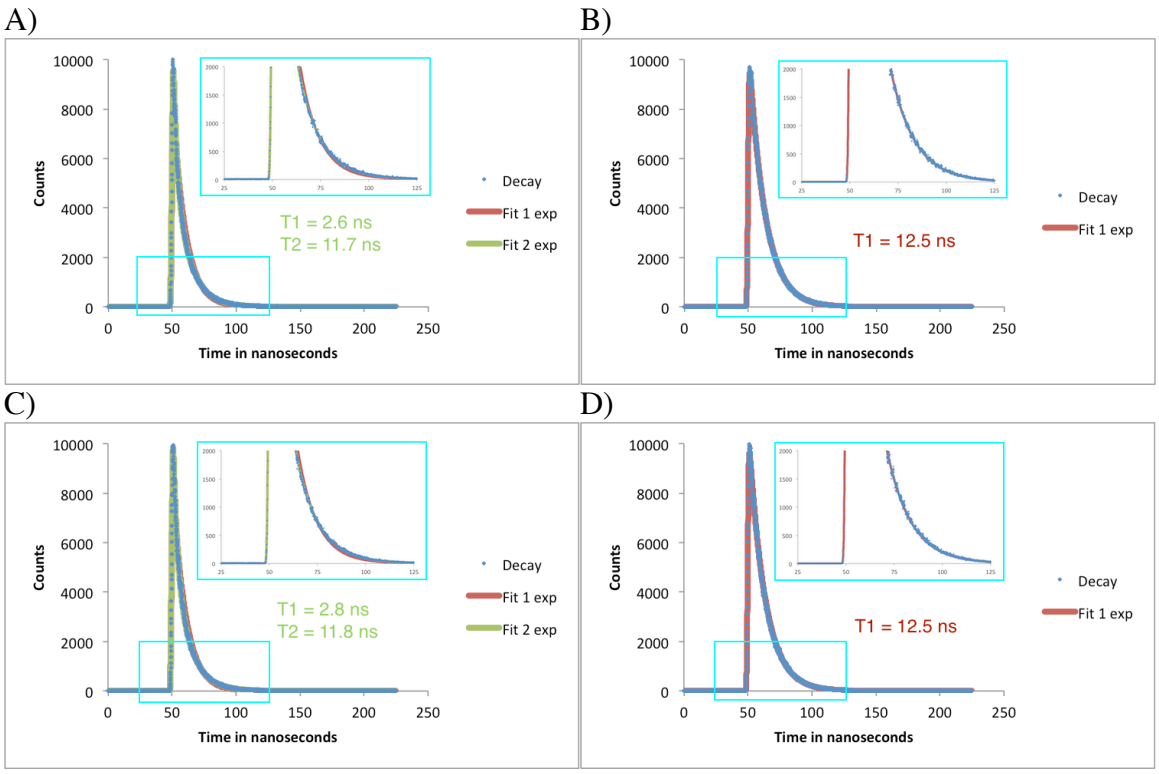

Figure 2.43: Fluorescence lifetime data, λ_{ex} = 371 nm (LED diode), λ_{em} = 417 nm. Repetition rate 1 MHz, measurement range 200 ns. Slit width 2.5 nm. A) 12 μM **2.1**. B) 12 μM **2.1**, 50 mM fructose. C) Same experiment as A, the following day. D) Same experiment as B, the following day.

Figure 2.43A shows that one exponential does not adequately fit the decay data, which indicates that there are two fluorescent species – monomer and excimer. In contrast, the data in 2.43B fits well when only one exponential is used. This result was expected, since fructose has been observed to diminish the fluorescence of the excimer. Since the shorter lifetime (2.6 ns) was not observed in 2.43B, this lifetime must correspond to the excimer, whereas the longer lifetime (11.7-12.5 ns) must belong to the monomer. Repeating the same experiments the following day (Figure 2.43C and D) produced no change. It could be that twenty-four hours was not enough time for the excimer lifetime to be eliminated, which is consistent with previous experiments.

Figure 2.44 shows the data collected with λ_{ex} = 371 nm (LED diode) and λ_{em} = 520 nm (wavelength of the excimer fluorescence). Figure 2.44A shows the data collected from a solution of 12 μM **2.1**, and B shows that from a solution of 12 μM **2.1** and 50 mM fructose. C and D are collected from the same solutions as A and B, respectively, the following day.

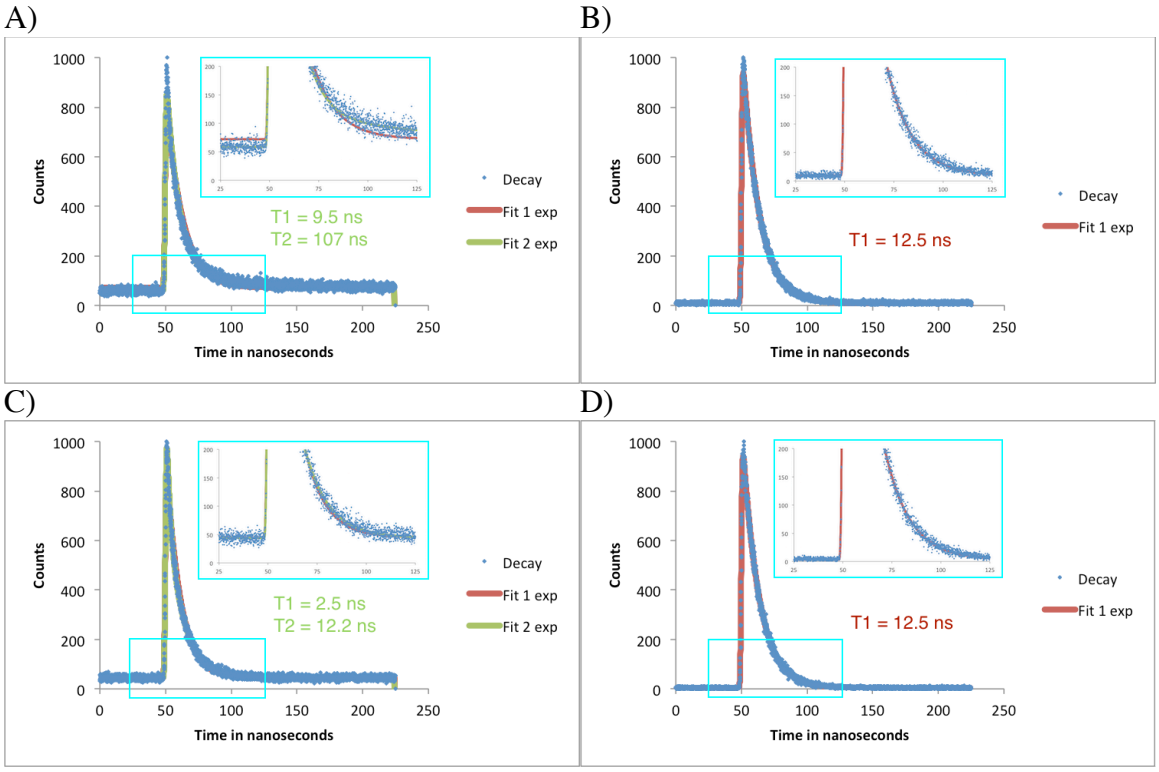

Figure 2.44: Fluorescence lifetime data, λ_{ex} = 371 nm (LED diode), λ_{em} = 520 nm. Repetition rate 1 MHz, measurement range 200 ns. Slit width 2.5 nm. A) 12 μM **2.1**. B) 12 μM **2.1**, 50 mM fructose. C) Same experiment as A, the following day. D) Same experiment as B, the following day.

In Figure 2.44A, one exponential does not adequately fit the decay data. Two exponentials fit well, but one of the calculated lifetimes (107 ns) is exceptionally long, as compared to those calculated in Figure 2.43. In the presence of fructose, however, the familiar lifetime of 12.5 ns is calculated. This is despite the fact that the wavelength of excimer fluorescence is being monitored. Figure 2.44C shows the long lifetime to be absent, and values closer to the already calculated lifetimes return.

Figure 2.45 shows the data collected with λ_{ex} = 402 nm (LED diode) and λ_{em} = 520 nm (wavelength of the excimer fluorescence). Figure 2.45A shows the data collected from a solution of 12 μM **2.1**, and B shows that from a solution of 12 μM **2.1** and 50 mM

fructose. C and D are collected from the same solutions as A and B, respectively, the following day. The diode used for excitation is not an ideal excitation wavelength; 402 nm excites both the monomer and the aggregate that forms the excimer. However, this was the closest wavelength diode to 408 nm, which excites only aggregate.

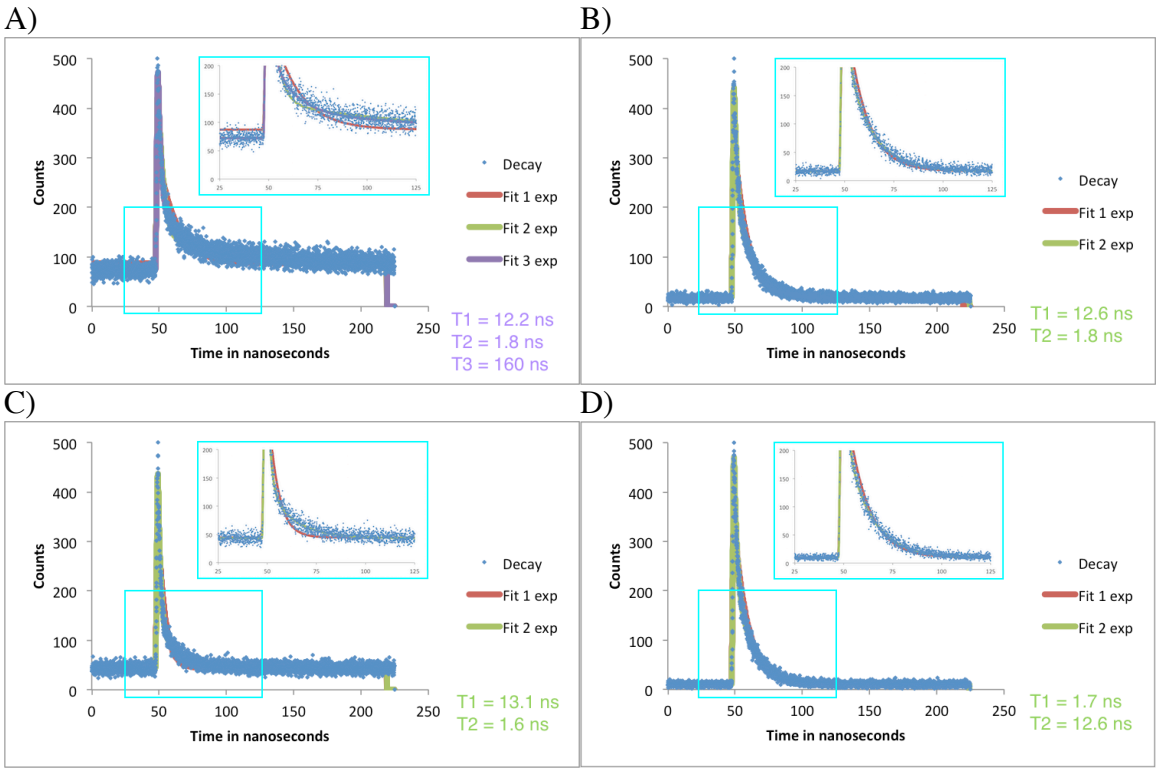

Figure 2.45: Fluorescence lifetime data, λ_{ex} = 402 nm (LED diode), λ_{em} = 520 nm. Repetition rate 1 MHz, measurement range 200 ns. Slit width 2.5 nm. A) 12 μM **2.1**. B) 12 μM **2.1**, 50 mM fructose. C) Same experiment as A, the following day. D) Same experiment as B, the following day.

In Figure 2.45A, even two exponentials do not fit the decay data, so three were required. Once again, one of the calculated lifetimes (160 ns) is exceptionally long. In the presence of fructose, however, only the two familiar lifetimes are calculated (assuming 1.8 ns corresponds to the same lifetime as 2.5-2.8 ns). This is despite the fact that the

wavelength of excimer fluorescence is being monitored. Figure 2.45C shows the long lifetime to be absent, and the observed monomer and excimer lifetimes are calculated.

2.2.5 Miscellaneous Controls and Other Studies

2.2.5.1 Fluorescence pH Titrations

The fluorescence pH titrations of **2.1** (12 μM) in the presence and absence of fructose (50 mM) carried out by Shinkai/James and Wang were reproduced (Figure 2.46). The titration is in agreement with previous reports, indicating pK_as of approximately 6.5-7 (hydroxylation of the boron atom) and 11 (deprotonation of the ammonium group).

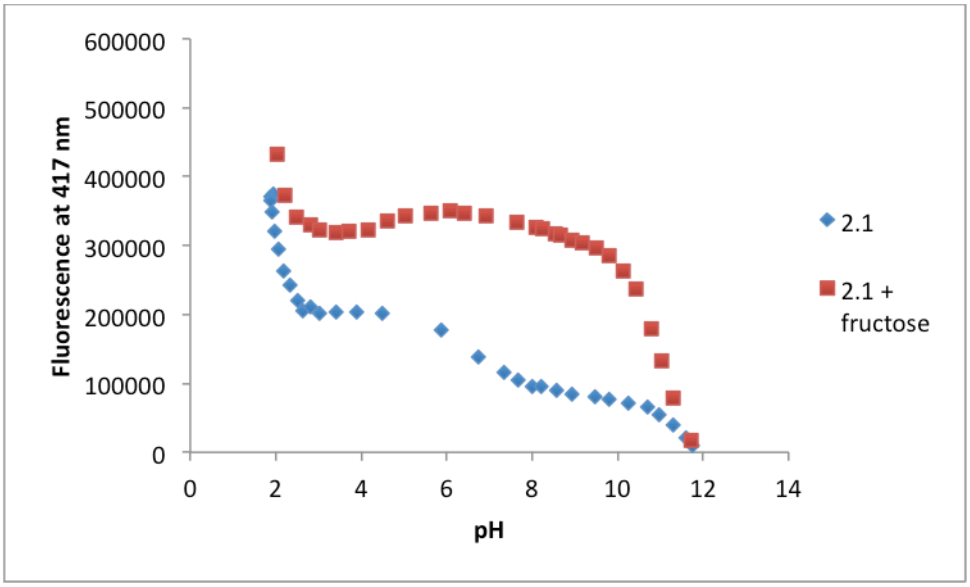

Figure 2.46: Fluorescence pH titration of 12 μM **2.1** in the presence and absence of 50 mM fructose.

A similar titration was performed with **2.13** (12 μM) in the presence and absence of fructose (50 mM) (Figure 2.47). The pH profiles show one pK_a, corresponding to deprotonation of the ammonium group, at approximately 7.5. The pK_a does not differ in

the presence versus absence of fructose, but the intensity of fluorescence response is much greater with fructose in solution.

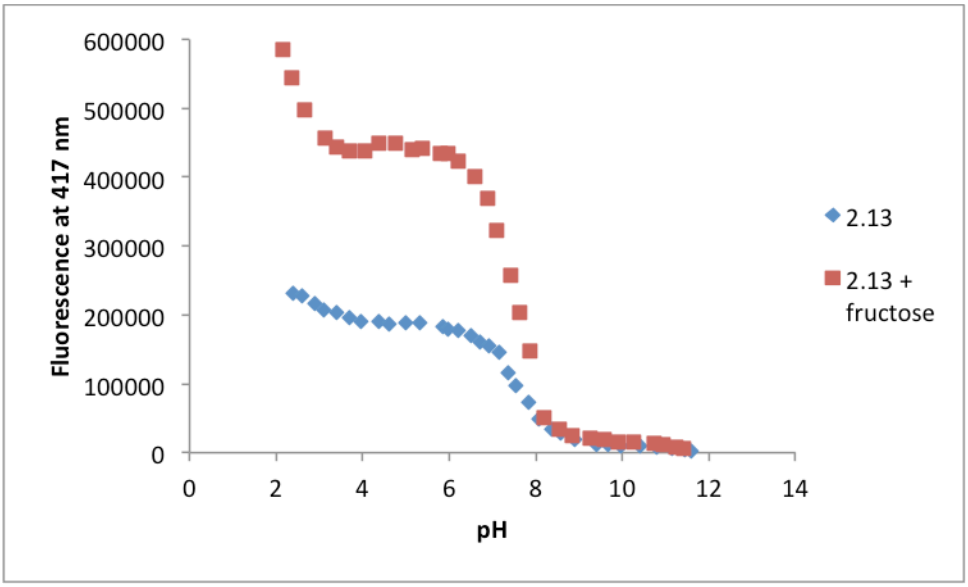

Figure 2.47: Fluorescence pH titration of 12 μM **2.13** in the presence and absence of 50 mM fructose.

2.2.5.2 Fluorescence of Fructose

A joint report from the Fossey and Anslyn groups shows that fructose has weak fluorescence on its own, and that this fluorescence can be confounded with the fluorescence of weak fluorophores.[69] To verify that fructose was not interfering with the fluorescence of **2.1**, 200 mM fructose was subjected to excitation scans with λ_{ex} = 368 nm (Figure 2.48). For comparison, a solution of 12 μM **2.1** and a solution of 12 μM **2.1** and 200 mM fructose are plotted on the same axes. The very weak fluorescence from fructose is likely due largely to scatter. It is too low in intensity to compete with the fluorescence of **2.1** alone, and certainly cannot be responsible for the large fluorescence turn-on of **2.1** in the presence of fructose. Thus, it can be concluded that the fluorescence of fructose is negligible for the studies of **2.1**.

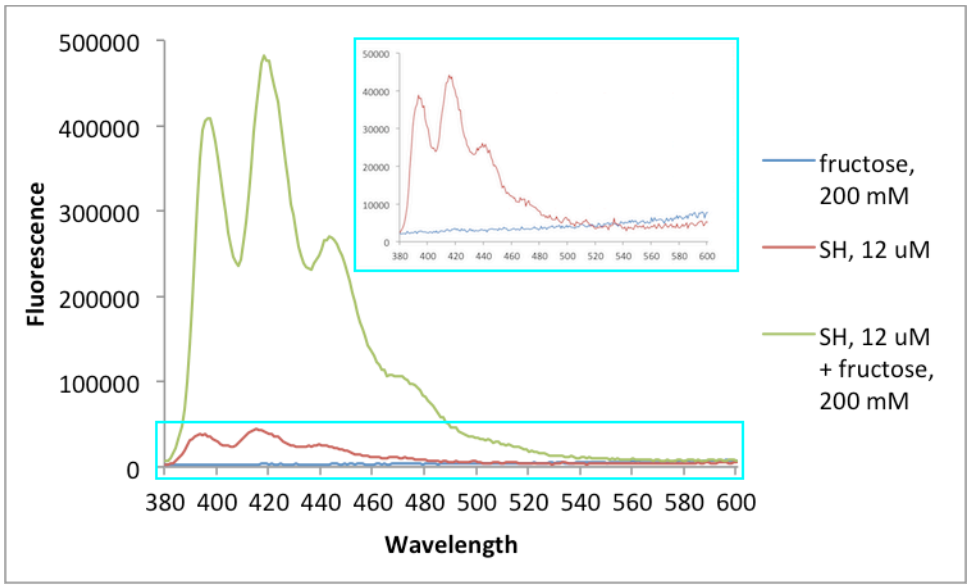

Figure 2.48: Fluorescence spectra of fructose, **2.1**, and **2.1** in the presence of fructose are compared. 12 μM **2.1** and 200 mM fructose, λ_{ex} = 368 nm.

2.2.5.3 Fluorescence of 9-Methylanthracene

A colleague suggested to us that if **2.1** formed a radical cation on the nitrogen atom, 9-methylanthracene could be produced, and that this would cause a small shift in the fluorescence spectrum of a solution of **2.1** over time. This seemed unlikely, since the nitrogen atom is expected to be protonated at neutral pH and would not have a free electron to donate. However, the hypothesis was tested so that we could be certain. The fluorescence spectrum (with λ_{ex} = 368 nm) of 9-methylanthracene is compared to that of **2.1** in Figure 2.49A. Compared to **2.1**, 9-methylanthracene's maximum emission wavelength is blue-shifted by about 3 nm. In contrast, the maximum emission wavelength does not change over time for a solution of **2.1** (Figure 2.49B) and is red-shifted by about 2 nm in the presence of fructose (Figure 2.49C). Thus, we conclude that 9-methylanthracene is not being generated during titrations or on exposure to light.

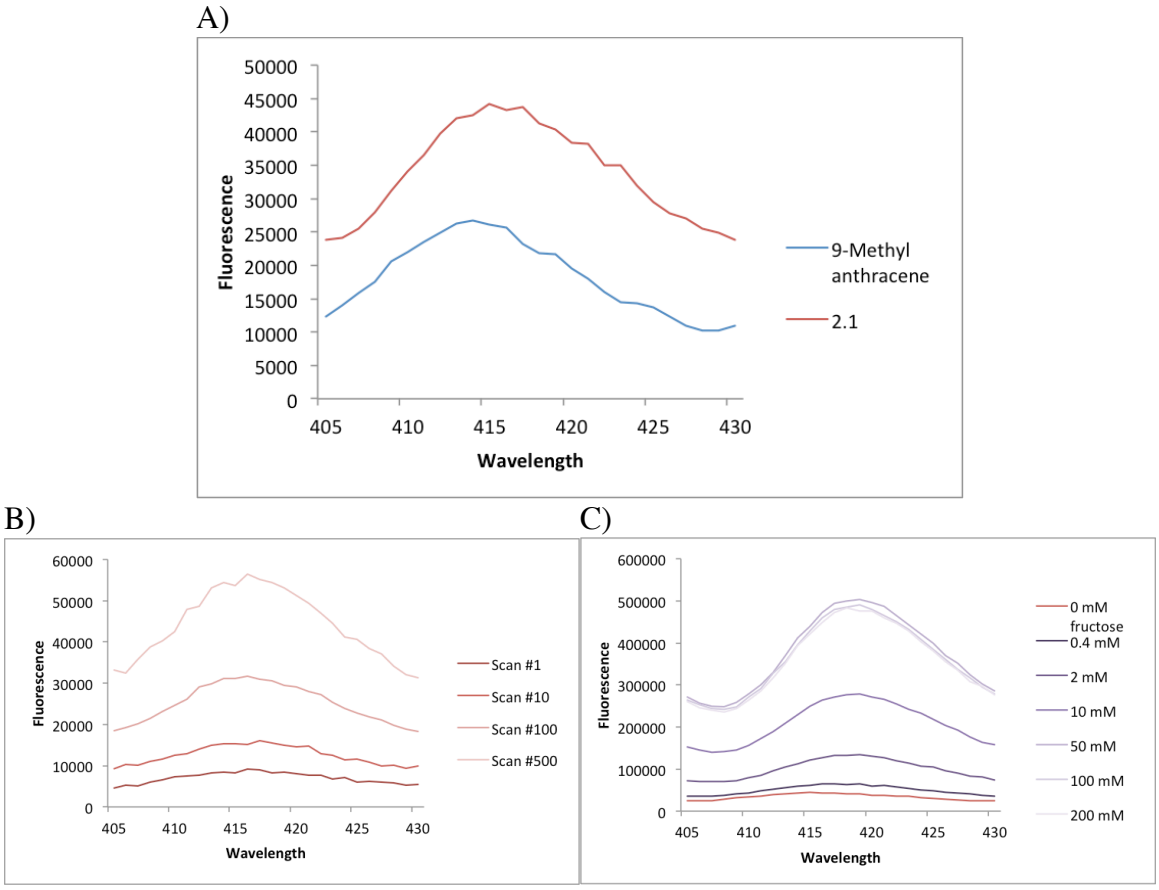

Figure 2.49: Comparison of the fluorescence spectra of 9-methylanthracene and **2.1**. A) Fluorescence spectra of 9-methylanthracene and **2.1**, both 12 μM in 2:1 water/methanol with 50 mM NaCl. λ_{ex} = 368 nm. B) Fluorescence spectra of **2.1** after selected numbers of scans, 12 μM in 2:1 water/methanol with 50 mM NaCl. λ_{ex} = 368 nm. C) Fluorescence spectra of **2.1** with increasing concentrations of fructose. 12 μM **2.1** and 0-200 mM fructose in 2:1 water/methanol with 50 mM NaCl, λ_{ex} = 368 nm.

2.2.5.4 Facilitation of Aggregation by Boroxines

It was hypothesized that **2.1** could form boroxines such as **2.14** and **2.15** (Figure 2.50) in solution. If these structures were formed, two (or more) anthracene moieties could be brought into close proximity to one another, either by two "arms" of the same

boroxine, or by stacking multiple boroxine units. This ground-state interaction could lead to excimer formation after irradiation.

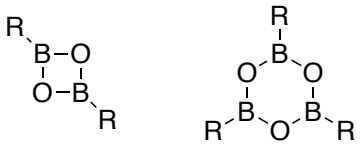

2.14 **2.15**

Figure 2.50: Two possible boroxines that can be formed from boronic acids.

An attempt to synthesize a boroxine of **2.1** was made, but the desired product was not observed. Instead, commercial phenylboronic acid was studied by ^{1}H NMR for comparison. In $CDCl_3$, two sets of aromatic peaks were observed, indicating that two species, a boronic acid and a boroxine, were both present. In CD_3OD, there was only one set of aromatic peaks. This suggests that the boroxine underwent solvolysis upon dissolution in methanol, and that the one set of aromatic peaks belongs to the boronic acid. It was concluded that a boroxine of **2.1** could not survive in water and methanol and thus boroxines could not be the cause of ground-state aggregation of **2.1**.

2.2.5.5 Dynamic Light Scattering

Following the example of Davis and coworkers,[67] an attempt was made to prove that a change in aggregation state of **2.1** took place over time using dynamic light scattering (DLS). Ideally, data would have shown larger particle sizes disappearing as smaller particle sizes dominated over time. However, this technique produced sporadic particle size measurements, and the analysis software consistently reported that the size data was of low quality. We interpret this to mean that in a homogeneous solution of **2.1** in 2:1 water/methanol with 50 mM NaCl, the particle size is too small to be accurately

measured by the instrument. This points to small aggregates, or potentially even simply dimers, rather than very large structures.

2.2.5.6 Diffusion-Ordered NMR Spectroscopy

Diffusion-ordered (DOSY) NMR was explored as another potential method for proving a change in aggregation over time and/or concentration. The goal was to show that at higher concentrations of **2.1**, the diffusion coefficient would decrease, meaning that the compound experienced slower diffusion as a result of larger particle size. Additionally, the same sample could have been analyzed over time in order to demonstrate that diffusion increased due to smaller particle size over time. Unfortunately, **2.1** could not be made concentrated enough to be detected by ^{1}H NMR in the 2:1 D_2O/CD_3OD mixture. Instead, analysis was carried out in pure CD_3OD, but samples with differing concentrations produced the same diffusion coefficient, likely because no aggregation was taking place at all in pure methanol.

2.2.5.7 Phosphorescence Lifetime Studies

In addition to fluorescence emission, anthracene derivatives, including **2.1**, also phosphoresce. Phosphorescence lifetimes are much longer than fluorescence lifetimes, and thus are distinguishable. A solution of 50 μM **2.1** in 2:1 water/methanol with 50 mM NaCl was subjected to 100 repeated excitations with a 300 Hz frequency. Lifetime data was collected for λ_{ex} = 368 nm and λ_{em} = 417 nm (Figure 2.51), λ_{ex} = 368 nm and λ_{em} = 520 nm (Figure 2.52), and λ_{ex} = 408 nm and λ_{em} = 520 nm (Figure 2.53). All three plots fit one exponential well, with no need for a second or third exponential, indicating that only the monomer emits phosphorescence. The three measurements also produce approximately the same phosphorescence lifetime of 5.9-6.9 μs.

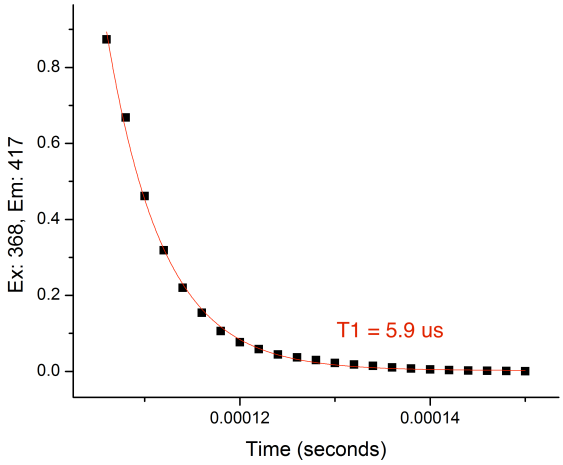

Figure 2.51: Phosphorescence lifetime data, λ_{ex} = 368 nm, λ_{em} = 417 nm. Repetition rate 300 Hz, 100 shots, measurement range 900 μs. Slit width 2 nm. 50 μM **2.1** in 2:1 water/methanol with 50 mM NaCl.

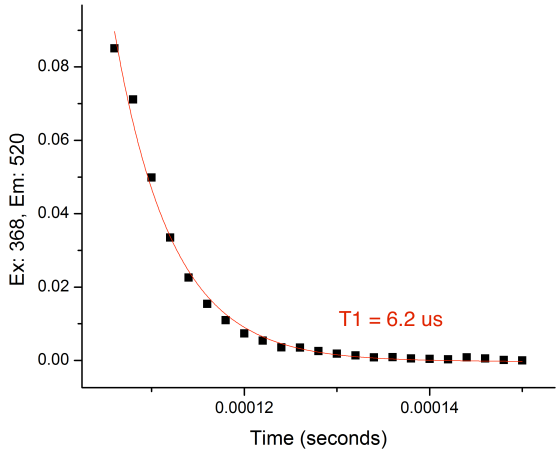

Figure 2.52: Phosphorescence lifetime data, λ_{ex} = 368 nm, λ_{em} = 520 nm. Repetition rate 300 Hz, 100 shots, measurement range 900 μs. Slit width 2 nm. 50 μM **2.1** in 2:1 water/methanol with 50 mM NaCl.

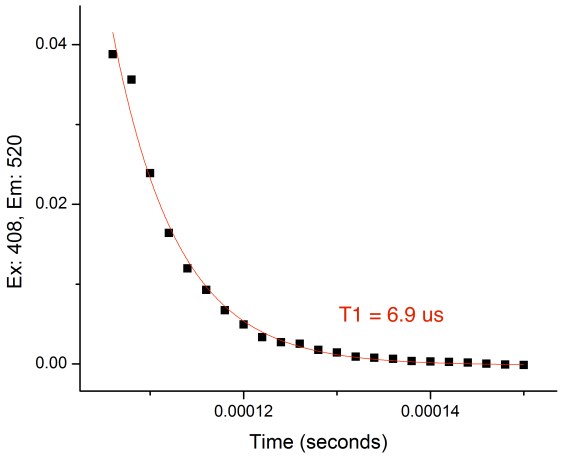

Figure 2.53: Phosphorescence lifetime data, λ_{ex} = 408 nm, λ_{em} = 520 nm. Repetition rate 300 Hz, 100 shots, measurement range 900 μs. Slit width 2 nm. 50 μM **2.1** in 2:1 water/methanol with 50 mM NaCl.

2.3 CONCLUSIONS

Shinkai's Host, **2.1**, forms ground-state aggregates in 2:1 water and methanol with 50 mM NaCl, and this aggregation leads to the formation of an excimer upon irradiation. Disaggregation can be observed *via* the monomer fluorescence emission at λ_{em} = 417 nm and the excimer (excited dimer) fluorescence emission at λ_{em} = 520 nm. An increase in monomer fluorescence and/or a decrease in excimer fluorescence represents a decrease in ground-state aggregation of **2.1**. Time, heat, and the presence of fructose all promote or catalyze the break-up of aggregates and thus modulate fluorescence. Excimer is not observed in pure methanol, and the fluorescence of the monomer does not increase over time or with the addition of fructose, indicating that **2.1** does not aggregate in methanol. This result also suggests that binding fructose does not modulate fluorescence. Fructose certainly binds, as shown by indicator displacement assays and isothermal titration calorimetry, but we assert that fluorescence modulation is unaffected by this phenomenon. This claim is supported by the fact that compound **2.13** also appears to

demonstrate binding when the fluorescence spectra in the presence of fructose are examined, despite the fact that it contains no boronic acid with which to bind fructose.

2.4 EXPERIMENTAL

2.4.1 Fluorescence Fructose Titrations

Solutions of 200 mM fructose and 24 μM host (**2.1**, **2.11**, **2.12**, or **2.13**) stock solutions in 2:1 water/methanol with 50 mM NaCl were prepared. The stock solutions, along with additional solvent, were used to prepare the samples in vials. First, various volumes of fructose stock solution were transferred to each vial, up to 500 μL. Then each sample was diluted to a total volume of 500 μL with solvent. This order of addition was chosen in order to prevent the host from being exposed to a high concentration of fructose before diluting. Finally, 500 μL of host stock solution was added to each vial, giving 12 μM host and 0-200 mM fructose. The vials were sealed and stored in the dark overnight.

Fluorescence spectra were recorded on a Photon Technology International Fluorescence Master fluorimeter. The source was a 75 W Xenon short arc lamp. Each sample was individually transferred to a clean semi-micro quartz cuvette and subjected to an emission scan with λ_{ex} = 368 nm. The excitation and emission slit widths were set to 2 nm, and the integration time was set to 1 s. To construct the binding curve, the fluorescence intensity at λ_{em} = 417 nm was plotted against the concentration of fructose. OriginPro 8.5.1 was used to plot and fit the curve using one-to-one binding (See Appendix).

2.4.2 NMR Parameters

^{11}B NMR spectra were recorded in quartz NMR tubes on a VARIAN DirectDrive 600 MHz spectrometer with a sweep width of 56818 Hz, a 90 degree flip angle, and 2

second acquisition time using BF_3•OEt_2 as an external reference. Each spectrum was processed with 10 Hz line broadening, and a back linear prediction of the first 32 points was used to remove the ^{11}B background of the probe.

2.4.3 Indicator Displacement Assay

All UV-Vis absorbance data was collected on an Agilent Technologies Cary 100 UV-Vis spectrophotometer in a 1 cm path length cuvette. A matched cuvette containing methanol was used as a baseline.

First, a one-to-one binding curve and equilibrium constant were established for Pyrocatechol Violet (PV) and **2.1**. A solution of 5 mM **2.1** and 80 μM PV in methanol was titrated into a solution of 80 μM PV in methanol. After each addition, an equilibration time of ten minutes was allowed before recording the absorbance spectrum. To construct the binding curve, the absorbance at 525 nm was plotted against the concentration of **2.1**. This wavelength was chosen because it demonstrated the largest dynamic range. OriginPro 8.5.1 was used to plot and fit the curve using one-to-one binding (See Appendix).

Next, an indicator displacement experiment was performed in order to calculate an equilibrium constant for the binding between **2.1** and fructose. A solution of 20 mM fructose, 80 μM PV, and 170 μM **2.1** in methanol was titrated into a solution of 80 μM PV and 170 μM **2.1** in methanol. After each addition, an equilibration time of ten minutes was allowed before recording the absorbance spectrum. To construct the binding curve, the absorbance at 610 nm was plotted against the concentration of fructose. This wavelength was chosen because it shows the greatest dynamic range and is a local maximum. OriginPro 8.5.1 was used to plot and fit the curve using equations for indicator displacement (See Appendix).

2.4.4 Isothermal Titration Calorimetry

Binding constants were measured on a MicroCal VP-ITC MicroCalorimeter. 10 mM diol (fructose, glucose, or ethylene glycol) in methanol was titrated into 1 mM host (**2.1**, **2.11**, **2.12**, or **2.13**) in methanol, with pure methanol in the reference cell. The temperature was set to 25 °C, the reference power was set to 5 μcal/sec, and the stir speed was set to 300. A 60 second initial delay was followed by a 6 μL injection, and then all following injections were 12 μL with a 600 second spacing between injections. MicroCal Origin was used to calculate binding constants.

2.4.5 Fluorescence and Phosphorescence Lifetimes

Fluorescence lifetimes were measured on a HORIBA Fluorolog 3 Fluorimeter. The 12 μM solution of **2.1** in 2:1 water/methanol with 50 mM NaCl was excited with LED diodes and emission was monitored at a single wavelength controlled by a monochromator. The sample was excited with a repetition rate of 1 MHz, and the emission was recorded from 40 ns after excitation to 240 ns after excitation. The slit width was 2.5 nm and the voltage was 1450 V. Lifetimes were calculated using Decay Analysis Software v6.8 from HORIBA.

Phosphorescence lifetimes were measured on a Photon Technology International Fluorescence Master fluorimeter. The source was a PTI Xenoflash lamp. A 50 μM solution of **2.1** in 2:1 water/methanol with 50 mM NaCl was excited with a Xenoflash lamp for 100 shots with a frequency of 300 Hz. The emission was recorded from 100 μs after excitation to 1000 μs after excitation. The slit widths were 2 nm. Lifetimes were calculated using OriginPro 8.5.1.

2.4.6 Fluorescence pH Titrations

Fluorescence pH titrations were recorded on a Photon Technology International Fluorescence Master in a 1 cm path length cuvette. The source was a 75 W Xenon short arc lamp.

Two aliquots of the same 12 μM solution of host (**2.1** or **2.13**) were adjusted to different pHs using an Orion 8103BN ROSS Combination Semi-micro pH electrode. One solution was adjusted with 2M aqueous HCl to pH ~2.5 and the other was adjusted with 2M NaOH to pH ~12. The solution at acidic pH was initially subjected to an emission scan with λ_{ex} = 368 nm. Then the basic solution was titrated into the acidic solution. After each addition, the pH was recorded and the same emission scan was carried out. The fluorescence intensity at 417 nm was plotted against pH.

The same procedure was followed for solutions of 12 μM host and 50 mM diol (fructose, glucose, or ethylene glycol).

2.4.7 Dynamic Light Scattering

DLS measurements were carried out on a Zetasizer Nano ZS in a 1 cm path length quartz cuvette. The sample was a saturated solution of **2.1** in 2:1 water/methanol with 50 mM NaCl.

2.4.8 Synthesis and Characterization of Hosts

*Synthesis of (2-(((anthracen-9-ylmethyl)(methyl)amino)methyl)phenyl)boronic acid, Shinkai's Host (**2.1**)*

2-Formylphenylboronic acid (4.5 mmol, 0.68 g), 9-(methylaminomethyl)anthracene (2.25 mmol, 0.50 g), and K_2CO_3 (0.225 mmol, 0.03 g) were combined in dry methanol (50 mL) and stirred at room temperature under nitrogen for 3.5 hours. Then $NaBH_4$ (4.5 mmol, 0.17 g) was added and the reaction was stirred at

room temperature for a further 1.5 hours. Solvent was removed *in vacuo* and DCM (25 mL) and water (25 mL) were added. The aqueous layer was extracted three times with DCM (3 x 25 mL) and the organic layers were combined, dried over $MgSO_4$, and concentrated *in vacuo*. The yellow residue was purified using a CombiFlash Companion/TS from Teledyne Isco automatic column machine and a RediSep Rf Gold C18Aq column with 5-90% acetonitrile in water. Acetonitrile was removed *in vacuo* and the resulting aqueous suspension was extracted three times with chloroform (2 x 25 mL). The organic layers were combined, dried over $MgSO_4$, and concentrated *in vacuo* to yield a pale yellow solid, 0.7181 g, 90% yield.

^{1}H NMR (600 MHz, CD_3OD, ppm): δ 2.48 (s, 3H), 4.46 (s, 2H), 5.14 (s, 2H), 7.28 (td, J = 7.37, 1.46 Hz, 1H), 7.38 (qd, J = 7.37, 1.23 Hz, 2H), 7.50-7.56 (m, 4H), 7.71 (d, J = 7.22 Hz, 1H), 8.12 (d, J = 7.72 Hz, 2H), 8.22 (d, J = 8.60 Hz, 2H), 8.68 (s, 1H).

^{11}B NMR (600 MHz, CD_3OD, ppm): δ 7.25.

^{13}C NMR (600 MHz, CD_3OD, ppm): δ 50.1, 54.8, 64.3, 124.9, 126.4, 128.3, 129.0, 130.5, 131.7, 132.9, 133.0, 135.4.

HRMS: ESI-MS: *m/z* calculated for $C_{23}H_{22}BNO_2$ $[M+H]^+$ 356.18200, found 356.18190.

*Synthesis of (3-(((anthracen-9-ylmethyl)(methyl)amino)methyl)phenyl)boronic acid (**2.11**)*

3-Formylphenylboronic acid (1.5 mmol, 0.23 g), 9-(methylaminomethyl)anthracene (0.75 mmol, 0.17 g), and K_2CO_3 (0.075 mmol, 0.01 g) were combined in dry methanol (20 mL) with 3Å molecular sieves and heated at reflux under nitrogen for 17 hours. Then the reaction was allowed to cool to room temperature and $NaBH_4$ (1.5 mmol, 0.06 g) was added and the reaction was stirred at room temperature for 4 hours. Solvent was removed *in vacuo* and DCM (10 mL) and water (10 mL) were added. The aqueous layer was extracted three times with DCM (3 x 10 mL)

and the organic layers were combined, dried over $MgSO_4$, and concentrated *in vacuo*. The yellow residue was purified using a CombiFlash Companion/TS from Teledyne Isco automatic column machine and a RediSep Rf Gold C18Aq column with 5-90% acetonitrile in water. Acetonitrile was removed *in vacuo* and the resulting aqueous suspension was extracted three times with chloroform (3 x 10 mL). The organic layers were combined, dried over $MgSO_4$, and concentrated *in vacuo* to yield a pale yellow solid, 0.0397 g, 15% yield.

^{1}H NMR (600 MHz, CD_3OD, ppm): δ 2.72 (s, 3H), 4.90 (s, 2H), 4.95 (s, 2H), 7.54 (ddd, J = 8.31, 6.52, 0.92 Hz, 4H), 7.64 (ddd, J = 8.93, 6.54, 1.34 Hz, 4H), 8.11 (dt, J = 8.48, 0.65 Hz, 2H), 8.39 (dd, J = 8.96, 0.86 Hz, 2H), 8.59 (s, 1H).

^{11}B NMR (600 MHz, CD_3OD, ppm): δ 28.4.

^{13}C NMR (600 MHz, CD_3OD, ppm): δ 34.1, 41.3, 62.5, 123.3, 124.5, 124.9, 126.5, 128.6, 129.0, 130.5, 131.2, 131.5, 131.6.

HRMS: ESI-MS: *m/z* calculated for $C_{23}H_{22}BNO_2$ $[M+H]^+$ 356.18200, found 356.18230.

*Synthesis of (4-(((anthracen-9-ylmethyl)(methyl)amino)methyl)phenyl)boronic acid (**2.12**)*

4-Formylphenylboronic acid (1.5 mmol, 0.23 g), 9-(methylaminomethyl)anthracene (0.75 mmol, 0.17 g), and K_2CO_3 (0.075 mmol, 0.01 g) were combined in dry methanol (20 mL) with 3Å molecular sieves and heated at reflux under nitrogen for 15 hours. Then the reaction was allowed to cool to room temperature and $NaBH_4$ (1.5 mmol, 0.06 g) was added and the reaction was stirred at room temperature for 5 hours. Solvent was removed *in vacuo* and DCM (10 mL) and water (10 mL) were added. The aqueous layer was extracted three times with DCM and the organic layers were combined, dried over $MgSO_4$, and concentrated *in vacuo*. The yellow residue was purified using a CombiFlash Companion/TS from Teledyne Isco automatic column

machine and a RediSep Rf Gold C18Aq column with 5-90% acetonitrile in water. Acetonitrile was removed *in vacuo* and the resulting aqueous suspension was extracted three times with chloroform (3 x 10 mL). The organic layers were combined, dried over $MgSO_4$, and concentrated *in vacuo* to yield a pale yellow solid, 0.0284 g, 11% yield.

^{1}H NMR (600 MHz, CD_3OD, ppm): δ 2.73 (s, 3H), 4.90 (s, 2H), 4.96 (s, 2H), 7.54 (ddd, J = 8.43, 6.52, 0.87 Hz, 4H), 7.64 (ddd, J = 8.94, 6.53, 1.35 Hz, 4H), 8.11 (d, J = 8.65 Hz, 2H), 8.39 (d, J = 8.65 Hz, 2H), 8.59 (s, 1H).

^{11}B NMR (600 MHz, CD_3OD, ppm): δ 27.9.

^{13}C NMR (600 MHz, CD_3OD, ppm): δ 41.3, 45.5, 62.2, 110.0, 123.3, 124.5, 124.9, 126.5, 128.3, 128.6, 129.0, 130.5, 131.2, 131.5, 131.6.

HRMS: ESI-MS: *m/z* calculated for $C_{23}H_{22}BNO_2$ $[M+H]^+$ 356.18200, found 356.18240.

*Synthesis of 1-(anthracen-9-yl)-N-benzyl-N-methylmethanamine (**2.13**)*

Benzyl bromide (0.75 mmol, 89 μL), 9-(methylaminomethyl)anthracene (0.75 mmol, 0.17 g), and K_2CO_3 (3.75 mmol, 0.52 g) were combined in dry THF (50 mL) and heated at reflux under nitrogen for 20 hours. Solvent was removed *in vacuo* and DCM (10 mL) and water (10 mL) were added. The aqueous layer was extracted three times with DCM (3 x 10 mL) and the organic layers were combined, dried over $MgSO_4$, and concentrated *in vacuo* to yield a pale yellow solid, 0.233 g, quantitative yield.

^{1}H NMR (600 MHz, $CDCl_3$, ppm): δ 2.36 (s, 3H), 3.81 (s, 2H), 4.59 (s, 2H), 7.37-7.41 (m, 1H), 7.43-7.50 (m, 4H), 7.57-7.67 (m, 4H), 8.10 (d, J = 9.08 Hz, 2H), 8.50 (s, 1H), 8.61 (d, J = 8.96 Hz, 2H).

^{13}C NMR (600 MHz, $CDCl_3$, ppm): δ 42.2, 53.6, 62.6, 124.9, 125.2, 125.7, 127.2, 127.6, 128.3, 129.1, 129.3, 130.4, 131.5, 131.6, 139.4.

HRMS: ESI-MS: *m/z* calculated for $C_{23}H_{21}N$ $[M+H]^+$ 312.17470, found 312.17530.

2.5 Acknowledgements

Dr. Joseph Larkin is gratefully acknowledged for his collaborative work on this project. Dr. Claudia Turro, Dr. Dario Bassani, and Dr. Tony Davis are thanked for their suggestions and advice. Steve Sorey and Angela Spangenberg are thanked for their help with NMR spectroscopy, Dr. Raluca Gearba is recognized for her help with fluorescence lifetime studies, and Dr. Tiddo Mooibroek is acknowledged for his help with ITC corrections.

2.6 References

(1) Kuivila, H. G.; Keough, A. H.; Soboczenski, E. J. Areneboronates From Diols and Polyols. *J. Org. Chem.* **1954**, *19* (5), 780–783.

(2) James, T. D.; Shinkai, S. Artificial Receptors as Chemosensors for Carbohydrates. *Top. Curr. Chem.* **2002**, *218*, 159–200.

(3) James, T. D.; Phillips, M. D.; Shinkai, S. *Boronic Acids in Saccharide Recognition*; Royal Society of Chemistry, 2006.

(4) James, T. D.; Sandanayake, K. R. A. S.; Shinkai, S. Saccharide Sensing with Molecular Receptors Based on Boronic Acid. *Angew. Chemie Int. Ed. English* **1996**, *35* (17), 1911–1922.

(5) Jin, S.; Cheng, Y.; Reid, S.; Li, M.; Wang, B. Carbohydrate Recognition by Boronolectins, Small Molecules, and Lectins. *Med. Res. Rev.* **2010**, *30* (2), 171–257.

(6) Hall, D. G. *Boronic Acids: Preparation, Applications in Organic Synthesis and Medicine*; John Wiley & Sons, 2006.

(7) Wright, A. T.; Griffin, M. J.; Zhong, Z.; McCleskey, S. C.; Anslyn, E. V; McDevitt, J. T. Differential Receptors Create Patterns That Distinguish Various Proteins. *Angew. Chem. Int. Ed. Engl.* **2005**, *44* (39), 6375–6378.

(8) Zaubitzer, F.; Buryak, A.; Severin, K. Cp*Rh-Based Indicator-Displacement Assays for the Identification of Amino Sugars and Aminoglycosides. *Chemistry* **2006**, *12* (14), 3928–3934.

(9) Bicker, K. L.; Sun, J.; Harrell, M.; Zhang, Y.; Pena, M. M.; Thompson, P. R.; Lavigne, J. J. Synthetic Lectin Arrays for the Detection and Discrimination of Cancer Associated Glycans and Cell Lines. *Chem. Sci.* **2012**, *3*, 1147–1156.

(10) Gray, C. W.; Houston, T. A. Boronic Acid Receptors for α-Hydroxycarboxylates:

High Affinity of Shinkai's Glucose Receptor for Tartrate. *J. Org. Chem.* **2002**, *67* (15), 5426–5428.

(11) Wang, W.; Gao, X.; Wang, B. Boronic Acid-Based Sensors. *Curr. Org. Chem.* **2002**, *6* (14), 1285–1317.

(12) Lee, J. W.; Lee, J.-S.; Chang, Y.-T. Colorimetric Identification of Carbohydrates by a pH indicator/pH Change Inducer Ensemble. *Angew. Chem. Int. Ed.* **2006**, *45* (39), 6485.

(13) Schiller, A.; Wessling, R. A.; Singarum, B. A Fluorescent Sensor Array for Saccharides Based on Boronic Acid Appended Bipyridinium Salts. *Angew. Chem. Int. Ed.* **2007**, *46* (34), 6457–6459.

(14) Edwards, N. Y.; Sager, T. W.; McDevitt, J. T.; Anslyn, E. V. Boronic Acid Based Peptidic Receptors for Pattern-Based Saccharide Sensing in Neutral Aqueous Media, an Application in Real-Life Samples. *J. Am. Chem. Soc.* **2007**, *129* (44), 13575–13583.

(15) Musto, C. J.; Lim, S. H.; Suslick, K. S. Colorimetric Detection and Identification of Natural and Artificial Sweeteners. *Anal. Chem.* **2009**, *81* (15), 6526–6533.

(16) Zhang, X.; You, L.; Anslyn, E. V.; Qian, X. Discrimination and Classification of Ginsenosides and Ginsends Using Bis-Boronic Acid Receptors in Dynamic Multicomponent Indicator Displacement Sensor Arrays. *Chem. Eur. J.* **2012**, *18* (4), 1102–1110.

(17) Springsteen, G.; Wang, B. A Detailed Examination of Boronic Acid-Diol Complexation. *Tetrahedron* **2002**, *58* (26), 5291–5300.

(18) Yasuda, H.; Kurokawa, T.; Fujii, Y.; Yamashita, A.; Ishibashi, S. Decreased D-Glucose Transport across Renal Brush-Border Membrane Vesicles from Streptozotocin-Induced Diabetic Rats. *Biochim. Biophys. Acta* **1990**, *1021* (2), 114–118.

(19) Fedorak, R. N.; Gershon, M. D.; Field, M. Induction of Intestinal Glucose Carriers in Streptozocin-Treated Chronically Diabetic Rats. *Gastroenterology* **1989**, *96* (1), 37.

(20) Mallia, A. K.; Hermanson, G. T.; Krohn, R. I.; Fujimoto, E. K.; Smith, P. K. Preparation and Use of a Boronic Acid Affinity Support for Separation and Quantitation of Glycosylated Hemoglobins. *Anal. Lett.* **1981**, *14* (B8), 649–661.

(21) Fang, H.; Kaur, G.; Wang, B. Progress in Boronic Acid-Based Fluorescent Glucose Sensors. *Fluorescence* **2004**, *14* (5), 481–489.

(22) Yang, W.; Gao, S.; Gao, X.; Karnati, V. V. R.; Ni, W.; Wang, B.; Hooks, W. B.; Carson, J.; Weston, B. Diboronic Acids as Fluorescent Probes for Cells Expressing Sialyl Lewis X. *Bioorg. Med. Chem. Lett.* **2002**, *12* (16), 2175–2177.

(23) Dai, C.; Cazares, L. H.; Wang, L.; Chu, Y.; Wang, S. L.; Troyer, D. A.; Semmes, O. J.; Drake, R. R.; Wang, B. Using Boronolectin in MALDI-MS Imaging for the Histological Analysis of Cancer Tissue Expressing the Sialyl Lewis X Antigen. *Chem. Commun.* **2011**, *47* (37), 10338–10340.

(24) Goldberg, R. N.; Tewari, Y. B. Thermodynamic and Transport Properties of Carbohydrates and Their Monophosphates: The Pentoses and Hexoses. *J. Phys. Chem. Ref. Data* **1989**, *18* (2), 809–880.

(25) Hinz, H. *Thermodynamic Data for Biochemistry and Biotechnology*; Springer-Verlag, 1986.

(26) Franks, F. Physical Chemistry of Small Carbohydrates-Equilibrium Solution Properties. *Pure Appl. Chem.* **1987**, *59* (9), 1189–1202.

(27) Varki, A.; Cummings, R. D.; Esko, J. D.; Freeze, Hudson, H.; Stanley, P.; Bertozzi, C. R.; Hart, G. W.; Etzler, M. E. The Expanding World of Glycobiology: Essentials of Glycobiology, 2nd Edition. *Nat. Chem. Biol.* **2009**, *5* (6), 373.

(28) Moulin, E.; Cormos, G.; Giuseppone, N. Dynamic Combinatorial Chemistry as a Tool for the Design of Functional Materials and Devices. *Chem. Soc. Rev.* **2012**, *41* (3), 1031–1049.

(29) Lehn, J.-M. From Supramolecular Chemistry towards Constitutional Dynamic Chemistry and Adaptive Chemistry. *Chem. Soc. Rev.* **2007**, *36* (2), 151–160.

(30) Lehn, J.-M. *Supramolecular Chemistry: Concepts and Perspectives*; VCH: Weinheim, 1995.

(31) Rowan, S. J.; Cantrill, S. J.; Cousins Graham, R. L.; Sanders, J. K. M.; Stoddart, F. J. Dynamic Covalent Chemistry. *Angew. Chem. Int. Ed.* **2002**, *41* (6), 898–952.

(32) Corbett, P. T.; Leclaire, J.; Vial, L.; West, K. R.; Wietor, J.-L.; Sanders, J. K. M.; Otto, S. Dynamic Combinatorial Chemistry. *Chem. Rev.* **2006**, *106* (9), 3652–3711.

(33) Cougnon, F. B. L.; Sanders, J. K. M. Evolution of Dynamic Combinatorial Chemistry. *Acc. Chem. Res.* **2012**, *45* (12), 2211–2221.

(34) Nagai, Y.; Kobayashi, K.; Toi, H.; Aoyama, Y. Stabilization of Sugar-Boronic Esters of Indolylboronic Acid in Water via Sugar-Indole Interaction: A Notable Selectivity in Oligosaccharides. *Bull. Chem. Soc. Jpn.* **1993**, *66* (10), 2965–2971.

(35) Huang, C.-Y.; Cabell, L. A.; Anslyn, E. V. Molecular Recognition of Cyclitols by Neutral Polyaza-Hydrogen-Bonding Receptors: The Strength and Influence of Intramolecular Hydrogen Bonds between Vicinal Alcohols. *J. Am. Chem. Soc.* **1994**, *116* (7), 2778–2792.

(36) Ferrand, Y.; Crump, M.; Davis, A. P. A Synthetic Lectin Analog for Biomimetic Disaccharide Recognition. *Science (80-.).* **2007**, *318* (5850), 619–622.

(37) Wulff, G. Selective Binding to Polymers via Covalent Bonds. The Construction of Chiral Cavities as Specific Receptor Sites. *Pure Appl. Chem.* **1982**, *54* (11), 2093–2102.

(38) Weith, H. L.; Wiebers, J. L.; Gilham, P. T. Synthesis of Cellulose Derivatives Containing the Dihydroxyboryl Group and a Study of Their Capacity to Form Specific Complexes with Sugars and Nucleic Acid Components. *Biochem.* **1970**, *9* (22), 4396–4401.

(39) Lorand, J. P.; Edwards, J. O. Polyol Complexes and Structure of the Benzeneboronate Ion. *J. Org. Chem.* **1959**, *24* (769-774).

(40) Wulff, G.; Dederichs, W.; Grotstollen, R.; Jupe, C. On the Chemistry of Binding Sites, Part II: Specific Binding of Substances to Polymers by Fast and Reversible Covalent Interactions. In *Analytical Chemistry Symposia Series, Affinity Chromatography and Related Techniques*; Gribnau, T. C. J., Visser, J., Nivard, R. J. F., Eds.; Elsevier: Amsterdam, 1982; pp 207–216.

(41) Wulff, G.; Lauer, M.; Boehnke, H. Chemistry of Adhesive Groups. Part 5. Rapid Proton Transfer as Cause for an Uncommonly Large Neighboring Group Effect. *Angew. Chem.* **1984**, *96* (9), 714–716.

(42) Xing, Z.; Wang, H.-C.; Cheng, Y.; Zhu, C.; James, T. D.; Zhao, J. Selective Saccharide Recognition Using Modular Diboronic Acid Fluorescent Sensors. *Eur. J. Org. Chem.* **2012**, *2012* (6), 1223–1229.

(43) Li, H.; Liu, Y.; Liu, J.; Liu, Z. A Wulff-Type Boronate for Boronate Affinity Capture of Cis-Diol Compounds at Medium Acidic pH Condition. *Chem. Commun.* **2011**, *47* (28), 8169–8171.

(44) Kitamura, M.; Suzuki, T.; Abe, R.; Ueno, T.; Aoki, S. 11B NMR Sensing of D-Block Metal Ions in Vitro and in Cells Based on the Carbon-Boron Bond Cleavage of Phenylboronic Acid-Pendant Cyclen (Clyclen = 1,4,7,10-Tetraazacyclododecane). *Inorg. Chem.* **2011**, *50* (22), 11568–11580.

(45) James, T. D.; Sandanayake, K. R. A. S.; Shinkai, S. Novel Photoinduced Electron-Transfer Sensor for Saccharides Based on the Interaction of Boronic Acid and Amine. *J. Chem. Soc., Chem. Commun.* **1994**, No. 4, 477–478.

(46) James, T. D.; Sandanayake, K. R. A. S.; Shinkai, S. A Glucose-Specific Molecular Fluorescence Sensor. *Angew. Chem.* **1994**, *106* (21), 2287–2289.

(47) James, T. D.; Sandanayake, K. R. A. S.; Shinkai, S. Chiral Discrimination of Monosaccharides Using a Fluorescent Molecular Sensor. *Nature* **1995**, *374* (6520), 345–347.

(48) Noeth, H.; Wrackmeyer, B. *NMR Basic Principles and Progress, Vol. 14: Nuclear Magnetic Resonance Spectroscopy of Boron Compounds*; Springer-Verlag: Berlin, 1978.

(49) James, T. D. Saccharide-Selective Boronic Acid Based Photoinduced Electron Transfer (PET) Fluorescent Sensors. *Top. Curr. Chem.* **2007**, *277*, 107–152.

(50) de Silva, A. P.; Gunnlaugsson, T.; Rice, T. E. Recent Evolution of Luminescent Photoinduced Electron Transfer Sensors. A Review. *Analyst* **1996**, *121* (12), 1759–1762.

(51) Bissell, R. A.; de Silva, A. P.; Gunaratne, H. Q. N.; Lynch, P. L. M.; Maguire, G. E. M.; McCoy, C. P.; Sandanayake, K. R. A. S. Fluorescent PET (Photoinduced Electron Transfer) Sensors. *Top. Curr. Chem.* **1993**, *168*, 223–264.

(52) Franzen, S.; Ni, W.; Wang, B. Study of the Mechanism of Electron-Transfer Quenching by Boron-Nitrogen Adducts in Fluorescent Sensors. *J. Phys. Chem. B* **2003**, *107* (47), 12942–12948.

(53) Ni, W.; Kaur, G.; Springsteen, G.; Wang, B. Regulating the Fluorescence Intensity of an Anthracene Boronic Acid System: A B-N Bond or a Hydrolysis Mechanism? *Bioorg. Chem.* **2004**, *32* (6), 571–581.

(54) Wiskur, S. L.; Lavigne, J. J.; Ait-Haddou, H.; Lynch, V.; Chiu, Y. H.; Canary, J. W.; Anslyn, E. V. pKa Values and Geometries of Secondary and Tertiary Amines Complexed to Boronic Acids - Implications for Sensor Design. *Org. Lett.* **2001**, *3* (9), 1311–1314.

(55) Zhu, L.; Shabbir, S. H.; Gray, M.; Lynch, V.; Sorey, S.; Anslyn, E. V. A Structural Investigation of the N-B Interaction in an O-(N,N-Dialkylaminomethyl)arylboronate System. *J. Am. Chem. Soc.* **2006**, *128* (4), 1222–1232.

(56) Larkin, J. D.; Fossey, J. S.; James, T. D.; Brooks, B. R.; Bock, C. W. A Computational Investigation of the Nitrogen-Boron Interaction in O-(N,N-Dialkylaminomethyl)arylboronate Systems. *J. Phys. Chem. A* **2010**, *114* (47), 12531–12539.

(57) Matsumura, T.; Iwatsuki, S.; Ishihara, K. Direct Kinetic Measurements for the Fast Interconversion Process between Trigonal Boronic Acid and Tetragonal Boronate Ion at Low Temperatures. *Inorg. Chem. Commun.* **2005**, *8* (8), 713–716.

(58) Collins, B. E.; Metola, P.; Anslyn, E. V. On the Rate of Boronate Ester Formation in Ortho-Aminomethyl-Functionalized Phenyl Boronic Acids. *Supramol. Chem.* **2013**, *25* (2), 79–86.

(59) Anslyn, E. V.; Dougherty, D. A. *Modern Physical Organic Chemistry*; University Science, 2005.

(60) Collins, B. E.; Sorey, S.; Hargrove, A. E.; Shabbir, S. H.; Lynch, V.; Anslyn, E. V. Probing Intramolecular B-N Interactions in Ortho-Aminomethyl Arylboronic Acids. *J. Org. Chem.* **2009**, *74* (11), 4055–4060.

(61) Chandross, E. A. Photolytic Dissociation of Dianthracene. *J. Chem. Phys.* **1965**, *43*

(11), 4175–4176.

(62) Chandross, E. A.; Ferguson, J.; McRae, E. G. Absorption and Emission Spectra of Anthracene Dimers. *J. Chem. Phys.* **1966**, *45* (10), 3546–3553.

(63) McVey, J. K.; Shold, D. M.; Yang, N. C. Direct Observation and Characterization of Anthracene Excimer in Solution. *J. Chem. Phys.* **1976**, *65* (8), 3375–3376.

(64) Birks, J. B. Excimers. *Rep. Prog. Phys.* **1975**, *38*, 903–974.

(65) Tomlinson, W. J.; Chandross, E. A.; Fork, R. L.; Pryde, C. A.; Lamola, A. A. Reversible Photodimerization. New Type of Photochromism. *Appl. Opt.* **1972**, *11* (3), 533–548.

(66) Shore, J. *Colorants and Auxiliaries*, 2nd ed.; Shore, J., Ed.; Society of Dyers and Colourists, 1990.

(67) Renney, C. M.; Fukuhara, G.; Inoue, Y.; Davis, A. P. Binding or Aggregation? Hazards of Interpretation in Studies of Molecular Recognition by Porphyrins in Water. *Chem. Commun.* **2015**, *51*, 9551–9554.

(68) Shabbir, S. H.; Regan, C. J.; Anslyn, E. V. A General Protocol for Creating High-Throughput Screening Assays for Reaction Yield and Enantiomeric Excess Applied to Hydrobenzoin. *Proc. Natl. Acad. Sci.* **2009**, *106* (26), 10487–10492.

(69) Zhai, W.; Chapin, B. M.; Yoshizawa, A.; Wang, H.-C.; Hodge, S. A.; James, T. D.; Anslyn, E. V.; Fossey, J. S. "Click-Fluors": Triazole-Linked Saccharide Sensors. *Org. Chem. Front.* **2016**, *3* (8), 918–928.

Chapter 3: ^{11}B NMR, its Uses in Structural Characterization of Boronic Acids and Boronate Esters, and its Application in Structural and Equilibrium Studies of *ortho*-Iminoarylboronate Systems

3.1 Introduction to ^{11}B NMR[a]

Boronic acids and boronate esters[1] serve a myriad of purposes, and the discovery of the Suzuki–Miyaura reaction[2] facilitated the widespread interest and application of organoboron compounds. This palladium-catalyzed C-C bond forming reaction initiated a renewed interest in the preparation of diversely functionalized boronic acids that would lead to valuable products. From this synthetic standpoint, Suzuki coupling reactions have been employed in the production of natural products[3–5] and the preparation of materials of interest.[6–10] The search for interesting starting materials for the Suzuki reaction produced a series of methods to prepare boronic acids so these species could be exploited in further applications. These compounds can be easily synthesized *via* transmetalation or hydroboration reactions,[11–13] or through asymmetric conjugate addition.[14] Additionally, boronic acids and boronate esters have been shown to function as catalytic inhibitors in enzymes and other biologically relevant proteins,[15–21] in the building of macromolecular scaffolds,[22–24] and as molecular recognition units with a special focus on sugars.[25–28] As highly versatile moieties, a profound and comprehensive understanding of their structural and electronic behavior is of relevance to the entire chemical community.

Boron-containing molecules have been thoroughly studied *via* ^{11}B NMR spectroscopy, and the resulting chemical shift information has been correlated to different structural patterns.[29–31] The technique is not usually employed as a definitive

[a] Sections 3.1-3.4 are adapted from a published book chapter: Metola, P.; Chapin, B. M.; Anslyn, E. V. ^{11}B NMR and Its Uses in Structural Characterization of Boronic Acids and Boronate Esters. In *Boron: Sensing, Synthesis and Supramolecular Self-Assembly*; Li, M.; Fossey, J. S.; James, T. D., Eds.; Royal Society of Chemistry, 2015; pp 44-60. Pedro Metola and Eric Anslyn cowrote the chapter and Brette Chapin edited it.

characterization tool. Rather, it has been used to partially assign general structural features directly from measurements of chemical shift values, J coupling constants, and information obtained from ^{1}H-^{11}B NMR correlated two-dimensional spectra.[29] The significant difference in chemical shift between tricoordinated and tetracoordinated boron translates into discrimination between such geometries. This allows for the use of ^{11}B NMR as a technique to monitor and study behavior of boronic acid-based constructs or systems, particularly those where a change in coordination and hybridization accompanies a reaction or transformation of interest.

3.2 ^{11}B NMR TECHNIQUE

Practical understanding of the particulars concerning ^{11}B NMR spectroscopy begins with the comparison of the boron nucleus to those nuclei that are traditionally studied: hydrogen and carbon. Table 3.1 contains parameters relevant to NMR spectroscopy for these nuclei.

Nucleus	Percent Abundance	Spin number (*I*)	Gyromagnetic Ratio (γ)[b]	Relative Sensitivity[c]	Larmor Frequency[d]	Quadrupole Moment[e]
^{1}H	99.99	1/2	26.75	1.00	400	0
^{13}C	1.07	1/2	6.73	1.70×10^{-4}	100.58	0
^{10}B	19.90	3	2.87	3.95×10^{-3}	42.98	0.111
^{11}B	80.10	3/2	8.58	0.132	128.34	3.55×10^{-2}

Table 3.1: Nuclear properties of hydrogen, carbon, and boron isotopes.

[b] Gyromagnetic ratio is expressed in 10^{7} rad $T^{-1}s^{-1}$
[c] Relative sensitivity when compared to ^{1}H
[d] Larmor frequency expressed in MHz at a magnetic field 9.4T
[e] Quadrupole moment expressed in 10^{-24} cm^{2}

The ^{11}B nucleus, with a smaller quadrupole moment and nuclear spin, is more sensitive and yields sharper and less complex signals than ^{10}B. The ^{10}B nucleus splits protons attached to it into a heptet, while the ^{11}B nucleus leads to a quartet. In addition, ^{11}B has a greater nuclear magnetic momentum than the other active isotope, which generally translates into a higher signal-to-noise ratio. Given these factors, ^{11}B is generally the boron nucleus of choice for these types of experiments.[32]

However, the high natural abundance and relatively high sensitivity (when compared to ^{13}C for example) do not necessarily translate into well-resolved spectral signals. The aforementioned spin coupling of ^{1}H with ^{10}B and ^{11}B and quadrupole moments often lead to broad signals.[33] On a different practical note, there is another issue that must be considered when aiming to undertake ^{11}B NMR analysis: most glass equipment that is used in scientific settings is composed of boron-containing species. These borosilicates will have an effect on the output NMR spectra. The contribution of the glass from the NMR tubes to this interference is something that can be avoided by employing considerably more expensive quartz tubes. But one must keep in mind that most NMR probes also have a glass component and therefore readings are marred with a substantial background signal. Unless the facilities provide a probe that is specifically tailored for boron analysis, or can reliably account for the background footprint, quantitative studies using ^{11}B NMR spectroscopy will be difficult to impossible.

The availability of X-ray crystallography instrumentation and data has made a significant difference to how chemical shifts are assigned to structural motifs or chemical environments around the boron atom. This solid-state evidence provides a true image of the geometry of the species under study and its binding modes. Caution must be taken, however, since these details might not remain consistent when the molecule is in solution.

3.3 ^{11}B NMR Chemical Shifts

As a result of numerous ^{11}B NMR studies, chemical shift values have been reported for a variety of boron-containing species. What follows is a compilation of chemical shifts corresponding to different common boranes and related species as recorded in the original bodies of work (Figure 3.1). The list includes single-boron compounds, polyboranes, carboranes and borates. Historically, chemical shift values have been reported relative to numerous reference standards, and the definition of upfield versus downfield has not always been consistent. All chemical shift values herein are given in relation to the external reference standard BF_3•Et_2O and rounded to within 0.1 ppm.

To delineate general trends, there exists a direct correlation between the p-donor ability of the groups attached to the boron atom and the frequencies for the ^{11}B resonances.[34] As the π-donating character of the ligands increases, an upfield shift is observed, as evidenced by the systematic decrease of the ^{11}B chemical shift that occurs when alkyl groups are replaced with electron-donating ligands with increased back-bonding abilities.[34] This electron donation is a similar phenomenon to the switch to lower ppm values that can be observed upon addition of a fourth group onto boron's p orbital that remains empty in tricoordinated boron compounds. As expected, factors that decrease p-bonding, such as steric hindrance around the boron center, are prone to cause a shift of the signal towards higher frequencies.[34]

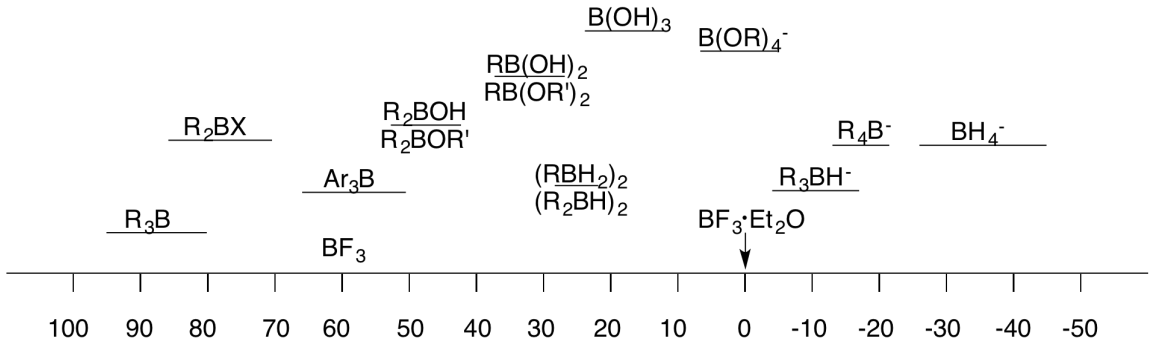

Figure 3.1: Relation of ^{11}B NMR resonances for different boron-containing species.

3.3.1 Tricoordinate Boranes and Trialkylboranes

Borane (BH_3) and trialkylboranes have well-defined resonance values. Trialkylboranes rarely show resonances outside the narrow low field range of 80-95 ppm regardless of the structure of the alkyl group. The chemical shifts of alkylboranes of the formula BRH_2 or BR_2H, however, cannot be as easily predicted and are highly dependent upon the structure of the alkyl groups on the boron atom (see Table 3.2).

Regarding cyclic boranes, the size of the ring has a direct effect on the position of the signal. Small rings show a pronounced downfield shift to higher ppm values. Five-membered rings are on average 6 ppm further downfield than their six-membered ring counterparts, which display approximately the same chemical shifts as acyclic alkylboranes.[34]

When there exists a B-H bond, the ^{11}B NMR spectrum will show a B-H coupling. This coupling will display the corresponding signal multiplicity as described earlier. The degree of B-H splitting and signal complexity increases with the number and electronegativity of the ligands.

Formation of a dimerized species is common in tricoordinated boranes lacking steric hindrance. Their presence leads to a shift towards lower resonance frequencies and the possibility of more convoluted spectra by virtue of additional coupling interactions.

Dative interactions with boron, where the two electrons forming the bond originate from another molecule (the solvent or a basic ligand), also lead to higher field shifts.

Structure	Resonance (ppm)
BH_3	+57.1[35] neat
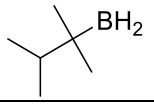	+24.0[36] diethyl ether
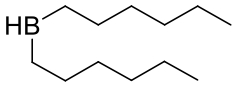	+30.5[37] neat
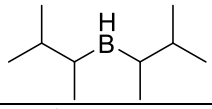	+30.0[38] tetrahydrofuran
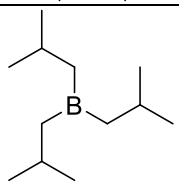	+87.1[39] neat
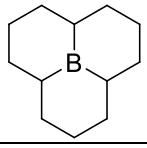	+71.2[40] tetrahydrofuran

Table 3.2: ^{11}B NMR chemical shifts for tricoordinated boranes and alkylboranes.

3.3.2 Unsaturation and Heteroatoms in Alkylboranes

Varying the unsaturated substituents on the boron atom has a larger effect on the ^{11}B chemical shifts than saturated analogs (see Table 3.3). Ligands with π-bonds adjacent to the central boron atom are more prone to donate into boron's empty p orbital due to orbital mixing. This can cause a consistent upfield shift of the ^{11}B resonance relative to the alkyl peaks. Alkyne ligands are also believed to contribute to this effect through anisotropy.

Similarly, the introduction of heteroatoms such as oxygen, nitrogen, or halogens, results in lower chemical shifts when compared to alkylboranes. The reason for this resides in the inter- or intramolecular donation of the lone pairs of the heteroatom into the p orbital of the central boron. This has the same effect as unsaturated systems, leading to upfield shifts of ^{11}B signals.

Structure	**Resonance (ppm)**
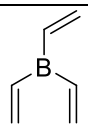	+55.2[41] neat
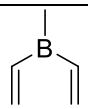	+64.4[41] neat
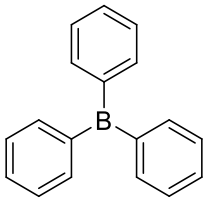	+60.2[41] neat
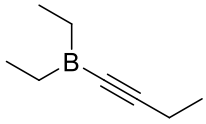	+72.9[42] pentane
	+60.1[43] chloroform
	+75.5[43] neat
	+78.8[44] neat
	+47.1[45] neat
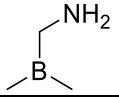	+48.4[46] neat

Table 3.3: ^{11}B NMR chemical shifts for unsaturated and substituted alkylboranes.

3.3.3 Boron Compounds with Oxygen Ligands

Numerous boronates have been prepared that have oxygen atoms attached directly to the central boron atom. As expected of strong π-donors, introduction of hydroxyl or alkoxy groups shifts the ^{11}B signals upfield relative to the analogous trialkylborane. The structural features of the alkoxy group apparently have little influence on the final position of the resonances, with signals only slightly shifted upfield for aromatic or vinylic groups. Cyclic anhydrides of the boronic acids are known as boroxines, and they show a slight shift downfield from the boronates, as shown in Table 3.4.

Structure	Resonance (ppm)
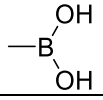	+31.9[43] water
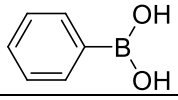	+28.4[47] chloroform
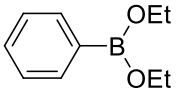	+28.6[48] chloroform
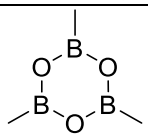	+33.2[43] neat

Table 3.4: ^{11}B NMR chemical shifts for tricoordinated boranes bound to oxygen ligands.

3.3.4 Borohydrides, Alkylborohydrides, and Tetraalkylborates

Another important class of boron-containing species has four substituent groups. The borohydrides (BH_4^-) can show more complicated spectra than expected. This is largely based on whether the nature of these species is covalent or ionic, as the interactions of the counterion with the borohydride hydrogens will differ. Generally, if exchange between binding modes is fast on the NMR time scale, only one type of hydrogen is observed. As expected, ^{11}B NMR resonances for borohydrides appear at high

field, -26 to -45 ppm (Table 3.5). These species represent some of the furthest upfield chemical shifts for boron species. Effects that interfere with the solvation of the counterion have a substantial effect on the position of the signals. When an alkyl group replaces one of the hydrogens, the resonances are shifted downfield to varying degrees. Tetraalkylborates appear between -15 and -22 ppm and the dependence on counterion and solvent is much less pronounced. The behavior of four-coordinated boron species containing heteroatom-bound ligands are harder to predict. Most of these examples show that the upfield shift compared to tricoordinated boron is not as pronounced as in tetraalkylborates, which is due to differences in electron donation between a purely covalent or dative interaction.

Structure	**Resonance (ppm)**
$Al(BH_4)_3$	-33.0[49] benzene
$Li\ BH_4$	-38.2[50] diethyl ether
$Li(BEt_4)$	-17.5[51] diethyl ether
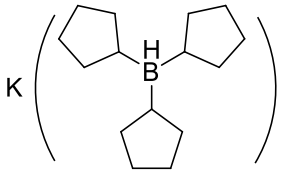	-10.7[40] tetrahydrofuran
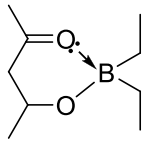	+14.2[52] tetrahydrofuran
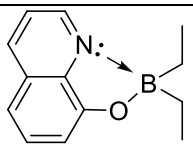	+14.4[52] benzene

Table 3.5: ^{11}B NMR chemical shifts for tetracoordinated boron species.

3.4 ^{11}B NMR IN BORONIC ACID SYSTEMS

Pizer and Tihal made the first significant contribution to the methodology of employing ^{11}B NMR spectroscopy as a means of confirming or validating a mechanistic and/or kinetic hypothesis in the boronic acid field in 1992 (Scheme 3.1).[53] This technique was employed to complement the results obtained *via* pH titrations in order to describe reaction pathways, equilibria, and rate constants associated with the reaction of trigonal and four-coordinated methylboronic acid with several diols. They found that tetrahedral boron was important for enhancing the binding affinity for diols. This important conclusion helped set the stage for future work on boronic acids. The same group also took advantage of the power of ^{11}B NMR in 1996 to study the different behaviors of the boron atom in trigonal vs. tetrahedral form in boronic acids.[54] In particular, they focused on rates of interconversion between the two different species.

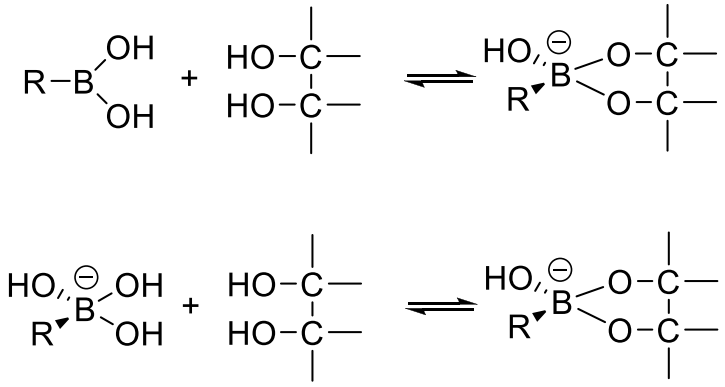

Scheme 3.1: Boronate ester formation reaction pathways studied.

In a simple, yet elegant, analysis of Lewis acid-base interactions between fluoride anions and boron, James *et al*. used ^{11}B NMR to examine the change in boron hybridization upon complexation to a fluoride anion (Scheme 3.2).[55] This process had the added allure of offering the possibility of a fluorescent sensor for fluoride. The boron chemical shift of **3.1** relative to a BMe_3 external reference occurs at 13.2 ppm. This

chemical shift corresponds to a single sp^2 boron. In the case of **3.2**, they observed two signals at 14.5 and 2.5 ppm, corresponding to one sp^2 free boron signal and one sp^3 boron signal due to coordination of the adjacent nitrogen atom, respectively. Upon addition of one equivalent of KF, the boron signal of **3.1** shifts to 12.0 ppm and further shifts to 7.4 ppm after addition of five equivalents of KF due to a change in hybridization (sp^2 to sp^3) upon complexation with fluoride. For **3.2**, the signal at 14.5 ppm shifted to 13.5 ppm upon addition of one equivalent of KF. When five equivalents of KF were added to **3.2**, only one signal at 2.5 ppm was observed. These data are indicative of a switch from trigonal planar sp^2 boron to tetrahedral boron.

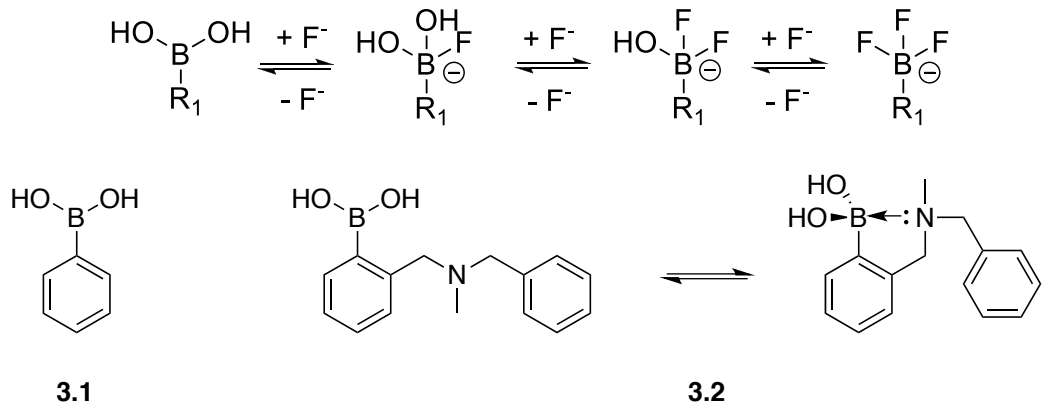

Scheme 3.2: Consecutive reactions of a boronic acid with fluoride anions.

In 1998, Todd *et al*. studied the thermodynamics and mode of coordination of the reaction of tetrahydroxyborate (**B**$^-$) with three different carbohydrates (**3.3**, **3.4** and **3.5**) as a preliminary test to aid in the design of polymers capable of removing boron from aqueous solutions (Scheme 3.3).[56] Quantification and determination of the boron-carbohydrate complexes were cleverly performed using ^{11}B NMR spectroscopy due to the ease with which the various boron complexes can be distinguished based on chemical shifts. While the complex with **3.3** showed that borate monoesters of the **BL** type were

the preferred mode of interaction, carbohydrate **3.4** favored borate diesters $\mathbf{BL_2}$. Interestingly, for the complex formed with **3.5**, it was found that the product of complexation was a combination of intramolecular tetradentate borate diesters and oligomeric chains of **3.5** attached *via* intermolecular borate diesters.

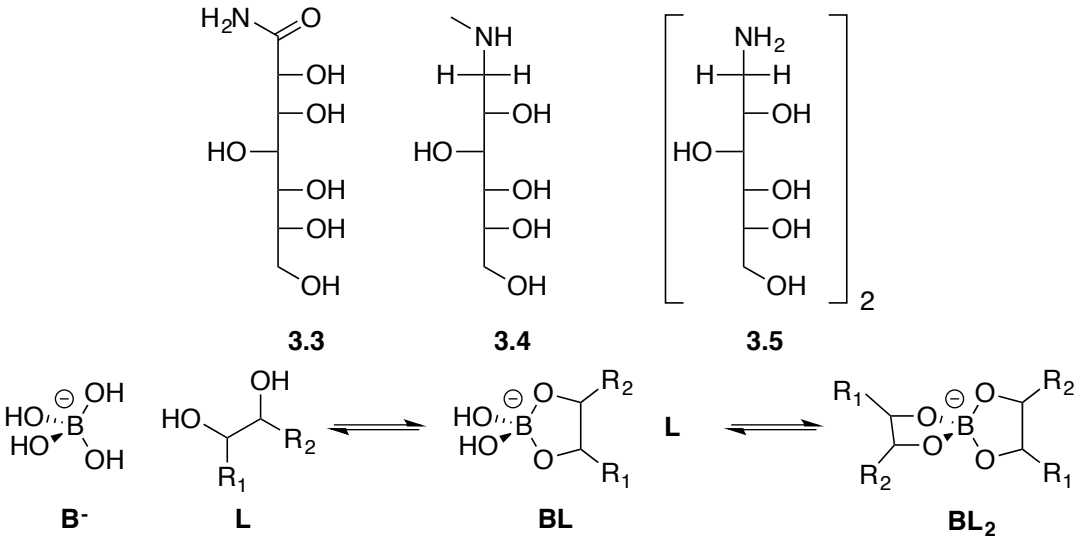

Scheme 3.3: Complexation between borate and diol ligands.

The reaction of borate $\mathbf{B^-}$ with the hydroxyl-containing polymer **PACL** (poly(1-(acrylamido)-1-deoxylactitol)) was studied by Kurth *et al*.[57] Using ^{11}B NMR spectroscopy they quantified the types of borate complexes formed and their binding constants. This study was placed within the framework of an investigation into factors affecting the intrinsic viscosity of certain classes of polymers. This body of work focused on complexes formed between tetrahydroxyborate and three different ligands: **3.6** (subunit of **PACL**), the monomer **3.7**, and **PACL**, with modes of interaction analogous to those described in Equations 3 and 4. Assembly of **B**-**3.6** and **B**-**3.7** complexes were performed first to help with peak assignments in the polymeric **B**-**PACL** complex due to foreseeable

peak broadening. The α,ß-bidentate, α,ß-dimer and α,γ-bidentate structures were recorded for the complexes with **3.6** and **3.7** (Scheme 3.4). The polymeric **B-PACL** structure showed a broad α,ß peak and a dimeric α,ß peak. The boric acid/borate-**3.7** complex was shown to have the greatest binding affinity as indicated by a decreased amount of free boric acid or borate present in the NMR spectrum.

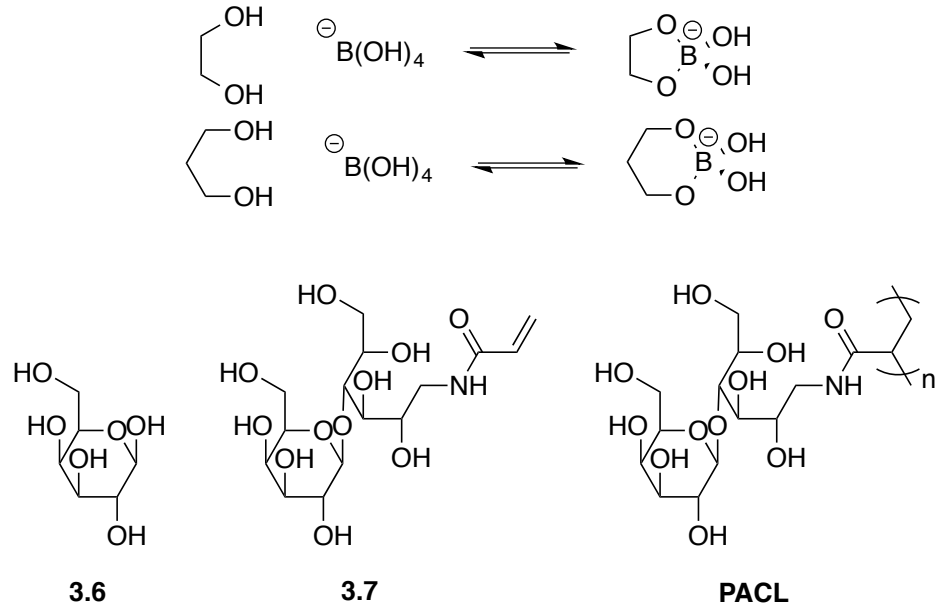

Scheme 3.4: Modes of complexation between borate 1,2- and 1,3-diols.

Anslyn *et al*. used ^{11}B NMR spectroscopy in conjunction with molecular modeling and X-ray crystallography analysis to distinguish between the modes of interaction between the nitrogen and boron atoms in a series of molecules based on the *ortho*-aminomethylphenylboronic acid moiety. This particular substructure is of special importance as it is the foundation for a number of efficient fluorescent polyol sensors.[25–28,58,59] The studies served to identify the factors involved in the formation of a dative N-B bond or the insertion of a molecule of solvent between the N and B atoms, with polar

aprotic media such as acetonitrile or chloroform favoring the former case and polar protic solvents such as methanol and water promoting the latter. This work also deserves mention based on the fact that it established a clear differentiation between ^{11}B NMR signals for the two different modes of tetrahedral boron. These shifts were determined to be 13-15 ppm for the N-B bond in structure **3.8** and 9-11 ppm for solvent-inserted boron in structure **3.9** (Figure 3.2). These assignments were further corroborated by X-ray studies.[60]

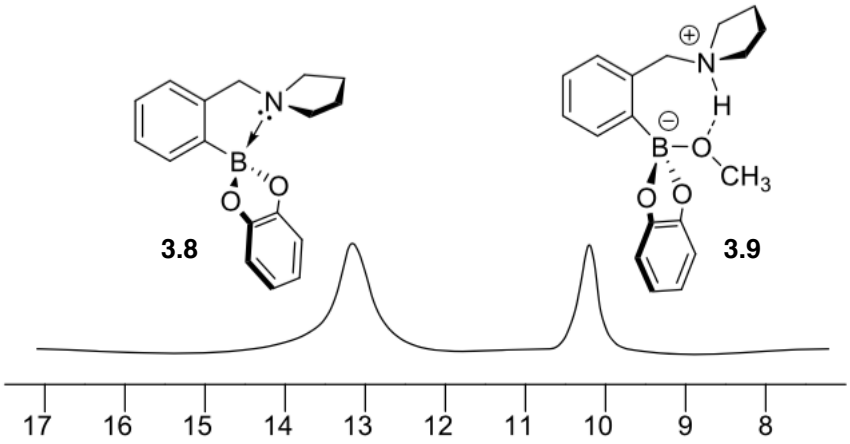

Figure 3.2: Modes of boron-nitrogen interaction in an *ortho*-aminomethylphenylboronic acid and their resonances in a ^{11}B NMR spectrum.

The complexation of boric acid with salicylic acid (**3.10**-**3.12**, Scheme 3.5) was studied by Yoshimura *et al*. in 2008. Interestingly, an ^{11}B NMR spectrum of boric acid and **3.10** at pH 4 yielded three boron signals: one at ~20 ppm corresponding to the free boric acid, and two signals at 2.9 and 3.3 ppm. First, **3.11** can complex boric acid in a 1:1 ratio (Scheme 3.6). This complexation leads to the monochelate **3.13,** which corresponds to the boron signal at 2.9 ppm. This monochelate can then undergo condensation with neutral **3.10** to yield the 1:2 bischelate **3.14** which corresponds to the boron signal at 3.3

ppm. They then used this information to further study the complexation of boric acids with other salicylic acid derivatives.[61]

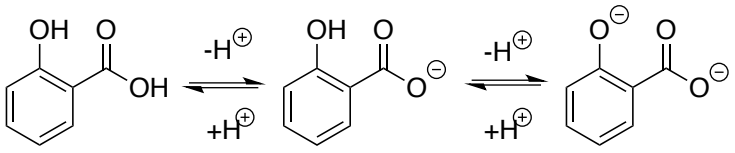

Scheme 3.5: Acid-base equilibrium for salicylic acid.

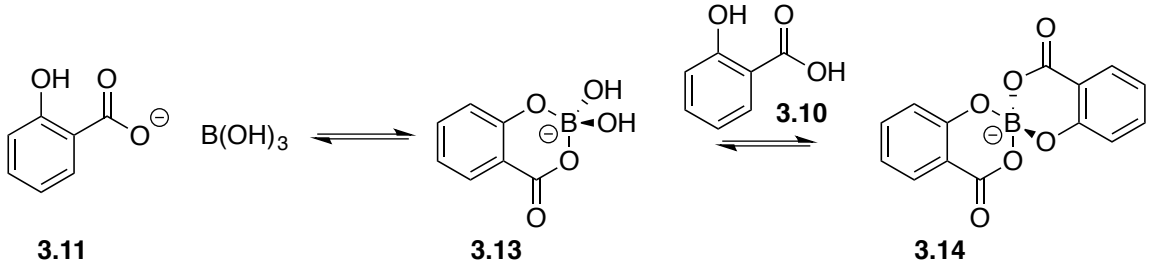

Scheme 3.6: Chelation of salicylic acid to boric acid.

In a recent report by James *et al*., the structures of macrocyclic Schiff base complexes incorporating 2-formylarylboronic acids and 1,2-amino alcohols were explored.[24] Using ^{11}B NMR spectroscopy, the authors were able to determine the geometry of these complexes. In contrast to the phenyl-derived boracyclic complexes **3.15** (10.5-11.5 ppm) (Scheme 3.7), the furan-derived boracycles **3.16** were shown to have more tetrahedral character (4.6-5.4 ppm) owing to the incorporation of a more geometrically strained furan ring into the complex (Scheme 3.8).

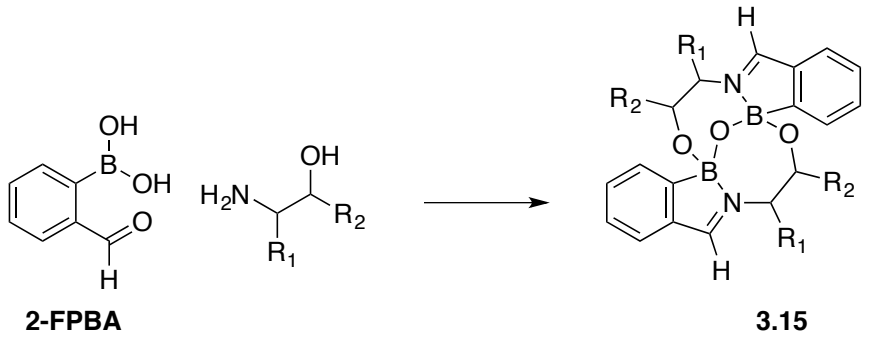

2-FPBA **3.15**

Scheme 3.7: Reaction of 1,2-aminoalcohols with 2-formylphenylboronic acid.

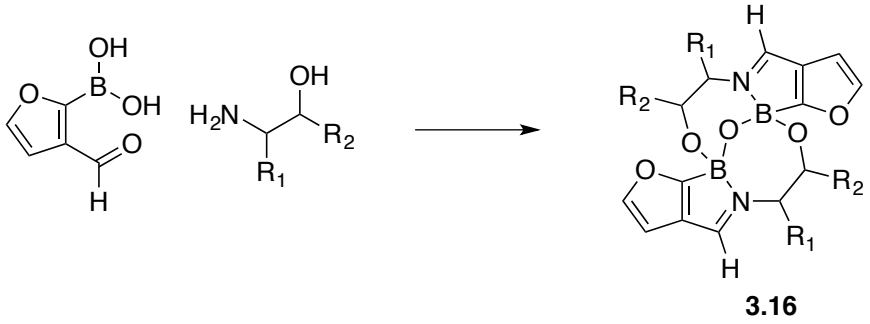

3.16

Scheme 3.8: Reaction of 1,2-aminoalcohols with 3-formyl-2-furanylboronic acid.

The rules affecting modes of interaction between boron and nitrogen were further studied by Anslyn *et al*. in 2009. They conducted analyses with the boronate ester formation of several *ortho*-aminomethylphenylboronic acids with different degrees of substitution around the nitrogen atom (Scheme 3.9). The experimental results showed that in polar protic solvents, increasing the number of substituents on the amine group correlated with a slight increase in the ratio of N-B dative bond to solvent insertion in polar protic solvents. Further, they found that the hydrogen atom from the inserted methanol was located closer to the amine than to the methanolic oxygen, indicating ionization of the solvent and the formation of a zwitterionic species.[62]

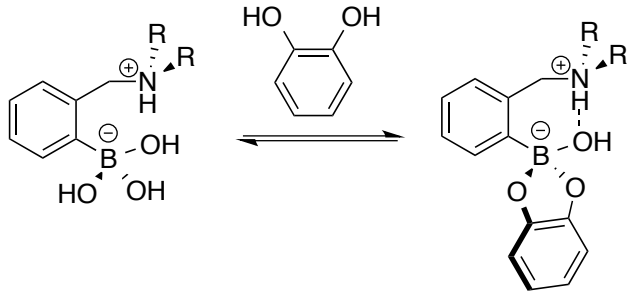

Scheme 3.9: Boronate ester formation from *ortho*-aminomethylphenylboronic acids.

To study the interaction of phenylboronic acids with amines in water, Yatsimirsky *et al*. used ^{11}B NMR spectroscopy to probe the charged state of the boron when complexing with an amine. At neutral pH (~7.0), 2-formylphenylboronic acid (**2-FPBA**) shows two boron resonances at 29.3 and 8.6 ppm. Acidification of the solution to pH 6.5 results in the complete disappearance of the 8.6 ppm peak. Hence, the peak at 29.3 ppm corresponds to the neutral boronic acid **2-FPBA**. Increasing the pH of the solution to pH 9.0 shows elimination of the 29.3 ppm signal. This means that the peak at 8.6 ppm corresponds to the anionic boron in **3.17** (Scheme 3.10). In order to deduce which side was favored in the complex equilibrium between neutral **3.18** and zwitterionic **3.19**, they examined which of the two boron signals (neutral versus anionic) were present with increasing equivalents of amine (Scheme 3.11). For both amines employed in the ^{11}B NMR aqueous titrations, disappearance of the neutral boron **2-FPBA** peak at 29.3 ppm, absence of peaks around the 13-16 ppm region, and a growing signal at around 9 ppm with increasing equivalents of amine gave clear evidence that the zwitterion **19** was present in solution.[63]

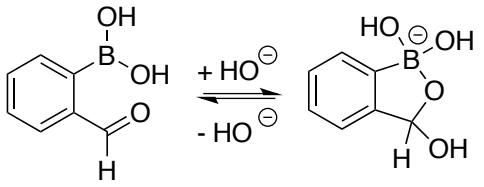

2-FPBA **3.17**

Scheme 3.10: Equilibrium between FPBA and its hemiacetal form.

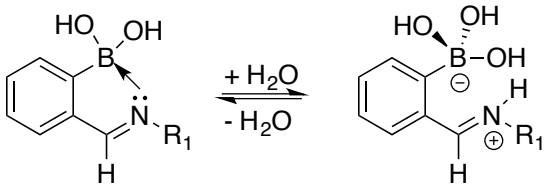

3.18 **3.19**

Scheme 3.11: Modes of nitrogen-boron interaction in *ortho*-iminomethylphenylboronic acids.

To fully study the binding properties and formation constants of boronate esters with 1,2-ethanediol and 1,3-propanediol, Yoshimura *et al*. employed ^{11}B-NMR spectroscopy in combination with computer-generated modeling. For boronate-1,2-ethanediol interactions, their results showed that besides the formation of the well-known 1:1 (**3.20**) and 1:2 (**3.21**) borate-1,2-ethandiol complexes, two other complexes were found representing a monochelated complex 1:1 (**3.22**) and a bischelated complex 1:2 (**3.23**). For the borate-1,3-propanediol interactions, the same types of complexes were found: 1:1 (**3.24**), 1:2 (**3.25**), 1:1 (**3.26**) and 1:2 (**3.27**). Interestingly, upon mixing all three components, (borate, 1,2-ethandiol, 1,3-propanediol) a new boron signal appeared at ~5 ppm appeared. This was suggested to be a bischelate 1:2 complex, **3.28**, comprised of all three components (Figure 3.3).[64]

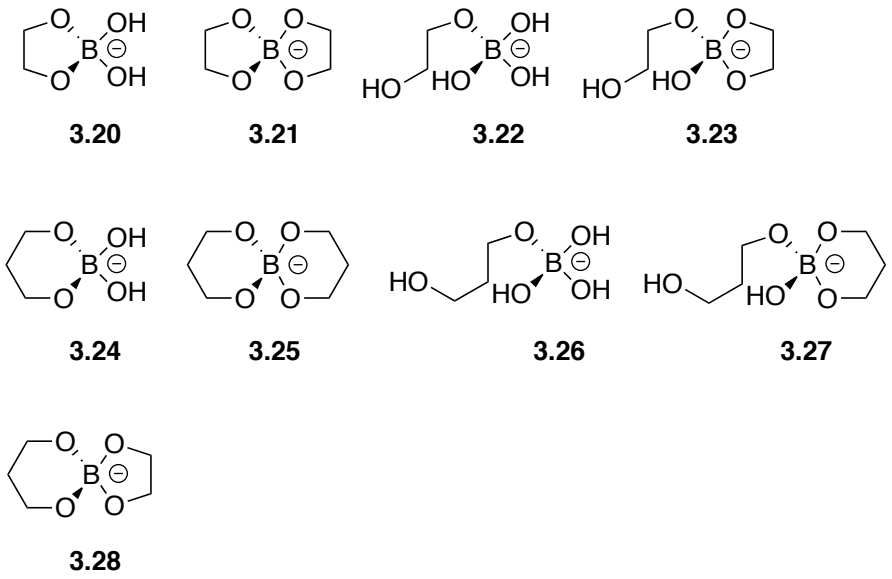

Figure 3.3: Complexes formed upon addition of 1,2-ethanediol and/or 1,3-propanediol to borate.

Yatsimirsky *et al*. used various spectroscopic titration methods to determine the effect of substituents on boronic acids **3.29**, **3.1**, and **3.30** with several diols.[65] The observed equilibrium constants (K_{obs}) were additionally determined by ^{11}B NMR spectroscopy by titration of **3.31** into solutions of the three boronic acids. For this experiment, **3.29**, **3.1**, and **3.30** each showed only one boron signal at 31.0, 31.8 and 31.6 ppm, respectively. These signals corresponded to the free boronic acid in the trigonal planar ester geometry. Titration of **3.31** into the solution of boronic acid at pH 5.5 showed the appearance of new peaks at 12.9, 13.4 and 13.5 ppm, for **3.29**, **3.1**, and **3.30**, respectively. These chemical shifts indicated the formation of the tetrahedral ester complex (Scheme 3.12). Unfortunately, the K_{obs} found using the ^{11}B NMR titration experiment was significantly lower than the K_{obs} calculated using spectrophotometric titrations. The authors suggested that the quadrupolar interactions of the ^{11}B nucleus and the aryl aromatic rings enhanced signal broadening which perturbs the NMR signal areas.

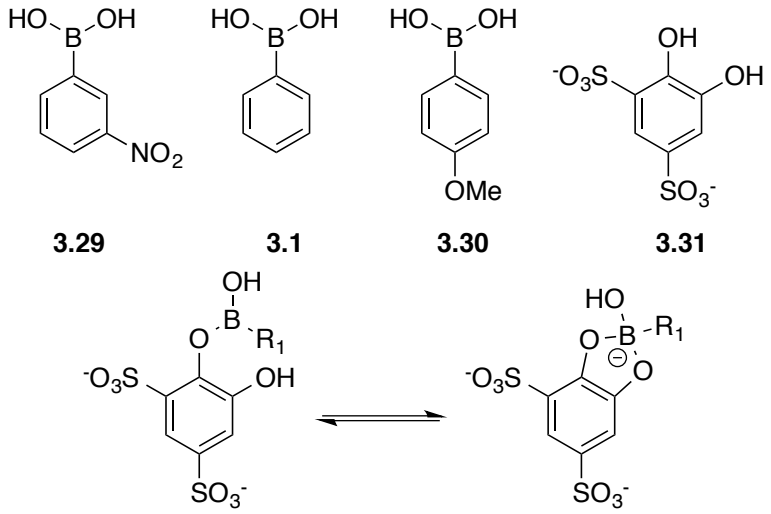

Scheme 3.12: Equilibrium between modes of complexation.

3.5[f] STRUCTURAL STUDIES OF *ORTHO*-IMINOARYLBORONATE SYSTEMS

The Bull and James groups have developed a series of three-component assemblies using boronic acids with the goal of generating chiral shift reagents.[66–71] The enantio-discriminating unit is formed by the reaction of enantiopure 1,1'-bi-2-naphthol (**BINOL**), 2-formylphenylboronic acid (**2-FPBA**), and an α-chiral primary amine. The three-component assembly forms a Schiff base and a boronate ester (Scheme 3.13). The different diastereomers formed have distinct ^{1}H NMR spectra, and the intensities thereof can be directly related to the enantiomeric composition of the original amine. This reaction is fast, highly efficient, and relatively simple, requiring no purification steps.

[f] Sections 3.5-3.6 were written in parallel with a manuscript for publication: Chapin, B. M.; Metola, P.; Lynch, V. M.; Stanton, J. F.; James, T. D.; Anslyn, E. V. Structural and Thermodynamic Analysis of a Three-Component Assembly Forming *ortho*-Iminophenylboronate Esters. *J. Org. Chem.* Accepted July 27, 2016.

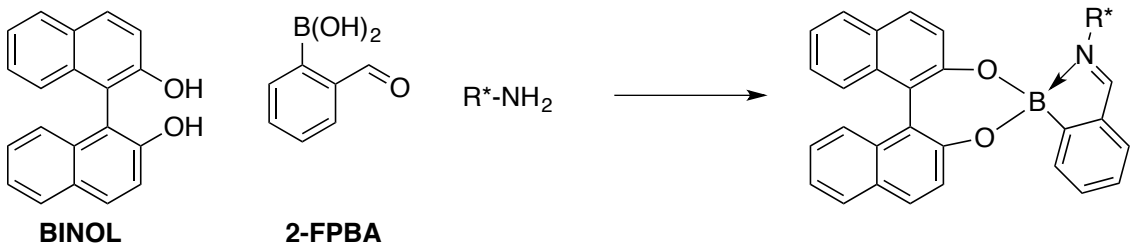

Scheme 3.13: Three-component assembly developed by the James and Bull groups.

While the Bull-James assembly employs an *ortho*-imino group, one of the most common design elements that facilitate the recognition of diols at neutral pH is an *ortho*-aminomethyl group on a phenylboronic acid. This functionality leads to an increase in binding under physiological conditions.[72,73] One consequence of the interest in such systems was the discovery by the Anslyn group of the prevalence of two different types of interactions between the boronic acid functionality and the amine, as described in Section 3.4.[60] Through the use of several coupled analytical techniques, such as ^{11}B NMR spectroscopy, X-ray diffraction, and computational modeling, it was determined that distinct ^{11}B NMR chemical shift values could be assigned to the two binding modes of tetrahedral boron. These shifts were determined to be 13-15 ppm for N-B bonded structures, and 9-11 ppm for solvent-inserted structures. One of the main conclusions of this work was that aprotic solvents favor the N-B bonded form while protic solvents promote near exclusive formation of the solvent-inserted mode of interaction. This was found for both boronic acids and boronate esters.

We reasoned that the same kind of analysis employed to structurally characterize *ortho*-aminomethylphenylboronate complexes could be used to characterize *ortho*-iminoarylboronate complexes such as those that arise in the Bull-James assembly. Thus, we set out to decipher the extents of N-B bond or solvent insertion using our group's previously developed ^{11}B NMR spectroscopic methods. The system we elected to

characterize is the three-component binding of *ortho*-formylphenylboronic acid (**2-FPBA**, B), catechol (D), and benzylamine (A) (Scheme 3.14).

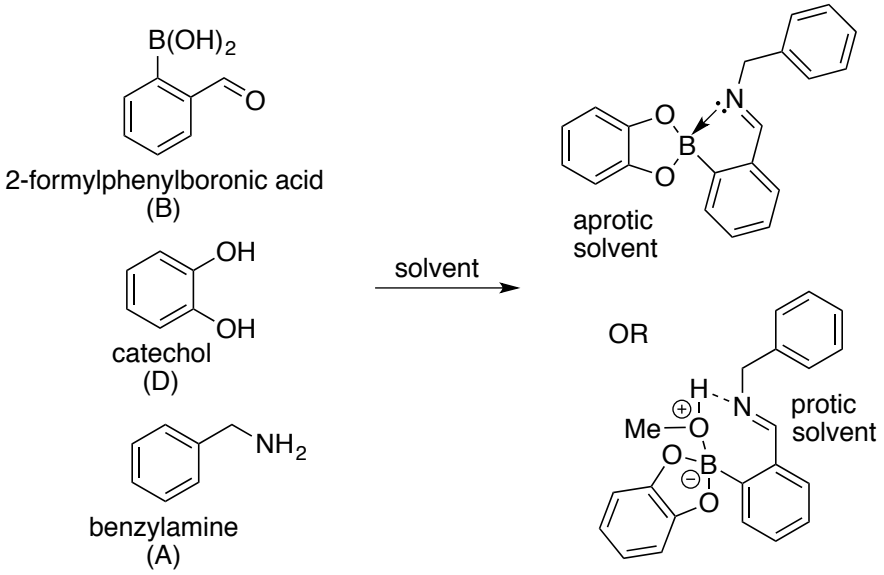

Scheme 3.14: Three-component assembly with 2-FPBA, catechol, and benzylamine.

In an effort to characterize the coordination modes and structures of the components involved in the Bull-James assembly, a number of ^{11}B NMR titrations were undertaken. The chemical shifts for the boron resonances were referenced to numbers obtained and established in prior work.[60,62] While such resonances present clear distinctions, several other resonances appear in the experiments discussed below, which are attributed to intermediates in the condensation mechanisms. Some of these assignments are speculative, albeit quite logical, based upon the mechanisms of Schiff-base formation, boronate ester formation, and the pK_a values of iminium and ammonium groups. Additionally, ^{1}H NMR titrations run in parallel with the ^{11}B NMR titrations were used to confirm or correct the ^{11}B assignments. While ^{1}H NMR was a useful tool in this sense, ^{11}B NMR still brings with it the benefits of having less complicated spectra and distinctive chemical shifts for the two modes of binding for tetrahedral boron.

3.5.1 ^{11}B and ^{1}H NMR Experiments Performed in Aprotic Solvent

Four titrations were carried out in acetonitrile-d_3 in order to observe each pairwise interaction, as well as the formation of the full three-component assembly. Figure 3.4 shows all of the structures that have been assigned to the NMR peaks in the titrations that follow.

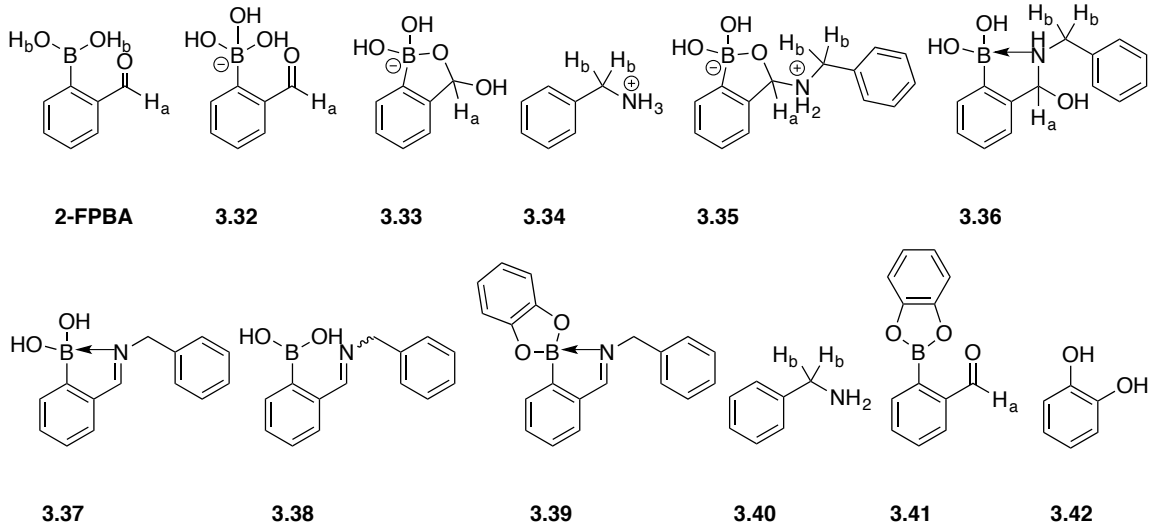

Figure 3.4: Structures assigned to the peaks in the ^{11}B and ^{1}H NMR titrations in aprotic solvent.

In the first study, benzylamine (A, 0-12 mM) was titrated into 2-FPBA (B, 10 mM) in acetonitrile, and an equivalent of catechol (D, 10 mM) was added at the end of the titration (Figure 3.5). The first ^{11}B spectrum (Figure 3.5A) shows **2-FPBA** alone, with only one signal at 29.5 ppm, corresponding to a trigonal boron atom. When benzylamine is first added, a second signal at 7.5 ppm grows in. We attribute this peak to a structure with a hydroxylated boron atom, **3.32**, a result of the ionization of the small amount of water that is present in solution by the weakly basic amine. This supposition is supported by the presence of the downfield aldehyde peak at 10.4 ppm in the ^{1}H spectrum (Figure 3.5B). Compound **3.32** would be in equilibrium with **3.33**, a cyclic hemiacetal. Structure

3.33 is consistent with the very small ^{1}H peak at 8.6 ppm. The hypothesis that structures **3.32** and/or **3.33** form upon ionization of water is supported by a control experiment in which triethylamine was added to 2-FPBA in acetonitrile. A ^{11}B peak at 6.5 ppm in the presence of triethylamine is comparable to the peak at 7.5 ppm in Figure 2a. Since triethylamine is a tertiary amine and cannot form an imine, this result is consistent with formation of a tetrahedral, anionic boron species. The counterion for either **3.32** or **3.33** is benzylammonium, **3.34**. As additional amine is added, a third ^{11}B signal arises at 9 ppm. For this peak, we propose the hemiaminal species **3.35** and **3.36** as potential structures. These species would explain the presence of the ^{1}H peak at 8.25 ppm, corresponding to the methine proton, and the methylene peak is reasonably expected to overlap with the methylene peak of **3.34**, because the nitrogen atom either carries a positive formal charge or is the donor in a dative bond. In this interpretation of the ^{11}B NMR spectra, the first addition of amine acts to dehydrate the solution by being protonated and delivering an equivalent of hydroxide to the boron. As additional amine is added, it begins to incorporate into the assembly. Peaks corresponding to **2-FPBA** and the hydroxylated 2-FPBA species (**3.32** and **3.33**) both disappear as the **3.35/3.36** peak grows. With increasing concentration of amine, a signal at 15.7 ppm dominates the ^{11}B spectrum, while a minor peak at 26.6 ppm appears. The peak at 15.7 ppm is consistent with a N-B interaction, as shown in structure **3.37**, and the peak at 26.6 ppm is a new trigonal species. We attribute this peak to a small amount of an open-form structure **3.38**. That is, we believe this is an imine without a Schiff base interaction. It appears that the N-B bonded and open-form structures, **3.37** and **3.38**, respectively, are in equilibrium with one another, as the ratio between them remains constant. The open-form could be the *E*-imine without the N-B bond, but we suspect that it is more likely the *Z*-imine, which cannot form the N-B bond. Finally, when catechol is added, the ^{11}B spectrum shows only one

peak at 13.5 ppm. This chemical shift is consistent with an N-B interaction, and since it is distinct from the shift of the boronic acid, **3.37**, we attribute this peak to the full assembly, **3.39**.

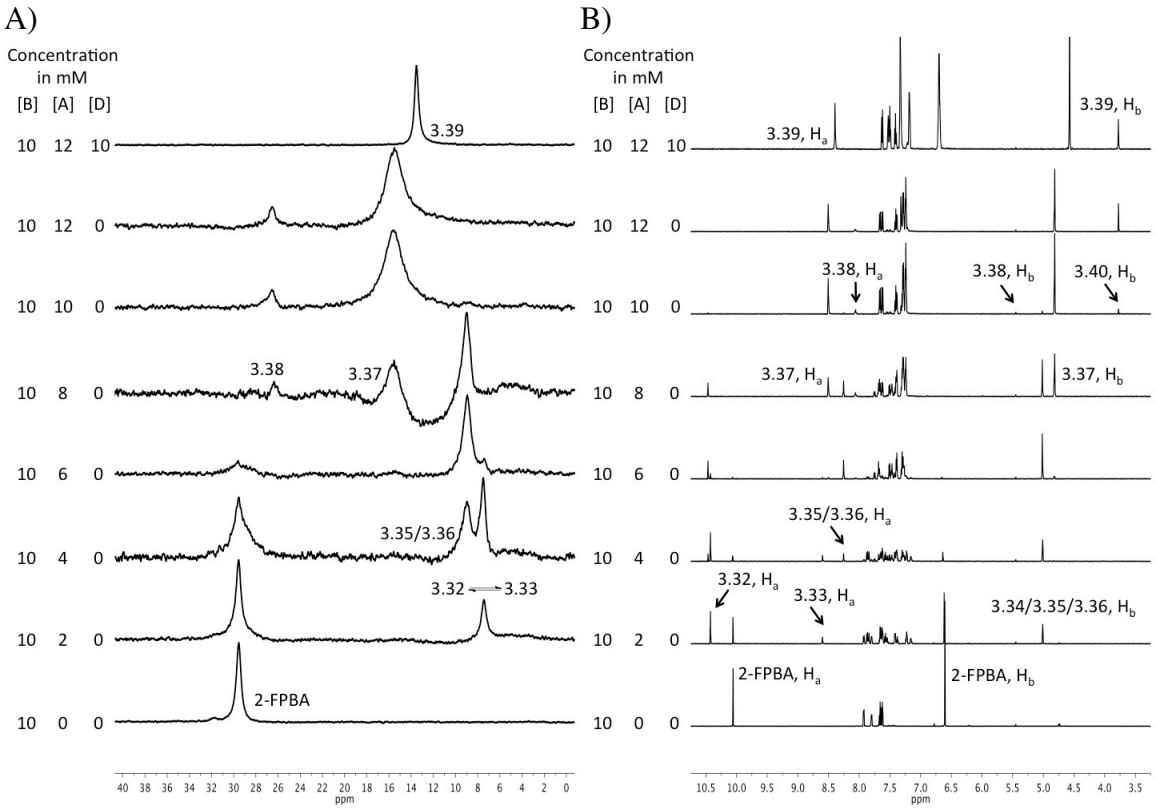

Figure 3.5: ^{11}B (A) and ^{1}H (B) spectra showing the addition of benzylamine (0-12 mM) into 2-FPBA (10 mM) in CD_3CN with the addition of one equivalent (10 mM) of catechol at the end of the titration. The bottom spectrum is 2-FPBA alone.

In the second titration, catechol (D, 0-12 mM) was added to 2-FPBA (B, 10 mM) and benzylamine (A, 10 mM) (Figure 3.6) in acetonitrile. The first ^{11}B spectrum (Figure 3.6A) shows **2-FPBA** alone, with one signal at 29.5 ppm, corresponding to a trigonal boron atom. The 1:1 mixture of 2-FPBA and benzylamine gives a signal at 15.7 ppm, which can be attributed to the N-B bonded imine **3.37**. As well, the peak attributed to

structure **3.38** is present and still appears to be at equilibrium with **3.37**. As expected, this spectrum is identical to the spectrum with one equivalent of amine in Figure 3.5. As catechol is added, the ^{11}B signal for the imine disappears and is replaced by a signal at 13.5 ppm, which represents the full three-component assembly, **3.39**. The imine presumably has a weaker N-B bond than the full assembly, as its signal is further downfield. This change suggests positive cooperativity in the sense that the binding of the diol to boronic acid strengthens the binding (increases the binding constant) of amine binding to the boronic acid.

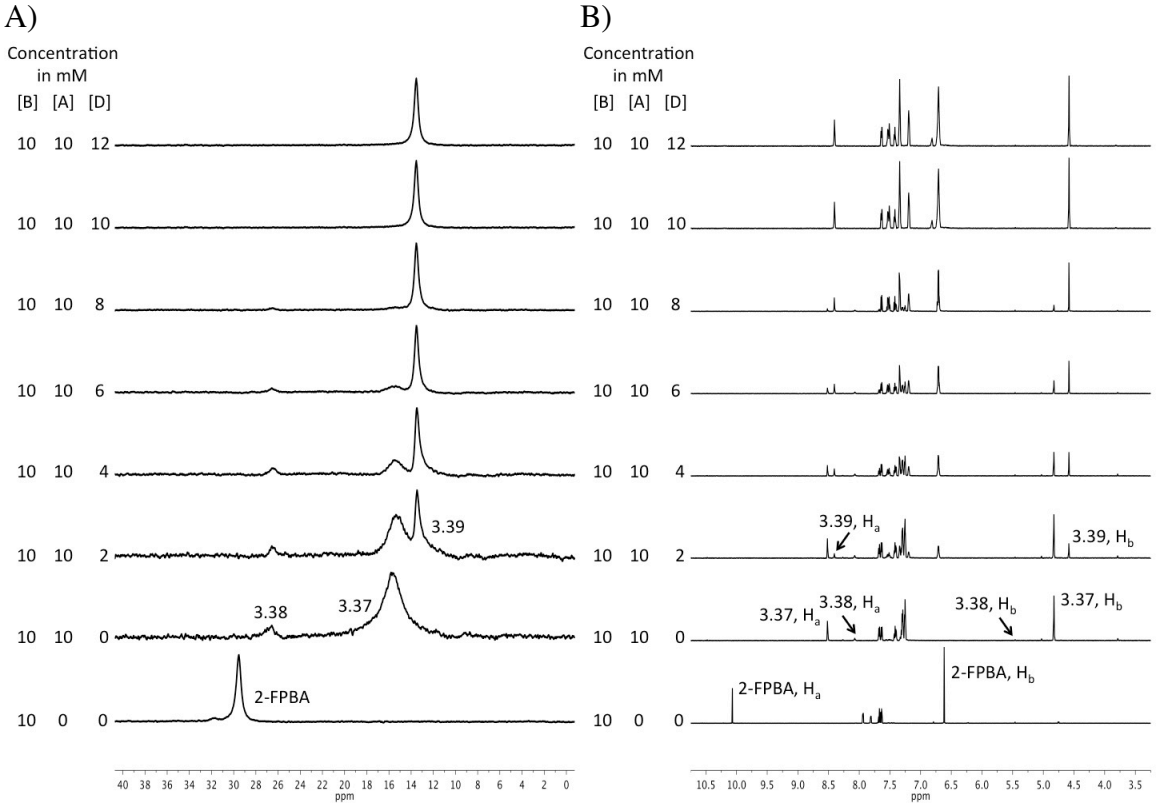

Figure 3.6: ^{11}B (A) and ^{1}H (B) spectra showing the addition of catechol (0-12 mM) into 2-FPBA (10 mM) and benzylamine (10 mM) in CD_3CN. The bottom spectrum is 2-FPBA alone.

In the third titration, catechol (D, 0-12 mM) was titrated into 2-FPBA (B, 10 mM) and an equivalent of benzylamine (A, 10 mM) was added at the end of the titration. (Figure 3.7). The first ^{11}B spectrum (Figure 3.7A) shows **2-FPBA** alone. The 1:1 mixture of 2-FPBA and catechol shows signals for the boronic acid **2-FPBA** as well as the boronate ester **3.41**, at 32.4 ppm. The addition of catechol to form the boronate ester results in a downfield shift, suggesting that catechol is more electron-withdrawing than the hydroxyl groups. The ^{1}H spectrum (Figure 3.7B) is consistent with this assignment, as the catechol peaks centered at 6.7 ppm (**3.42**) shift to 7.3 ppm (**3.41**). Unlike the addition of amine that leads to full condensation on the aldehyde at one or slightly more than one equivalent, the combination of catechol is far from complete with the boronic acid at one equivalent. Yet, addition of an equivalent of amine leads to full complexation of the catechol. Thus, it appears that the amine cooperatively assists the condensation of catechol.

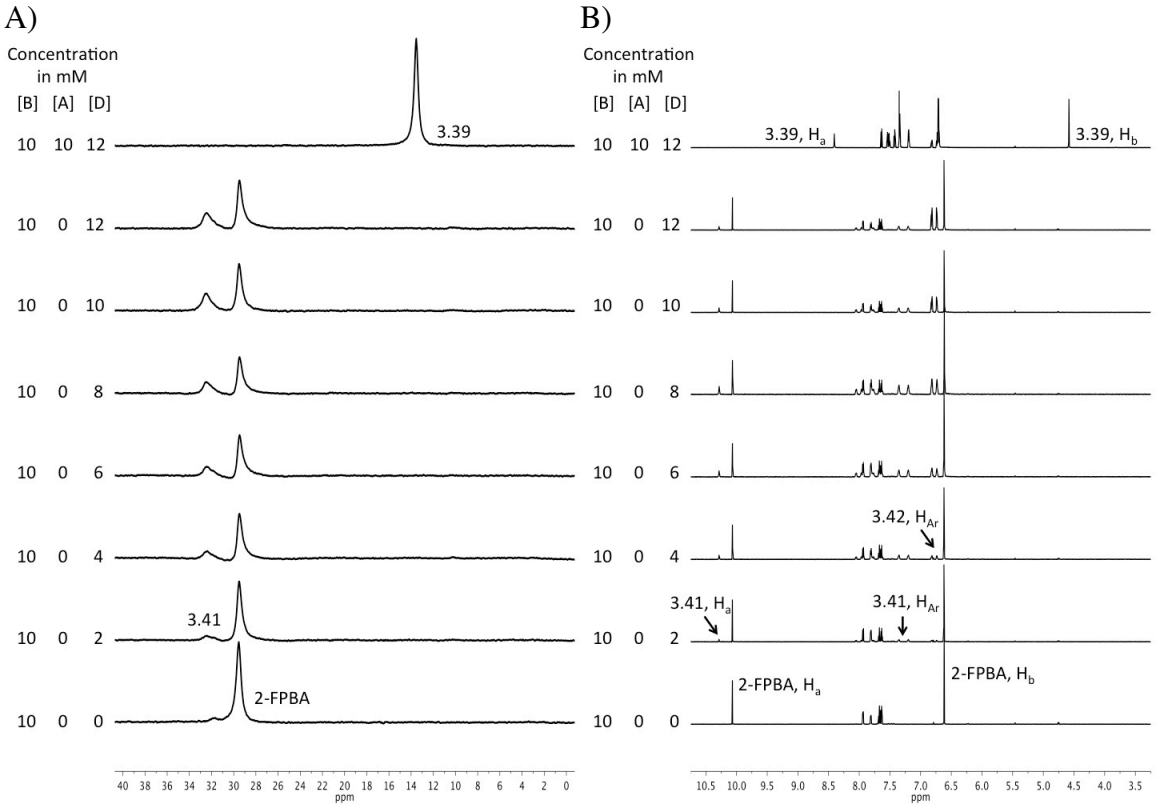

Figure 3.7: ^{11}B (A) and ^{1}H (B) spectra showing the addition of catechol (0-12 mM) into 2-FPBA (10 mM) in CD_3CN with the addition of one equivalent (10 mM) of benzylamine at the end of the titration. The bottom spectrum is 2-FPBA alone.

In the fourth titration, benzylamine (A, 0-12 mM) was titrated into 2-FPBA (B, 10 mM) and catechol (D, 10 mM) (Figure 3.8). The first ^{11}B spectrum (Figure 3.8A) shows 2-FPBA alone. The 1:1 mixture of 2-FPBA and catechol again shows signals for the boronic acid **2-FPBA** and the boronate ester **3.41**. The ^{1}H shift of the catechol peaks in Figure 3.7B is also evident in Figure 3.8B. As benzylamine is added, the signal for the three-component assembly begins to dominate and then becomes the sole signal when [A] = 10 mM.

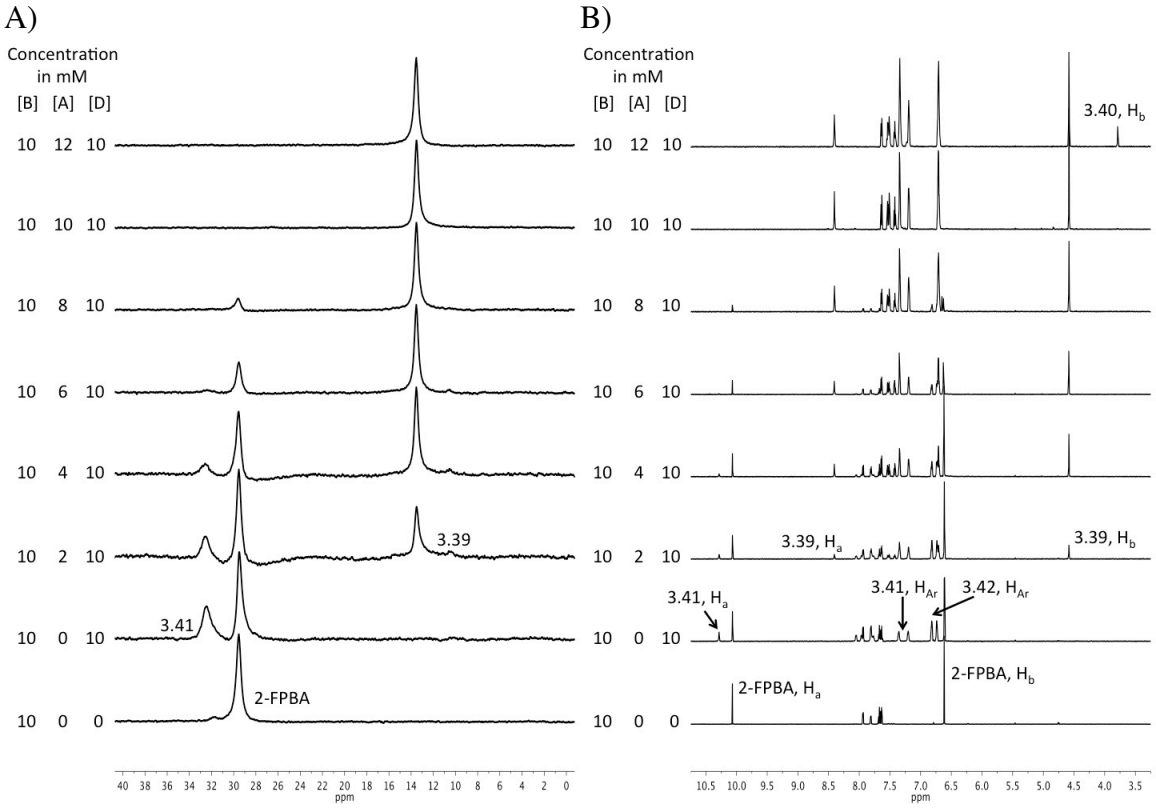

Figure 3.8: ^{11}B (A) and ^{1}H (B) spectra showing the addition of benzylamine (0-14 mM) into 2-FPBA (10 mM) and catechol (10 mM) in CD_3CN. The bottom spectrum is 2-FPBA alone.

Throughout these four titrations, various hemiaminal and N-B bonded species were assigned using a combination of ^{11}B and ^{1}H peaks. A crystal grown from acetonitrile confirms our assignment of the N-B bond in the 1:1:1 complex (Figure 3.9). This N-B bond measures 1.65 Å, which is consistent with a dative bond. The imine bond is 1.28 Å, which is a typical bond length for a C=N bond.

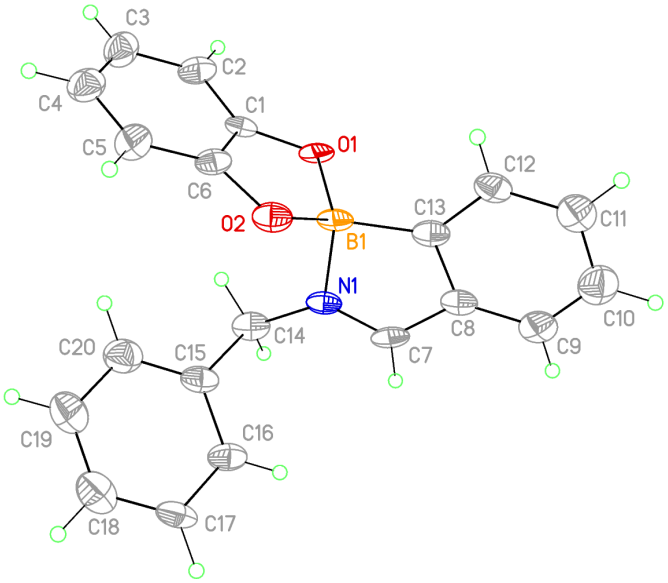

Figure 3.9[g]: Crystal structure of 2-formylphenylboronic acid, catechol, and benzylamine. The crystal was grown in acetonitrile.

3.5.2 ^{11}B and ^{1}H NMR Experiments Performed in Protic Solvent

Four titrations were carried out in methanol-d_4 in order to observe each pairwise interaction, as well as the formation of the full three-component assembly. Figure 3.10 shows all of the structures that have been assigned to the NMR peaks in the titrations that follow.

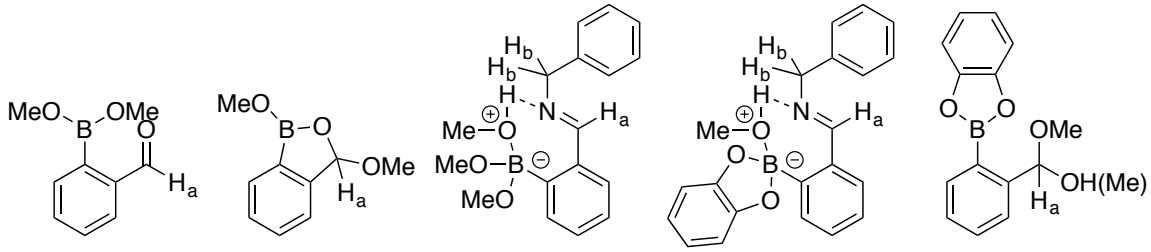

3.43 **3.44** **3.45** **3.46** **3.47**

Figure 3.10: Structures assigned to the peaks in the ^{11}B and ^{1}H NMR titrations in protic solvent.

[g] The crystal was grown by Dr. Pedro Metola and its structure was solved by Dr. Vincent Lynch.

For the first study in protic media, benzylamine (A, 0-14 mM) was titrated into 2-FPBA (B, 10 mM) in methanol, and an equivalent of catechol (D, 10 mM) was added at the end of the titration (Figure 8). The first ^{11}B spectrum (Figure 8a) shows 2-FPBA alone, with two signals at 30 and 31 ppm, corresponding to trigonal boron. We attribute one signal to the boronate ester formed with the solvent (**3.43**), and the other signal to a cyclic boronate acetal (**3.44**). This is consistent with the ^{1}H spectrum (Figure 8b), which shows a singlet at 6 ppm for the acetal proton. As amine is added, a ^{11}B signal at 10.6 ppm emerges. This signal corresponds to the solvent-inserted imine, **3.45**. When an equivalent of catechol is added, no new peaks emerge, and the signal remains at 10.6 ppm. Presumably, the imine and the full assembly, **3.46**, coincidentally have the same chemical shift. The same coincidental overlap was observed in studies of *ortho*-(aminomethyl)phenylboronic acid condensation with diols in methanol.[60]

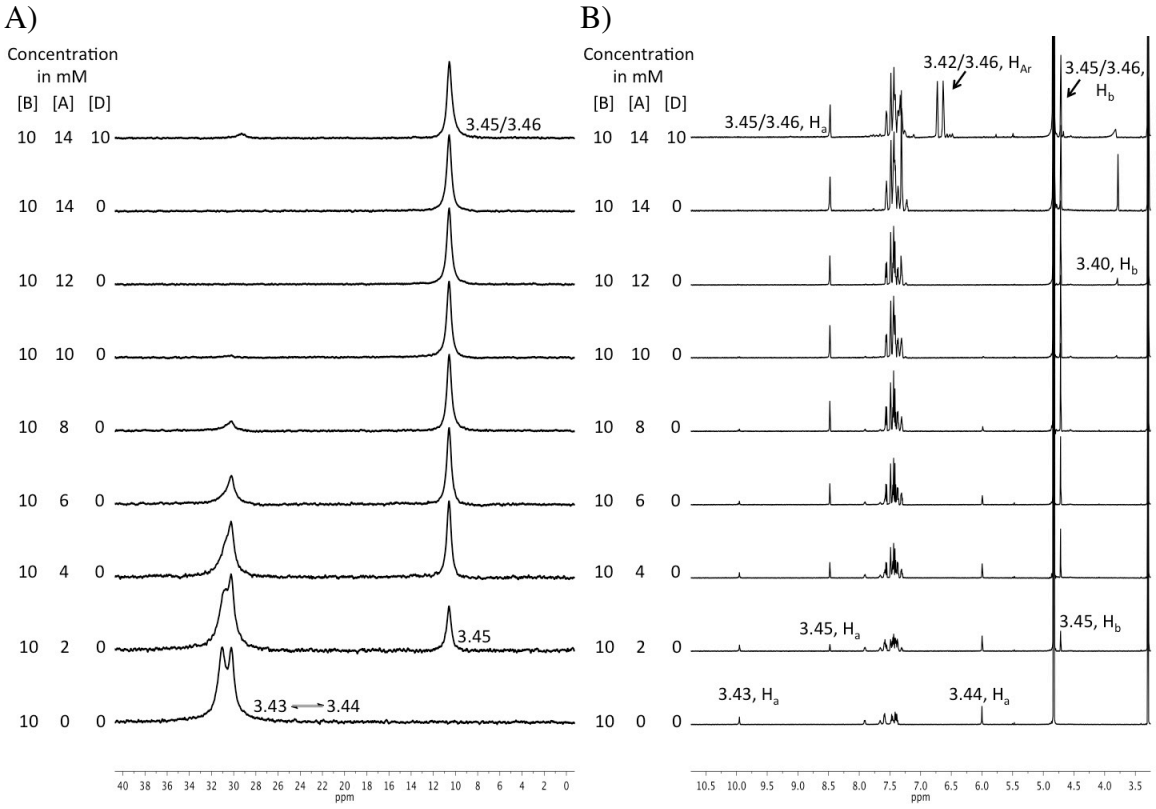

Figure 3.11: ^{11}B (A) and ^{1}H (B) spectra showing the addition of benzylamine (0-14 mM) into 2-FPBA (10 mM) in CD_3OD with the addition of one equivalent (10 mM) of catechol at the end of the titration. The bottom spectrum is 2-FPBA alone.

In the second titration, catechol (D, 0-12 mM) was titrated into 2-FPBA (B, 10 mM) and benzylamine (A, 10 mM) (Figure 3.12). The first ^{11}B spectrum (Figure 3.12A) shows 2-FPBA alone. The 1:1 mixture of 2-FPBA and benzylamine gives a signal at 10.6 ppm, and titrating in catechol does not effect any change due to the chemical shift overlap of **3.45** and **3.46**. Importantly, in this titration there is only one set of aromatic peaks for catechol in the ^{1}H spectrum (Figure 3.12A). It is possible that catechol is thus only in one form (all bound or none bound) or that in the ^{1}H spectrum, as well as the ^{11}B spectrum, there is chemical shift overlap between species.

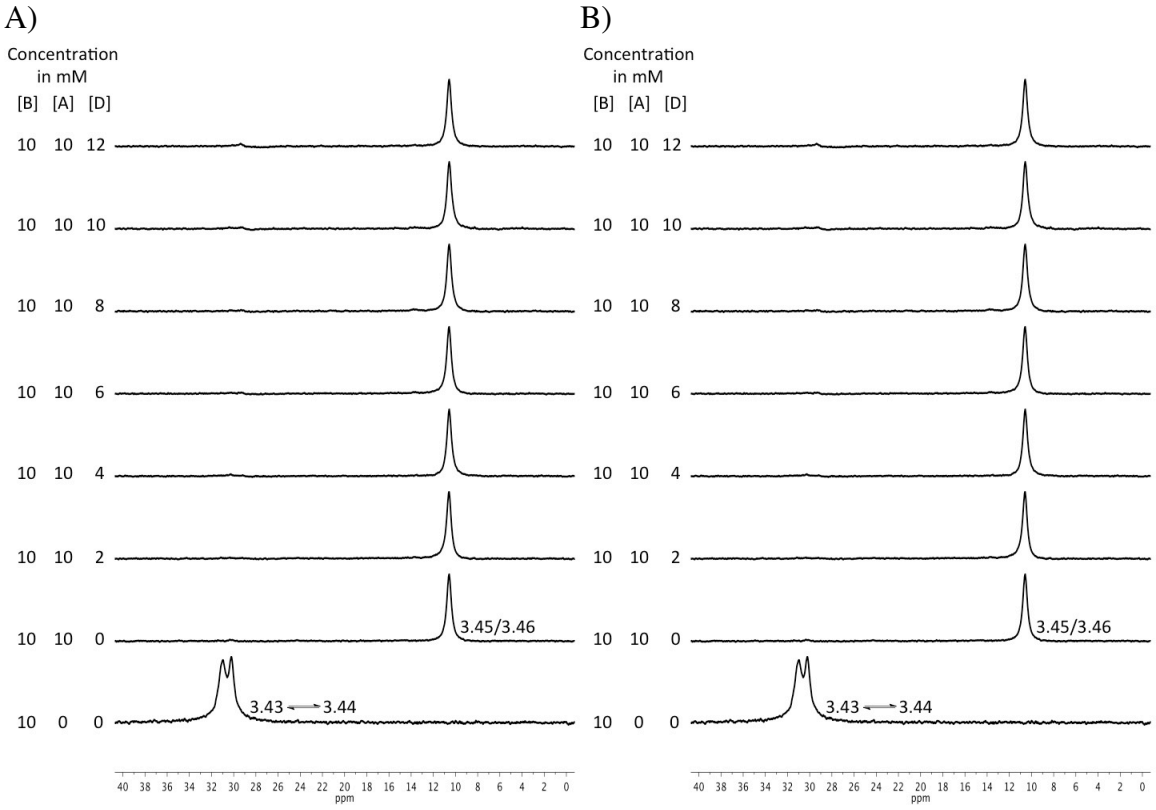

Figure 3.12: ^{11}B (A) and ^{1}H (B) spectra showing the addition of catechol (0-12 mM) into 2-FPBA (10 mM) and benzylamine (10 mM) in CD_3OD. The bottom spectrum is 2-FPBA alone.

In the third titration, catechol (D, 0-60 mM) was titrated into 2-FPBA (B, 10 mM) and an equivalent of benzylamine (A, 10 mM) was added at the end of the titration (Figure 3.13). The first ^{11}B spectrum (Figure 3.13A) shows 2-FPBA alone. As catechol was added, a peak grew in at 29.3 ppm. This peak in the trigonal boron region was thought to be the boronate ester formed with catechol, **3.41**. However, the only aldehyde peak in the ^{1}H spectrum (Figure 3.13B) is for the methanol ester, **3.43**. For this reason, we propose structure **3.47**, which still contains a boronate ester, but no longer contains an aldehyde due to attack of the solvent. This is reasonable because the acetal **3.44** is observed, so the acetal or hemiacetal **3.47** can be expected to form under the same

conditions. After one equivalent of benzylamine was added, the signal at 10.6 ppm demonstrated formation of the three-component assembly, **3.46**. Once again, as in acetonitrile, catechol does not bind strongly enough to fully convert the boronic acid (in this case, methyl boronate ester) to catechol boronate ester until an equivalent of amine is added. Note here that formation of the catechol boronate ester doesn't go to completion even in the presence of six equivalents of catechol. This titration shows that there is indeed chemical shift overlap between species; even as **3.43**, **3.44**, and **3.47** can be seen to form **3.45** and **3.46** in the ^{11}B spectrum as amine is added, the peaks for catechol in the ^{1}H spectrum still remain unchanged.

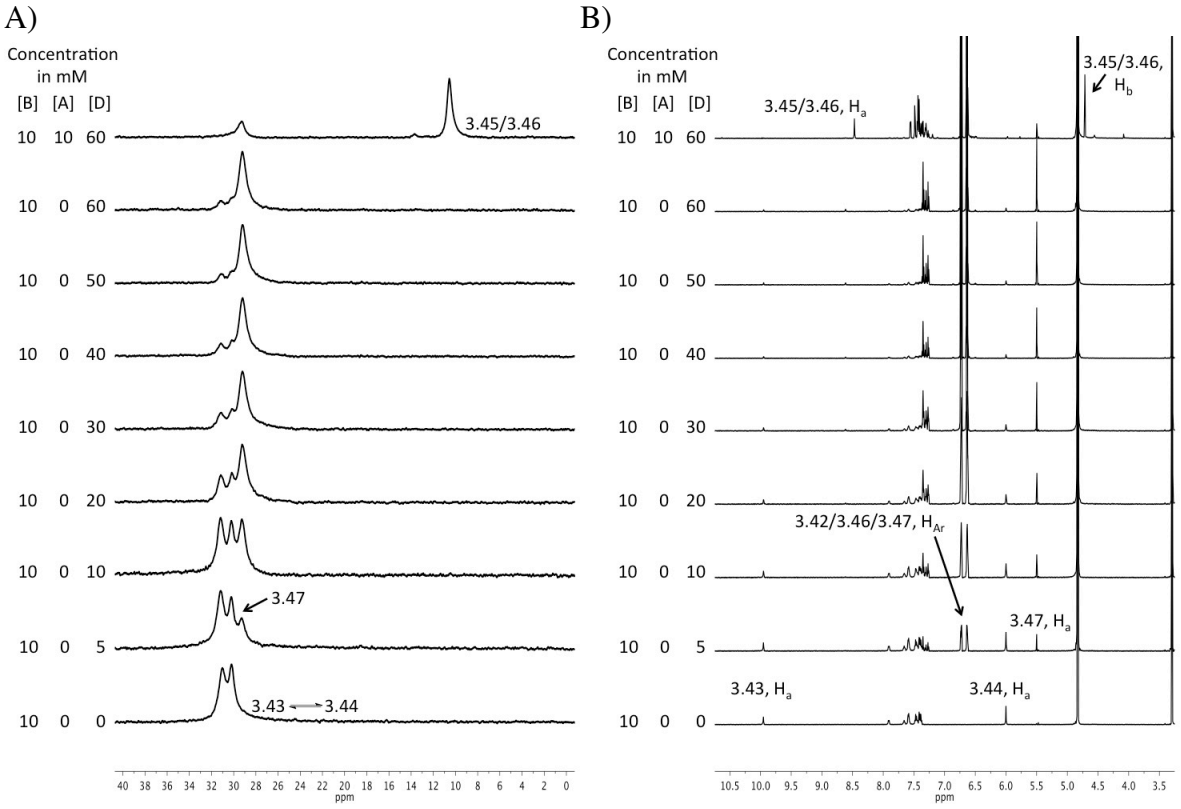

Figure 3.13: ^{11}B (A) and ^{1}H (B) spectra showing the addition of catechol (0-60 mM) into 2-FPBA (10 mM) in CD_3OD with the addition of one equivalent (10 mM) of benzylamine at the end of the titration. The bottom spectrum is 2-FPBA alone.

In the fourth titration, benzylamine (A, 0-14 mM) was titrated into 2-FPBA (B, 10 mM) and catechol (D, 10 mM) (Figure 3.14). The first ^{11}B spectrum (Figure 3.14A) shows 2-FPBA alone. The 1:1 mixture of 2-FPBA and catechol shows signals for the methanolic boronate ester **3.43**, the boronate acetal **3.44** and the catechol boronate ester **3.47**, just as in Figure 3.13. As benzylamine is added, the signal for the three-component assembly begins to dominate.

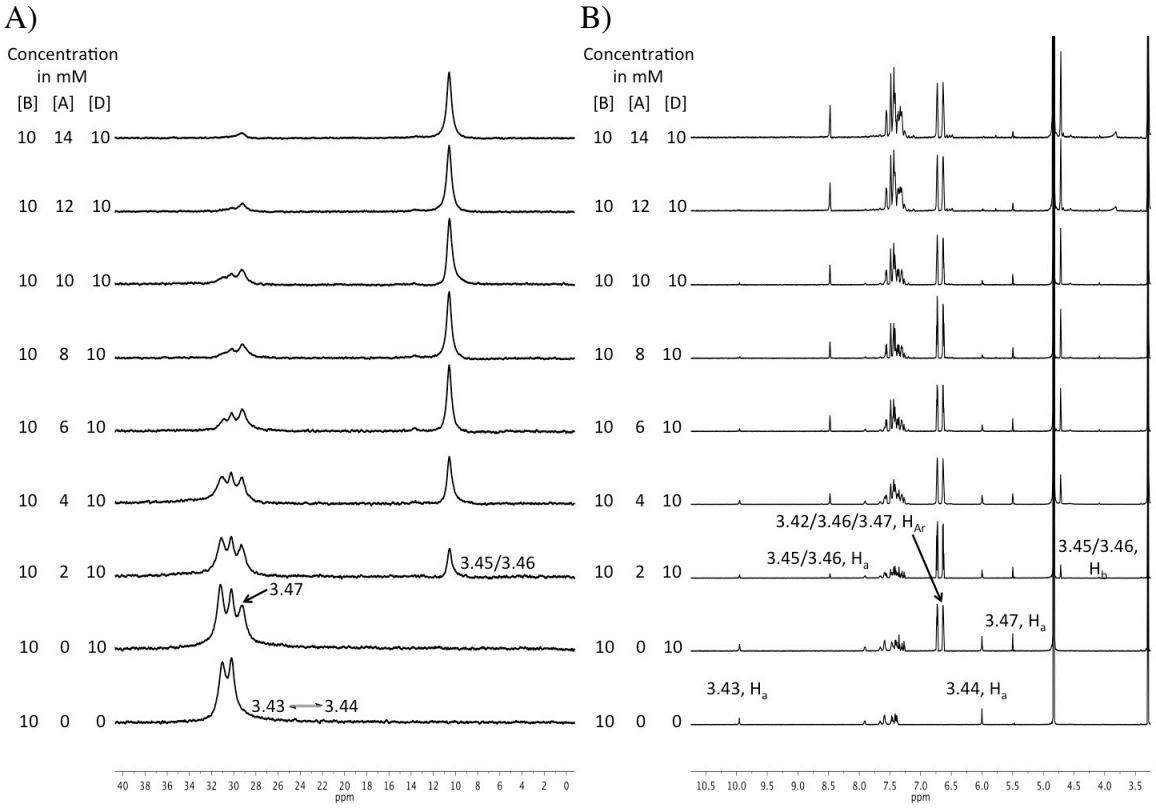

Figure 3.14: ^{11}B (A) and ^{1}H (B) spectra showing the addition of benzylamine (0-14 mM) into 2-FPBA (10 mM) and catechol (10 mM) in CD_3OD. The bottom spectrum is 2-FPBA alone.

In the four titrations in methanol, tetrahedral boron was always in the range of what has been assigned to solvent-inserted species in *ortho*-(aminomethyl)phenylboronic acids, and thus the *ortho*-iminophenylboronic acids and boronate esters were assigned to solvent-inserted species as well.

3.6 EQUILIBRIUM STUDIES OF *ORTHO*-IMINOARYLBORONATE SYSTEMS

Host-guest equilibrium chemistry is typically described by one-to-one or two-to-one binding, and our group and others have previously published algebraic equations to describe the associated equilibria.[74,75] However, a mathematical description of a system in

which one host binds two distinct guests has not yet been described. Such a three-component assembly allows for the possibilities of either guest binding the host first, or, potentially, an entropically unlikely simultaneous binding of both guests in a termolecular reaction. If, as expected, the two guests do not bind simultaneously, there is also a possibility for either positive or negative cooperativity – that is, binding of the first guest could increase or decrease, respectively, the binding constant of the second guest relative to the binding constant in the absence of the first guest.

In the following sections, we lay out the derivation and application of a seventh-order polynomial to describe the complex equilibria at play in the paradigmatic Bull-James assembly. This assembly serves as a model system, but the same equations could be applied to any system that involves one host and two distinct guests.

3.6.1 Deriving a Polynomial for the Three-Component Assembly

For the purposes of deriving the mathematical equations that describe the complex equilibrium of the three-component assembly, the binding constants and species involved will be defined as shown in Scheme 3.15.

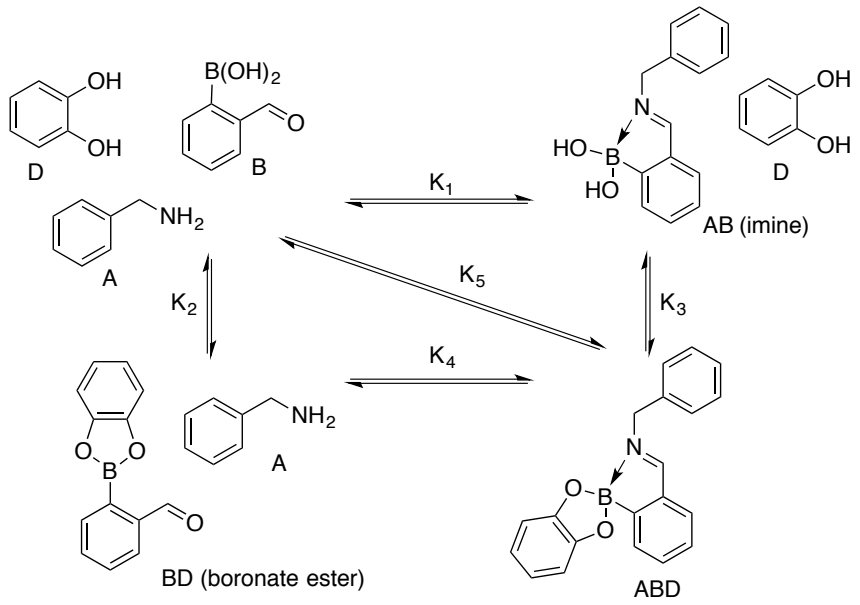

Scheme 3.15: Binding constants and species involved in the formation of the three-component assembly. The analogous structures for AB and ABD in methanol would have inserted solvent.

We begin the process by outlining the system of equations as defined by the association constant expressions (Equations 3.1 – 3.5) and the mass balances (Equations 3.6 – 3.8).

$K_1[A][B] = [AB]$ Equation 3.1

$K_2[B][D] = [BD]$ Equation 3.2

$K_3[AB][D] = [ABD]$ Equation 3.3

$K_4[BD][A] = [ABD]$ Equation 3.4

$K_5[A][B][D] = [ABD]$ Equation 3.5

$[A]_T = [A] + [AB] + [ABD]$ Equation 3.6

$[B]_T = [B] + [AB] + [BD] + [ABD]$ Equation 3.7

$[D]_T = [D] + [BD] + [ABD]$ Equation 3.8

Our objective is to express [ABD] as a function of the constants K_i, $[A]_T$, $[B]_T$, $[D]_T$ and the variable [B]. Note that $[X]_T$ denotes the initial concentration of X, and the total amount of all species that contain X at equilibrium.

Substitute Equations 3.1 and 3.2 into Equation 3.7 to arrive at Equation 3.9.

$$[B]_T = [B] + K_1[A][B] + K_2[B][D] + [ABD] \quad \text{Equation 3.9}$$

Substitute Equations 3.1 and 3.2 into Equations 3.6 and 3.8, respectively, and rearrange Equations 3.6 and 3.8 to solve for [A] and [D], respectively, giving Equations 3.10 and 3.11.

$$[A] = \frac{[A]_T - [ABD]}{1+K_1[B]} \quad \text{Equation 3.10}$$

$$[D] = \frac{[D]_T - [ABD]}{1+K_2[B]} \quad \text{Equation 3.11}$$

Substitute Equations 3.10 and 3.11 into Equation 3.9 to reach Equation 3.12.

$$[B]_T = [B] + K_1[B]\left(\frac{[A]_T - [ABD]}{1+K_1[B]}\right) + K_2[B]\left(\frac{[D]_T - [ABD]}{1+K_2[B]}\right) + [ABD] \quad \text{Equation 3.12}$$

Rearrange to isolate [ABD] to produce Equation 3.13.

$$[ABD] = \frac{[B]_T - [B] - \frac{[A]_T K_1[B]}{1+K_1[B]} - \frac{[D]_T K_2[B]}{1+K_2[B]}}{1 - \frac{K_1[B]}{1+K_1[B]} - \frac{K_2[B]}{1+K_2[B]}} \quad \text{Equation 3.13}$$

Multiply Equation 3.13 by $\frac{(1+K_1[B])(1+K_2[B])}{(1+K_1[B])(1+K_2[B])}$ and simplify to get Equation 3.14.

$$[ABD] = \frac{(1+K_1[B])(1+K_2[B])([B]_T - [A]_T - [D]_T - [B]) + (1+K_2[B])[A]_T + (1+K_1[B])[D]_T}{1 - K_1K_2[B]^2} \quad \text{Equation 3.14}$$

Now define $f_i \equiv 1 + K_i[B]$ and rewrite Equation 3.14 as Equation 3.15.

$$[ABD] = \frac{f_1 f_2([B]_T - [A]_T - [D]_T - [B]) + f_2[A]_T + f_1[D]_T}{1 - K_1K_2[B]^2} \quad \text{Equation 3.15}$$

Define the numerator as W, so that in Equation 3.16,

$$W \equiv f_1 f_2([B]_T - [A]_T - [D]_T - [B]) + f_2[A]_T + f_1[D]_T, \quad \text{Equation 3.16}$$

and in Equation 3.17,

$$[ABD] = \frac{W}{1-K_1K_2[B]^2}\,. \quad \text{Equation 3.17}$$

Return to Equation 3.5 and express [ABD] using Equations 3.10 and 3.11 to generate 3.18.

$$[ABD] = K_5 \frac{[B]([A]_T-[ABD])([D]_T-[ABD])}{(1+K_1[B])(1+K_2[B])} \quad \text{Equation 3.18}$$

Substitute Equation 3.17 into Equation 3.18 to reach Equation 3.19.

$$[ABD] = K_5 \frac{[B]\left([A]_T-\frac{W}{1-K_1K_2[B]^2}\right)\left([D]_T-\frac{W}{1-K_1K_2[B]^2}\right)}{(1+K_1[B])(1+K_2[B])} \quad \text{Equation 3.19}$$

Set Equations 3.17 and 3.19 equal to one another to achieve Equation 3.20.

$$\frac{W}{1-K_1K_2[B]^2} = K_5 \frac{[B]\left([A]_T-\frac{W}{1-K_1K_2[B]^2}\right)\left([D]_T-\frac{W}{1-K_1K_2[B]^2}\right)}{f_1f_2} \quad \text{Equation 3.20}$$

Multiply both sides of Equation 3.20 by $f_1f_2(1-K_1K_2[B]^2)^2$ to give Equation 3.21.

$$f_1f_2(1-K_1K_2[B]^2)W = K_5[B]([A]_T(1-K_1K_2[B]^2)-W)([D]_T(1-K_1K_2[B]^2)-W)$$

Equation 3.21

Finally, Wolfram Mathematica can be used to solve for a polynomial in [B] using the inputs shown below. First, substitutions for f_i and W must be entered (In[1] – In[3]). Then each side of Equation 3.21 must be defined with respect to f_i and W (In[4] and

In[7]). For each side of the equation, Mathematica is used to generate a list of coefficients for each ordered term in the polynomial in [B] (In[5] and In[8]) and to subsequently simplify each list (In[6] and In[9]).

```
In[1]:= f1 = 1 + K1*B

Out[1]= 1 + B K1

In[2]:= f2 = 1 + K2*B

Out[2]= 1 + B K2

In[3]:= W = f1*f2*(BT - AT - DT - B) + f2*AT + f1*DT

Out[3]= DT(1 + B K1) + AT(1 + B K2) + (-AT - B + BT - DT)(1 + B K1)(1 + B K2)

In[4]:= LHS = f1*f2*W*(1 - K1*K2*B^2)

Out[4]= (1 + B K1)(1 + B K2)(1 - B^2 K1 K2)(DT(1 + B K1) + AT(1 + B K2) + (-AT -
        B + BT - DT)(1 + B K1)(1 + B K2))

In[5]:= CoefficientList[LHS,B]

Out[5]= {BT, -1 - AT K1 + 2 BT K1 + 2 BT K2 - DT K2, -2 K1 - AT K1^2 + BT K1^2 -
        2 K2 - 2 AT K1 K2 + 3 BT K1 K2 - 2 DT K1 K2 + BT K2^2 - DT K2^2, -K1^2 -
        3 K1 K2 - AT K1^2 K2 - DT K1^2 K2 - K2^2 - AT K1 K2^2 - DT K1 K2^2, AT
        K1^3 K2 - BT K1^3 K2 + AT K1^2 K2^2 - 3 BT K1^2 K2^2 + DT K1^2 K2^2 -
        BT K1 K2^3 + DT K1 K2^3, K1^3 K2 + 3 K1^2 K2^2 + 2 AT K1^3 K2^2 - 2
        BT K1^3 K2^2 + DT K1^3 K2^2 + K1 K2^3 + AT K1^2 K2^3 - 2 BT K1^2
        K2^3 + 2 DT K1^2 K2^3, 2 K1^3 K2^2 + 2 K1^2 K2^3 + AT K1^3 K2^3 - BT
        K1^3 K2^3 + DT K1^3 K2^3, K1^3 K2^3}

In[6]:= Simplify[%5]

Out[6]= {BT, -1 - AT K1 - DT K2 + 2 BT(K1 + K2), (-AT + BT)K1^2 + K2(-2 + BT K2
        - DT K2) - K1(2 + 2 AT K2 - 3 BT K2 + 2 DT K2), -K2^2 - K1^2 (1 + AT K2 +
        DT K2) - K1 K2 (3 + AT K2 + DT K2), K1 K2 (AT K1(K1 + K2) + DT K2(K1 +
        K2) - BT(K1^2 + 3 K1 K2 + K2^2)), K1 K2 (K2^2 + K1^2 (1 + 2 AT K2 - 2 BT
        K2 + DT K2) + K1 K2(3 + AT K2 - 2 BT K2 + 2 DT K2)), K1^2 K2^2 (2 K2 +
        K1(2 + AT K2 - BT K2 + DT K2)), K1^3 K2^3}

In[7]:= RHS = K5*B*(AT*(1-K1*K2*B^2)-W)*(DT*(1-K1*K2*B^2)-W)
```

Out[7]= B(-DT(1 + B K1) - AT(1 + B K2) - (-AT - B + BT - DT)(1 + B K1)(1 + B K2) + AT(1 - B^2 K1 K2))(-DT(1 + B K1) - AT(1 + B K2) - (-AT - B + BT - DT)(1 + B K1)(1 + B K2) + DT(1 - B^2 K1 K2))K5

In[8]:= CoefficientList[RHS,B]

Out[8]= {0, -AT BT K5 + BT^2 K5 + AT DT K5 - BT DT K5, AT K5 - 2 BT K5 + DT K5 + AT^2 K1 K5 - 3 AT BT K1 K5 + 2 BT^2 K1 K5 + AT DT K1 K5 - BT DT K1 K5 - AT BT K2 K5 + 2 BT^2 K2 K5 + AT DT K2 K5 - 3 BT DT K2 K5 + DT^2 K2 K5, K5 + 3 AT K1 K5 - 4 BT K1 K5 + DT K1 K5 + AT^2 K1^2 K5 - 2 AT BT K1^2 K5 + BT^2 K1^2 K5 + AT K2 K5 - 4 BT K2 K5 + 3 DT K2 K5 + AT^2 K1 K2 K5 - 4 AT BT K1 K2 K5 + 4 BT^2 K1 K2 K5 + 2 AT DT K1 K2 K5 - 4 BT DT K1 K2 K5 + DT^2 K1 K2 K5 + BT^2 K2^2 K5 - 2 BT DT K2^2 K5 + DT^2 K2^2 K5, 2 K1 K5 + 2 AT K1^2 K5 - 2 BT K1^2 K5 + 2 K2 K5 + 4 AT K1 K2 K5 - 8 BT K1 K2 K5 + 4 DT K1 K2 K5 + AT^2 K1^2 K2 K5 - 3 AT BT K1^2 K2 K5 + 2 BT^2 K1^2 K2 K5 + AT DT K1^2 K2 K5 - BT DT K1^2 K2 K5 - 2 BT K2^2 K5 + 2 DT K2^2 K5 - AT BT K1 K2^2 K5 + 2 BT^2 K1 K2^2 K5 + AT DT K1 K2^2 K5 - 3 BT DT K1 K2^2 K5 + DT^2 K1 K2^2 K5, K1^2 K5 + 4 K1 K2 K5 + 3 AT K1^2 K2 K5 - 4 BT K1^2 K2 K5 + DT K1^2 K2 K5 + K2^2 K5 + AT K1 K2^2 K5 - 4 BT K1 K2^2 K5 + 3 DT K1 K2^2 K5 - AT BT K1^2 K2^2 K5 + BT^2 K1^2 K2^2 K5 + AT DT K1^2 K2^2 K5 - BT DT K1^2 K2^2 K5, 2 K1^2 K2 K5 + 2 K1 K2^2 K5 + AT K1^2 K2^2 K5 - 2 BT K1^2 K2^2 K5 + DT K1^2 K2^2 K5, K1^2 K2^2 K5}

In[9]:= Simplify[%8]

Out[9]= {0, -(AT-BT)(BT-DT)K5, (AT - 2 BT + DT)(1 + AT K1 + DT K2 - BT(K1+K2))K5, (1 + DT K1 + 3 DT K2 + DT^2 K1 K2 + DT^2 K2^2 + AT^2 K1(K1 + K2) + BT^2 (K1^2 + 4 K1 K2 + K2^2) - 2 BT (2 K1(1 + DT K2) + K2 (2 + DT K2)) + AT(-2 BT K1^2 + K2 + K1(3 - 4 BT K2 + 2 DT K2)))K5, ((AT - BT)K1^2 (2 + AT K2 - 2 BT K2 + DT K2) + 2 K2(1 - BT K2 + DT K2) + K1(2 + 4 DT K2 + 2 BT^2 K2^2 + DT^2 K2^2 + AT K2(4 - BT K2 + DT K2) - BT K2 (8 + 3 DT K2)))K5, (K2^2 + K1 K2(4 + AT K2 - 4 BT K2 + 3 DT K2) + K1^2 (1 + DT K2 + BT^2 K2^2 - BT K2 (4 + DT K2) + AT K2(3 - BT K2 + DT K2)))K5, K1 K2(2 K2 + K1(2 + AT K2 - 2 BT K2 + DT K2))K5, K1^2 K2^2 K5}

In summary, Mathematica produces two seventh-order polynomials (LHS and RHS) in [B], which can be neatly expressed as a single polynomial, as in Equation 3.22.

$$Polynomial([B]) = \sum_{k=0}^{7} [B]^k (K_5 \rho_k - \lambda_k), \qquad \text{Equation 3.22}$$

where the ρ_k and λ_k terms are as follows.

$$\boldsymbol{\rho_0} = 0$$

$$\boldsymbol{\rho_1} = -([A]_T - [B]_T)([B]_T - [D]_T)$$

$$\boldsymbol{\rho_2} = ([A]_T - 2[B]_T + [D]_T)(1 + K_1[A]_T + K_2[D]_T - (K_1 + K_2)[B]_T)$$

$$\boldsymbol{\rho_3} = 1 + K_1[D]_T + 3K_2[D]_T + K_1K_2[D]_T^2 + K_2^2[D]_T^2 + K_1(K_1 + K_2)[A]_T^2 + (K_1^2 + 4K_1K_2 + K_2^2)[B]_T^2 - 2\big(2K_1(1 + K_2[D]_T) + K_2(2 + K_2[D]_T)\big)[B]_T + \big(-2K_1^2[B]_T + K_2 + K_1(3 - 4K_2[B]_T + 2K_2[D]_T)\big)[A]_T$$

$$\boldsymbol{\rho_4} = K_1^2([A]_T - [B]_T)(2 + K_2[A]_T - 2K_2[B]_T + K_2[D]_T) + 2K_2(1 - K_2[B]_T + K_2[D]_T) + K_1(2 + 4K_2[D]_T + 2K_2^2[B]_T^2 + K_2^2[D]_T^2 + K_2(4 - K_2[B]_T + K_2[[D]]_T)[A]_T - K_2(8 + 3K_2[D]_T)[B]_T)$$

$$\boldsymbol{\rho_5} = K_2^2 + K_1K_2(4 + K_2[A]_T - 4K_2[B]_T + 3K_2[D]_T) + K_1^2(1 + K_2[D]_T + K_2^2[B]_T^2 - K_2(4 + K_2[D]_T)[B]_T + K_2(3 - K_2[B]_T + K_2[D]_T)[A]_T)$$

$$\boldsymbol{\rho_6} = K_1K_2(2K_2 + K_1(2 + K_2[A]_T - 2K_2[B]_T + K_2[D]_T))$$

$$\boldsymbol{\rho_7} = K_1^2K_2^2$$

$$\boldsymbol{\lambda_0} = [B]_T$$

$$\boldsymbol{\lambda_1} = -1 - K_1[A]_T - K_2[D]_T + 2(K_1 + K_2)[B]_T$$

$$\boldsymbol{\lambda_2} = K_1^2(-[A]_T + [B]_T) + K_2(-2 + K_2[B]_T - K_2[D]_T) - K_1(2 + 2K_2[A]_T - 3K_2[B]_T + 2K_2[D]_T)$$

$$\boldsymbol{\lambda_3} = -K_2^2 - K_1^2(1 + K_2[A]_T + K_2[D]_T) - K_1K_2(3 + K_2[A]_T + K_2[D]_T)$$

$$\boldsymbol{\lambda_4} = K_1K_2(K_1(K_1 + K_2)[A]_T + K_2(K_1 + K_2)[D]_T - (K_1^2 + 3K_1K_2 + K_2^2)[B]_T)$$

$$\boldsymbol{\lambda_5} = K_1K_2(K_2^2 + K_1^2(1 + 2K_2[A]_T - 2K_2[B]_T + K_2[D]_T) + K_1K_2(3 + K_2[A]_T - 2K_2[B]_T + 2K_2[D]_T))$$

$$\boldsymbol{\lambda_6} = K_1^2K_2^2(2K_2 + K_1(2 + K_2[A]_T - K_2[B]_T + K_2[D]_T))$$

$$\boldsymbol{\lambda_7} = K_1^3K_2^3$$

3.6.2 Application of the Polynomial to the Three-Component Assembly

Now we turn to the application of the polynomial derived in the section above. In theory, K_1 could be determined using the integrations from Figure 3.5 (aprotic media) and Figure 3.11 (protic media), K_3 could be determined using Figures 3.6 and 3.12, K_2 could be determined using Figures 3.7 and 3.13, and K_4 could be determined using Figures 3.8 and 3.14. However, some of these theoretically possible calculations have complications that render this approach impossible. In acetonitrile, K_1 cannot be determined because formation of the imine (AB) is not represented by a single step, and doesn't even generate a single form of AB. In acetonitrile, K_3 cannot be determined because the three-component assembly forms nearly quantitatively from AB and D. Thus, the binding constant is too large to calculate using NMR spectroscopy. In methanol, K_3 cannot be calculated because the chemical shift of AB is indistinguishable from the chemical shift of ABD. In both solvents, K_4 cannot be calculated because the first step, formation of the boronate ester (BD), is not complete, and thus adding amine would conflate the two steps whose individual binding constants we wish to measure.

This means that the only individual steps we can measure by integration of the ^{11}B NMR spectra is the formation of BD in both solvents, which is represented by the binding constant K_2, and the formation of AB in methanol, which is represented by the binding constant K_1. Thus, we focused solely on analysis in methanol because both K_1 and K_2 could be determined.

K_2 was calculated in methanol by integrating the ^{11}B B and BD signals for three different concentrations of [D], as shown in Figure 3.15. The three spectra shown were chosen because the overlapping B and BD peaks were similar enough in size to make a vertical division in their integrations and still reasonably estimate their areas, as shown in the figure. The resulting calculated concentrations of B, BD, and D (calculated as [D] =

$[D]_T - [BD]$) are shown in Table 3.6. Then the values of K_2 were computed and averaged over the three measurements to give $K_2 = 112\ M^{-1}$. Importantly, the three values are consistent and thus a credible estimation of the value of K_2. The value of K_1 in methanol was calculated to be 1100 M^{-1} using ^{11}B integrations from Figure 3.11, revealing that in protic media, the amine condensation is favorable but still amenable to NMR analysis.

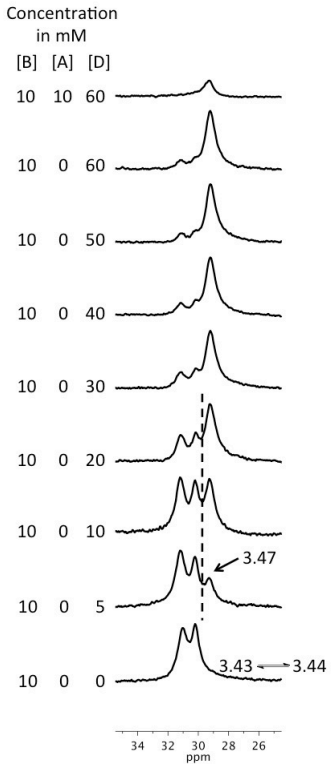

Figure 3.15: Portion of Figure 11a showing the integrations of the B (structures 13 and 14) and BD (structure 17) peaks.

$[D]_T$	[B]	[BD]	[D]	K_2
5 mM	7.61 mM	2.39 mM	2.61 mM	121 M^{-1}
10 mM	6.04 mM	3.96 mM	6.04 mM	109 M^{-1}
20 mM	4.03 mM	5.97 mM	14.0 mM	106 M^{-1}
			Average	**112 M^{-1}**

Table 3.6: Calculated values of [B], [BD], and [D] from the integrations of ^{11}B NMR peaks corresponding to B and BD.

While the polynomial can only be applied to the equilibria of Scheme 3.15 in methanol, the single binding constant that could be extracted in acetonitrile was calculated. The ^{11}B peaks in Figure 3.7 were integrated, concentrations were calculated, and four values of K_2 between 94 and 101 gave an average of $K_2 = 98\ M^{-1}$. Likewise, the precision of the calculated binding constants lends credibility to the value.

Only K_1 and K_2 were able to be calculated directly and empirically in methanol, but the other values can be calculated using the polynomial([B]). With K_1 and K_2 given, K_5 is the only unknown in the polynomial and it can be calculated using K_1 and K_2. A termolecular reaction is unlikely, and therefore is not meant to reflect a mechanism, but K_5 does represent a thermodynamic parameter. Given the fact that $K_5 = K_1 \times K_3 = K_2 \times K_4$, and with K_1, K_2, and K_5 known, we can calculate K_3 and K_4. To execute this approach, Figure 3.14 was reexamined. K_4 could not be calculated from this titration because the reaction corresponding to K_2 was incomplete, but this titration can still be used because it contains A, B, and D, all simultaneously. For a given concentration of $[A]_T = 4$ mM, [B] was calculated by integrating all ^{11}B peak areas to give [B] = 5.417 mM. With a constant $[A]_T$ and measured variable [B], K_5 was calculated to be 2.69×10^6

M^{-2} using Wolfram Mathematica. The calculated values of K_1, K_2, and K_5 were then used to determine K_3 and K_4. The summary of binding constants is shown in Table 3.7.

Binding Constant	Value
K_1	1100 M^{-1}
K_2	112 M^{-1}
K_3	2.45 x 10^3 M^{-1}
K_4	2.40 x 10^4 M^{-1}
K_5	2.69 x 10^6 M^{-2}

Table 3.7: Summary of binding constants in methanol.

To evaluate cooperativity, the values of K_1 and K_4 should be compared (since these binding constants correspond to addition of amine) and the values of K_2 and K_3 should be compared (since these binding constants correspond to the addition of diol). Since K_4 is greater than K_1 and K_3 is greater than K_2, it can be concluded that both guests experience positive cooperativity. In other words, the binding of a guest is improved when the other guest has already bound, and the two binding events reinforce one another. In this way, the numerical analysis mirrors the structural interpretation of binding throughout the ^{11}B and ^{1}H NMR titrations.

3.6.3 Isothermal Titration Calorimetry

In an attempt to confirm the values of K_1 and K_2, we turned to isothermal titration calorimetry (ITC). Figure 3.16 shows the addition of catechol to 2-FPBA in methanol, while Figure 3.17 shows the addition of benzylamine to 2-FPBA in methanol.

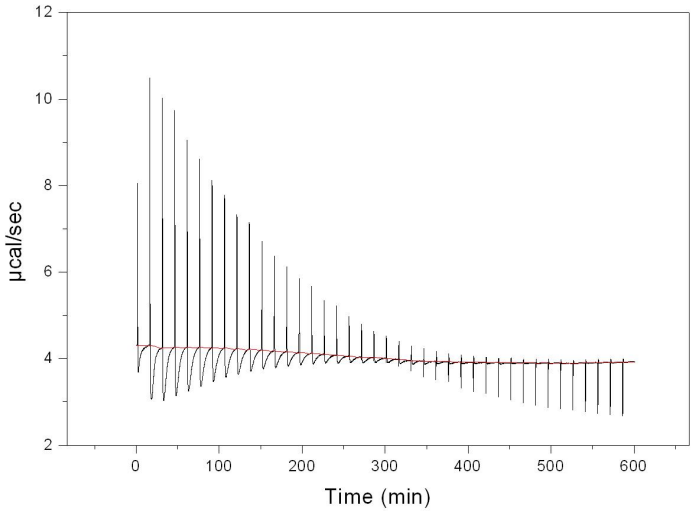

Figure 3.16: ITC of 60 mM catechol added to 4 mM 2-FPBA in methanol. 25 ºC, reference power 5 µcal/sec, stir speed 300. Initial delay 60 s, initial injection 3 µL, all following injections 6 µL with 900 s spacing.

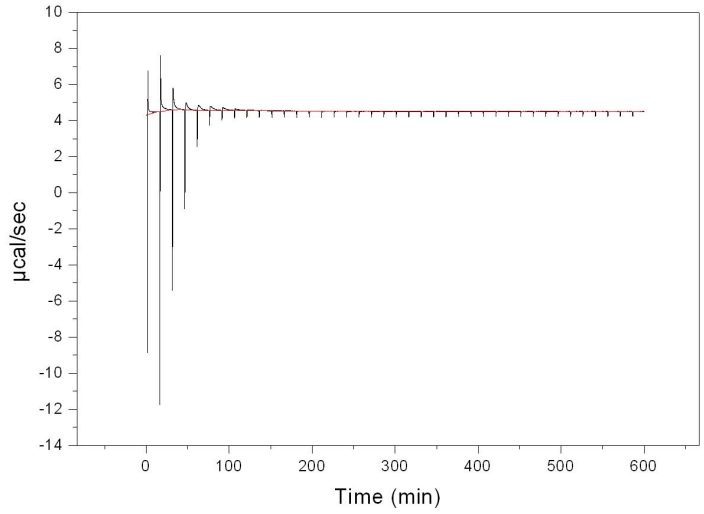

Figure 3.17: ITC of 10 mM benzylamine added to 1.5 mM 2-FPBA in methanol. 25 ºC, reference power 5 µcal/sec, stir speed 300. Initial delay 60 s, initial injection 3 µL, all following injections 6 µL with 900 s spacing.

The ITC results were surprising because straight-forward measurement of the binding constants was expected. However, what was found instead was a combination of exothermic and endothermic steps in the additions, which has been previously been observed in other systems.[76] Figure 3.16 illustrates an initial endothermic phase after each addition of catechol, followed by an exothermic phase. Figure 3.17 shows just the opposite, with the exothermic phase taking place initially, and the endothermic step following. Unfortunately, this multi-phase behavior makes it impossible to calculate a binding constant from the titration data.

Figures 3.18 and 3.19 show the same additions of catechol and benzylamine to 2-FPBA in acetonitrile.

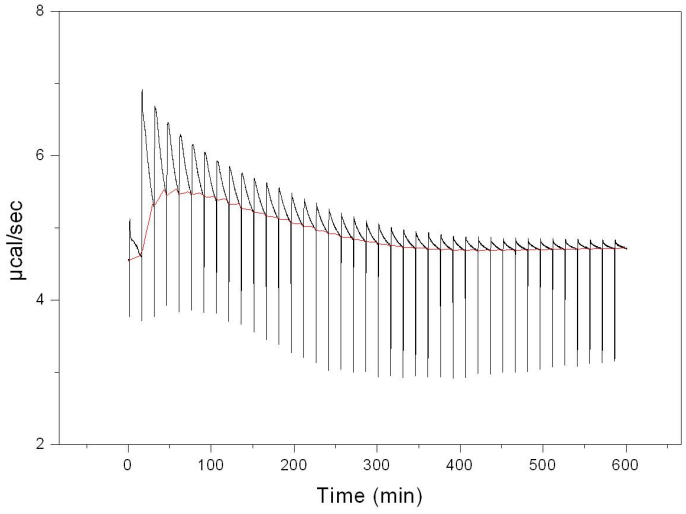

Figure 3.18: ITC of 50 mM catechol added to 4 mM 2-FPBA in acetonitrile. 25 ºC, reference power 5 µcal/sec, stir speed 300. Initial delay 60 s, initial injection 3 µL, all following injections 6 µL with 900 s spacing.

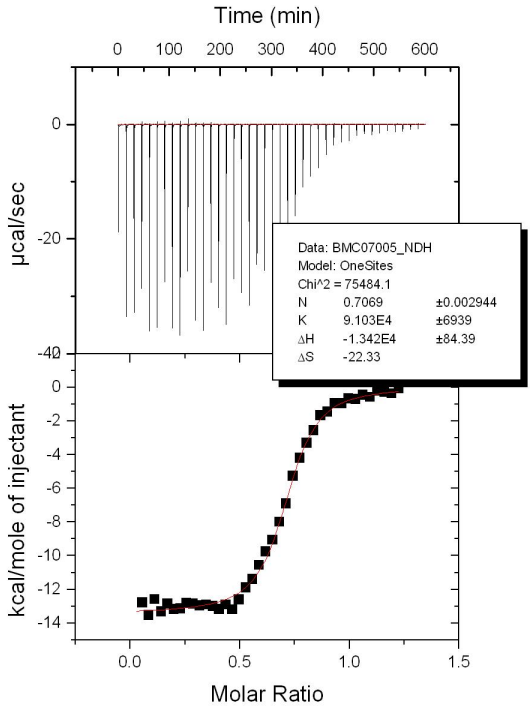

Figure 3.19: ITC of 10 mM benzylamine added to 1.5 mM 2-FPBA in acetonitrile. 25 ºC, reference power 36 µcal/sec, stir speed 300. Initial delay 60 s, initial injection 3 µL, all following injections 6 µL with 900 s spacing.

Figure 3.18 illustrates an initial exothermic phase upon addition of catechol, following by an endothermic step – the opposite result of its addition in methanol. Figure 3.19 shows the only titration that does not exhibit two phases; it shows a simple exothermic response to the addition of benzylamine to 2-FPBA in acetonitrile. However, even this data cannot be used because the software calculates N = 0.71. This binding event is 1:1, and so N = 1 is expected. When N is set to equal 1, the software fails to fit the data at all. The result is that ITC was unable to verify any of the binding constants for the Bull-James system.

3.7 CONCLUSIONS

^{11}B NMR spectroscopy is a valuable technique suited for the qualitative monitoring of electronic or structural changes in the chemical environment of a boron atom. Moreover, in many cases the quantitative aspect of this spectroscopy can be employed to take advantage of the analysis of those changes. As the various examples have shown, ^{11}B NMR spectroscopy has led to insights about the hybridization and charge state of the boron atom in various interactions, the binding stoichiometry and mode of binding, and the binding affinity and position of equilibria.

In particular, we have examined the binding of a three-component assembly that forms *ortho*-iminophenylboronate esters. Like *ortho*-(aminomethyl)phenylboronic acids and boronate esters, these assemblies form N-B bonds in aprotic solvent and solvent-inserted species in protic solvent. We have also demonstrated that the equilibrium between one host and two distinct guests can be described by a seventh-order polynomial, and that this polynomial can be used along with ^{11}B NMR data to calculate the five equilibrium constants involved in this complex equilibrium in methanol. Finally, the comparison of these five equilibrium constants leads to the conclusion that guest binding is cooperative, in that binding one guest strengthens the binding of the second guest.

3.8 EXPERIMENTAL

3.8.1 Materials

Reagents and solvents were used as purchased from commercial sources, with the exception of 2-formylphenylboronic acid. 2-FPBA was recrystallized from dichloromethane in order to remove boric acid. When present, boric acid displays a ^{11}B NMR signal at 19 ppm.

3.8.2 Instruments and Methods

^{1}H and ^{11}B NMR spectra were collected on an Agilent VNMRS 600 MHz spectrometer with a sweep width of 56818 Hz, a 90 degree flip angle, and 2 second acquisition time using BF_3•OEt_2 as an external reference. Each spectrum was processed with 10 Hz line broadening, and a back linear prediction of the first 32 points was used to remove the ^{11}B background.

ITC experiments were carried out on a MicroCal VP-ITC MicroCalorimeter. MicroCal Origin was used to fit the data.

3.8.3 Procedure for ^{11}B NMR Titrations

Stock solutions of 2-formylphenylboronic acid, benzylamine, and catechol were made to be 70 mM in either CD_3OD or CD_3CN. Then each (separate) quartz NMR tube was loaded according to the following tables. The samples were stored overnight in a refrigerator and ^{11}B NMR spectra (as well as ^{1}H spectra, in order to support structural assignments) were obtained the next day.

Volume 2-FPBA	Volume catechol	Volume benzylamine	Volume solvent	[FPBA]	[catechol]	[benzylamine]
100 μL	0 μL	20 μL	580 μL	10 mM	0 mM	2 mM
100 μL	0 μL	40 μL	560 μL	10 mM	0 mM	4 mM
100 μL	0 μL	60 μL	540 μL	10 mM	0 mM	6 mM
100 μL	0 μL	80 μL	520 μL	10 mM	0 mM	8 mM
100 μL	0 μL	100 μL	500 μL	10 mM	0 mM	10 mM
100 μL	0 μL	120 μL	480 μL	10 mM	0 mM	12 mM
100 μL	0 μL	140 μL	460 μL	10 mM	0 mM	14 mM
100 μL	100 μL	140 μL	360 μL	10 mM	10 mM	14 mM

Table 3.8: Titration of benzylamine into 2-FPBA with catechol added at end.

Volume 2-FPBA	Volume catechol	Volume benzylamine	Volume solvent	[FPBA]	[catechol]	[benzylamine]
100 μL	100 μL	0 μL	500 μL	10 mM	10 mM	0 mM
100 μL	100 μL	20 μL	480 μL	10 mM	10 mM	2 mM
100 μL	100 μL	40 μL	460 μL	10 mM	10 mM	4 mM
100 μL	100 μL	60 μL	440 μL	10 mM	10 mM	6 mM
100 μL	100 μL	80 μL	420 μL	10 mM	10 mM	8 mM
100 μL	100 μL	100 μL	400 μL	10 mM	10 mM	10 mM
100 μL	100 μL	120 μL	380 μL	10 mM	10 mM	12 mM

Table 3.9: Titration of benzylamine into 2-FPBA and catechol.

Volume 2-FPBA	Volume catechol	Volume benzylamine	Volume solvent	[FPBA]	[catechol]	[benzylamine]
100 μL	50 μL	0 μL	550 μL	10 mM	5 mM	0 mM
100 μL	100 μL	0 μL	500 μL	10 mM	10 mM	0 mM
100 μL	150 μL	0 μL	450 μL	10 mM	15 mM	0 mM
100 μL	200 μL	0 μL	400 μL	10 mM	20 mM	0 mM
100 μL	300 μL	0 μL	300 μL	10 mM	30 mM	0 mM
100 μL	400 μL	0 μL	200 μL	10 mM	40 mM	0 mM
100 μL	500 μL	0 μL	100 μL	10 mM	50 mM	0 mM
100 μL	500 μL	100 μL	0 μL	10 mM	50 mM	10 mM

Table 3.10: Titration of catechol into 2-FPBA with benzylamine added at end.

Volume 2-FPBA	Volume catechol	Volume benzylamine	Volume solvent	[FPBA]	[catechol]	[benzylamine]
100 μL	0 μL	100 μL	500 μL	10 mM	0 mM	10 mM
100 μL	20 μL	100 μL	480 μL	10 mM	2 mM	10 mM
100 μL	40 μL	100 μL	460 μL	10 mM	4 mM	10 mM
100 μL	60 μL	100 μL	440 μL	10 mM	6 mM	10 mM
100 μL	80 μL	100 μL	420 μL	10 mM	8 mM	10 mM
100 μL	100 μL	100 μL	400 μL	10 mM	10 mM	10 mM
100 μL	120 μL	100 μL	380 μL	10 mM	12 mM	10 mM

Table 3.11: Titration of catechol into 2-FPBA and benzylamine.

3.9 Acknowledgements

Steve Sorey and Angela Spangenberg are thanked for their help with NMR spectroscopy. Dr. John Stanton is thanked for his help in solving the polynomial.

3.10 References

(1) Hall, D. G. *Boronic Acids: Preparation, Applications in Organic Synthesis and Medicine*; John Wiley & Sons, 2006.

(2) Miyaura, N.; Yamada, K.; Suzuki, A. A New Stereopecific Cross-Coupling by the Palladium-Catalyzed Reaction of 1-Alkenylboranes with 1-Alkenyl or 1-Alkynyl Halides. *Tetrahedron Lett.* **1979**, *36*, 3437–3740.

(3) Miyaura, N.; Suzuki, A. Palladium-Catalyzed Cross-Coupling Reactions of Organoboron Compounds. *Chem. Rev.* **1995**, *95* (7), 2457–2483.

(4) Suzuki, A. Recent Advances in the Cross-Coupling Reactions of Organoboron Derivatives with Organic Electrophiles, 1995-1998. *Organomet. Chem.* **1999**, *576* (1-2), 147–168.

(5) Al-Zoubi, R. M.; Marion, O.; Hall, D. G. Direct and Waste-Free Amidation and Cycloadditions by Organocatalytic Activation of Carboxylic Acids at Room Temperature. *Angew. Chem. Int. Ed.* **2008**, *47* (15), 2876–2879.

(6) Cote, A. P.; Benin, A. I.; Ockwig, N. W.; O'Keefe, M.; Matzger, A. J.; Yaghi, O. M. Porous, Crystalline, Covalent Organic Frameworks. *Science (80-.).* **2005**, *310* (5751), 1166–1170.

(7) El-Kaderi, H. M.; Hunt, J. R.; Medoza-Cortes, J. L.; Cote, A. P.; Taylor, R. E.; O'Keefe, M.; Yaghi, O. M. Designed Synthesis of 3D Covalent Organic Frameworks. *Science (80-.).* **2007**, *316* (5822), 268–272.

(8) Rambo, B. M.; Lavigne, J. J. Defining Self-Assembly Linear Oligo(dioxaborole)s. *Chem. Mater.* **2007**, *19* (15), 3732–3739.

(9) Korich, A. L.; Iovine, P. M. Boroxine Chemistry and Applications: A Perspective. *Dalt. trans.* **2010**, *39* (6), 1423–1431.

(10) Adamczyk-Wozniak, A.; Cyranski, M. K.; Jakubczyk, Michal Klimentowska, P.; Koll, A.; Kolodziejczak, J.; Pojmaj, G.; Zubrowska, A.; Zukowska, G. Z.; Sporzynski, A. Influence of the Substituents on the Structure and Properties of Benzoxaboroles. *J. Phys. Chem. A* **2010**, *114* (6), 2324–2330.

(11) Brown, H. C. *Organic Syntheses via Boranes Vol. 1*; Aldrich Chemical: Milwaukee, WI, 1997.

(12) Brown, H. C.; Zaidlewicz, M. *Organic Syntheses via Boranes. Vol. 2*; Aldrich Chemical: Milwaukee, WI, 2001.

(13) Suzuki, A.; Brown, H. C. *Organic Syntheses via Boranes*. *Vol. 3*; Aldrich Chemical: Milwaukee, WI, 2003.

(14) Takaya, Y.; Ogasawara, M.; Hayashi, T.; Sakai, M.; Miyaura, N. Rhodium-Catalyzed Asymmetric 1,4-Addition of Aryl- and Alkenylboronic Acids to Enones. *J. Am. Chem. Soc.* **1998**, *120* (22), 5579–5580.

(15) Kettner, C.; Mersinger, L.; Knabb, R. The Selective Inhibition of Thrombin by Peptides of Boroarginine. *J. Biol. Chem.* **1990**, *265* (30), 18289–18297.

(16) Spencer, J.; Burd, A. P.; Goodwin, C. A.; Merette, S. A. M.; Scully, M. F.; Adatia, T.; Deadman, J. J. Synthesis of Ortho-Modified Mercapto- and Piperazino-Methyl-Phenylboronic Acid Derivatives. *Tetrahedron* **2002**, *58* (8), 1551–1556.

(17) Strynadka, N. C. J.; Adachi, H.; Jensen, S. E.; Johns, K.; Sielecki, A.; Betzel, C.; Sutoh, K.; James, M. N. G. Molecular Structure of the Acyl-Enzyme Intermediate in Beta-Lactam Hydrolysis at 1.7 A Resolution. *Nature* **1992**, *359* (6397), 700–705.

(18) Flentke, G. R.; Munoz, E.; Huber, B. T.; Plaut, A. G.; Kettner, C. A.; Bachovin, W. W. Inhibition of Dipeptidyl Aminopeptidase IV (DP-IV) by Xaa-boroPro Dipeptides and Use of These Inhibitors to Examine the Role of DP-IV in T-Cell Function. *Proc. Natl. Acad. Sci.* **1991**, *88* (4), 1556–1559.

(19) Dunsdon, R. M.; Greening, J. R.; Jones, P. S.; Jordan, S.; Wilson, F. X. Solid Phase Synthesis of Aminoboronic Acids: Potent Inhibitors of the Hepatitis C Virus NS3 Proteinase. *Bioorg. Med. Chem. Lett.* **2000**, *10* (14), 1577–1579.

(20) Bukhtiyarova, M.; Rizzo, C. J.; Kettner, C. A.; Korant, B. D.; Scarnati, H. T.; King, R. W. Inhibition of the Bovine Viral Diarrhoea Virus NS3 Serine Protease by a Boron-Modified Peptidyl Mimetic of Its Natural Substrate. *Antivir. Chem. Chemother.* **2002**, *12* (6), 367–373.

(21) Hiratake, J.; Oda, J. Aminophosphonic and Aminoboronic Acids as Key Elements of a Transition State Analog Inhibitor of Enzymes. *Biosci. Biotech. Biochem.* **1997**, *61* (2), 211–218.

(22) Arnal-Herault, C.; Pase, A.; Michau, M.; Cot, D.; Petit, E.; Barboiu, M. Functional G-Quartet Macroscopic Membrane Films. *Angew. Chem. Int. Ed.* **2007**, *46* (44), 8409–8413.

(23) Hutin, M.; Bernardinelli, G.; Nitschke, J. R. An Iminoboronate Construction Set for Subcomponent Self-Assembly. *Chem. Eur. J.* **2008**, *14* (15), 4585–4593.

(24) Galbraith, E.; Kelly, A. M.; Fossey, J. S.; Kociok-Koehn, G.; Davidson, M. G.; Bull, S. D.; James, T. D. Dynamic Covalent Self-Assembled Macrocycles Prepared from 2-Formyl-Aryl-Boronic Acids and 1,2-Amino Alcohols. *New J. Chem.* **2009**, *33* (1), 181–185.

(25) James, T. D.; Sandanayake, K. R. A. S.; Shinkai, S. Novel Photoinduced Electron-Transfer Sensor for Saccharides Based on the Interaction of Boronic Acid and Amine. *J. Chem. Soc., Chem. Commun.* **1994**, *4*, 477–478.

(26) James, T. D.; Sandanayake, K. R. A. S.; Shinkai, S. A Glucose-Specific Molecular Fluorescence Sensor. *Angew. Chem.* **1994**, *106* (21), 2287–2289.

(27) James, T. D.; Sandanayake, K. R. A. S.; Shinkai, S. Chiral Discrimination of Monosaccharides Using a Fluorescent Molecular Sensor. *Nature* **1995**, *374* (6520), 345–347.

(28) James, T. D. Saccharide-Selective Boronic Acid Based Photoinduced Electron Transfer (PET) Fluorescent Sensors. *Top. Curr. Chem.* **2007**, *277*, 107–152.

(29) Siedle, A. R. Boron-11 NMR Spectroscopy. *Annu. Rep. NMR Spectrosc.* **1982**, *12*, 177–261.

(30) Siedle, A. R. Boron-11 NMR Spectroscopy. *Annu. Rep. NMR Spectrosc.* **1988**, *20*, 205–314.

(31) Wrackmeyer, B. Nuclear Magnetic Resonance Spectroscopy of Boron Compounds Containing Two-, Three- and Four-Coordinate Boron. *Annu. Rep. NMR Spectrosc.* **1988**, *20*, 61–203.

(32) Smith, W. L. Boron-11 NMR. *J. Chem. Ed.* **1977**, *54* (8), 469–473.

(33) Eaton, G. R. N. M. R. of Boron Compounds. *J. Chem. Ed.* **1969**, *46* (9), 547–556.

(34) Noeth, H.; Wrackmeyer, B. *Nuclear Magnetic Resonance Spectroscopy of Boron Compounds*; Springer-Verlag: Berlin, 1978.

(35) Noeth, H.; Vahrenkamp, H. Nuclear Resonance Investigations on Boron Compounds. I. 11B Nuclear Resonance Spectra of Boranes with Substituents from the First Eight-Membered Period of the Periodic System. *Chem. Ber.* **1966**, *99* (3), 1049–1067.

(36) Brown, H. C.; Nazer, B.; Cha, J. S.; Sikorski, J. A. Selective Reductions. 38. Reaction of Thexylchloroborane-Methyl Sulfide Complex in Methylene Chloride with Selected Organic Compounds Containing Representative Functional Groups. Comparison of the Reducing Characteristics of Thexylchloroborane, Thexylbora. *J. Org. Chem.* **1986**, *51* (26), 5264–5270.

(37) Brown, H. C.; Cole, T. E.; Srebnik, M.; Kim, K. W. Hydroboration. 79. Preparation and Properties of Methylborane and Dimethylborane and Their Characteristics as Hydroborating Agents. Synthesis of Tertiary Alcohols Containing Methyl Groups via Hydroboration. *J. Org. Chem.* **1986**, *51* (25), 4925–4930.

(38) Chandraskharan, J.; Brown, H. C. Hydroboration Kinetics. 11. A Reinvestigation of the Kinetics of Hydroboration of Representative Alkenes with Disiamylborane

Dimer. Conclusive Evidence for the Dissociation Mechanism in the Hydroboration of Alkenes with Dialkylborane Dimers. *J. Org. Chem.* **1985**, *50* (4), 518–520.

(39) Mikhailov, B. M.; Ter-Sarkisyan, G. S.; Nikolaeva, N. A. Organoboron Compounds. CCXXXVI. Reactions of 1,4-Naphthoquinone with Trialkylboranes. *Zh. Obs. Khim.* **1971**, *41* (8), 1721–1725.

(40) Brown, H. C.; Kramer, G. W.; Hubbard, J. L.; Krishnamurthy, S. Addition Compounds of Alkali Metal Hydrides. XVIII. Reaction of Trialkylboranes with Tert-Butyllithium. A General, Convenient Method for the Preparation of Lithium Trialkylborohydrides. *J. Organometal. Chem.* **1980**, *188* (1), 1–10.

(41) Good, C. D.; Ritter, D. M. Alkenylboranes. II. Improved Preparative Methods and New Observations on Methylvinylboranes. *J. Am. Chem. Soc.* **1962**, *84*, 1162–1166.

(42) Brown, H. C.; Sinclair, J. A. Organoboranes. XVIII. Reaction of Lithium Alkynes with Methyl Dialkylborinate: The Synthesis of B-1-Alkynyldialkylboranes. *J. Organometal. Chem.* **1977**, *131* (2), 163–169.

(43) de Moor, J. E.; van der Kelen, G. P. Studies on Trivalent Boron Compounds. I. The Boron and Proton Magnetic Resonance Spectra of Some Trivalent Boron Compounds. *J. Organometal. Chem.* **1966**, *6* (3), 235–241.

(44) Paetzold, P. I.; Hansen, H. J. Chemistry of Boron Azides. VI. Dimethylborazide and Its Amino Complexes. *Anorg. Chem.* **1966**, *345* (1-2), 79–86.

(45) Noeth, H.; Vahrenkamp, H. Nuclear Magnetic Resonance Spectroscopic Studies of Boron Compounds. II. Monomer-Dimer Equilibriums in Aminoboranes. *Chem. Ber.* **1967**, *100* (10), 3353–3362.

(46) Schaeffer, R.; Todd, L. J. Boron-Nitrogen Compounds. IX. Synthesis and Properties of Some Substituted Trimethylboranes. *J. Am. Chem. Soc.* **1965**, *87* (3), 488–494.

(47) Dewar, M. J. S.; Jones, R. New Heteroaromatic Compounds. XXV. Studies of Salt Formation in Boron Oxyacids by Boron-11 Nuclear Magnetic Resonance. *J. Am. Chem. Soc.* **1967**, *89* (10), 2408–2410.

(48) Phillips, W. D.; Miller, H. C.; Muetterties, E. L. B11 Magnetic Resonance Study of Boron Compounds. *J. Am. Chem. Soc.* **1959**, *81*, 4496–4500.

(49) James, B. D.; Nanda, R. K.; Wallbridge, M. G. H. Spectroscopic Studies of Borohydride Derivatives of Zirconium and Hafnium. *J. Chem. Soc., Inorg., Phys., Theor.* **1966**, *2*, 182–184.

(50) Onak, T. P.; Landesman, H.; Williams, R. E.; Shapiro, I. The B11 Nuclear Magnetic Resonance Chemical Shifts and Spin Coupling Values for Various Compounds. *J. Phys. Chem.* **1959**, *63*, 1533–1535.

(51) Thompson, R. J.; Davis, J. C. J. Electronegativeity Effects on 11B Chemical Shifts in Tetrahedral BX4- Ions. *Inorg. Chem.* **1965**, *4* (10), 1464–1467.

(52) Toporcer, L. H.; Dessy, R. E.; Green, S. I. E. Preparation and Properties of Some Tetracoordinate Boron Compounds. The Pseudo-Metal Ion Concept. *Inorg. Chem.* **1965**, *4* (11), 1649–1655.

(53) Pizer, R.; Tihal, C. Equilibria and Reaction Mechanism of the Complexation of Methylboronic Acid with Polyols. *Inorg. Chem.* **1992**, *31* (15), 3243–3247.

(54) Pizer, R. D.; Tihal, C. A. Mechanism of Boron Acid/polyol Complex Formation. Comments on the Trigonal/tetrahedral Interconversion on Boron. *Polyhedron* **1996**, *15* (19), 3411–3416.

(55) Cooper, C. R.; Spencer, N.; James, T. D. Selective Fluorescence Detection of Fluoride Using Boronic Acids. *Chem. Commun.* **1998**, *13*, 1365–1366.

(56) Smith, B. M.; Owens, J. L.; Bowman, C. N.; Todd, P. Thermodynamics of Borate Ester Formation by Three Readily Grafted Carbohydrates. *Carbohydr. Res.* **1998**, *308* (1-2), 173–179.

(57) Wilson, M. E.; Najdi, S.; Krochta, J. M.; Hsieh, Y.-L.; Kurth, M. J. Complexation of Borate with Poly(1-(Acrylamido)-1-Deoxyactitol): Dilute Solution Viscosity, 11B NMR, and 13C NMR Studies. *Macromolecules* **1998**, *31* (14), 4486–4492.

(58) James, T. D.; Sandanayake, K. R. A. S.; Shinkai, S. Saccharide Sensing with Molecular Receptors Based on Boronic Acid. *Angew. Chemie Int. Ed. English* **1996**, *35* (17), 1910–1922.

(59) Fang, H.; Kaur, G.; Wang, B. Progress in Boronic Acid-Based Fluorescent Glucose Sensors. *Fluorescence* **2004**, *14* (5), 481–489.

(60) Zhu, L.; Shabbir, S. H.; Gray, M.; Lynch, V.; Sorey, S.; Anslyn, E. V. A Structural Investigation of the N-B Interaction in an O-(N,N-Dialkylaminomethyl)arylboronate System. *J. Am. Chem. Soc.* **2006**, *128* (4), 1222–1232.

(61) Miyazaki, Y.; Matsuo, H.; Fujimori, T.; Takemura, H.; Matsuoka, S.; Okobira, T.; Uezu, K.; Yoshimura, K. Interaction of Boric Acid with Salicyl Derivatives as an Anchor Group of Boron-Selective Adsorbents. *Polyhedron* **2008**, *27* (13), 2785–2790.

(62) Collins, B. E.; Sorey, S.; Hargrove, A. E.; Shabbir, S. H.; Lynch, V.; Anslyn, E. V. Probing Intramolecular B-N Interactions in Ortho-Aminomethyl Arylboronic Acids. *J. Org. Chem.* **2009**, *74* (11), 4055–4060.

(63) Gutierrez-Moreno, N. J.; Medrano, F.; Yatsimirsky, A. K. Schiff Base Formation and Recognition of Amino Sugars, Aminoglycosides and Biological Polyamines by 2-Formylphenylboronic Acid in Aqueous Solution. *Org. Biomol. Chem.* **2012**, *10* (34), 6960–6972.

(64) Miyazaki, Y.; Fujimori, T.; Okita, H.; Hirano, T.; Yoshimura, K. Thermodynamics of Complexation Reactions of Borate and Phenylboronate with Diol, Triol and Tetritol. *Dalt. Trans.* **2013**, *42* (29), 10473–10486.

(65) Martinez-Aguirre, M. A.; Villamil-Ramos, R.; Guerrero-Alvarez, J. A.; Yatsimirsky, A. K. Substituent Effects and pH Profiles for Stability Constants of Arylboronic Acid Diol Esters. *J. Org. Chem.* **2013**, *78* (10), 4674–4684.

(66) Perez-Fuentes, Y.; Kelly, A. M.; Fossey, J. S.; Powell, M. E.; Bull, S. D.; James, T. D. Simple Protocols for NMR Analysis of the Enantiomeric Purity of Chiral Primary Amines. *Nat. Protoc.* **2008**, *3* (2), 210–214.

(67) Kelly, A. M.; Perez-Fuentes, Y.; Fossey, J. S.; Yeste, S. L.; Bull, S. D.; James, T. D. Simple Protocols for NMR Analysis of the Enantiomeric Purity of Chiral Diols. *Nat. Protoc.* **2008**, *3* (2), 215–219.

(68) Yeste, S. L.; Powell, M. E.; Bull, S. D.; James, T. D. Simple Chiral Derivatization Protocols for 1H NMR and 19F NMR Spectroscopic Analysis of the Enantiopurity of Chiral Diols. *J. Org. Chem.* **2009**, *74* (1), 427–430.

(69) Mirri, G.; Bull, S. D.; Horton, P. N.; James, T. D.; Male, L.; Tucker, J. H. R. Electrochemical Method for the Determination of Enantiomeric Excess of Binol Using Redox-Active Boronic Acids as Chiral Sensors. *J. Am. Chem. Soc.* **2010**, *132* (26), 8903–8905.

(70) Metola, P.; Anslyn, E. V.; James, T. D.; Bull, S. D. Circular Dichroism of Multi-Component Assemblies for Chiral Amine Recognition and Rapid Ee Determination. *Chem. Sci.* **2012**, *3* (1), 156–161.

(71) Shcherbakova, E. G.; Minami, T.; Brega, V.; James, T. D.; Anzenbacher, P. J. Determination of Enantiometic Excess in Amine Derivatives with Molecular Self-Assemblies. *Angew. Chem. Int. Ed.* **2015**, *54* (24), 7130–7133.

(72) Wulff, G. Selective Binding to Polymers via Covalent Bonds. The Construction of Chiral Cavities as Specific Receptor Sites. *Pure Appl. Chem.* **1982**, *54* (11), 2093–2102.

(73) Wulff, G.; Lauer, M.; Boehnke, H. Chemistry of Adhesive Groups. Part 5. Rapid Proton Transfer as Cause for an Uncommonly Large Neighboring Group Effect. *Angew. Chem.* **1984**, *96* (9), 714–716.

(74) Hargrove, A. E.; Zhong, Z.; Sessler, J. L.; Anslyn, E. V. Algorithms for the Determination of Binding Constants and Enantiomeric Excess in Complex Host : Guest Equilibria Using Optical Measurements. *New J. Chem.* **2010**, *34* (2), 348–354.

(75) Thordarson, P. Determining Association Constants from Titration Experiments in Supramolecular Chemistry. *Chem. Soc. Rev.* **2011**, *40* (3), 1305–1323.

(76) Blasie, C. A.; Berg, J. M. Kinetics and Thermodynamics of Copper(II) Binding to Apoazurin. *J. Am. Chem. Soc.* **2003**, *125* (23), 6866–6867.

Chapter 4: The Bull-James Assembly in Pedagogy and in Kinetic Resolution of a Terminal Alkyne Amine *via* Copper-Catalyzed Azide-Alkyne Cycloaddition

4.1 The Bull-James Assembly in an Undergraduate Teaching Laboratory[a]

As was mentioned in Chapter 3, the Bull and James groups developed a three-component boronic acid-based assembly[1,2] that has been used by them and others[3–6] as a chiral shift reagent. This series of chiral shift reagents employs 2-formylphenylboronic acid (2-FPBA) and either an enantiopure amine to measure the enantiomeric excess (*ee*) of a chiral diol, or an enantiopure diol to measure the *ee* of a chiral primary amine, using ^{1}H NMR spectroscopy. This is possible because introducing one enantiomer of one component to both enantiomers of the other component produces two diastereomeric complexes, which can be distinguished by ^{1}H NMR.

Determining the enantiomeric excess (*ee*) of an asymmetric transformation is an everyday task for synthetic chemists, and being able to accurately measure the enantioenrichment of a product is crucial to a wide range of chemistry, especially in areas such as asymmetric catalysis.[7]

Being able to quickly and accurately measure the *ee* of a reaction mixture has been a focus for development in industrial and academic settings due to increased demand of quick *ee* determination in high-throughput screening (HTS) methodologies.[8–10] Established means of analysis (chiral HPLC) are not ideal for these applications, where hundreds, if not thousands of asymmetric transformations can need to be quantified daily, requiring long method development and lengthy run times. ^{1}H NMR spectroscopy is a methodology which has been targeted for HTS because a ^{1}H NMR spectrum can be

[a] Sections 4.1 and 4.3-4.5 were adapted from a manuscript and supporting materials co-written by Brette Chapin and members of Dr. John Fossey's research group at the University of Birmingham (UK).

obtained in under five minutes and thus can reduce analysis times compared with established chiral chromatography methods.[11–13] Undergraduate students should be aware of techniques which can form diastereomeric mixtures from enantiomeric mixtures (e.g. Mosher's acid derivitisation) and should develop an appreciation that these can be applied to *ee* determination using NMR.[14,15]

However, undergraduate students do not often have opportunities to gain practical experience in measuring *ee*. We wished to tackle this through research-informed teaching, applying cutting-edge *ee* determination methodology as well as reinforcing multidisciplinary aspects of undergraduate learning, such as supramolecular, organic, and analytical chemistry. Developing an undergraduate practical procedure based upon chiral HPLC could be both time-consuming and expensive, especially in institutions that do not already possess chiral HPLC capacity. Therefore, we have developed an undergraduate protocol for determination of *ee* based on ^{1}H NMR spectroscopy and supramolecular assemblies, using commercially available materials, and demonstrating the impact of real-life research in the undergraduate laboratory.

4.2 Preliminary Experiments and Modifications[b]

The system that was chosen for the undergraduates to study was 2-formylphenylboronic acid (2-FPBA), (*R*)-1,1'-bi-2-naphthol ((*R*)-BINOL), and various *ee*s of α-methylbenzylamine (α-MBA) (Scheme 4.1).

[b] The studies in section 4.2 were carried out by Brette Chapin as a visiting student in Dr. John Fossey's research group at the University of Birmingham (UK).

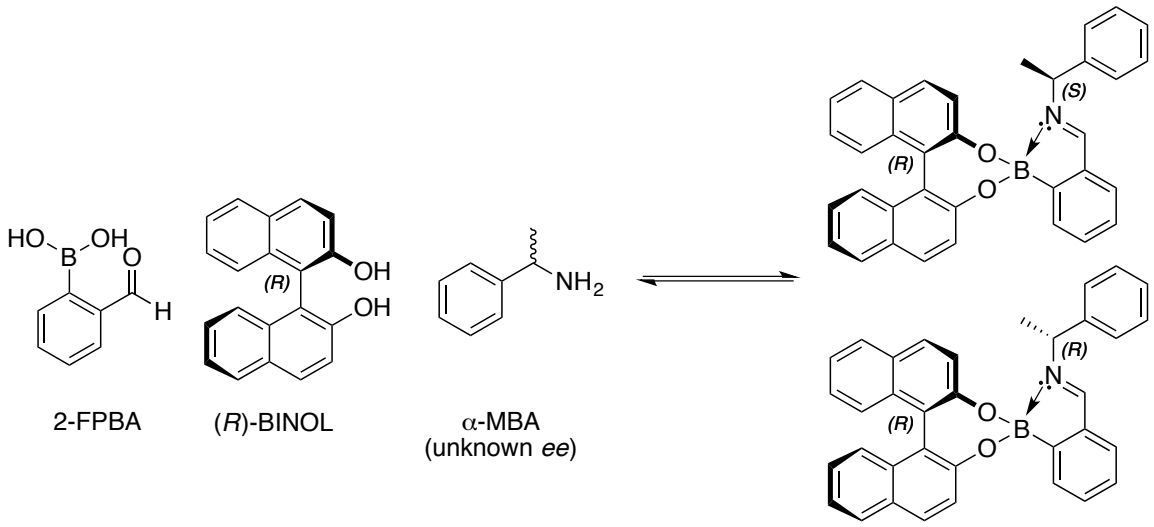

2-FPBA (*R*)-BINOL α-MBA (unknown *ee*)

Scheme 4.1: The Bull-James assembly under study: 2-FPBA, (*R*)-BINOL, and α-MBA.

The Bull-James protocol recommends using a 1:1.1:1 ratio of 2-FPBA, BINOL, and amine, which gave the spectrum shown below in chloroform-*d* (Figure 4.1).[1] The sharp peak at 5.2 ppm is the alcohol peak for the excess (*S*)-BINOL.

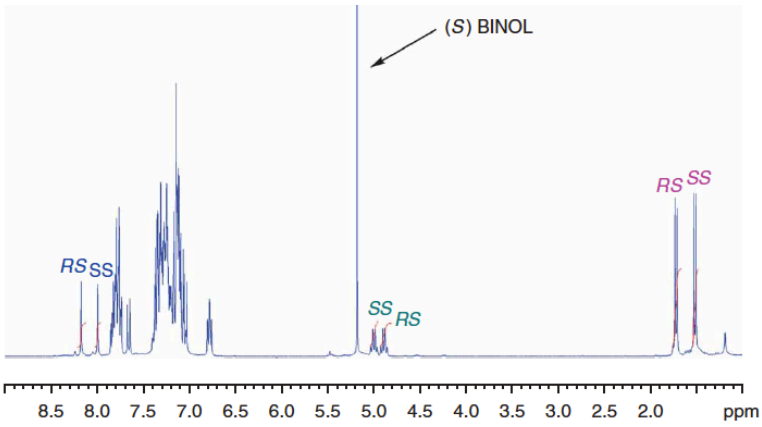

Figure 4.1[1]: The Bull-James assembly with 2-FPBA, (*S*)-BINOL, and α-MBA in a 1:1.1:1 ratio. (Note that they used (*S*)-BINOL while this report uses its enantiomer.)

However, adventitious water within the solvent can cause exchange with the BINOL alcohols and thus the peak at 5.2 ppm can appear significantly broadened (Figure 4.2). This broad peak overlaps with the peaks corresponding to benzylic methine protons from the two complexes. This interferes with integrating their areas and thus can be detrimental to the accuracy of the methodology.

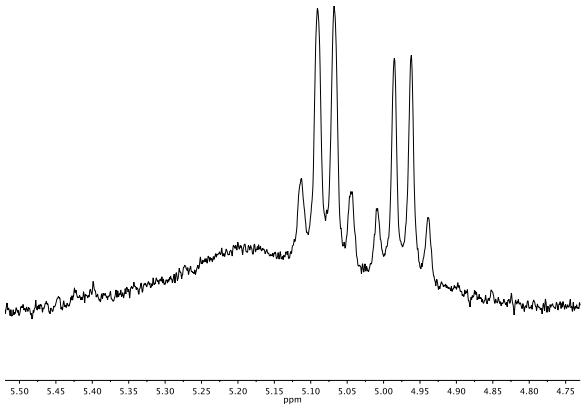

Figure 4.2: The alcohol peak of BINOL broadens and overlaps the benzylic methine proton peaks when the solvent (chloroform-*d*) is not dry.

Keeping an NMR solvent completely dry in an undergraduate teaching laboratory seemed unachievable, especially considering the fact that molecular sieves alone did not achieve sufficient dryness. As such, the system was adapted to accommodate 2-FPBA, BINOL, and amine in a 1:1:1.2 ratio in order to prevent BINOL from being in excess, in addition to drying each solution over 4Å molecular sieves. Importantly, before adopting this approach, it needed to be tested whether adding racemic amine in excess would result in preferential complexation of one of the enantiomers. Luckily, the relative integrations of the two diastereomeric methine proton signals were constant, regardless of the amount of α-MBA in solution (Table 4.1). Thus, it was concluded that there was no kinetic resolution effect occurring.

Equivalents of *rac*-α-MBA, relative to 2-FPBA and (*R*)-BINOL (1:1)	**Ratio of (*R*)- and (*S*)-α-MBA bound in the three-component assembly**
1.0 equiv.	1 (*R*) : 0.79 (*S*)
1.2 equiv.	1 (*R*) : 0.82 (*S*)
1.5 equiv.	1 (*R*) : 0.79 (*S*)
2.0 equiv.	1 (*R*) : 0.78 (*S*)

Table 4.1: Ratio of bound α-MBA depending on the number of equivalents of racemic amine.

The results in Table 4.1 were encouraging in the sense that the ratio of (*R*)- and (*S*)-α-methylbenzylamine was independent of the number of equivalents of amine. However, the observed ratio was not accurate at all, since the racemic mixture should give a ratio of 1:1. For this reason, the use of calibration curves to mitigate this discrepancy was investigated. Five assembly formations with different *ee*s of α-MBA were carried out and analyzed with ^{1}H NMR spectroscopy. The diastereomeric regions are highlighted with colored boxes in Figure 4.3 and expanded in Figure 4.4. The green (methyl group) and blue (benzylic methine proton) regions each contain a peak for the unbound amine. The red (imine) region contains a peak for the imine formed between 2-FPBA and α-MBA, but which is "unbound" in the sense that BINOL is not coordinated. This occurs as a result of adventitious water competing with BINOL to reform the boronic acid from the boronate ester.

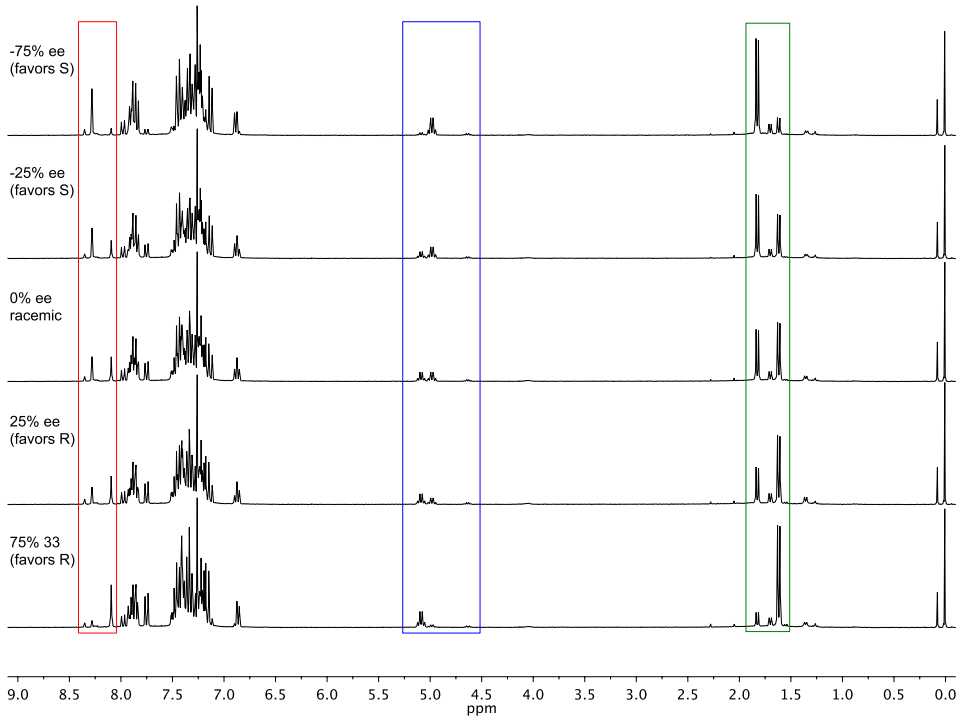

Figure 4.3: NMR spectra used to construct the calibration curves. The three sets of diastereomeric peaks are highlighted with colored boxes. 2-FPBA, (*R*)-BINOL, and α-MBA are present in a 1:1:1.2 ratio.

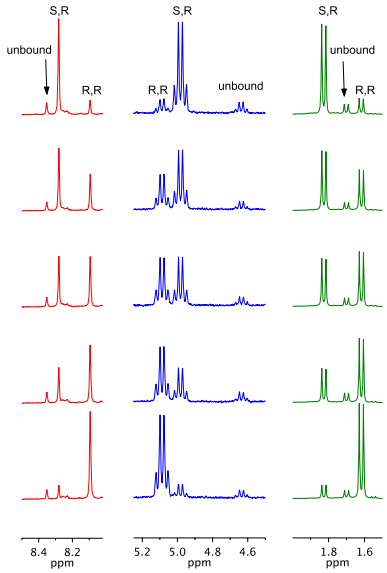

Figure 4.4: The diastereomeric peaks from Figure 4.3 are expanded and labeled.

Integrations of the diastereomeric signals in Figures 4.3 and 4.4 were used to calculate the measured *ee*, which was plotted against the "true" or intended *ee* of the amine in each solution. An *ee* favoring the (*S*)-enantiomer is defined as negative, while an *ee* favoring the (*R*)-enantiomer is defined as positive. The integrations for the imine peaks are plotted in Figure 4.5, while the integrations for the benzylic methine proton peaks are plotted in Figure 4.6. The integrations of the methyl group peaks could also be used to construct a calibration curve, but this study focused on the two regions that would be common to many α-chiral primary amines. This allows for broader applicability in undergraduate teaching laboratories, where investigating a range of chiral amines might be a goal.

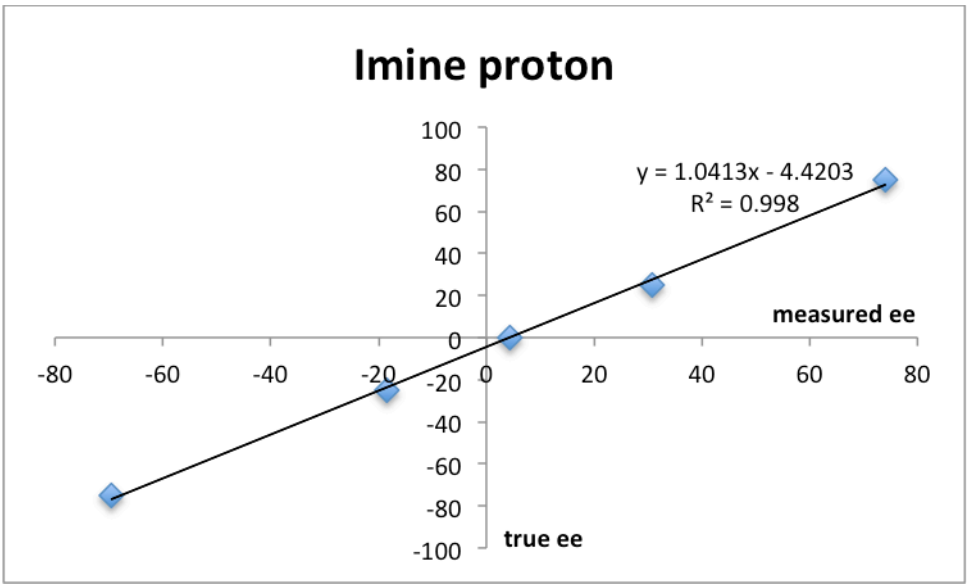

Figure 4.5: Plot of true *ee* versus measured *ee* determined using the imine protons. The integrations for the signals at 8.3 ppm (corresponding to the bound (*S*)-amine) and 8.1 ppm (corresponding to the bound (*R*)-amine) were used to calculate the measured *ee*, and these values were plotted against the true or intended *ee* of each solution.

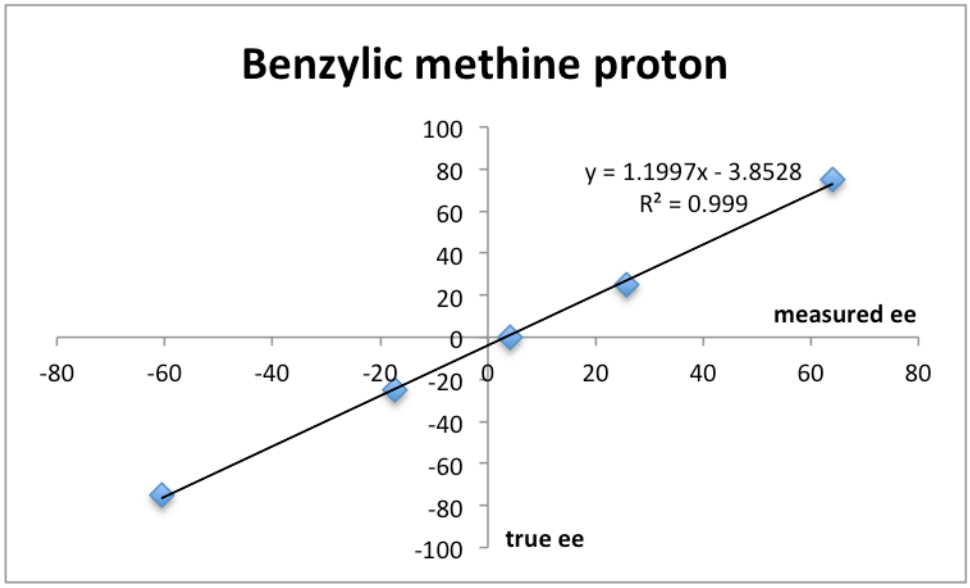

Figure 4.6: Plot of true *ee* versus measured *ee* determined using the benzylic methine protons. The integrations for the signals at 5.1 ppm (corresponding to the bound (*R*)-amine) and 5.0 ppm (corresponding to the bound (*S*)-amine) were used to calculate the measured *ee*, and these values were plotted against the true or intended *ee* of each solution.

Next, three assembly formations with varying *ee*s of amine were prepared and their *ee*s were measured by integration of the NMR signals. Then their measured *ee*s were used to solve for their calibrated *ee*s using the equations of the best-fit lines in Figures 4.5 and 4.6. The results are summarized in Table 4.2.

	Imine signals				Benzylic signals			
True % ee	**(*R*)**	**(*S*)**	**Measured % ee**	**Calibrated % ee**	**(*R*)**	**(*S*)**	**Measured % ee**	**Calibrated % ee**
89.3	14.39	1	87.0	86.3	1	0.13	77.0	88.6
-10.7	0.93	1	-3.6	-8.2	1	1.1	-4.8	-9.6
-50.0	0.38	1	-44.9	-51.3	1	2.28	-39.0	-50.7

Table 4.2: Comparison of the true, measured, and calibrated *ee*s using the two calibration curves shown in Figures 4.5 and 4.6.

The results in Table 4.2 show small errors for the calibrated *ee*s, with 0.7-1.1% error for the imine signals and 1.3-3.0% error for the benzylic signals. These errors are very low, since the error for NMR spectroscopy is generally agreed to be about 5%. Importantly, the errors were small for low, middle, and high *ee* values, with either enantiomer in excess.

These preliminary experiments showed that by adjusting the ratio of components and using a calibration curve, *ee*s could be determined accurately, even with unbound amine and adventitious water present. These modifications served as a critical component for writing a procedure for the undergraduate teaching laboratories.

4.3 THE LABORATORY MANUAL

In order for the undergraduate cohort to be able to carry out this reaction efficiently, a laboratory manual was required. This manual begins by introducing students to chirality in biological systems, and as a result, in the pharmaceutical industry. This establishes the relevance of this procedure to science in the "real world". The term enantiomeric excess (*ee*) is defined conceptually and mathematically, and it is explained that historically, *ee* has been determined using optical rotation. However, high-

performance liquid chromatography (HPLC) is now used much more commonly, despite the fact that this approach can be time-consuming and expensive. ^{1}H NMR spectroscopy is then presented as a possible alternative to combat both of these limitations. It is explained that in order to observe enantiomers (which have the same chemical and physical properties) by ^{1}H NMR, they must be converted to diastereomers (which have different chemical and physical properties), which can be accomplished with chiral shift reagents. Three examples of chiral shift reagents are given: Mosher's acid chloride, lanthanide reagents such as europium tris[(heptafluoropropylhydroxymethylene)-(+)-camphorate] ($Eu(hfc)_3$), and the Bull-James assembly. These details place the Bull-James assembly and the experimental procedure that follows within a context of the strengths and weaknesses of other methods for *ee* determination.

The manual then introduces (or reinforces) three important features of the Bull-James assembly. The first is that BINOL has axial chirality and forms atropisomers, rather than having a "chiral carbon". This is a structural feature that students may or may not have been exposed to previously, but they will need to understand atropisomerism in order to understand that the three-component assembly has two diastereomers. Then it is explained that the three-component assembly forms due to two types of reversible covalent bonding. The students are reminded of reversible imine formation from an aldehyde and primary amine, which they are expected to be familiar with, and they are introduced to the formation of a cyclic boronate ester from a boronic acid and a vicinal diol, which they are most likely unfamiliar with. This is a brief introduction to the reversible covalent bonding of some host-guest chemistry.

Finally, the students are instructed to work in groups of five. The procedure details how the groups will work together to prepare stock solutions of the three components. Each individual is made responsible for preparing one NMR sample from

the stock solutions for the five-point calibration curves (as in Figures 4.5 and 4.6), and one NMR sample of unknown *ee*. Then, as a team, they will use their NMR data to construct their calibration curve and use it to calculate the *ee*s of the unknown samples, as in Table 4.2.

4.4 Student Assessment

In their post-laboratory assignment, students were asked to show their calibration curves and report their calculated *ee*s for the five unknown samples. Then they were asked to critically evaluate their findings. Several selected questions are shown as examples below.

Comment on the quality of each calibration curve judging by the R^2 values. Discuss any anomalous points and try to rationalize why they occurred. Can these points be eliminated from the curve? Most students correctly compared their R^2 values to the ideal value of R = 1. Rationalizations for anomalous points varied, but we wanted students to have a valid reason (they observed something that went wrong with that sample in the laboratory) for eliminating a point, rather than the simple observation that one point was an outlier from the best-fit line. This brings up the ethical matter of when it is acceptable to exclude a data point from a set of data.

In an ideal case, what you would expect the best-fit equation for the calibration curves to be? Discuss the accuracy and precision of your calibration curves. Which curve do you expect to give you the most accurate ee *values for the unknown solutions?* With this question, we wanted students to state that ideally, the best-fit equation would be y = x and that this best-fit line would demonstrate perfect accuracy. The fact that this is not the best-fit equation is what necessitates the use of a calibration curve in the first place. Instead, the students found that their calibration curves were not very accurate, as

individual points on the curve represented large differences between true and measured *ee*, including y-intercept ≠ 0. The calibrations curves were, nonetheless, often precise, sometimes with $R^2 > 0.99$. When asked to choose which calibration curve would be most accurate, some students made a decision based on one R^2 value being much higher than the other, but some groups had two very precise R^2 values and they cited the fact that one set of NMR signals was much easier for them to integrate due to lack of overlap with other signals, and that they therefore trusted the accuracy of those integrations better.

What is the function of molecular sieves and why are they added to the solutions in this experiment. We wanted students to state that molecular sieves absorb water, but we also wanted them to state the importance of this function. Correct answers included that removing water would prevent imine hydrolysis or reduce the competition between water and (*R*)-BINOL for binding to boron, that it would stop the formation of tetrahedral borate or hemiaminals, or that it would remove water as a protic solvent, which could interfere with the nitrogen-boron bond.

4.5 Conclusions from the Undergraduate Teaching Laboratory

This experiment was successfully run with a cohort of 113 students at the University of Birmingham (UK). Several observations were made that may assist others who want to carry out this teaching experiment in the future.

During the data analysis session, it was noted that a thorough introduction into NMR processing software was required. The majority of students had no experience with NMR data processing, and they struggled to use the programs effectively without detailed instructions. Additionally, the construction of the calibration curves was achieved with variable success. A key training point should be the construction of these graphs; however, applying these to the inference of the *ee* of unknown samples was performed

well. The students produced data that could be successfully used to determine a diastereomeric ratio to give an inferred *ee* value accurate to within ±10% of the true *ee* value. Students found it difficult to deal with open-ended questions, such as where the potential for error was introduced into this experiment, and many students provided answers relating to human-based errors or specific examples that they encountered. The essay-style questions were designed to challenge the critical thinking of the students and to encourage them to assess and question the validity of the data they obtained; some students found it challenging to answer these questions. Some were reluctant to comment on the quality of their data, perhaps feeling that critical self-assessment would lead to a lower score. However, the grading rubric has been specifically designed to encourage the critical evaluation of data, regardless of the results obtained, and students could be reassured of this during the experiment.

Overall, we have demonstrated that the Bull-James assembly can be used as a practical introduction into the use of ^{1}H NMR spectroscopy as a technique for inferring the *ee* of a primary amine. In addition to this, the experiment reminds students of the relationships between diastereomers and enantiomers and reinforces knowledge of carbonyl chemistry. It also introduces them to the reversible, covalent, supramolecular interactions between boronic acids and diols and aims to encourage students to critically analyze their decisions both in the laboratory and during data analysis.

4.6 Introduction to Kinetic Resolution

Kinetic resolution is a process in which one enantiomer of a racemic mixture reacts more readily than the other to form a product. As shown in Figure 4.7, the two enantiomers have, by definition, the same free energy. The two products also have the same free energy. The resolution is a result of a difference in transition state energies

(hence, *kinetic* resolution) in the presence of another chiral reagent or a chiral catalyst. Due to the difference in transition state energies for the two enantiomers, k_R and k_S are unequal. This inequality in the two reaction rates means that if the reaction is stopped at some point between 0% and 100% conversion, it can be possible to form and isolate enantioenriched products, as well as recover enantioenriched starting materials, as one enantiomer of starting materal is being consumed faster than the other, and thus the corresponding enantiomer of product is forming faster than the other.

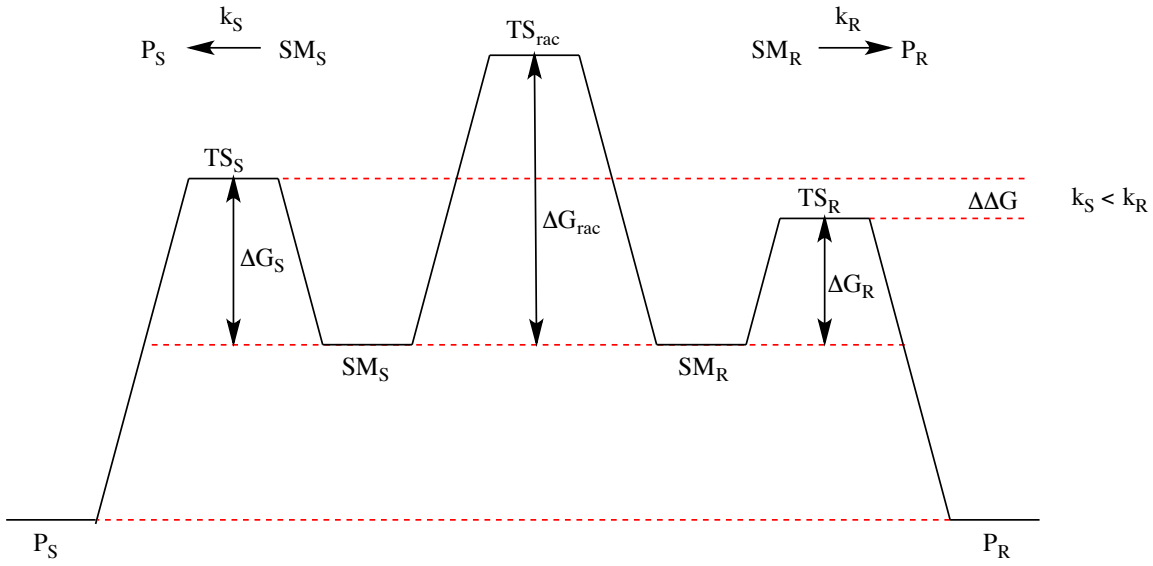

Figure 4.7: A reaction coordinate diagram illustrates the origin of kinetic resolution.

The success of a kinetic resolution is measured with a term called the selectivity factor, *s*. The selectivity factor is a ratio of the rates of reaction for the two enantiomers of the starting material (Equation 4.1).[16]

$$s = \frac{k_1}{k_2}, \qquad \text{Equation 4.1}$$

where k_1 is the rate of reaction for the faster-reacting enantiomer, and k_2 is that of the slower-reacting enantiomer. For example, if one enantiomer is reacting ten times faster than the other, the selectivity factor will be ten. Alternatively, *s* can be expressed in terms of the conversion, C, and the *ee* of the starting material (Equation 4.2).[16]

$$s = \frac{ln[(1-C)(1-ee)]}{ln[(1-C)(1+ee)]}. \qquad \text{Equation 4.2}$$

4.6.1 Kinetic Resolution Using Copper-Catalyzed Azide-Alkyne Cycloadditions

The first (and so far, only) kinetic resolution of azides *via* a copper-catalyzed azide-alkyne cycloaddition (CuAAC) was reported in 2005 by Meng and coworkers.[17] An α-benzylic azide was resolved using copper(I) iodide and an indole-appended pyridine bisoxazoline (PyBOX) ligand (Figure 4.8).

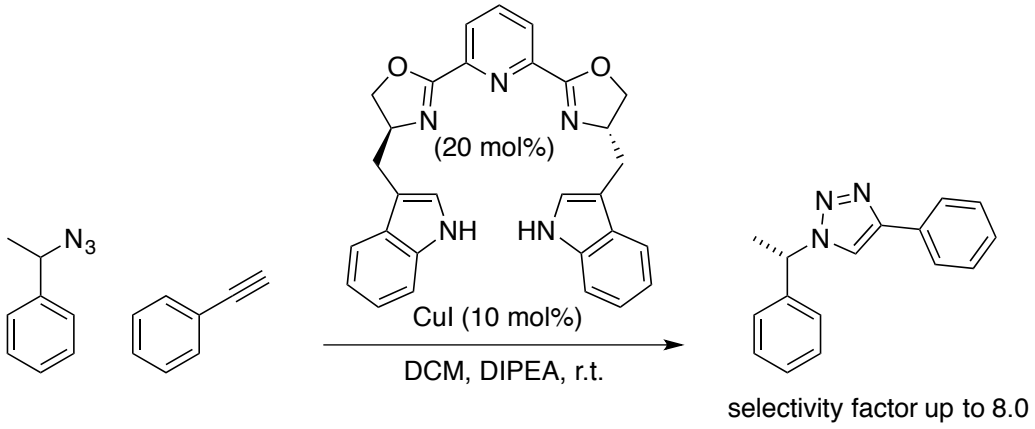

Figure 4.8: Kinetic resolution of an azide *via* CuAAC with copper iodide and an indole-appended PyBOX ligand.

The highest selectivity factor achieved was 8.0; this was a modest result, but it is significant as the first of its kind. The authors also reported an unsuccessful attempt to kinetically resolve terminal alkynes *via* CuAAC, and attributed this failure to the only moderate proximity of the stereocenter on the alkyne to the chiral influence of the ligand.

The first kinetic resolution of a terminal alkyne *via* CuAAC was achieved a full decade after Meng and coworkers' unsuccessful attempt. In 2015, Brittain and coworkers reported a resolution of an alkyne-appended oxindole using copper(I) chloride and a phenyl-substituted PyBOX ligand (Figure 4.9).[18] The largest selectivity factor found for this system was $s = 22$ when the reaction was carried out in 2,5-hexanedione. This result not only proves the applicability of this method to terminal alkynes, but the excellent selectivity also suggests its possible synthetic utility.

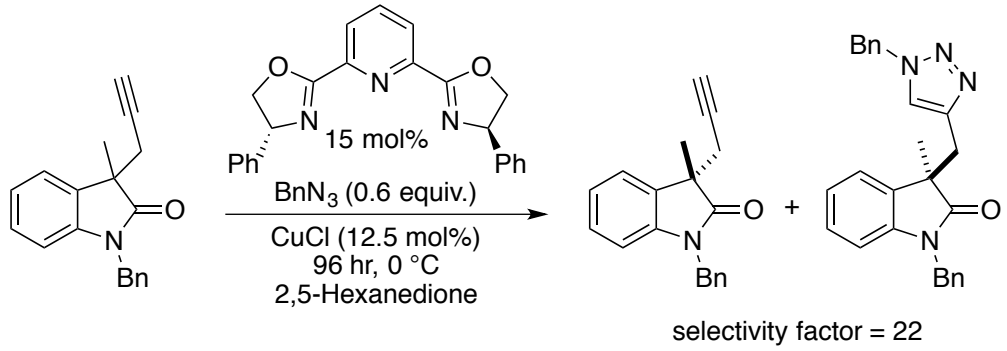

Figure 4.9: Kinetic resolution of a terminal alkyne *via* CuAAC with copper chloride and a phenyl-substituted PyBOX ligand.

Kinetic resolution and other asymmetric methods *via* CuAAC are small in number compared with many common metal-mediated transformations,[19] and there is a lot of methodology left to be developed.

4.7 The Bull-James Assembly as a Dual Chiral Auxiliary and Chiral Shift Reagent for *in situ* Kinetic Resolution of an Alkyne Amine *via* CuAAC[c]

It was proposed that the three-component Bull-James assembly could bind an alkyne-appended amine, and that the hanging alkyne could undergo CuAAC. The goal was for the Bull-James assembly to act as a chiral auxiliary, effecting kinetic resolution, in addition to its usual role of measuring *ee*s by converting a pair of enantiomers to a pair of diastereomers. In this way, it would serve simultaneously as a synthetic and analytical tool, measuring the *ee*s that it brought about (Scheme 4.10). The amine **4.1** was chosen because it is an important building block for several biologically active compounds such as peptide isoteres, analogues of oxotremorine,[20] and benzo[b]furan compounds.[21] In addition, the associated triazole has previously been studied for its antimicrobial activity.[22] Therefore, kinetic resolution would allow access to compounds and intermediates with previously proven biological activity in an enantioenriched form.

[c] Sections 4.7-4.10 were adapted from a manuscript for publication: Brittain, W. D. G.; Chapin, B. M.; Zhai, W.; Lynch, V. M.; Buckley, B. R.; Anslyn, E. V.; Fossey, J. S. The Bull-James Assembly as a Chiral Auxiliary and Shift Reagent in Kinetic Resolution of Alkyne Amines by the CuAAC Reaction. *Org. Biomol. Chem.* Accepted August 9, 2016. The experiments in sections 4.7-4.8 were carried out by William Brittain, Wenlei Zhai, and Brette Chapin.

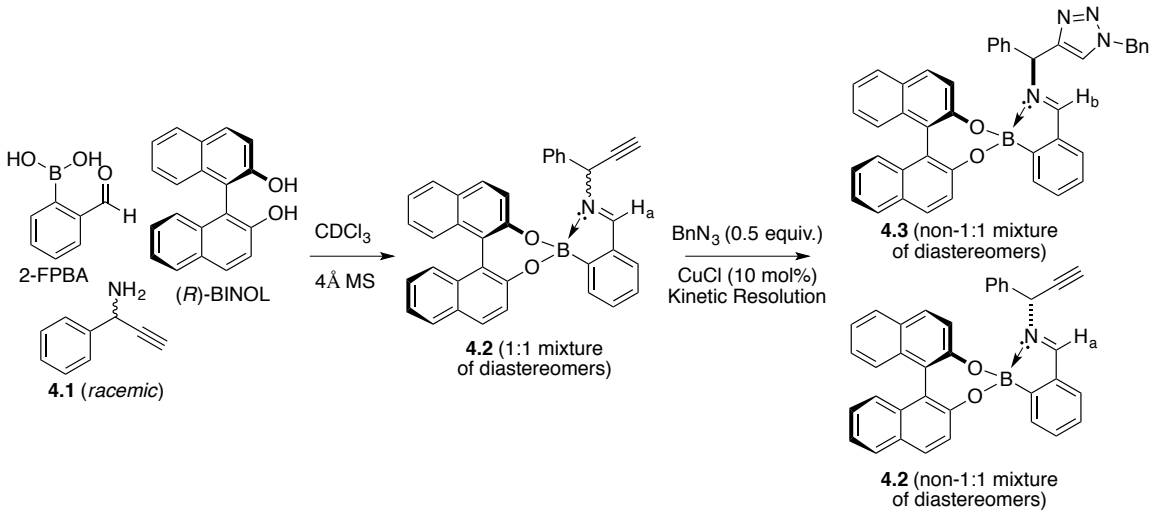

Scheme 4.2: The Bull-James assembly employed simultaneously as a chiral auxiliary for effecting kinetic resolution and as an analytical platform for measuring the degree of kinetic resolution.

It was found that combining 2-FPBA, (*R*)-BINOL, and amine **4.1** formed the assembly **4.2**, and then upon addition of half an equivalent of benzyl azide and 10 mol% copper(I) chloride, CuAAC occurred to form a mixture of assemblies **4.3** and **4.2**. ^{1}H NMR spectroscopy revealed that the integrations corresponding to diastereomers of both alkyne and triazole imine peaks (**4.2**, H_a, and **4.3**, H_b, respectively) were in non-1:1 ratios (Figure 4.10). This showed that after formation of a 1:1 mixture of diastereomers of the assembly **4.2** with amine **4.1**, the alkyne of one diastereomer was consumed more rapidly than the other, which implies that a non-racemic triazole was being formed.

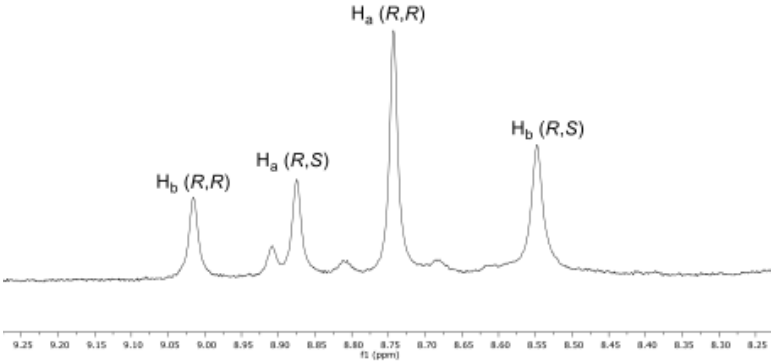

Figure 4.10: Imine region of the ^{1}H NMR spectrum, showing two diastereomers of each complex (**4.2** and **4.3**). Integration of the H_b signals gives a ratio of diastereomers that leads to an inferred *ee* of 37%.

In order to provide data to support that the NMR spectroscopic analysis was giving an accurate measure of *ee* during the kinetic resolution process, we first used chiral HPLC as a standard with which to compare the relative NMR peak integrations. In order to use HPLC for analysis, the manipulations shown in Scheme 4.3 were performed.

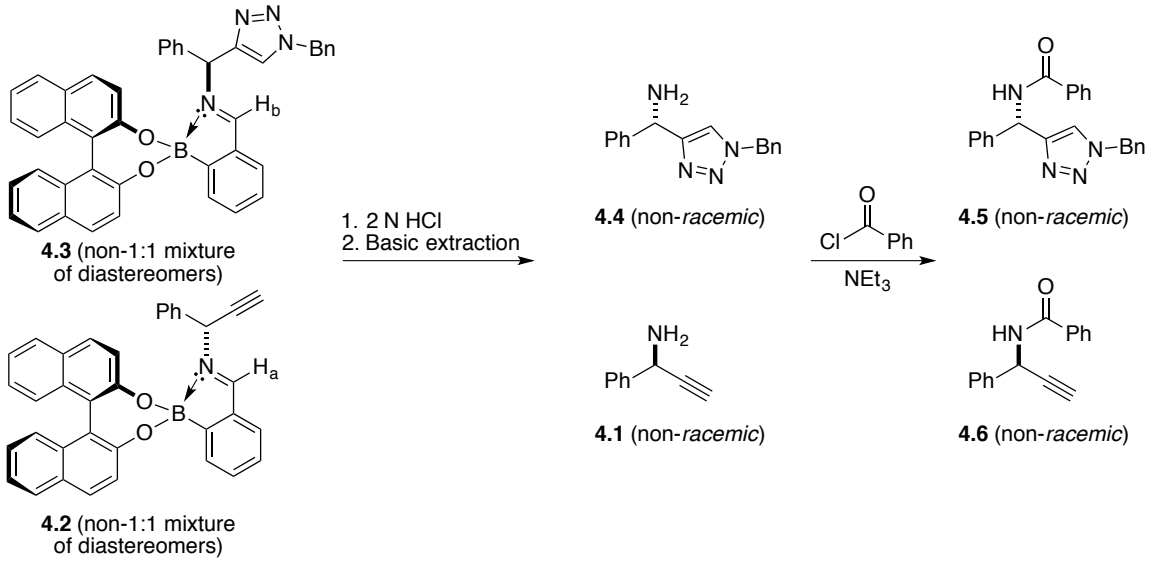

Scheme 4.3: Hydrolysis of the assemblies and benzoylation of the free amines to generate HPLC-separable material.

Hydrolysis of the mixture of assembly **4.2** and **4.3** (following kinetic resolution) with 2 N HCl and subsequent basic extraction led to the recovery of the alkyne amine **4.1** and triazole amine **4.4** with minimal amounts of 2-FPBA and BINOL remaining (Scheme 4.3). The amine was then protected using benzoyl chloride in the presence of triethylamine to give HPLC-separable enantiomers of **4.6** and **4.5**. The calculated *ee*s from HPLC integration were within ±5% *ee* agreement with the level of enantioenrichment determined by *in situ* ^{1}H NMR spectroscopic integration analysis of a mixture of **4.2** and **4.3** during the reaction. As additional evidence for the accuracy of the *in situ* method, it was found that a chiral GC method could be used to measure the *ee* of the starting amine **4.1** without need for derivatization (Figure 4.11).

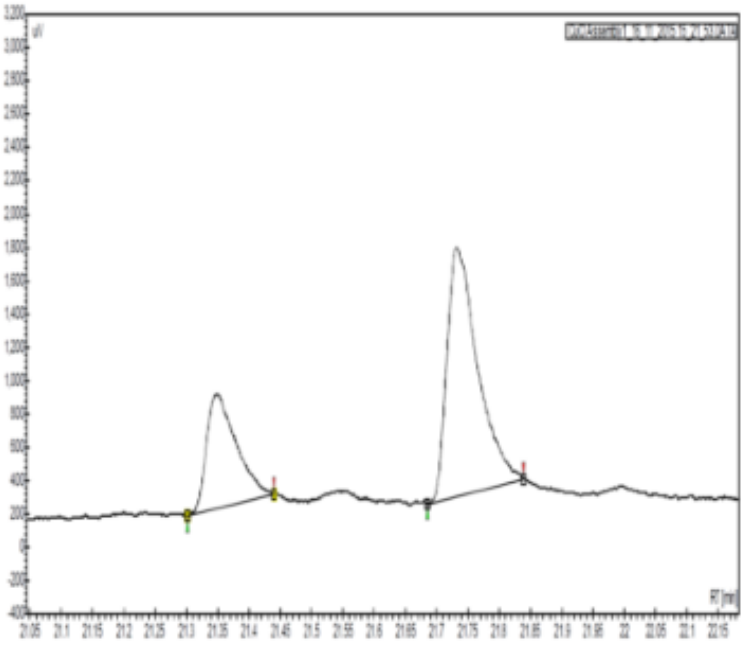

Figure 4.11: Chiral GC trace of amine **4.1** after hydrolysis of the assembly. Integration of the peak areas gives a ratio of diastereomers that leads to an inferred *ee* of 39%. This can be compared to the 37% *ee* calculated from the NMR data in Figure 4.10 from the same reaction.

The chiral GC integration values and the *in situ* NMR spectroscopic integration data of the mixture of diastereiosomers **4.2** and **4.3** during kinetic resolution was shown to be within ±3% *ee* of each other. The agreement of the *ee* values determined by chiral chromatography with the ^{1}H NMR integrations of the imine signals corresponding to the mixture of diastereoisomers **4.2** and **4.3** during kinetic resolution allowed us to conclude that the assembly was successfully doubling as a dual-function chiral auxiliary and *ee* measurement ensemble of *both* the starting material and product *in situ*.

We found that, due to the reversible nature of the boronic acid-diol binding, adventitious water led to the appearance of additional peaks in the proton NMR spectrum. We found that rigorous drying of the BINOL and 2-FPBA and the addition of molecular sieves to all solutions led to the minimization of these side-products.

4.8 Screening Reaction Conditions

After confirming that the three-component assembly was acting as a dual *ee* determination ensemble and chiral auxiliary, we began to screen reaction conditions in the hope of improving the selectivity. First, the copper source was varied, and a range of commercially available Cu(II), Cu(I) and Cu(0) sources were tested (Table 4.3). Of the copper sources tested, our initial choice, CuCl, was confirmed as superior in terms of selectivity (s = 4.1) while still giving reasonable conversion (30%) after 24 hours. CuBr gave slightly increased conversion (34%) but with slightly reduced selectivity (s = 3.7) while CuI was very sluggish and required doubling of the reaction time to 48 hours to give a reasonable conversion (39%) with poorer selectivity (s = 2.4). CuOAc gave no conversion to triazole and Cu(OTf)•0.5 Toluene gave decreased selectivity (s = 2.8). $Cu(MeCN)_4$•BF_4 and $[Cu(CH_3CN)_4]PF_6$ both gave increased conversions (54% and 50%, respectively). However, selectivity was lower (s = 1.9 and s = 3.0, respectively). The

addition of tris[(1-benzyl-1*H*-1,2,3-triazol-4-yl)methyl]amine (TBTA) caused greatly increased conversion (68%) but with decreased selectivity (*s* = 1.7). A range of Cu(II) sources did not improve conversion or selectivity. Copper powder did not catalyze the reaction, but surprisingly, Copper turnings do seem to have some catalytic ability and with respectable selectivity (*s* = 3.3). Conversions were determined by integration of the ^{1}H NMR spectra of the assembly, comparing the imine proton of the starting material and the triazolic product. Values for *ee* were determined *via* comparison of the integration values of the imine region diastereomers in the ^{1}H NMR spectrum of the assembly.

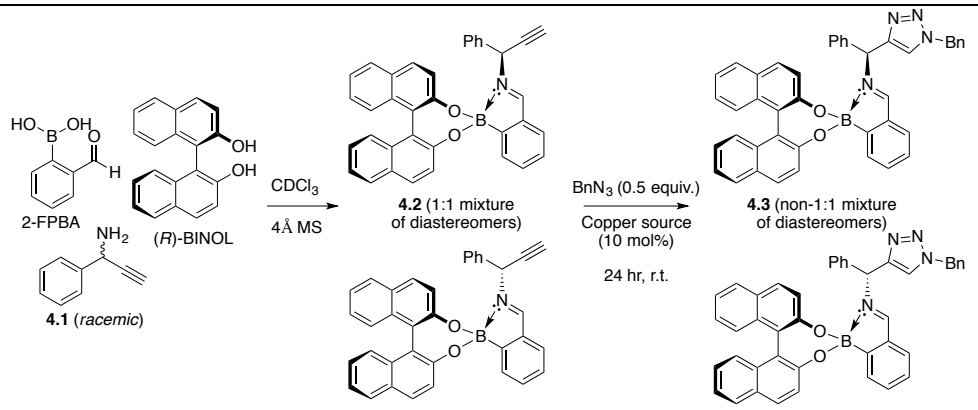

Copper Source	Conversion (%)	ee of S.M. (%)	ee of P (%)	s
CuCl	30	23	39	4.1
CuBr	34	25	48	3.7
CuI	39	21	13	2.4
CuOAc	0	5	-	-
Cu(OTf)•0.5 Toluene	31	18	31	2.8
$Cu(MeCN)_4•BF_4$	54	25	15	1.9
$[Cu(CH_3CN)_4]PF_6$	50	36	16	3.0
CuCl + TBTA 1:1	68	30	13	1.7
$Cu(OAc)_2$	11	6	19	3.1
$CuSO_4$	0	0	-	-
$Cu(OTf)_2$	22	10	28	2.3
$Cu(NO_3)_2•3H_2O$	0	0	-	-
Copper acetylacetonate	0	0	-	-
Copper carbonate basic	0	0	-	-
Cu powder	0	0	-	-
Cu turnings	36	25	23	3.3

Table 4.3: Summary of results for the screening of copper sources.

Next, solvent effects were investigated to determine their influence on both enantioselectivity and spectra analysis. We found that DMSO-d_6 and DMF-d_7 led to broad spectra, which were difficult to integrate to give reliable values, even after drying over molecular sieves. To our surprise, we found that acetonitrile-d_4 and toluene-d_8 both led to precipitation of the assembly. On closer inspection of the acetonitrile case, only one diastereomer (*R*,*R*) precipitated, which was recrystallized and analyzed through XRD to obtain the structure shown in Figure 4.12. Chloroform-*d* was thus determined to be the best choice, as it is amenable to drying with molecular sieves and removal *in vacuo*. In addition, chloroform-*d* has an economic advantage over other more expensive deuterated solvents.

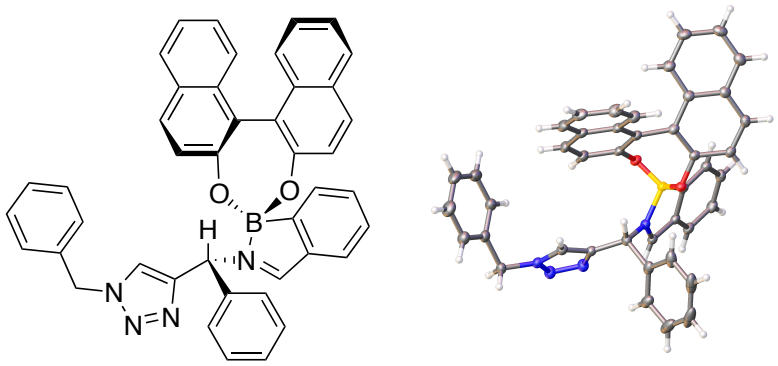

Figure 4.12: Crystal structure of the assembly that precipitated from a mixture of the components in acetonitrile. The chirality of the diastereomer was determined to be (*R*,*R*) from the known chirality of the (*R*)-BINOL.

Next the diol component of the assembly was varied to determine whether this had an effect on the observed enantioselectivity and the ability to determine *ee* (Table 4.4).

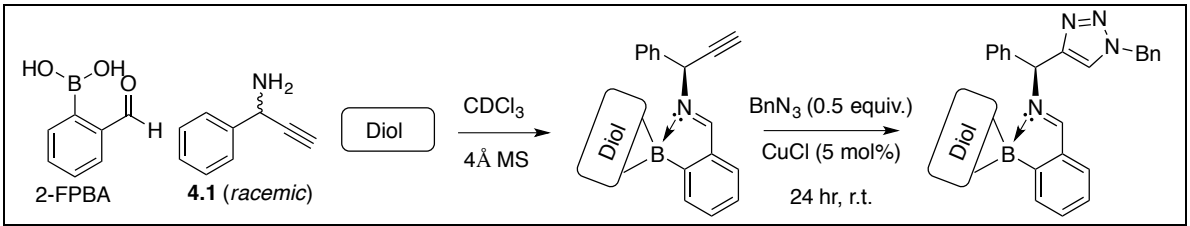

Diol	Conversion (%)	ee of S.M. (%)	ee of P (%)	s
Dimethy-L-tartrate	25	15	5	3.0
(*S*)-1,2-propanediol	40	3	2	1.1
(*2S*,*3S*)-butanediol	3	-	-	-
(*R*)-1,1,2-triphenyl-1,2-ethanediol	40	29	19	3.3
(*R*,*R*)-1,2-dicyclohexyl-1,2-ethanediol	82	2	9	1.0
(*S*)-1-phenyl-1,2-ethanediol	0	-	-	-

Table 4.4: Summary of results for the screening of chiral diols.

After testing this range of diols, it was clear that BINOL was the best choice. The chiral diols listed in Table 4.4 were likely not bulky enough to exert a chiral influence on the reactions. In contrast, very bulky BINOL derivatives lacked sufficient solubility for NMR analysis. The BINOL derivatives that were explored were: (*R*)-3,3'-dibromo-1,1'-bi-2-naphthol, (*R*)-6,6'-dibromo-1,1'-bi-2-naphthol, and (*R*)-3,3'-bis(9-anthracenyl)-1,1'-bi-2-naphthol. (*R*)-2,2'-Diphenyl-3,3'-(4-biphenanthrol) ((*R*)-VAPOL) was also explored but was likewise insufficiently soluble.

4.9 Conclusions

These preliminary findings show that chiral boronic acid-based assemblies designed for *ee* analysis of amines *via* ^{1}H NMR spectroscopy can also be used as chiral

auxiliaries. This allows for the catalysis and analysis of the reaction mixture to be carried out by the same auxiliary. It was shown that this assembly can effect, and accurately measure, the enantioenrichment of primary amine alkynes and primary amine triazoles in a kinetic resolution reaction. Since kinetic resolution of terminal alkynes *via* CuAAC is presently a challenging reaction, it is a robust test of this dual chiral auxiliary sensing system. This system allows for rapid and relatively accurate measurement of an ongoing asymmetric transformation *in situ*, and thus analysis time is shortened compared with standard chiral chromatography. We anticipate that the concept of using a chiral appendage as both an asymmetric induction unit and as an NMR chiral shift reagent will be applicable to other asymmetric transformations.

4.10 EXPERIMENTAL

4.10.1 General

Reagents were used as purchased from suppliers without further purification, with the exception of 2-FPBA. 2-FPBA was recrystallized from dichloromethane and hexane before use. ^{1}H NMR spectra were recorded at 300 MHz and 400 MHz using Bruker AVIII 300 and Bruker AVIII 400 NMR, Varian DirectDrive 400 spectrometers. ^{13}C NMR experiments were carried out on a Bruker AVIII 400 NMR and Varian DirectDrive 400 NMR spectrometer recorded at 101 MHz. HPLC analysis was carried out using an Agilent 1260 Infinity and Chiralpak IA column, and traces were recorded at eight UV wavelengths: 210, 214, 230, 250, 254, 260, 273 and 280 nm. Calculations were carried out using the traces recorded at 254 nm. GC analysis was carried out on a Varian 430-GC using a Chiralsil-Dex CB chiral column using a UV detector. Column chromatography was carried out using a Combiflash R*f* 200i and column traces were recorded at two UV wavelengths (254 nm and 280 nm).

4.10.2 Synthesis

Synthesis of 1-phenylprop-2-yn-1-ol

Under an atmosphere of nitrogen, a solution of benzaldehyde (1.0 mL, 10.0 mmol) in THF (10 mL) was stirred at -78 °C using a dry ice and acetone bath. To this solution, ethynylmagnesium bromide (24 mL, 0.5 M in THF) was added dropwise over a period of 10 minutes with stirring. This was then allowed to slowly warm to room temperature and stirred for a further 3 h. The reaction mixture was then quenched with sat. NH_4Cl solution, and extracted with DCM (3 x 50 mL). The combined organic fractions were washed with water (100 mL), dried with $MgSO_4$, and concentrated *in vacuo*. The resulting brown oil was purified by automated flash column chromatography combiflash Rf (0-100% EtOAc : hexane gradient, 20 mins) to yield the product as a yellow oil, 1.2 g, 91% yield.

Characterization was consistent with literature.[23] δ_H (400 MHz, $CDCl_3$) 7.58 – 7.51 (2H, m), 7.41 – 7.31 (3H, m), 5.45 (1H, d, *J* 1.5), 2.66 (1H, d, *J* 2.3), 2.44 (1H, br s); δ_C (101 MHz, $CDCl_3$) 140.05, 128.70, 128.58, 126.63, 83.52, 74.86, 64.43; IR ν_{max} (ATR)/cm^{-1} 3431, 3289, 3066, 3032, 1453, 1019, 947; MS AP^- *m/z* 131.0 [M-H]; HRMS (AP^--TOF) Calculated for $C_9H_7O^-$ = 131.0502 Found = 131.0494.

Synthesis of N-*(1-phenylprop-2-yn-1-yl)acetamide*

To a mixture of 1-phenyl-2-propynyl-1-ol (1.11 g, 8.4 mmol) and anhydrous sodium sulfate (1.2 g, 8.4 mmol) in acetonitrile (20 mL) at 0 °C was added a solution of 95% sulfuric acid (4.28 g, 42 mmol, 2.9 mL) in acetonitrile (10 mL). The mixture was allowed to warm to room temperature and stirred for 48 h. The solution was then concentrated *in vacuo* and the residue poured onto ice. This mixture was then extracted with EtOAc (3 x 50 mL) and then DCM (50 mL). The combined organic fractions were dried with $MgSO_4$ and concentrated *in vacuo*. The crude mixture was subjected to

automated flash column chromatography combiflash Rf (0-100% EtOAc : Hexane gradient, 20 mins) to yield the product as a cream-colored solid 0.87 g, 59% yield. Characterization was consistent with literature.[24] δ_H (400 MHz, $CDCl_3$) 7.51 – 7.49 (2H, m), 7.40 – 7.30 (3H, m), 6.03 (1H, s), 2.51 – 2.48 (1H, m), 2.02 (3H, s); δ_C (101 MHz, $CDCl_3$) 168.79, 138.27, 128.78, 128.29, 127.05, 81.70, 72.99, 44.53, 23.18; IR ν_{max} (ATR)/cm^{-1} 3280, 3038, 1648, 1532, 1452, 1371, 1309, 1092; MS AP+ *m/z* 174.1 [M+H]; HRMS (AP+-TOF) Calculated for $C_{11}H_{12}NO^+$ = 174.0913 Found = 174.0913; MP 89 – 90 °C.

Synthesis of 1-phenylprop-2-yn-1-amine

To a solution of *N*-(1-phenylprop-2-yn-1-yl)acetamide (0.10 g, 0.76 mmol) in methanol (1 mL) was added 3.0 N aqueous HCl (20 mL) and the reaction mixture heated to 70 °C for 18 h. The resulting solution was extracted with EtOAc (50 mL). The aqueous phase was basified with aqueous 2.0 N NaOH solution to pH ~10. This was then extracted with EtOAc (3 x 50 mL), the organic layers were combined, dried with $MgSO_4$, and concentrated *in vacuo* to afford sufficiently pure 1-phenylprop-2-yn-1-amine as a yellow oil 0.036 g 35% yield. It was found that this compound will degrade if stored in its pure form; material was stored as a solution in chloroform in the freezer. Characterization was consistent with literature.[25] δ_H (300 MHz, $CDCl_3$) 7.58 – 7.50 (2H, m), 7.40 – 7.29 (3H, m), 4.78 (1H, d, *J* 1.9), 2.49 (1H, d, *J* 2.3), 1.91 (2H, br s); δ_C (101 MHz, $CDCl_3$) 141.59, 128.67, 127.82, 126.67, 86.01, 72.30, 47.31; IR ν_{max} (ATR)/cm^{-1} 3666, 3288, 1492, 1451, 1275; MS AP+ *m/z* 132.1 [M+H]; HRMS (AP+-TOF) Calculated for $C_{11}H_{12}NO^+$ = 132.0913 Found = 132.0814.

Synthesis of N-*((1-benzyl-1*H*-1,2,3-triazol-4-yl)(phenyl)methyl)acetamide*

To a solution of *N*-(1-phenylprop-2-yn-1-yl)acetamide (0.050 g, 0.30 mmol) and benzyl azide (0.044 g, 0.33 mmol) in methanol (20 mL) was added sodium L-ascorbate

(0.059 g, 0.30 mmol) and copper sulfate pentahydrate (0.008 g, 0.03 mmol). The mixture was allowed to stir at 50 °C for 3 h. The reaction mixture was quenched with 5% aqueous ammonia solution (10 mL). The solution was extracted with EtOAc (3 x 25 mL) and the combined organic extracts were washed with water (100 mL), dried with $MgSO_4$, and concentrated *in vacuo* to give the pure triazole as a cream-colored solid, 0.081 g, 87% yield.

Characterization was consistent with literature.[22] δ_H (400 MHz, $CDCl_3$) 7.39 – 7.21 (11H, m), 6.95 (1H, d, *J* 7.7), 6.27 (1H, d, *J* 7.9), 5.47 (2H, q, *J* 14.8), 2.01 (3H, s); δ_C (101 MHz, $CDCl_3$) 169.26, 147.98, 140.88, 134.30, 129.17, 128.86, 128.71, 128.11, 127.73, 127.26, 121.53, 54.25, 49.56, 23.27; IR ν_{max} (ATR)/cm^{-1} 1721, 1653, 1489, 1345, 1278, 1154; MS ESI *m/z* 329.1 [M+Na]; MP 155 – 156 °C.

*Synthesis of (1-benzyl-1*H*-1,2,3-triazol-4-yl)(phenyl)methanamine*

To a solution of *N*-((1-benzyl-1*H*-1,2,3-triazol-4-yl)(phenyl)methyl)acetamide (0.25 g, 3.24 mmol) in methanol (2 mL) was added 3.0 N aqueous HCl (20 mL). The mixture heated to 70 °C for 18 h, after which the reaction mixture was extracted with EtOAc (50 mL), the aqueous phase basified to pH ~10 with 2.0 N aqueous NaOH, extracted with EtOAc (3 x 50 mL), dried with $MgSO_4$, and concentrated *in vacuo* to give the product as a cream-colored solid, 0.48 g, 56% yield.

δ_H (400 MHz, $CDCl_3$) 7.44 – 7.13 (11H, m), 5.45 (2 H, s), 5.36 (1 H, s) δ_C (101 MHz, $CDCl_3$) 152.76, 143.79, 134.64, 129.07, 128.66, 128.05, 127.50, 126.86, 120.73, 54.15, 52.54. IR ν_{max} (ATR)/cm^{-1} 3366, 3122, 3064, 2925, 2853, 1494, 1454, 1216; MS ESI *m/z* 287.1 [M+Na]; HRMS (ESI-TOF) Calculated for $C_{16}H_{16}N_4Na^-$ = 287.1278 Found = 287.1274.; MP 86 - 88°C.

Synthesis of N-(1-phenylprop-2-yn-1-yl)benzamide

To a solution of 1-phenylprop-2-yn-1-amine (10 mg, 0.08 mmol) in DCM (10 mL) cooled in an ice bath was added benzoyl chloride (11 mg, 8.8 μL, 0.08 mmol) and TEA (8.0 mg, 10 μL, 0.08 mmol). The reaction was allowed to warm to room temperature and stirred for 2 h. The reaction was then quenched with water (10 mL) and extracted with EtOAc (3 x 25 mL). The organic fractions were combined, dried over $MgSO_4$, and concentrated *in vacuo*. The crude mixture was purified by automated flash column chromatography combiflash Rf (0-100% EtOAc : Hexane gradient, 20 mins) to yield the product as a white solid, 15 mg, 84% yield.

δ_H (400 MHz, $CDCl_3$) 7.83 – 7.77 (2 H, m), 7.62 – 7.57 (2 H, m), 7.55 – 7.49 (1 H, m), 7.47 – 7.31 (5 H, m), 6.57 (1 H, d, *J* 7.9), 6.25 (1 H, dd, *J* 8.4, 2.4), 2.55 (1 H, d, *J* 2.4); δ_C (101 MHz, $CDCl_3$) 166.20, 138.21, 133.67, 131.92, 128.85, 128.66, 128.36, 127.11, 81.64, 73.33, 44.99; IR ν_{max} (ATR)/cm^{-1} 3291, 3034, 1639, 1522, 1488, 1331; MS AP+ *m/z* 236.1 [M+H]; HRMS (AP+-TOF) Calculated for $C_{16}H_{14}NO^+$ = 236.1070 Found = 236.1073; MP 131 – 132 °C; HPLC (IA) Hexane/IPA 80:20, 1.0 mL/min, λ = 254 nm, t_{major} = 7.9 min, t_{minor} = 8.8 min.

Synthesis of N-*((1-benzyl-1*H*-1,2,3-triazol-4-yl)(phenyl)methyl)benzamide*

To a solution of (1-benzyl-1*H*-1,2,3-triazol-4-yl)(phenyl)methanamine (0.079 g, 0.3 mmol) in DCM (10 mL) cooled in an ice bath was added benzoyl chloride (0.042 g, 35 μL, 0.3 mmol) and TEA (0.030 g, 42 μL, 0.3 mmol). The reaction allowed to warm to room temperature and stirred for 2 h. The reaction was then quenched with water (10 mL) and extracted with EtOAc (3 x 25 mL). The organic fractions were combined, dried over $MgSO_4$, and concentrated *in vacuo*. The crude mixture was purified by automated flash column chromatography combiflash Rf (0-100% EtOAc : Hexane gradient, 20 mins) to yield the product as a white solid 0.102 g, 93% yield.

δ_H (400 MHz, $CDCl_3$) 7.83 (2 H, dd, *J* 5.2, 3.3), 7.58 (1 H, d, *J* 7.4), 7.52 – 7.21 (13 H, m), 6.46 (1 H, d, *J* 7.5), 5.49 (2 H, ABq, *J* 14.8); δ_C (101 MHz, $CDCl_3$) 166.51, 147.97, 140.93, 134.29, 134.03, 131.68, 129.18, 128.87, 128.77, 128.55, 128.13, 127.79, 127.30, 127.18, 121.58, 54.30, 50.12; IR ν_{max} (ATR)/cm^{-1} 3378, 3116, 1639, 1515, 1487, 1354; MS ESI *m/z* 391.2 [M+Na]; HRMS (ESI-TOF) Calculated for $C_{23}H_{20}N_4ONa^-$ = 391.1540 Found = 391.1541; MP 207 – 209 °C; HPLC (IA) Hexane/IPA 80:20, 1.0 mL/min, λ = 214 nm, t_{major} = 16.7 min, t_{minor} = 18.3 min.

4.10.3 Catalysis

A mixture of 2-FPBA (5.7 mg, 0.038 mmol, 1 equiv.) and (*R*)-BINOL (10.9 mg, 0.038 mmol, 1 equiv.) were placed in a vial and dried under high vacuum for 2 hours. The mixture was removed from high vacuum and a solution of amine **4.1** (5.0 mg, 0.038 mmol, 1 equiv.) in $CDCl_3$ (0.5 mL) and dried over 4A MS was added. A small number of 4A MS were added to the vial and the contents stirred at rt for 20 mins. To this, 0.1 mL of benzyl azide stock solution (24 μL per 1 mL, 0.5 equiv.) was added, along with CuCl (0.19 mg, 0.0019 mmol, 5 mol%) and the reaction was allowed to stir at r.t. for 24 h. After this time a ^1H NMR was taken of the reaction mixture to give the conversion and enantiomeric excess of **4.1** and **4.4**. To recover the alkyne **4.1** and triazole **4.4** after the reaction was completed, 2.0 N HCl solution (5 mL) was added to the NMR sample and the combined solution was left to stir vigorously for 30 minutes. The mixture was then extracted with EtOAc (25 mL) and water (25 mL). The aqueous phase was then basified to pH ~10 using 2.0 N NaOH. The basified solution was then extracted with EtOAc (3 x 25 mL) and the combined organic fractions were dried with $MgSO_4$ and concentrated *in vacuo* to give alkyne **4.1** and triazole **4.4** with minimal amounts of the other assembly components. Selected examples of *ee* were verified *via* either chiral GC or chiral HPLC

methodology. For HPLC determination, benzoylation of the recovered mixture of components was carried out as detailed above.

4.11 Acknowledgements

Dr. John Fossey and the entire Fossey group, but particularly William Brittain, Wenlei Zhai, and Daniel Payne, are gratefully acknowledged for their collaboration with the work presented in this chapter.

4.12 References

(1) Perez-Fuentes, Y.; Kelly, A. M.; Fossey, J. S.; Powell, M. E.; Bull, S. D.; James, T. D. Simple Protocols for NMR Analysis of the Enantiomeric Purity of Chiral Primary Amines. *Nat. Protoc.* **2008**, *3* (2), 210–214.

(2) Kelly, A. M.; Perez-Fuentes, Y.; Fossey, J. S.; Yeste, S. L.; Bull, S. D.; James, T. D. Simple Protocols for NMR Analysis of the Enantiomeric Purity of Chiral Diols. *Nat. Protoc.* **2008**, *3* (2), 215–219.

(3) Yeste, S. L.; Powell, M. E.; Bull, S. D.; James, T. D. Simple Chiral Derivatization Protocols for 1H NMR and 19F NMR Spectroscopic Analysis of the Enantiopurity of Chiral Diols. *J. Org. Chem.* **2009**, *74* (1), 427–430.

(4) Mirri, G.; Bull, S. D.; Horton, P. N.; James, T. D.; Male, L.; Tucker, J. H. R. Electrochemical Method for the Determination of Enantiomeric Excess of Binol Using Redox-Active Boronic Acids as Chiral Sensors. *J. Am. Chem. Soc.* **2010**, *132* (26), 8903–8905.

(5) Metola, P.; Anslyn, E. V.; James, T. D.; Bull, S. D. Circular Dichroism of Multi-Component Assemblies for Chiral Amine Recognition and Rapid Ee Determination. *Chem. Sci.* **2012**, *3* (1), 156–161.

(6) Shcherbakova, E. G.; Minami, T.; Brega, V.; James, T. D.; Anzenbacher, P. J. Determination of Enantiometic Excess in Amine Derivatives with Molecular Self-Assemblies. *Angew. Chem. Int. Ed.* **2015**, *54* (24), 7130–7133.

(7) Cao, Z.-Y.; Brittain, W. D. G.; Fossey, J. S.; Zhou, F. Recent Advances in the Use of Chiral Metal Complexes with Achiral Ligands for Application in Asymmetric Catalysis. *Catal. Sci. Technol.* **2015**, *5* (7), 3441–3451.

(8) Jo, H. H.; Gao, X.; You, L.; Anslyn, E. V.; Krische, M. J. Application of a High-Throughput Enantiomeric Excess Optical Assay Involving a Dynamic Covalent Assembly: Parallel Asymmetric Allylation and Ee Sensing of Homoallylic Alchohols. *Chem. Sci.* **2015**, *6* (12), 6747–6753.

(9) Jo, H. H.; Lin, C.-Y.; Anslyn, E. V. Rapid Optical Methods for Enantiomeric Excess Analysis: From Enantioselective Indicator Displacement Assays to Exciton-Coupled Circular Dichroism. *Acc. Chem. Res.* **2014**, *47* (7), 2212–2221.

(10) Dragna, J. M.; Gade, A. M.; Tran, L.; Lynch, V. M.; Anslyn, E. V. Chiral Amine Enantiomeric Excess Determination Using Self-Assembled Octahedral Fe(II)-Imine Complexes. *Chirality* **2015**, *27* (4), 294–298.

(11) Dalvit, C.; Flocco, M.; Knapp, S.; Mostardini, M.; Perego, R.; Stockman, B. J.; Veronesi, M.; Varasi, M. High-Throughput NMR-Based Screening with Competition Binding Experiments. *J. Am. Chem. Soc.* **2002**, *124* (26), 7702–7709.

(12) Reetz, M. T.; Eipper, A.; Tielmann, P.; Mynott, R. A Practical NMR-Based High-Throughput Assay for Screening Enantioselective Catalysts and Biocatalysts. *Adv. Synth. Catal.* **2002**, *344* (9), 1008–1016.

(13) Chen, A.; Shapiro, M. J. NOE Pumping as High-Throughput Method To Determine Compounds with Binding Affinity to Macromolecules by NMR. *J. Am. Chem. Soc.* **2000**, *122* (2), 414–415.

(14) Dale, J. A.; Dull, D. L.; Mosher, H. S. Alpha-Methoxy-Alpha-Trifluoromethylphenylacetic Acid, a Versatile Reagent Forthe Determination of Enantiomeric Composition of Alcohols and Amines. *J. Org. Chem.* **1969**, *34* (9), 2543–2549.

(15) Dale, J. A.; Mosher, H. S. Nuclear Magnetic Resonance Enantiomer Reagents. Configurational Correlations via Nuclear Magnetic Resonance Chemical Shifts of Diastereomeric Mandelate, O-Methylmandelate, and Alpha-Methoxy-Alpha-Trifluoromethylphenylacetate (MTPA) Esters. *J. Am. Chem. Soc.* **1973**, *95* (2), 512–519.

(16) Kagan, H. B.; Fiaud, J. C. Kinetic Resolution. In *Topics in Stereochemistry, Volume 18*; Eliel, E. L., Wilen, S. H., Eds.; John Wiley & Sons, 1988; pp 249–330.

(17) Meng, J.; Fokin, V. V.; Finn, M. G. Kinetic Resolution by Copper-Catalyzed Azide-Alkyne Cycloaddition. *Tetrahedron Lett.* **2005**, *46*, 4543–4546.

(18) Brittain, W. D. G.; Buckley, B. R.; Fossey, J. S. Kinetic Resolution of Alkyne-Substituted Quaternary Oxindoles via Copper Catalysed Azide-Alkyne Cycloadditions. *Chem. Commun.* **2015**, *51* (97), 17217–17220.

(19) Brittain, W. D. G.; Buckley, B. R.; Fossey, J. S. Asymmetric Copper-Catalyzed Azide-Alkyne Cycloadditions. *ACS Catal.* **2016**, *6*, 3629–3636.

(20) Nilsson, B. M.; Vargas, H. M.; Ringdahl, B.; Hacksell, U. Phenyl-Substituted Analogs of Oxotremorine as Muscarinic Antagonists. *J. Med. Chem.* **1992**, *35* (2), 285–294.

(21) Messina, F.; Botta, M.; Corelli, F.; Schneider, M. P.; Fazio, F. Resolution of (±)-1-Aryl-2-Propynlamines via Acyl Transfer Catalyzed by Candida Antarctica Lipase. *J. Org. Chem.* **1999**, *64* (10), 3767–3769.

(22) Castagnolo, D.; Dessi, F.; Radi, M.; Botta, M. Synthesis of Enantiomerically Pure Alpha-[4-(1-Substituted)-1,2,3-Triazol-4-Yl]-Benzylacetamides via Microwave-Assisted Click Chemistry: Towards New Potential Antimicrobial Agents. *Tetrahedron: Asymmetry* **2007**, *18* (11), 1345–1350.

(23) Ye, L.; He, W.; Zhang, L. Gold-Catalyzed One-Step Practical Synthesis of Oxetan-3-Ones from Readily Available Propargylic Alcohols. *J. Am. Chem. Soc.* **2010**, *132* (25), 8550–8551.

(24) Ni, Z.; Giordano, L.; Tenaglia, A. Cyclobutene Formation in PtCl2-Catalyzed Cycloisomerizations of Heteroatom-Tethered 1,6-Enynes. *Chem. Eur. J.* **2014**, *20* (37), 11703–11706.

(25) Nilsson, B. M.; Hacksell, U. Base-Catalyzed Cyclization of N-Propargylamides to Oxazoles. *J. Heterocycl. Chem.* **1989**, *26* (2), 269–275.

Chapter 5: Exploring the Reversibility of Azide-Alkyne Cycloadditions

5.1 Introduction

The term "click chemistry" was coined by K.B. Sharpless in 2001 to describe a broad class of reactions that meet a number of criteria.[1] These reactions must be modular, wide in scope, selective, high-yielding, and cannot generate offensive byproducts, according to Sharpless' definition. They must require only readily available starting materials and be carried out under simple conditions to generate easily isolable products. The term was originally applied to many reactions, such as nucleophilic ring-opening reactions, cycloadditions, and even reactions that are typically used to introduce protecting groups. Perhaps the most well-known click reaction is the Huisgen dipolar [3 + 2] cycloadditon. This reaction brings together an azide and an alkyne to form 1,4- and 1,5-disubstituted 1,2,3-triazoles.[2] This reaction was described as the "cream of the crop" by Sharpless and co-workers[1] due to the azide's orthogonal reactivity. Azides remain latent until a dipolarophile (such as an alkyne or alkene) is present, and then react readily and specifically.

In 2002, Sharpless and Meldal simultaneously reported the copper(I)-catalyzed azide-alkyne cycloaddition (CuAAC).[3,4] CuAAC is stepwise, rather than concerted, and generates the 1,4-disubstituted triazole exclusively. The catalytic cycle for the reaction is shown in Scheme 5.1. In the first step, the terminal alkyne is deprotonated and coordinates in a sigma fashion to a copper(I) ion to form a copper acetylide. The proximal nitrogen of the azide then coordinates to copper, and the substituents cyclize to form a six-membered metallocycle. The ring contracts to exclude copper, which is then replaced by a proton to produce a 1,2,3-triazole and regenerate the active copper(I)

catalyst. Over time, the term “click chemistry” has come to be colloquially associated with this specific reaction.

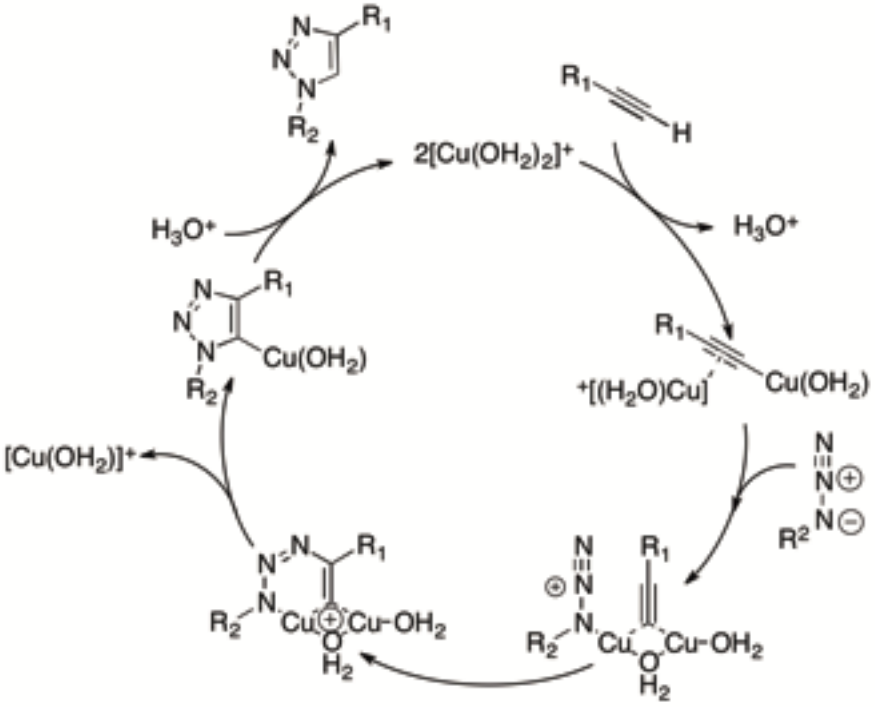

Scheme 5.1: Catalytic cycle for CuAAC.

Whereas the uncatalyzed cycloaddition generates a 62% combined yield of the two triazole regioisomers after eight hours at 60 °C, the copper-catalyzed version produces a 92% yield of exclusively the 1,4-disubstituted product after one hour at room temperature.[5] This result demonstrates the power of CuAAC and implies that the reaction is quite exothermic. In fact, density functional theory (DFT) calculations predict the cycloaddition of an azide and an alkyne to be exothermic by approximately 50 kcal/mol. In the thermally promoted Huisgen [3 + 2] cycloaddition, the activation energy is predicted to be approximately 35 kcal/mol, which explains the need for elevated reaction temperatures. In the copper(I)-catalyzed version, the barrier to formation of the

metallocycle is the rate-determining step. This barrier has a calculated energy of 16 kcal/mol and is easily overcome at room temperature.[6]

The goal of this research project was to identify conditions under which the copper(I)-catalyzed azide-alkyne cycloaddition could be carried out chemically in both the forward and reverse directions. More specifically, the goal was for the forward and reverse reactions to take place simultaneously and dynamically. We envisioned conditions under which azides, alkynes, and triazoles existed at a thermodynamic equilibrium such that various reaction partners could cyclize reversibly to form the most stable triazole. Determining the factors that would allow this scenario to occur was of interest because such conditions would challenge the notion that this reaction is chemically irreversible. Additionally, reversibility of the click reaction would allow its use in applications that require dynamic reactions.

5.2 Approaches to Reversing CuAAC

A variety of conditions were explored in search of a system that would allow cycloreversion of a triazole to regenerate the parent azide and alkyne. We hypothesized that if a triazole is coordinated to a metal ion, it may be able to undergo a cycloreversion through the same intermediates that form in the forward direction, according to the principle of microscopic reversibility. Thus we explored a triazole derivative that allows recoordination. Two alternative approaches to address reversibility are based on oxidative addition of a triazole derivative to a metal ion. This system involves generation of a hypervalent metal that could be unstable enough to regenerate the component azide and alkyne. Each of the approaches that follow was influenced by different precedents and designed by different rationales, so each system will be introduced and described individually.

5.2.1 Microscopic Reversibility: Coordination of a Triazolium Salt

The last step of the copper(I)-catalyzed azide-alkyne cycloaddition mechanism is the concomitant release of copper and protonation of the triazole. According to the principle of microscopic reversibility, the reverse reaction would occur by proceeding through the same intermediates as the forward reaction. However, the copper-bound species is not accessible in the reverse direction because the triazole is not easily deprotonated. Our approach was to alter the triazole in such a way that this proton can be removed, and the resulting lone pair on the carbon at the 5-position could recoordinate to the copper catalyst. We hypothesized that this copper-coordinated triazole derivative could undergo a cycloreversion similar to that of a free triazole and could thus experience similar intermediates. 1,4-Triazoles have previously been methylated at the 3-position, and the resulting triazolium salts are known to undergo deuterium exchange of the triazolic proton in aqueous base.[7] Furthermore, these salts have been shown to coordinate to copper.[8] For these reasons, methylated triazolium salts were explored as a potential system for reversibility. Our proposed catalytic cycle for the reaction is shown in Scheme 5.2. In this proposal, an azide and an alkyne form a triazole, and this triazole is methylated by methyl iodide. The triazolium salt is then deprotonated at the triazolic proton, and the conjugate base coordinates to copper. Cycloreversion could occur, releasing a copper acetylide and a methylated azide. The methylated azide, which was expected to be very unstable, would then transfer a methyl group to another triazole and then cyclize with the copper acetylide generated in the previous step. Finally, a proton would take the place of copper to form a new triazole and regenerate the copper catalyst.

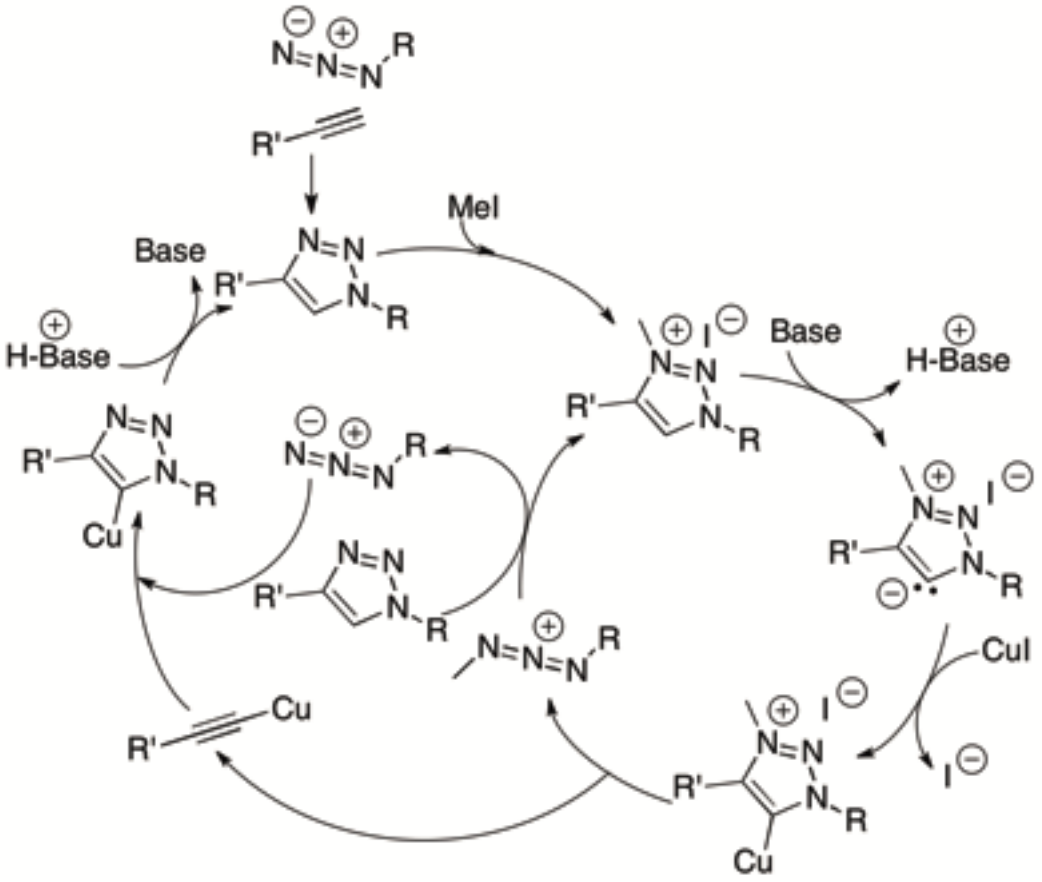

Scheme 5.2: Proposed catalytic cycle for the cycloreversion of a methylated triazolium salt.

The 1,4-disubstituted 1,2,3-triazoles were prepared[9] and methylated[10] according to literature procedures. The resulting triazolium salt was then combined with sodium deuteroxide in deuterated methanol and monitored by ^{1}H NMR spectroscopy. Deuterium exchange occurred rapidly, and the triazolic proton peak was invisible by NMR spectroscopy in less than ten minutes, showing that the proton was made acidic by the formal positive charge on the molecule. Triethylamine and potassium bicarbonate were also studied for promoting deuterium exchange. Exchange was successful, despite the fact that these are weaker bases than hydroxide. Deprotonation was also carried out in the

presence of copper iodide to determine whether coordination to the metal would occur, but no downfield shifts were observed by NMR spectroscopy, indicating that coordination did not take place. Although the copper-coordinated species is not observable in solution, this does not preclude its role as a high-energy intermediate that could exist undetected in low concentration. It was hypothesized that if copper participates in the reaction by coordinating the deprotonated triazole, a change in the rate of deuterium exchange would be observed. This hypothesis was investigated by plotting the time-dependent proportion of triazolic protons on the triazolium salt in the presence of base for one hour. Note that a lesser proportion of protonation indicates increased deuterium exchange of the triazolic proton. Copper(I) showed little effect on the rate of deuterium exchange, so other metals were investigated (Figure 5.1).

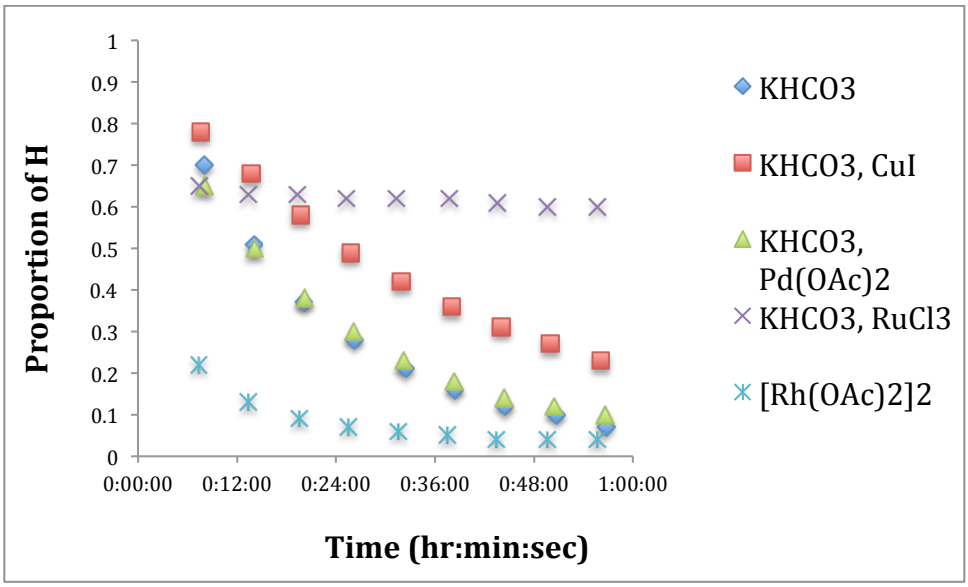

Figure 5.1: Proportion of H versus time in the presence of base and various metal salts.

Ruthenium(III)[11] and silver(I)[12] were chosen because they have been shown to be competent catalysts for azide-alkyne cycloadditions. Silver(I) and palladium(II) have

been shown to coordinate triazolium salts and were studied as well.[13] Palladium(II) appeared to have no effect on the rate of deuterium exchange, and any apparent effect of copper(I) is not statistically significant. Ruthenium(III) and rhodium(II) showed a significant effect on exchange, making them ideal for further exploration. The effects of $Pd(PPh_3)_4$ and $AgNO_3$ were also measured but are not shown in the figure. Complete deuterium exchange occurred almost immediately in the presence of these two metals, indicating that they play a role in facilitating exchange. Deuterium exchange also occurred immediately in the absence of base with both metals, indicating that oxidative addition, rather than deprotonation and subsequent coordination, was likely occurring.

A second exchange reaction that was studied is the transfer of a methyl group from a triazolium salt to a triazole. Triazole-triazolium salt pairs (**5.1**-**5.6** and **5.1a**-**5.6a**, Figure 5.2) were heated at reflux in various solvents in order to effect a nucleophilic substitution reaction (Table 5.1). In this reaction, the triazole was expected to act as a nucleophile and the triazolium methyl group was expected to act as an electrophile.

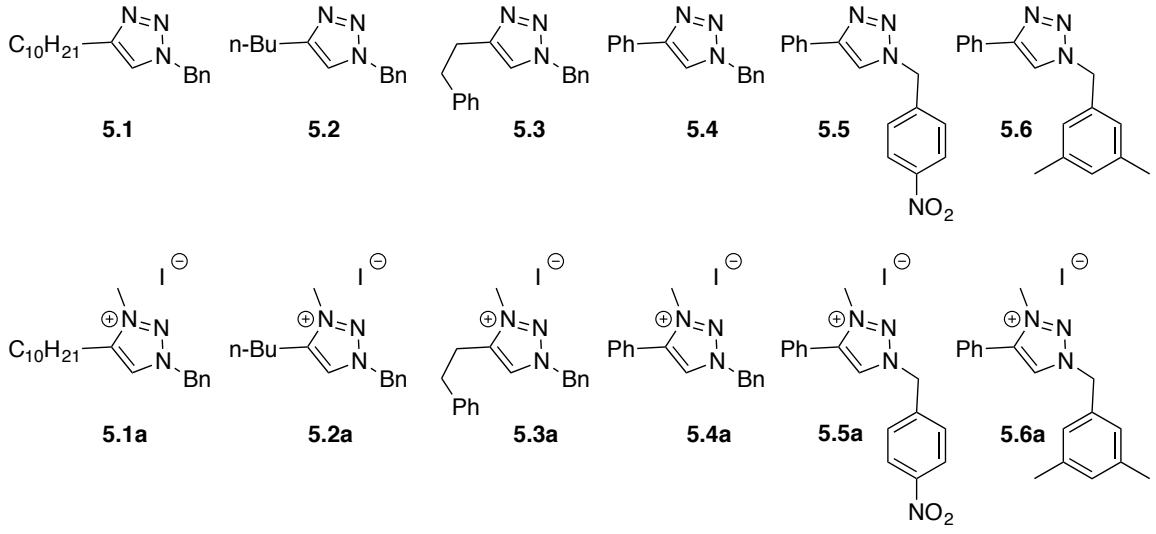

Figure 5.2: The triazoles and methylated triazolium salts that were explored in the attempted reactions in Table 5.1.

Methyl exchange reaction	Conditions	Result
5.1a + **5.2** → **5.1** + **5.2a**	MeCN	no reaction
5.1a + **5.3** → **5.1** + **5.3a**	MeCN	no reaction
5.1a + **5.4** → **5.1** + **5.4a**	MeCN	no reaction
5.1a + **5.4** → **5.1** + **5.4a**	1,4-dioxane	decomposition
5.1a + **5.4** → **5.1** + **5.4a**	MeOH, Cu(II), NaAsc, $KHCO_3$	no reaction
5.5a + **5.6** → **5.5** + **5.6a**	MeCN	decomposition

Table 5.1: Attempted methyl exchange reactions using the compounds in Figure 5.2. Each triazole-triazolium salt pair was heated at reflux in the indicated solvent.

When this result was not observed, it seemed likely that the triazolium methyl group was not electrophilic enough for the predicted substitution reaction. However, we reasoned that a methyl exchange could occur through a catalyzed mechanism instead. If the triazolium were to undergo a copper-catalyzed cycloreversion, a methylated azide would be produced. We expected this species to be unstable and therefore more capable of acting as a methylating agent, facilitating methyl transfer to a triazole. For this reason, a methyl exchange reaction was attempted in the presence of copper, but unfortunately no reaction occurred. Finally, an electron-poor triazole (**5.5**) was methylated to form its corresponding triazolium salt (**5.5a**) and combined with an electron-rich triazole (**5.6**). The electron-withdrawing character of the triazolium salt was expected to enhance electrophilicity, and the electron-rich triazole was thought to be a better nucleophile than those previously tested. However, the triazolic compounds decomposed rather than undergoing exchange of the methyl group. This result seemed to indicate that the methyl exchange would not occur under any conditions.

Although methyl exchange did not occur under the studied conditions, this did not prove that the cycloreversion was impossible; it simply showed that methyl exchange cannot operate as part of the mechanism of cycloreversion. We looked for evidence of catalyzed cycloreversion by combining pre-formed triazolium salts with free azides or alkynes. If the triazolium salt were to revert to starting materials, those starting materials would react with the free azide or alkyne to generate a different triazole or triazolium salt that could then be detected by NMR spectroscopy. It became clear that free alkynes could not be used in the presence of copper because copper acetylides form aggregates that remain inert after sequestering all of the copper present in the solution.[14] For this reason, only exchanges involving free azides were explored. For each of these experiments, a triazolium salt and a free azide (**5.7**) were heated at reflux in the presence of a variety of potential catalysts for cycloreversion. The results of these experiments are summarized in Table 5.2. In each case, the attempted reaction resulted in decomposition, indicating that destabilization caused by heating initiates a reaction other than the desired cycloreversion.

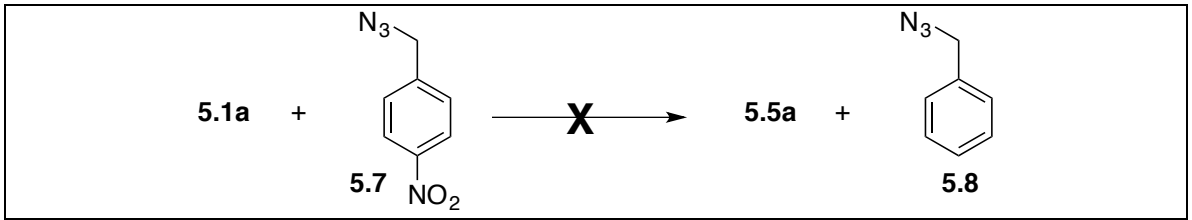

Conditions	Result
$CuSO_4 \bullet 5H_2O$, NaAsc, $KHCO_3$, MeOH	decomposition
$CuSO_4 \bullet 5H_2O$, NaAsc, Verkade's base, MeOH	decomposition
$Pd(PPh_3)_4$, MeOH	decomposition
$RuCl_3$, NEt_3, MeOH	decomposition
$[Rh(OAc)_2]_2$, NEt_3, MeOH	decomposition
$AgNO_3$, NEt_3, MeOH	decomposition

Table 5.2: Attempted azide exchange reactions with triazolium salts in the presence of various metals.

In order to gain a better understanding of the energetics of the proposed reactions, density functional theory (DFT) calculations were carried out in collaboration with the Stanton group. We were able to verify that the cycloaddition of phenylacetylide and benzyl azide to form 1-benzyl-4-phenyl-1*H*-1,2,3-triazole is exothermic by -51 kcal/mol. Additionally, methylation of this triazole was found to be exothermic by -24 kcal/mol (Figure 5.3). Unfortunately, the methylation of an azide by methyl iodide actually turned out to be exothermic by 1 kcal/mol, so the methylated azide must not be as unstable as expected. This means that the cycloreversion of a methylated triazolium salt is endothermic by 74 kcal/mol, to say nothing of the large activation barrier.

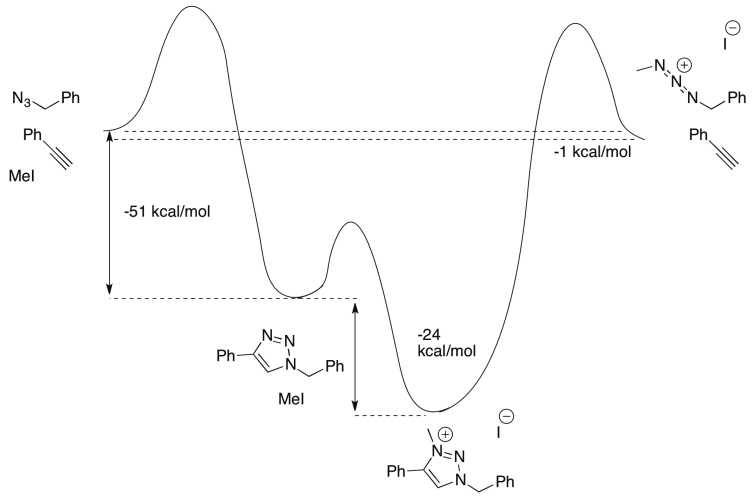

Figure 5.3: Summary of DFT calculations for the intermediates proposed in the cycloaddition of a methylated triazolium salt.

5.2.2 Oxidative Addition of a 5-Iodo-triazole

A second system that could allow for cycloreversion involves the oxidative addition of 5-iodo-triazoles to copper(I) iodide. Oxidative addition to copper(I) would generate an unstable copper(III) species. This species would likely have a short lifetime and could possibly be energetic enough to generate either starting materials or products. A recent review lends support to the possibility of forming this unstable copper(III) species as well as palladium(IV) species for a palladium(II) catalyst.[15] A potential catalytic cycle for this reaction is depicted in Scheme 5.3.

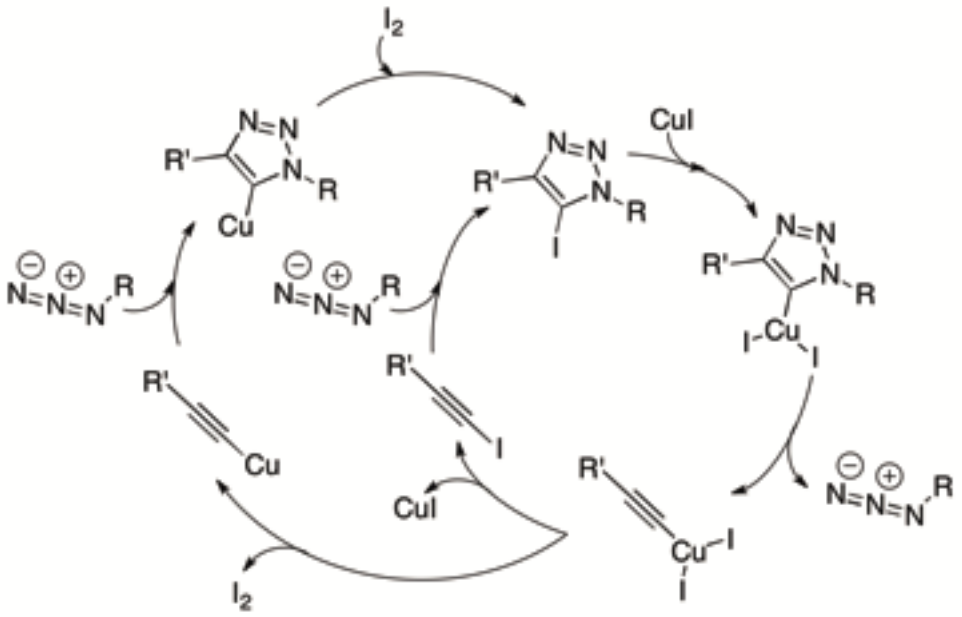

Scheme 5.3: Proposed catalytic cycle for the cycloreversion of 5-iodo-triazole. Two differing paths following cycloreversion are depicted.

In the proposed cycle, a 5-iodo-triazole undergoes oxidative addition to form a highly unstable copper(III) complex, which could be high enough in energy to surmount an activation barrier for cycloreversion that would release an azide and a copper(III) acetylide. The copper(III) acetylide is followed through two potential pathways. It could break up to form copper(I) iodide and an iodoalkyne, or it could form molecular iodine and a copper acetylide. In either case, the alkyne-containing species undergoes cycloaddition with an azide, either to form a new 5-iodo-triazole, or a copper complex which would then form a 5-iodo-triazole and regenerate copper(I) iodide.

5-Iodo-1,2,3-triazoles were synthesized according to literature procedure[16] and subjected to heating at reflux in the presence of a free azide (**5.7**) and a variety of potential metal catalysts. The results of these studies are summarized in Table 5.3.

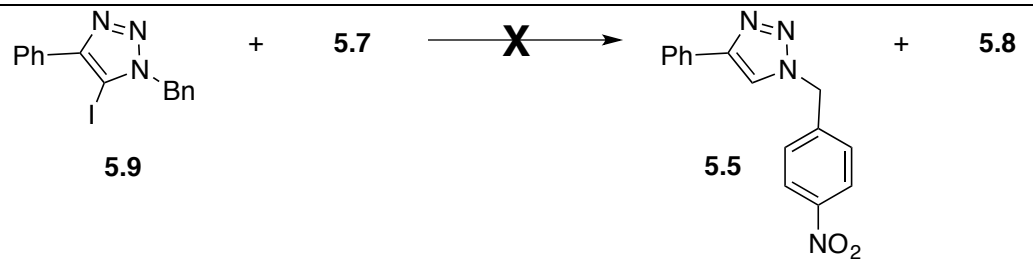

5.9 5.5

Conditions	Result
CuI, MeOH	no reaction
CuI, MeCN	no reaction
$Pd(PPh_3)_4$, MeOH	decomposition
$Pd(OAc)_2$, MeOH	no reaction
$RuCl_3$, MeOH	decomposition
$[Rh(OAc)_2]_2$, MeOH	decomposition
$AgNO_3$, MeOH	no reaction

Table 5.3: Attempted azide exchange reactions with 5-iodo-triazoles in the presence of various metals.

In all cases, the reaction mixture either decomposed or showed no evidence of any reaction. This result demonstrates that the barrier to the decomposition reaction(s) is lower than the barrier to cycloreversion.

5.2.3 Oxidative Addition of a 5-Iodo-triazolium Salt

The two previously described methods were combined in a third approach to triazole cycloreversion. This strategy involved methylation of a 5-iodo-triazole at the 3-position and attempts at oxidative addition of the resulting 5-iodo-triazolium to various metal salts. Just as the positive formal charge of the triazolium salt draws electron density and increases the acidity of the triazolic proton at the 5-position, a methyl group on a 5-iodo-triazolium salt is expected to draw electron density and lengthen the carbon-iodide

bond at the 5-position. This longer, weaker bond may be activated toward oxidative addition to copper(I) or another metal salt. This system utilizes the same strategy as that involving the 5-iodo-triazole: formation of an unstable copper(III) complex that could potentially be energetic enough to collapse to either products or starting materials. A 5-iodo-1,2,3-triazole was methylated and heated at reflux in the presence of a free azide and a variety of potential catalysts. The results of these experiments are summarized in Table 5.4.

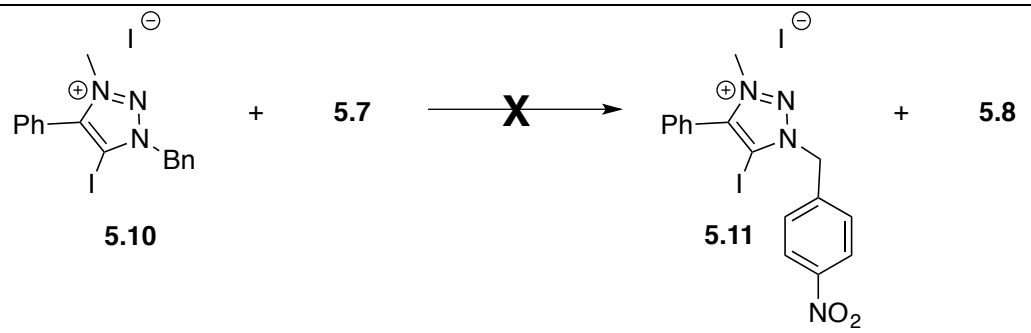

Conditions	Result
CuI, MeOH	no reaction
$Pd(PPh_3)_4$, MeOH	no reaction
$Pd(OAc)_2$, MeOH	decomposition
$RuCl_3$, MeOH	decomposition
$[Rh(OAc)_2]_2$, MeOH	decomposition
$AgNO_3$, MeOH	decomposition

Table 5.4: Attempted azide exchange reactions with 5-iodo-triazolium salts in the presence of various metals.

Once again, the reaction mixtures each produced either no reaction or decomposition, indicating that the methylated 5-iodo-triazolium salt is no more

susceptible to oxidative addition than the 5-iodo-triazole is. DFT results corroborate this conclusion in two ways. First, the methylation of a 5-iodo-triazole by methyl iodide is exothermic by 20 kcal/mol, so cycloreversion from that intermediate would be faced with a high activation barrier to overcome. Additionally, the C-I bond in the 5-iodotriazole and that in the methylated 5-iodotriazolium salt are the same length, which suggests that both species would be equally unlikely to surmount the activation barrier.

Unfortunately, the basis set proved to be insufficient to model the behavior of the copper atom, so calculation of copper-containing intermediates and transition states were not able to be completed.

5.3 Conclusions

The three approaches all unfortunately failed to produce any observable cycloreversion of triazoles or their derivatives. This failure was largely due to the fact that by altering the triazoles, they were made more stable, rather than less stable. This means that even if the transition state energies were not far above the energy of the starting materials, the overall activation barriers would still be incredibly high for the stabilized triazole derivatives. The CuAAC thus remains irreversible, at least under the conditions which we were able to devise and test.

5.4 Experimental

5.4.1 Synthesis

Organic azides,[17] 1,4-disubstituted 1,2,3-triazoles,[9] 1,3,4-trisubstituted 1,2,3-triazolium salts,[10] and 1,4-disubstituted 5-iodo-1,2,3-triazoles[16] were synthesized according to their respective literature procedures.

5.4.2 General Procedure for the Deprotonation of Triazolium Salts

A solution of 1-benzyl-4-decyl-3-methyl-1*H*-1,2,3-triazolium iodide (9 μmol) in CD_3OD (0.9 mL) and a metal salt (2 μmol) were combined in an NMR tube. A solution of potassium bicarbonate (3 μL, 2.4 M, 7 μmol) was added, the tube was inverted twice, and a timer was started. NMR spectra were acquired repeatedly for one hour, and the time was recorded as each spectrum finished acquiring. The triazolic proton peak was integrated and compared to two protons in the benzylic peak. The integrated value was plotted against time.

5.4.3 General Procedure for Methyl Exchange of Triazolium Salts

A triazolium salt and a triazole were combined in a 1:1 ratio and dissolved in acetonitrile (0.6 M). The mixture was heated at reflux for several days and monitored by NMR periodically. All but one of these attempted reactions were uncatalyzed, but in one case, 15 mol% $CuSO_4 \bullet 5H_2O$ and 20 mol% sodium ascorbate were added, and this reaction was attempted in methanol.

5.4.4 General Procedure for Azide Exchange of Triazolium Salts

1-benzyl-4-decyl-3-methyl-1*H*-1,2,3-triazolium iodide (0.045 mmol), 4-nitrobenzyl azide (3 equiv.), triethylamine (1 equiv.), and a metal salt (15 mol%), were combined in CD_3CN (0.045 M) in a J. Young valve NMR tube. An NMR spectrum was acquired, and the tube was placed in an 80 °C oil bath. Periodically over several days, the tube was removed from the bath and allowed to cool, and an NMR spectrum was acquired, and the tube was returned to the bath.

5.4.5 General Procedure for Azide Exchange of 5-Iodo-triazole

1-benzyl-5-iodo-4-phenyl-1*H*-1,2,3-triazole (0.025 mmol), 4-nitrobenzyl azide (5 equiv.), and a metal salt (15 mol%) were combined in CD_3CN (0.025 M) in a J. Young

valve NMR tube. An NMR spectrum was acquired, and the tube was placed in an 80 °C oil bath. Periodically over several days, the tube was removed from the bath and allowed to cool, and an NMR spectrum was acquired, and the tube was returned to the bath.

5.4.6 General Procedure for Azide Exchange of 5-Iodo-triazolium Salt

1-benzyl-5-iodo-3-methyl-4-phenyl-1*H*-1,2,3-triazolium iodide (0.005 mmol), 4-nitrobenzyl azide (5 equiv.), and a metal salt (15 mol%) were combined in CD_3OD (0.005 M) in a J. Young valve NMR tube. An NMR spectrum was acquired, and the tube was placed in an 80 °C oil bath. Periodically over several days, the tube was removed from the bath and allowed to cool, and an NMR spectrum was acquired, and the tube was returned to the bath.

5.4.7 Density Functional Theory

Optimized geometries, energies, and thermodynamic corrections at 298 K were calculated using the B3LYP[18–20] density functional theory method in QChem 4.0. 6-311G(d,p) was used for all atoms. Solvation energies in water were added as single point calculations with the basis set 3-21G for iodine and 6-31G* for all other atoms.

5.5 Acknowledgements

Dr. John Stanton and his student, Laura McCaslin, are thanked for their collaboration with DFT calculations.

5.6 References

(1) Kolb, H. C.; Finn, M. G.; Sharpless, K. B. Click Chemistry: Diverse Chemical Function from a Few Good Reactions. *Angew. Chem. Int. Ed. Engl.* **2001**, *40* (11), 2004–2021.

(2) Huisgen, R.; Szeimies, G.; Moebius, L. 1,3-Dipolar Cycloadditions. XXXII. Kinetics of the Addition of Organic Azides to Carbon-Carbon Multiple Bonds. *Chem. Ber.* **1967**, *100* (8), 2494–2507.

(3) Rostovtsev, V. V; Green, L. G.; Fokin, V. V; Sharpless, K. B. A Stepwise Huisgen Cycloaddition Process: copper(I)-Catalyzed Regioselective "ligation" of Azides and Terminal Alkynes. *Angew. Chem. Int. Ed. Engl.* **2002**, *41* (14), 2596–2599.

(4) Tornøe, C. W.; Christensen, C.; Meldal, M. Peptidotriazoles on Solid Phase: [1,2,3]-Triazoles by Regiospecific Copper(i)-Catalyzed 1,3-Dipolar Cycloadditions of Terminal Alkynes to Azides. *J. Org. Chem.* **2002**, *67* (9), 3057–3064.

(5) Himo, F.; Lovell, T.; Hilgraf, R.; Rostovtsev, V. V; Noodleman, L.; Sharpless, K. B.; Fokin, V. V. Copper(I)-Catalyzed Synthesis of Azoles. DFT Study Predicts Unprecedented Reactivity and Intermediates. *J. Am. Chem. Soc.* **2005**, *127* (1), 210–216.

(6) Cantillo, D.; Ávalos, M.; Babiano, R.; Cintas, P.; Jiménez, J. L.; Palacios, J. C. Assessing the Whole Range of CuAAC Mechanisms by DFT Calculations--on the Intermediacy of Copper Acetylides. *Org. Biomol. Chem.* **2011**, *9* (8), 2952–2958.

(7) Begtrup, M. Reactions Between Azolium Salts and Nucleophilic Reagents. *Acta Chem. Scand.* **1971**, *25*, 249–259.

(8) Hohloch, S.; Su, C.-Y.; Sarkar, B. Copper(I) Complexes of Normal and Abnormal Carbenes and Their Use as Catalysts for the Huisgen [3+2] Cycloaddition between Azides and Alkynes. *Eur. J. Inorg. Chem.* **2011**, *2011* (20), 3067–3075.

(9) Shah, J.; Khan, S.; Blumenthal, H.; Liebscher, J. 1,2,3-Triazolium-Tagged Prolines and Their Application in Asymmetric Aldol and Michael Reactions. *Synthesis (Stuttg).* **2009**, *2009* (23), 3975–3982.

(10) Hanelt, S.; Liebscher, J. A Novel and Versatile Access to Task-Specific Ionic Liquids Based on 1,2,3-Triazolium Salts. *Synlett* **2008**, *2008* (7), 1058–1060.

(11) Zhang, L.; Chen, X.; Xue, P.; Sun, H. H. Y.; Williams, I. D.; Sharpless, K. B.; Fokin, V. V; Jia, G. Ruthenium-Catalyzed Cycloaddition of Alkynes and Organic Azides. *J. Am. Chem. Soc.* **2005**, *127* (46), 15998–15999.

(12) McNulty, J.; Keskar, K.; Vemula, R. The First Well-Defined silver(I)-Complex-Catalyzed Cycloaddition of Azides onto Terminal Alkynes at Room Temperature. *Chem. Eur. J.* **2011**, *17* (52), 14727–14730.

(13) Saravanakumar, R.; Ramkumar, V.; Sankararaman, S. Synthesis and Structure of 1,4-Diphenyl-3-Methyl-1,2,3-Triazol-5-Ylidene Palladium Complexes and Application in Catalytic Hydroarylation of Alkynes. *Organometallics* **2011**, *30*, 1689–1694.

(14) Hein, J. E.; Fokin, V. V. Copper-Catalyzed Azide-Alkyne Cycloaddition (CuAAC) and beyond: New Reactivity of copper(I) Acetylides. *Chem. Soc. Rev.* **2010**, *39* (4), 1302–1315.

(15) Hickman, A. J.; Sanford, M. S. High-Valent Organometallic Copper and Palladium in Catalysis. *Nature* **2012**, *484* (7393), 177–185.

(16) Brotherton, W. S.; Clark, R. J.; Zhu, L. Synthesis of 5-Iodo-1,4-Disubstituted-1,2,3-Triazoles Mediated Y in Situ Generated Copper(I) Catalyst and Electrophilic Triiodide Ion. *J. Org. Chem.* **2012**, *77*, 6443–6455.

(17) Guo, Z.-F.; Yan, H.; Li, Z.-F.; Lu, Z.-L. Synthesis of Mono- and Di-[12]aneN3 Ligands and Study on the Catalytic Cleavage of RNA Model 2-Hydroxypropyl-P-Nitrophenyl Phosphate with Their Metal Complexes. *Org. Biomol. Chem.* **2011**, *9* (19), 6788–6796.

(18) Becke, A. D. Density-Functional Exchange-Energy Aproximation with Correct Asymptotic Behavior. *Phys. Rev. A* **1988**, *38* (6), 3098–3100.

(19) Lee, C.; Yang, W.; Parr, R. G. Development of the Colle-Salvetti Correlation-Energy Formula into a Functional of the Electron Density. *Phys. Rev. B* **1988**, *37* (2), 785–789.

(20) Becke, A. D. A New Mixing of Hartree-Fock and Local Density-Functional Theories. *J. Chem. Phys.* **1993**, *98* (2), 1372–1377.

Appendix: A Tutorial for Fitting 1:1 Binding and Indicator Displacement Assay Data to Calculate Binding Constants

A.1 Introduction

The equations used to calculate binding constants have already been derived by Hargrove *et al.*[1] This appendix is simply a practical guide to creating new fitting functions in OriginPro and using those fitting functions to solve for a binding constant. The instructions that follow were written using OriginPro 8.5.1 as a model.

A.2 Creating a New Fitting Function for 1:1 Binding

In OriginPro, click Analysis → Fitting → Nonlinear Curve Fit → Open Dialog. The window in Figure A.1 will open. Click on the Create New Fitting Function button, circled in green.

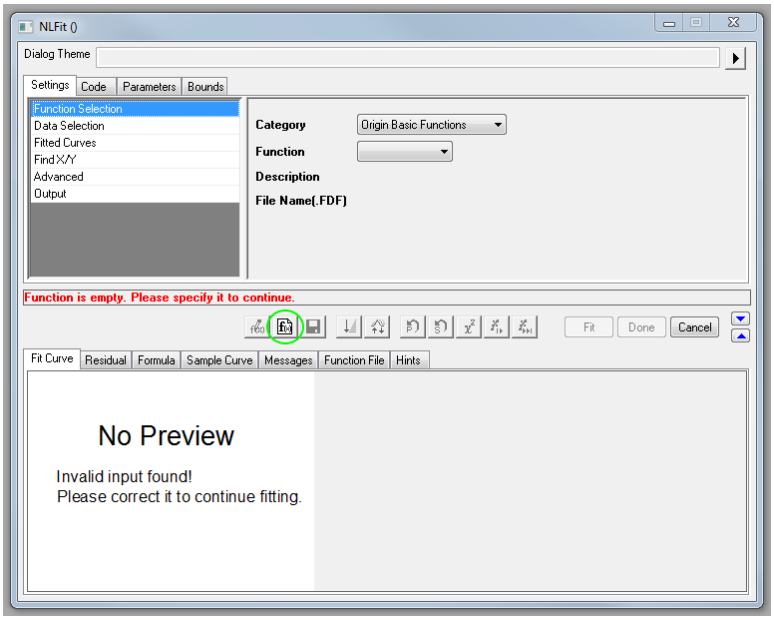

Figure A.1: Dialog window for curve fitting. The button for writing a new function is circled in green.

The Function Builder window in Figure A.2 will open. The Function Builder will first ask for Name and Type. Select Category: User Defined. Name the function and select Function Type: Expression. Click Next.

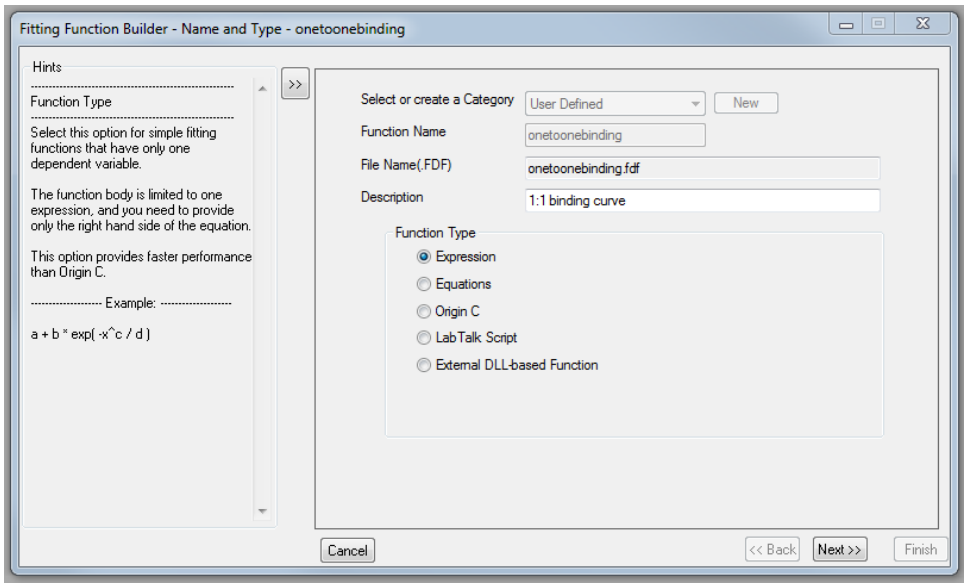

Figure A.2: Function Builder window, Name and Type.

The Function Builder will next ask for Variables and Parameters. Enter the variables and parameters described in this paragraph as shown in Figure A.3. The Independent Variable is xt. This is the total concentration of component X in solution. The letter X is chosen because the terms host, guest, and indicator can be confusing. If only a 1:1 binding curve is necessary, then the titration is between a host and a guest. However, if an indicator displacement assay is the next step in the analysis, the titration is between a host and an indicator, but this means the indicator is acting as a guest. Furthermore, host can be titrated into guest or guest can be titrated into host. To avoid this confusion, X is whichever component is changing in concentration during the titration. Thus, concentration of X is the independent variable, and changes in the

dependent variable will be related to changes in the concentration of X. The dependent variable is F. The letter F was chosen for fluorescence intensity, but it could be absorbance or even chemical shift. In any case, F is the variable being measured as a function of the concentration of X. The Parameters are K, n1, n2, and zt. K is the binding constant between component X and component Z. Z is the component that remains at a constant concentration during the titration, and the parameter zt is the total concentration of component Z in solution. The two n values, n1 and n2, are coefficients belonging to Z and XZ, respectively. These two coefficients are the molar absorptivities of Z and XZ if the dependent variable is absorbance, or a conglomeration of molar absorptivity and quantum yield if the dependent variable is fluorescence intensity. (It should be noted that one component, X, is assumed to be invisible to the measurement technique.) After entering the variables and parameters, click Next.

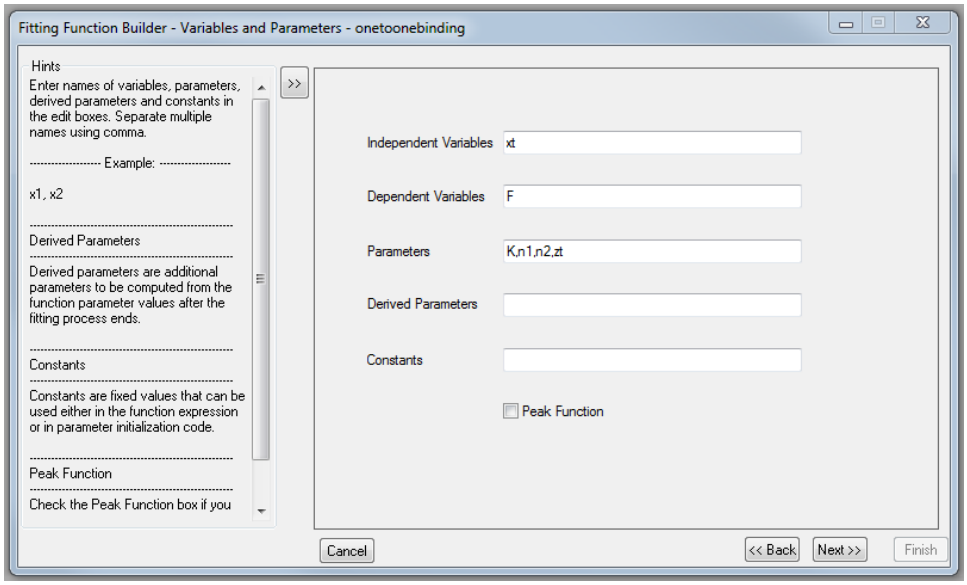

Figure A.3: Function Builder window, Variables and Parameters.

Next, the Function Builder will ask for the Expression Function (Figure A.4). The function to be entered as Function Body is as follows:

(1/(2*K))*(-1-K*xt+K*zt+(4*K*zt+(1+K*xt-K*zt)^2)^0.5)*(n1+((K*n2*xt)/(1+0.5*(-1-K*xt+K*zt+(4*K*zt+(1+K*xt-K*zt)^2)^0.5))))

This function is equivalent to Equation 11 in the Hargrove paper. After entering and double-checking the function, click Next.

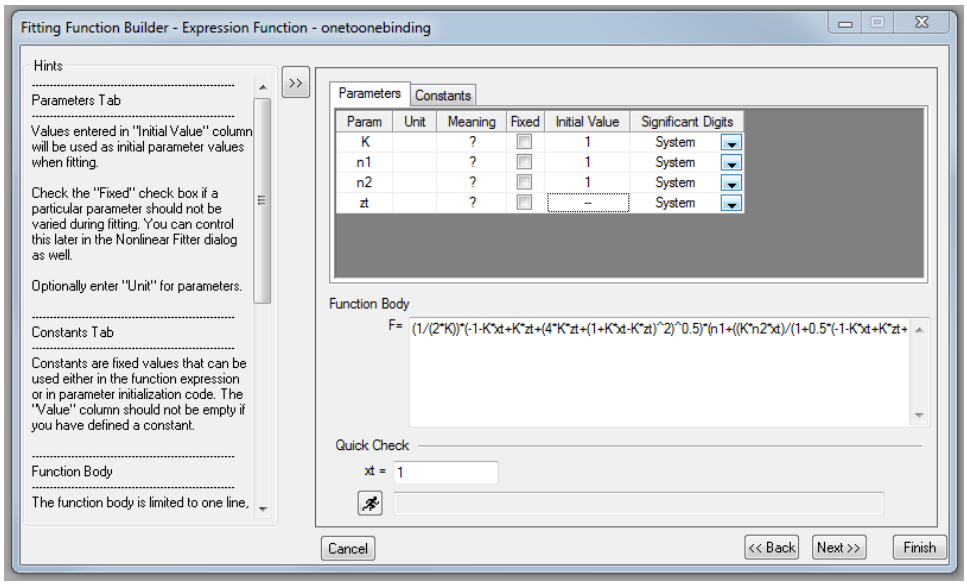

Figure A.4: Function Builder window, Expression Function.

Skip Initialization Code and click Next again. The Function Builder will ask for Bounds (Figure A.5). Set both coefficients to be greater than zero. To do this, double-click in the relevant cell in the "< or <=" column, and enter "0" in the Lower Bounds column. Then click Next.

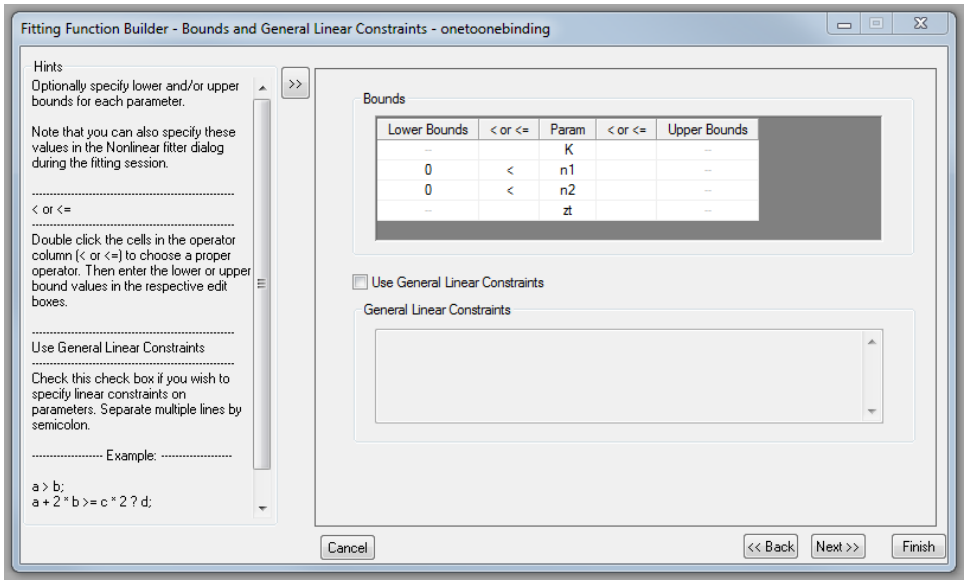

Figure A.5: Function Builder window, Bounds.

Skip Derived Parameters and click Next again. Skip Script Before or After Fitting and click Finish.

A.3 Testing the Fitting Function for 1:1 Binding

To test that the function fits properly, the data in Table A.1 can be used. This is the absorbance data from the 1:1 binding curve in Chapter 2, Section 2.2.3.2. When processing data for fitting, all concentrations should be converted to molar concentrations, not millimolar, etc. Additionally, the initial absorbance or fluorescence intensity measurement should be subtracted from all subsequent measurements so that the first data point is at [0,0]. If the measurement drops during the titration, the initial measurement can be added, so that the first data point's y-value is at 0 and all following points have negative y-values, or the initial measurement can be subtracted, so that all following points have positive y-values. This is largely a matter of personal preference.

[SH] in M	Change in Abs at 525
0	0
1.24688E-05	0.03499
2.48756E-05	0.0798
3.72208E-05	0.12735
4.9505E-05	0.18246
6.17284E-05	0.2111
7.38916E-05	0.24907
8.59951E-05	0.27816
9.80392E-05	0.30675
0.000110024	0.33417
0.000121951	0.355
0.000145631	0.38683
0.000169082	0.42458
0.000192308	0.44805
0.000215311	0.46273
0.000238095	0.48824
0.000283019	0.49327
0.000327103	0.53442
0.00037037	0.54102
0.000412844	0.56133
0.000454545	0.56855
0.000555556	0.58173
0.000652174	0.59259
0.000744681	0.58161
0.000833333	0.57894

Table A.1: 1:1 binding data with which to test the new 1:1 binding function. If this is being viewed digitally as a document, the data **can** be copied and pasted from the document to the OriginPro spreadsheet.

After pasting the data into OriginPro, some cells may read ########. If this occurs, widen the column until all the numbers can be displayed. Then highlight the data and click Analysis → Fitting → Nonlinear Curve Fit → Open Dialog. Select Category: User Defined, and Function: onetoonebinding (this is the function you created in section A.2) (Figure A.6).

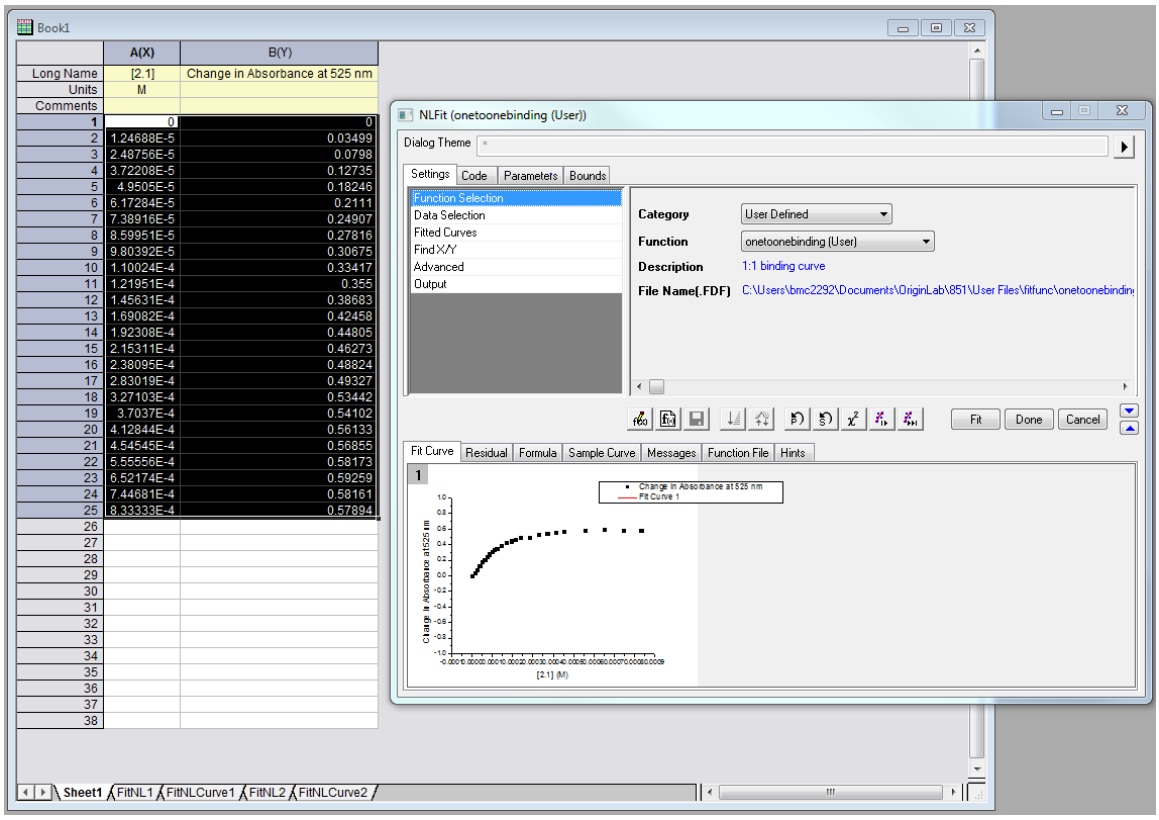

Figure A.6: Select onetoonebinding.

Next, click on the Parameters tab. Set zt = 0.00008 and select the adjacent Fixed? checkbox. (This value comes from the 1:1 binding titration presented in Chapter 2, Section 2.2.3.2.) Then click the One Iteration button, circled in green (Figure A.7).

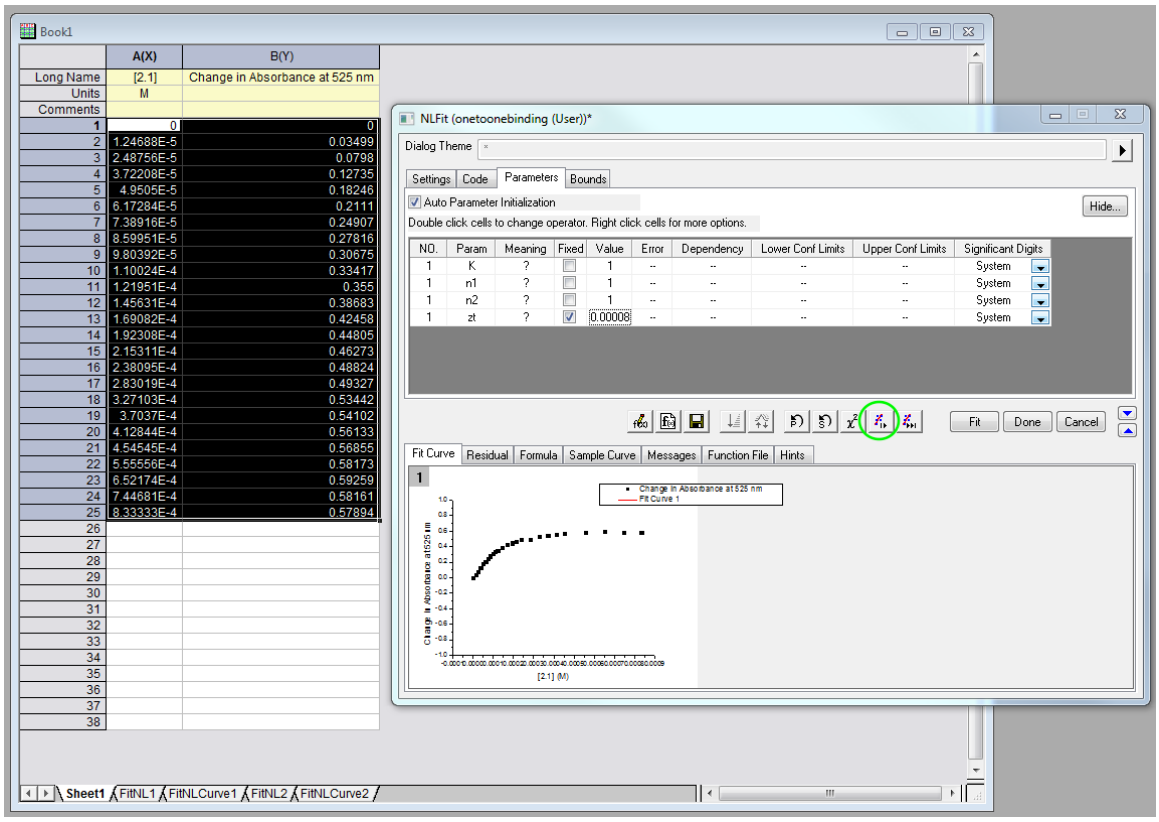

Figure A.7: Set parameters and iterate.

After only one iteration, the program has already made some bad guesses (Figure A.8). Sometimes additional iterations only make matters worse.

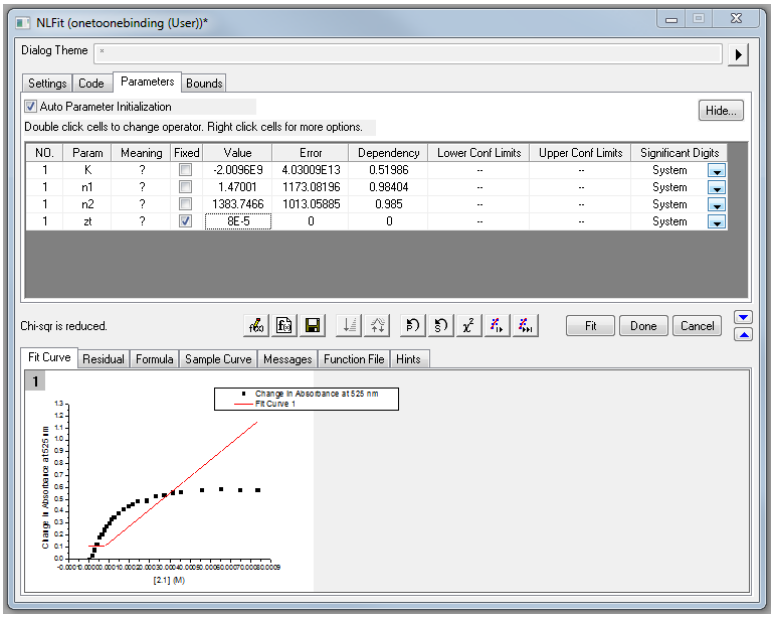

Figure A.8: Sometimes the program cannot fit the data without a reasonable guess.

It is often a good idea to provide a guess for one or more of the parameters. At this juncture, enter a value of 1000 for K, but do not select it as Fixed. Click on the One Iteration button again. Using the guessed K value, the program reaches a reasonable fit with one iteration (Figure A.9).

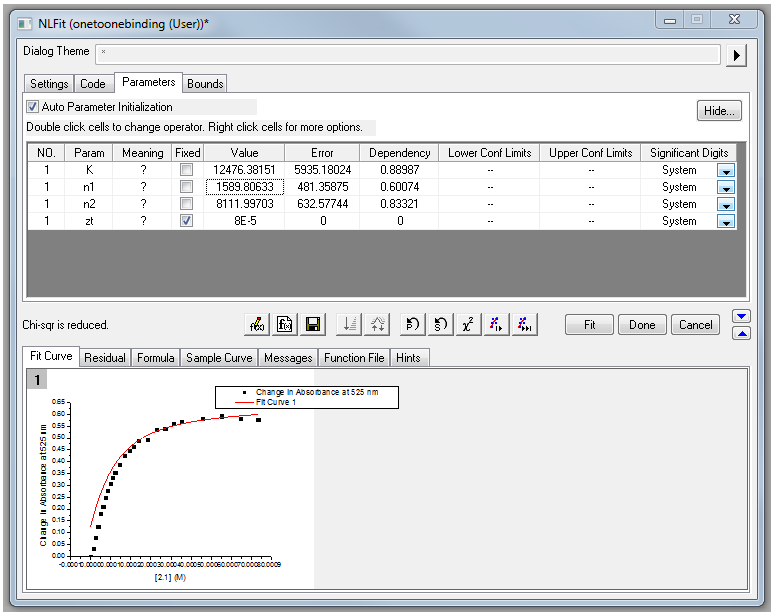

Figure A.9: The fit after one more iteration.

The One Iteration button can be clicked repeatedly, or since the fit appears to be close, the Iterate Until Converged button (to the right of the One Iteration button) can be clicked instead. When convergence is reached, the fit looks great (Figure A.10).

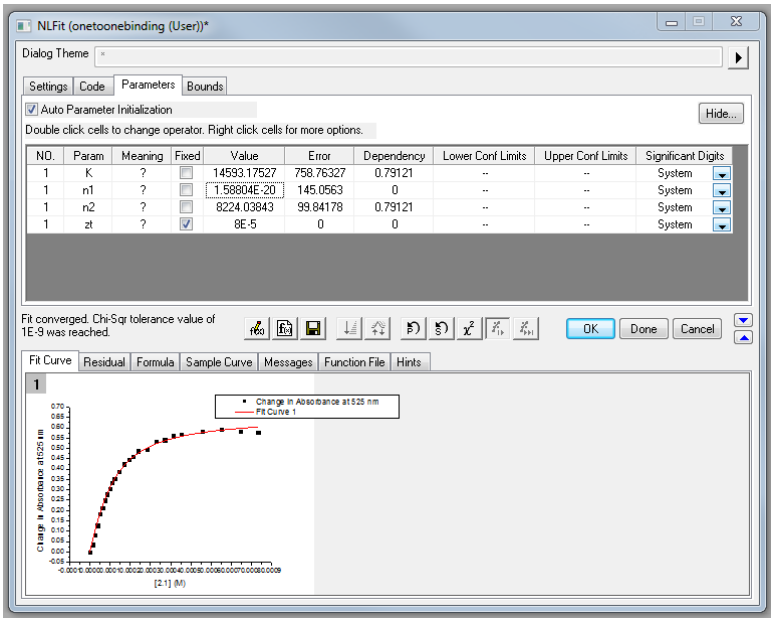

Figure A.10: The fit has converged.

Click OK. The program asks, “Do you want to switch to the report sheet?” Select Yes and click OK. The report sheet should contain the values shown in Figure A.11.

		Value	Standard Error
Change in Absorbance at 525 nm	K	14592.54179	758.7231
Change in Absorbance at 525 nm	n1	9.99249E-31	145.05631
	n2	8224.10719	99.84367
Change in Absorbance at 525 nm	zt	8E-5	0

Figure A.11: The parameters after fitting.

You are now ready to fit your own data. In OriginPro, copy and paste the concentrations of your titrant (in M) into column A(X). This is your independent variable, xt, the concentration of component X. Rename the A(X) column with the identity of your titrant. Copy and paste your data (as the change in signal, so that your first value is 0) into column B(Y). This is your dependent variable, F. Rename the B(Y)

column appropriately. Then the only parameter you must enter is zt, which is the concentration (in M) of the component that remained at constant concentration throughout the titration.

A.4 Creating a New Fitting Function for Indicator Displacement Assays

In OriginPro, open a new Book. Click Analysis → Fitting → Nonlinear Curve Fit → Open Dialog. Click on the Create New Fitting Function button. The Function Builder window in Figure A.12 will open. The Function Builder will first ask for Name and Type. Select Category: User Defined. Name the function and select Function Type: Lab Talk Script. Click Next.

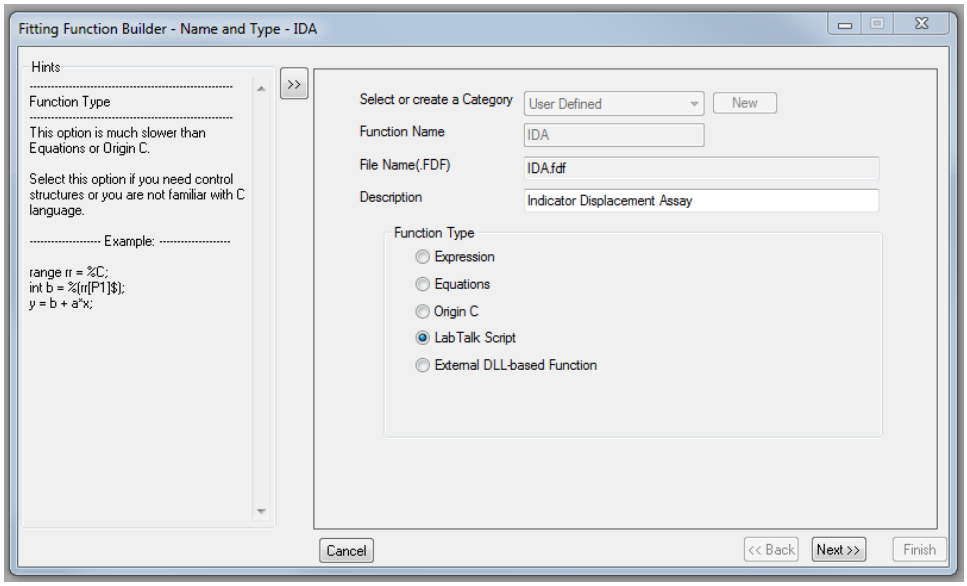

Figure A.12: Function Builder window, Name and Type.

The Function Builder will next ask for Variables and Parameters (Figure A.13). For the IDA function, we return to the familiar host (H), indicator (I), and guest (G) naming system. Thus, the independent variable is Gt, the total concentration of guest in solution. This is the one concentration that will change throughout the titration. The

dependent variable is F, for fluorescence, but could also be absorbance. The parameters Ht and It are the total concentrations of host and indicator, respectively, in solution. These concentrations will remain constant during the titration. The binding constants Ki and Kg are the binding constants for host to indicator and host to guest, respectively. The coefficients ni and nhi are the molar absorptivities and/or quantum yields for the indicator and the host-indicator complex, respectively. (The host, guest, and host-guest complex are assumed to be invisible to the measurement technique. If this were not true, an indicator displacement assay would not be necessary!)

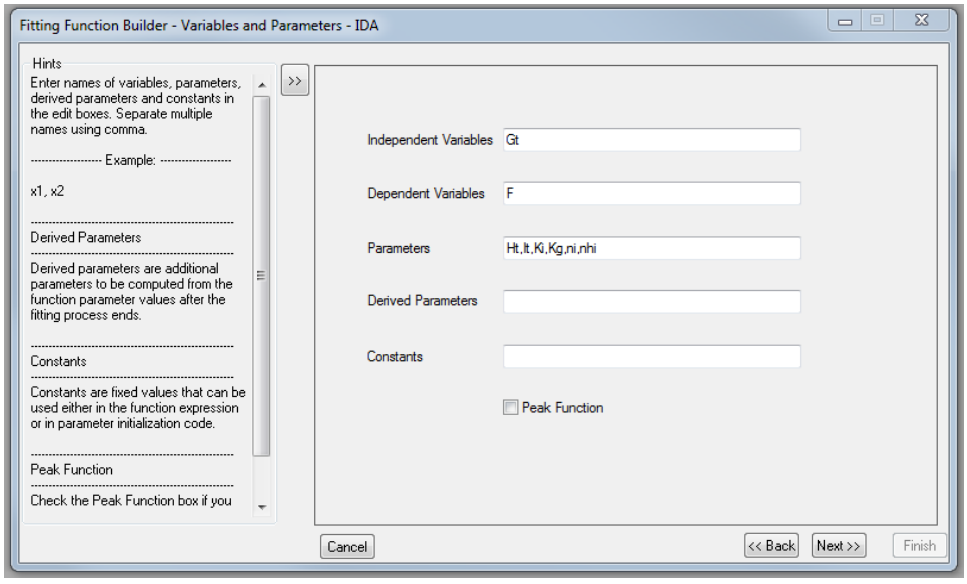

Figure A.13: Function Builder window, Variables and Parameters.

After entering the variables and parameters, click Next. The Function Builder will ask for the Expression Function (Figure A.14). The function to be entered as Function Body is as follows:

A=Ki*Kg;

B=Ki+Kg+Ki*Kg*It+Ki*Kg*Gt-Ki*Kg*Ht;

C=1+Ki*It+Kg*Gt-Ki*Ht-Kg*Ht;

D=-Ht;

for (H=Ht, step=1; abs(step)>1E-15; H=H-step){

step=(a*H*H*H+B*H*H+C*H+D)/(3*A*H*H+2*B*H+C);};

F=It*(ni+nhi*Ki*H)/(1+Ki*H)

This script is based on Equations 39 and 41 in the Hargrove paper. After entering and double-checking the function, click Next.

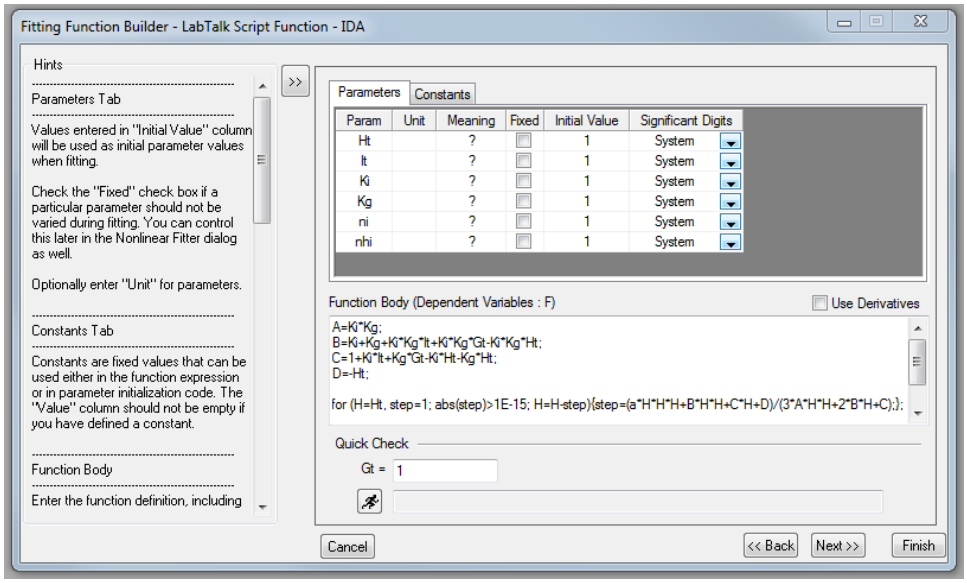

Figure A.14: Function Builder window, Expression Function.

Skip Initialization Code, Bounds, Derived Parameters, and Script Before or After Fitting, and click Finish.

A.5 Testing the Fitting Function for Indicator Displacement Assays

To test that the function fits properly, the data in Table A.2 can be used. This is the absorbance data from the indicator displacement assay in Chapter 2, Section 2.2.3.2.

[fructose] in M	Change in Abs 610
0	0
4.98753E-05	-0.05425
9.95025E-05	-0.08902
0.000148883	-0.13067
0.00019802	-0.16774
0.000246914	-0.20745
0.000295567	-0.24229
0.00034398	-0.28078
0.000392157	-0.31963
0.000440098	-0.35679
0.000487805	-0.39082
0.000582524	-0.43455
0.000676329	-0.47381
0.000769231	-0.50243
0.000861244	-0.54095
0.000952381	-0.56515
0.00113	-0.6085
0.00131	-0.65039
0.00148	-0.6896
0.00182	-0.74283
0.00222	-0.81291
0.00261	-0.85898
0.00333	-0.91803
0.004	-0.95553
0.00519	-0.98943
0.00621	-0.98822
0.0075	-1.01676
0.00889	-0.99627
0.01	-1.0174

Table A.2: Indicator displacement data with which to test the new IDA binding function. If this is being viewed digitally as a document, the data **can** be copied and pasted from the document to the OriginPro spreadsheet.

After pasting the data into OriginPro, highlight the data, then click Analysis → Fitting → Nonlinear Curve Fit → Open Dialog. Select Category: User Defined, and Function: IDA. Then click on the Parameters tab. Set Ht = 0.00017, It = 0.00008. (These

values come from the indicator displacement assay presented in Chapter 2, Section 2.2.3.2.) Set Ki = 14593. (This value for Ki is the one we found using the 1:1 binding fit function in section A.3) Select the adjacent Fixed? checkboxes for these three parameters (Figure A.15). Then click on the One Iteration button.

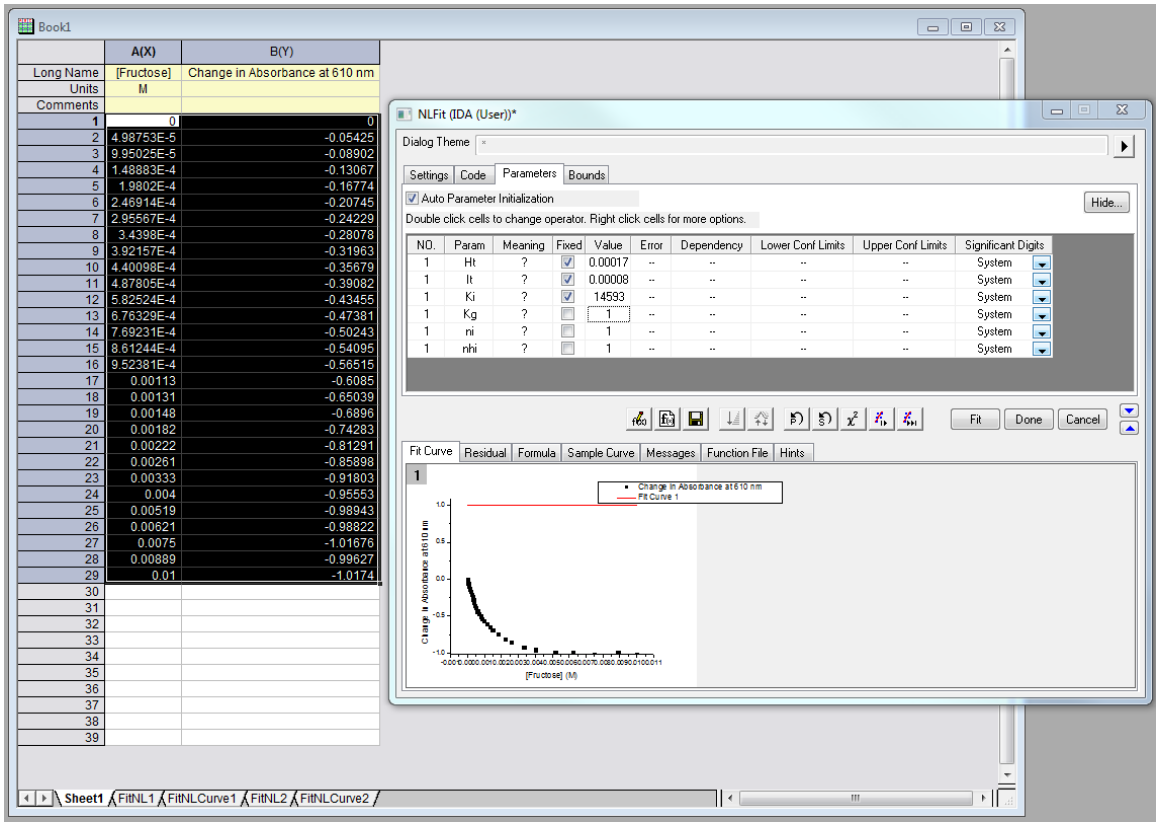

Figure A.15: Set parameters and iterate.

Once again, a few iterations produce fits that have little chance of finding their way. Continuing to iterate with these can result in the program simply reaching an ill-fitting local minimum, rather than the global minimum. To fix this, guess Kg to be somewhere between 1000 and 10000. Keep iterating until the fit converges. Then click OK and switch to the report sheet. The report sheet should contain the values shown in Figure A.16.

		Value	Standard Error
Change in Absorb	Ht	1.7E-4	0
	It	8E-5	0
	Ki	14593	0
	Kg	4332.38064	169.96062
	ni	-14210.048	123.55155
	nhi	8358.53565	148.02634

Figure A.16: The parameters after fitting.

You are now ready to fit your own data. In OriginPro, copy and paste the concentrations of your Guest (in M) into column A(X). Rename the A(X) column with the identity of your guest. Copy and paste your data (as the change in signal, so that your first value is 0) into column B(Y). This is your dependent variable, F. Rename the B(Y) column appropriately. Then enter the constant concentrations (in M) of Host and Indicator as Ht and It, respectively. Enter the binding constant for Ki that you found by fitting your 1:1 binding curve.

A.6 References

(1) Hargrove, A. E.; Zhong, Z.; Sessler, J. L.; Anslyn, E. V. *New J. Chem.* **2010**, *34* (2), 348–354.

References

Adamczyk-Wozniak, A.; Cyranski, M. K.; Jakubczyk, Michal Klimentowska, P.; Koll, A.; Kolodziejczak, J.; Pojmaj, G.; Zubrowska, A.; Zukowska, G. Z.; Sporzynski, A. Influence of the Substituents on the Structure and Properties of Benzoxaboroles. *J. Phys. Chem. A* **2010**, *114* (6), 2324–2330.

Akhani, R. K.; Moore, M. I.; Pribyl, J. G.; Wiskur, S. L. Linear Free-Energy Relationship and Rate Study on a Silylation-Based Kinetic Resolution: Mechanistic Insights. *J. Org. Chem.* **2014**, *79* (6), 2384–2396.

Al-Zoubi, R. M.; Marion, O.; Hall, D. G. Direct and Waste-Free Amidation and Cycloadditions by Organocatalytic Activation of Carboxylic Acids at Room Temperature. *Angew. Chem. Int. Ed.* **2008**, *47* (15), 2876–2879.

Amir, R. J.; Pessah, N.; Shamis, M.; Shabat, D. Self-Immolative Dendrimers. *Angew. Chem. Int. Ed.* **2003**, *42* (37), 4494–4499.

Anslyn, E. V.; Dougherty, D. A. *Modern Physical Organic Chemistry*; University Science, 2005.

Arnal-Herault, C.; Pase, A.; Michau, M.; Cot, D.; Petit, E.; Barboiu, M. Functional G-Quartet Macroscopic Membrane Films. *Angew. Chem. Int. Ed.* **2007**, *46* (44), 8409–8413.

Arumugam, K.; Varghese, B.; Brantley, J. N.; Konda, S. S. M.; Lynch, V. M.; Bielawski, C. W. 1,6-Enyne Cyclizations Catalyzed by N-Heterocyclic Carbene Supported Gold Complexes: Deconvoluting Sterics and Electronics. *Eur. J. Org. Chem.* **2014**, *2014* (3), 493–497.

Becke, A. D. Density-Functional Exchange-Energy Aproximation with Correct Asymptotic Behavior. *Phys. Rev. A* **1988**, *38* (6), 3098–3100.

Becke, A. D. A New Mixing of Hartree-Fock and Local Density-Functional Theories. *J. Chem. Phys.* **1993**, *98* (2), 1372–1377.

Begtrup, M. Reactions Between Azolium Salts and Nucleophilic Reagents. *Acta Chem. Scand.* **1971**, *25*, 249–259.

Bess, E. N.; Bischoff, A. J.; Sigman, M. S. Designer Substrate Library for Quantitative, Predictive Modeling of Reaction Performance. *Proc. Natl. Acad. Sci.* **2014**, *111* (41), 14698–14703.

Bicker, K. L.; Sun, J.; Harrell, M.; Zhang, Y.; Pena, M. M.; Thompson, P. R.; Lavigne, J. J. Synthetic Lectin Arrays for the Detection and Discrimination of Cancer Associated Glycans and Cell Lines. *Chem. Sci.* **2012**, *3*, 1147–1156.

Birks, J. B. Excimers. *Rep. Prog. Phys.* **1975**, *38*, 903–974.

Bissell, R. A.; de Silva, A. P.; Gunaratne, H. Q. N.; Lynch, P. L. M.; Maguire, G. E. M.; McCoy, C. P.; Sandanayake, K. R. A. S. Fluorescent PET (Photoinduced Electron Transfer) Sensors. *Top. Curr. Chem.* **1993**, *168*, 223–264.

Blasie, C. A.; Berg, J. M. Kinetics and Thermodynamics of Copper(II) Binding to Apoazurin. *J. Am. Chem. Soc.* **2003**, *125* (23), 6866–6867.

Brittain, W. D. G.; Buckley, B. R.; Fossey, J. S. Kinetic Resolution of Alkyne-Substituted Quaternary Oxindoles via Copper Catalysed Azide-Alkyne Cycloadditions. *Chem. Commun.* **2015**, *51* (97), 17217–17220.

Brittain, W. D. G.; Buckley, B. R.; Fossey, J. S. Asymmetric Copper-Catalyzed Azide-Alkyne Cycloadditions. *ACS Catal.* **2016**, *6*, 3629–3636.

Brotherton, W. S.; Clark, R. J.; Zhu, L. Synthesis of 5-Iodo-1,4-Disubstituted-1,2,3-Triazoles Mediated Y in Situ Generated Copper(I) Catalyst and Electrophilic Triiodide Ion. *J. Org. Chem.* **2012**, *77*, 6443–6455.

Brown, H. C. *Organic Syntheses via Boranes Vol. 1*; Aldrich Chemical: Milwaukee, WI, 1997.

Brown, H. C.; Cole, T. E.; Srebnik, M.; Kim, K. W. Hydroboration. 79. Preparation and Properties of Methylborane and Dimethylborane and Their Characteristics as Hydroborating Agents. Synthesis of Tertiary Alcohols Containing Methyl Groups via Hydroboration. *J. Org. Chem.* **1986**, *51* (25), 4925–4930.

Brown, H. C.; Kramer, G. W.; Hubbard, J. L.; Krishnamurthy, S. Addition Compounds of Alkali Metal Hydrides. XVIII. Reaction of Trialkylboranes with Tert-Butyllithium. A General, Convenient Method for the Preparation of Lithium Trialkylborohydrides. *J. Organometal. Chem.* **1980**, *188* (1), 1–10.

Brown, H. C.; Nazer, B.; Cha, J. S.; Sikorski, J. A. Selective Reductions. 38. Reaction of Thexylchloroborane-Methyl Sulfide Complex in Methylene Chloride with Selected Organic Compounds Containing Representative Functional Groups. Comparison of the Reducing Characteristics of Thexylchloroborane, Thexylbora. *J. Org. Chem.* **1986**, *51* (26), 5264–5270.

Brown, H. C.; Sinclair, J. A. Organoboranes. XVIII. Reaction of Lithium Alkynes with Methyl Dialkylborinate: The Synthesis of B-1-Alkynyldialkylboranes. *J. Organometal. Chem.* **1977**, *131* (2), 163–169.

Brown, H. C.; Zaidlewicz, M. *Organic Syntheses via Boranes. Vol. 2*; Aldrich Chemical: Milwaukee, WI, 2001.

Bukhtiyarova, M.; Rizzo, C. J.; Kettner, C. A.; Korant, B. D.; Scarnati, H. T.; King, R. W. Inhibition of the Bovine Viral Diarrhoea Virus NS3 Serine Protease by a Boron-Modified Peptidyl Mimetic of Its Natural Substrate. *Antivir. Chem. Chemother.* **2002**, *12* (6), 367–373.

Campbell, C. J.; Leigh, D. A.; Vitorica-Yrezabal, I. J.; Woltering, S. L. A Simple and

Highly Effective Ligand System for the Copper(I)-Mediated Assembly of Rotaxanes. *Angew. Chem. Int. Ed.* **2014**, *53* (50), 13771–13774.

Cantillo, D.; Ávalos, M.; Babiano, R.; Cintas, P.; Jiménez, J. L.; Palacios, J. C. Assessing the Whole Range of CuAAC Mechanisms by DFT Calculations--on the Intermediacy of Copper Acetylides. *Org. Biomol. Chem.* **2011**, *9* (8), 2952–2958.

Cao, Z.-Y.; Brittain, W. D. G.; Fossey, J. S.; Zhou, F. Recent Advances in the Use of Chiral Metal Complexes with Achiral Ligands for Application in Asymmetric Catalysis. *Catal. Sci. Technol.* **2015**, *5* (7), 3441–3451.

Castagnolo, D.; Dessi, F.; Radi, M.; Botta, M. Synthesis of Enantiomerically Pure Alpha-[4-(1-Substituted)-1,2,3-Triazol-4-Yl]-Benzylacetamides via Microwave-Assisted Click Chemistry: Towards New Potential Antimicrobial Agents. *Tetrahedron: Asymmetry* **2007**, *18* (11), 1345–1350.

Chandraskharan, J.; Brown, H. C. Hydroboration Kinetics. 11. A Reinvestigation of the Kinetics of Hydroboration of Representative Alkenes with Disiamylborane Dimer. Conclusive Evidence for the Dissociation Mechanism in the Hydroboration of Alkenes with Dialkylborane Dimers. *J. Org. Chem.* **1985**, *50* (4), 518–520.

Chandross, E. A. Photolytic Dissociation of Dianthracene. *J. Chem. Phys.* **1965**, *43* (11), 4175–4176.

Chandross, E. A.; Ferguson, J.; McRae, E. G. Absorption and Emission Spectra of Anthracene Dimers. *J. Chem. Phys.* **1966**, *45* (10), 3546–3553.

Chang, M. C. Y.; Pralle, A.; Isacoff, Ehud, Y.; Chang, C. J. A Selective, Cell-Permeable Optical Probe for Hydrogen Peroxide in Living Cells. *J. Am. Chem. Soc.* **2004**, *126* (47), 15392–15393.

Chen, A.; Shapiro, M. J. NOE Pumping as High-Throughput Method To Determine Compounds with Binding Affinity to Macromolecules by NMR. *J. Am. Chem. Soc.* **2000**, *122* (2), 414–415.

Collins, B. E.; Metola, P.; Anslyn, E. V. On the Rate of Boronate Ester Formation in Ortho-Aminomethyl-Functionalized Phenyl Boronic Acids. *Supramol. Chem.* **2013**, *25* (2), 79–86.

Collins, B. E.; Sorey, S.; Hargrove, A. E.; Shabbir, S. H.; Lynch, V.; Anslyn, E. V. Probing Intramolecular B-N Interactions in Ortho-Aminomethyl Arylboronic Acids. *J. Org. Chem.* **2009**, *74* (11), 4055–4060.

Cooper, C. R.; Spencer, N.; James, T. D. Selective Fluorescence Detection of Fluoride Using Boronic Acids. *Chem. Commun.* **1998**, *13*, 1365–1366.

Corbett, P. T.; Leclaire, J.; Vial, L.; West, K. R.; Wietor, J.-L.; Sanders, J. K. M.; Otto, S. Dynamic Combinatorial Chemistry. *Chem. Rev.* **2006**, *106* (9), 3652–3711.

Cote, A. P.; Benin, A. I.; Ockwig, N. W.; O'Keefe, M.; Matzger, A. J.; Yaghi, O. M. Porous, Crystalline, Covalent Organic Frameworks. *Science (80-.).* **2005**, *310* (5751), 1166–1170.

Cougnon, F. B. L.; Sanders, J. K. M. Evolution of Dynamic Combinatorial Chemistry. *Acc. Chem. Res.* **2012**, *45* (12), 2211–2221.

Dai, C.; Cazares, L. H.; Wang, L.; Chu, Y.; Wang, S. L.; Troyer, D. A.; Semmes, O. J.; Drake, R. R.; Wang, B. Using Boronolectin in MALDI-MS Imaging for the Histological Analysis of Cancer Tissue Expressing the Sialyl Lewis X Antigen. *Chem. Commun.* **2011**, *47* (37), 10338–10340.

Dale, J. A.; Dull, D. L.; Mosher, H. S. Alpha-Methoxy-Alpha-Trifluoromethylphenylacetic Acid, a Versatile Reagent Forthe Determination of Enantiomeric Composition of Alcohols and Amines. *J. Org. Chem.* **1969**, *34* (9), 2543–2549.

Dale, J. A.; Mosher, H. S. Nuclear Magnetic Resonance Enantiomer Reagents. Configurational Correlations via Nuclear Magnetic Resonance Chemical Shifts of Diastereomeric Mandelate, O-Methylmandelate, and Alpha-Methoxy-Alpha-Trifluoromethylphenylacetate (MTPA) Esters. *J. Am. Chem. Soc.* **1973**, *95* (2), 512–519.

Dalvit, C.; Flocco, M.; Knapp, S.; Mostardini, M.; Perego, R.; Stockman, B. J.; Veronesi, M.; Varasi, M. High-Throughput NMR-Based Screening with Competition Binding Experiments. *J. Am. Chem. Soc.* **2002**, *124* (26), 7702–7709.

de Moor, J. E.; van der Kelen, G. P. Studies on Trivalent Boron Compounds. I. The Boron and Proton Magnetic Resonance Spectra of Some Trivalent Boron Compounds. *J. Organometal. Chem.* **1966**, *6* (3), 235–241.

de Silva, A. P.; Gunnlaugsson, T.; Rice, T. E. Recent Evolution of Luminescent Photoinduced Electron Transfer Sensors. A Review. *Analyst* **1996**, *121* (12), 1759–1762.

Dewar, M. J. S.; Jones, R. New Heteroaromatic Compounds. XXV. Studies of Salt Formation in Boron Oxyacids by Boron-11 Nuclear Magnetic Resonance. *J. Am. Chem. Soc.* **1967**, *89* (10), 2408–2410.

Dragna, J. M.; Gade, A. M.; Tran, L.; Lynch, V. M.; Anslyn, E. V. Chiral Amine Enantiomeric Excess Determination Using Self-Assembled Octahedral Fe(II)-Imine Complexes. *Chirality* **2015**, *27* (4), 294–298.

Dunsdon, R. M.; Greening, J. R.; Jones, P. S.; Jordan, S.; Wilson, F. X. Solid Phase Synthesis of Aminoboronic Acids: Potent Inhibitors of the Hepatitis C Virus NS3 Proteinase. *Bioorg. Med. Chem. Lett.* **2000**, *10* (14), 1577–1579.

Eaton, G. R. N. M. R. of Boron Compounds. *J. Chem. Ed.* **1969**, *46* (9), 547–556.

Eaton, P. E.; Cole, T. W. J. Cubane. *J. Am. Chem. Soc.* **1964**, *86* (15), 3157–3158.

Edwards, N. Y.; Sager, T. W.; McDevitt, J. T.; Anslyn, E. V. Boronic Acid Based Peptidic Receptors for Pattern-Based Saccharide Sensing in Neutral Aqueous Media, an Application in Real-Life Samples. *J. Am. Chem. Soc.* **2007**, *129* (44), 13575–13583.

El-Kaderi, H. M.; Hunt, J. R.; Medoza-Cortes, J. L.; Cote, A. P.; Taylor, R. E.; O'Keefe, M.; Yaghi, O. M. Designed Synthesis of 3D Covalent Organic Frameworks. *Science (80-.).* **2007**, *316* (5822), 268–272.

Fang, H.; Kaur, G.; Wang, B. Progress in Boronic Acid-Based Fluorescent Glucose Sensors. *Fluorescence* **2004**, *14* (5), 481–489.

Fedorak, R. N.; Gershon, M. D.; Field, M. Induction of Intestinal Glucose Carriers in Streptozocin-Treated Chronically Diabetic Rats. *Gastroenterology* **1989**, *96* (1), 37.

Feng, J.; Garza, V. J.; Krische, M. J. Redox-Triggered C-C Coupling of Alcohols and Vinyl Epoxides: Diastereo- and Enantioselective Formation of All-Carbon Quaternary Centers via Tert-(Hydroxy)-Prenylation. *J. Am. Chem. Soc.* **2014**, *136* (25), 8911–8914.

Ferrand, Y.; Crump, M.; Davis, A. P. A Synthetic Lectin Analog for Biomimetic Disaccharide Recognition. *Science (80-.).* **2007**, *318* (5850), 619–622.

Flentke, G. R.; Munoz, E.; Huber, B. T.; Plaut, A. G.; Kettner, C. A.; Bachovin, W. W. Inhibition of Dipeptidyl Aminopeptidase IV (DP-IV) by Xaa-boroPro Dipeptides and Use of These Inhibitors to Examine the Role of DP-IV in T-Cell Function. *Proc. Natl. Acad. Sci.* **1991**, *88* (4), 1556–1559.

Franks, F. Physical Chemistry of Small Carbohydrates-Equilibrium Solution Properties. *Pure Appl. Chem.* **1987**, *59* (9), 1189–1202.

Franzen, S.; Ni, W.; Wang, B. Study of the Mechanism of Electron-Transfer Quenching by Boron-Nitrogen Adducts in Fluorescent Sensors. *J. Phys. Chem. B* **2003**, *107* (47), 12942–12948.

Galbraith, E.; Kelly, A. M.; Fossey, J. S.; Kociok-Koehn, G.; Davidson, M. G.; Bull, S. D.; James, T. D. Dynamic Covalent Self-Assembled Macrocycles Prepared from 2-Formyl-Aryl-Boronic Acids and 1,2-Amino Alcohols. *New J. Chem.* **2009**, *33* (1), 181–185.

Ge, S.; Green, R. A.; Hartwig, J. F. Controlling First-Row Catalysts: Amination of Aryl and Heteroaryl Chlorides and Bromides with Primary Aliphatic Amines Catalyzed by a BINAP-Ligated Single-Component Ni(0) Complex. *J. Am. Chem. Soc.* **2014**, *136* (4), 1617–1627.

Goldberg, R. N.; Tewari, Y. B. Thermodynamic and Transport Properties of Carbohydrates and Their Monophosphates: The Pentoses and Hexoses. *J. Phys. Chem. Ref. Data* **1989**, *18* (2), 809–880.

Good, C. D.; Ritter, D. M. Alkenylboranes. II. Improved Preparative Methods and New Observations on Methylvinylboranes. *J. Am. Chem. Soc.* **1962**, *84*, 1162–1166.

Gray, C. W.; Houston, T. A. Boronic Acid Receptors for α-Hydroxycarboxylates: High Affinity of Shinkai's Glucose Receptor for Tartrate. *J. Org. Chem.* **2002**, *67* (15), 5426–5428.

Guo, Z.-F.; Yan, H.; Li, Z.-F.; Lu, Z.-L. Synthesis of Mono- and Di-[12]aneN3 Ligands and Study on the Catalytic Cleavage of RNA Model 2-Hydroxypropyl-P-Nitrophenyl Phosphate with Their Metal Complexes. *Org. Biomol. Chem.* **2011**, *9* (19), 6788–6796.

Gutierrez-Moreno, N. J.; Medrano, F.; Yatsimirsky, A. K. Schiff Base Formation and Recognition of Amino Sugars, Aminoglycosides and Biological Polyamines by 2-Formylphenylboronic Acid in Aqueous Solution. *Org. Biomol. Chem.* **2012**, *10* (34), 6960–6972.

Hall, D. G. *Boronic Acids: Preparation, Applications in Organic Synthesis and Medicine*; John Wiley & Sons, 2006.

Hanelt, S.; Liebscher, J. A Novel and Versatile Access to Task-Specific Ionic Liquids Based on 1,2,3-Triazolium Salts. *Synlett* **2008**, *2008* (7), 1058–1060.

Hargrove, A. E.; Zhong, Z.; Sessler, J. L.; Anslyn, E. V. Algorithms for the Determination of Binding Constants and Enantiomeric Excess in Complex Host : Guest Equilibria Using Optical Measurements. *New J. Chem.* **2010**, *34* (2), 348–354.

Hein, J. E.; Fokin, V. V. Copper-Catalyzed Azide-Alkyne Cycloaddition (CuAAC) and beyond: New Reactivity of copper(I) Acetylides. *Chem. Soc. Rev.* **2010**, *39* (4), 1302–1315.

Hickman, A. J.; Sanford, M. S. High-Valent Organometallic Copper and Palladium in Catalysis. *Nature* **2012**, *484* (7393), 177–185.

Himo, F.; Lovell, T.; Hilgraf, R.; Rostovtsev, V. V; Noodleman, L.; Sharpless, K. B.; Fokin, V. V. Copper(I)-Catalyzed Synthesis of Azoles. DFT Study Predicts Unprecedented Reactivity and Intermediates. *J. Am. Chem. Soc.* **2005**, *127* (1), 210–216.

Hinz, H. *Thermodynamic Data for Biochemistry and Biotechnology*; Springer-Verlag, 1986.

Hiratake, J.; Oda, J. Aminophosphonic and Aminoboronic Acids as Key Elements of a Transition State Analog Inhibitor of Enzymes. *Biosci. Biotech. Biochem.* **1997**, *61* (2), 211–218.

Hohloch, S.; Su, C.-Y.; Sarkar, B. Copper(I) Complexes of Normal and Abnormal Carbenes and Their Use as Catalysts for the Huisgen [3+2] Cycloaddition between Azides and Alkynes. *Eur. J. Inorg. Chem.* **2011**, *2011* (20), 3067–3075.

Huang, C.-Y.; Cabell, L. A.; Anslyn, E. V. Molecular Recognition of Cyclitols by Neutral Polyaza-Hydrogen-Bonding Receptors: The Strength and Influence of Intramolecular Hydrogen Bonds between Vicinal Alcohols. *J. Am. Chem. Soc.* **1994**, *116* (7), 2778–2792.

Huisgen, R.; Szeimies, G.; Moebius, L. 1,3-Dipolar Cycloadditions. XXXII. Kinetics of the Addition of Organic Azides to Carbon-Carbon Multiple Bonds. *Chem. Ber.* **1967**, *100* (8), 2494–2507.

Hutin, M.; Bernardinelli, G.; Nitschke, J. R. An Iminoboronate Construction Set for Subcomponent Self-Assembly. *Chem. Eur. J.* **2008**, *14* (15), 4585–4593.

James, B. D.; Nanda, R. K.; Wallbridge, M. G. H. Spectroscopic Studies of Borohydride Derivatives of Zirconium and Hafnium. *J. Chem. Soc., Inorg., Phys., Theor.* **1966**, *2*, 182–184.

James, T. D. Saccharide-Selective Boronic Acid Based Photoinduced Electron Transfer (PET) Fluorescent Sensors. *Top. Curr. Chem.* **2007**, *277*, 107–152.

James, T. D.; Phillips, M. D.; Shinkai, S. *Boronic Acids in Saccharide Recognition*; Royal Society of Chemistry, 2006.

James, T. D.; Sandanayake, K. R. A. S.; Shinkai, S. Novel Photoinduced Electron-Transfer Sensor for Saccharides Based on the Interaction of Boronic Acid and Amine. *J. Chem. Soc., Chem. Commun.* **1994**, No. 4, 477–478.

James, T. D.; Sandanayake, K. R. A. S.; Shinkai, S. A Glucose-Specific Molecular Fluorescence Sensor. *Angew. Chem.* **1994**, *106* (21), 2287–2289.

James, T. D.; Sandanayake, K. R. A. S.; Shinkai, S. Chiral Discrimination of Monosaccharides Using a Fluorescent Molecular Sensor. *Nature* **1995**, *374* (6520), 345–347.

James, T. D.; Sandanayake, K. R. A. S.; Shinkai, S. Saccharide Sensing with Molecular Receptors Based on Boronic Acid. *Angew. Chemie Int. Ed. English* **1996**, *35* (17), 1911–1922.

James, T. D.; Shinkai, S. Artificial Receptors as Chemosensors for Carbohydrates. *Top. Curr. Chem.* **2002**, *218*, 159–200.

Jin, S.; Cheng, Y.; Reid, S.; Li, M.; Wang, B. Carbohydrate Recognition by Boronolectins, Small Molecules, and Lectins. *Med. Res. Rev.* **2010**, *30* (2), 171–257.

Jo, H. H.; Gao, X.; You, L.; Anslyn, E. V.; Krische, M. J. Application of a High-Throughput Enantiomeric Excess Optical Assay Involving a Dynamic Covalent Assembly: Parallel Asymmetric Allylation and Ee Sensing of Homoallylic Alchohols. *Chem. Sci.* **2015**, *6* (12), 6747–6753.

Jo, H. H.; Lin, C.-Y.; Anslyn, E. V. Rapid Optical Methods for Enantiomeric Excess Analysis: From Enantioselective Indicator Displacement Assays to Exciton-Coupled Circular Dichroism. *Acc. Chem. Res.* **2014**, *47* (7), 2212–2221.

Kagan, H. B.; Fiaud, J. C. Kinetic Resolution. In *Topics in Stereochemistry, Volume 18*; Eliel, E. L., Wilen, S. H., Eds.; John Wiley & Sons, 1988; pp 249–330.

Kelly, A. M.; Perez-Fuentes, Y.; Fossey, J. S.; Yeste, S. L.; Bull, S. D.; James, T. D. Simple Protocols for NMR Analysis of the Enantiomeric Purity of Chiral Diols. *Nat. Protoc.* **2008**, *3* (2), 215–219.

Kettner, C.; Mersinger, L.; Knabb, R. The Selective Inhibition of Thrombin by Peptides of Boroarginine. *J. Biol. Chem.* **1990**, *265* (30), 18289–18297.

Kitamura, M.; Suzuki, T.; Abe, R.; Ueno, T.; Aoki, S. 11B NMR Sensing of D-Block Metal Ions in Vitro and in Cells Based on the Carbon-Boron Bond Cleavage of Phenylboronic Acid-Pendant Cyclen (Clyclen = 1,4,7,10-Tetraazacyclododecane). *Inorg. Chem.* **2011**, *50* (22), 11568–11580.

Kolb, H. C.; Finn, M. G.; Sharpless, K. B. Click Chemistry: Diverse Chemical Function from a Few Good Reactions. *Angew. Chem. Int. Ed. Engl.* **2001**, *40* (11), 2004–2021.

Korich, A. L.; Iovine, P. M. Boroxine Chemistry and Applications: A Perspective. *Dalt. trans.* **2010**, *39* (6), 1423–1431.

Kuivila, H. G.; Keough, A. H.; Soboczenski, E. J. Areneboronates From Diols and Polyols. *J. Org. Chem.* **1954**, *19* (5), 780–783.

Larkin, J. D.; Fossey, J. S.; James, T. D.; Brooks, B. R.; Bock, C. W. A Computational Investigation of the Nitrogen-Boron Interaction in O-(N,N-Dialkylaminomethyl)arylboronate Systems. *J. Phys. Chem. A* **2010**, *114* (47), 12531–12539.

Lee, C.; Yang, W.; Parr, R. G. Development of the Colle-Salvetti Correlation-Energy Formula into a Functional of the Electron Density. *Phys. Rev. B* **1988**, *37* (2), 785–789.

Lee, J. W.; Lee, J.-S.; Chang, Y.-T. Colorimetric Identification of Carbohydrates by a pH indicator/pH Change Inducer Ensemble. *Angew. Chem. Int. Ed.* **2006**, *45* (39), 6485.

Lehn, J.-M. *Supramolecular Chemistry: Concepts and Perspectives*; VCH: Weinheim, 1995.

Lehn, J.-M. From Supramolecular Chemistry towards Constitutional Dynamic Chemistry and Adaptive Chemistry. *Chem. Soc. Rev.* **2007**, *36* (2), 151–160.

Li, H.; Liu, Y.; Liu, J.; Liu, Z. A Wulff-Type Boronate for Boronate Affinity Capture of Cis-Diol Compounds at Medium Acidic pH Condition. *Chem. Commun.* **2011**, *47* (28), 8169–8171.

Lorand, J. P.; Edwards, J. O. Polyol Complexes and Structure of the Benzeneboronate Ion. *J. Org. Chem.* **1959**, *24* (769-774).

Maier, G.; Pfriem, S.; Schaefer, U.; Matusch, R. Small Rings. 25. Tetra-Tert-Butyltetrahedrane. *Angew. Chem.* **1978**, *90* (7), 552–553.

Mallia, A. K.; Hermanson, G. T.; Krohn, R. I.; Fujimoto, E. K.; Smith, P. K. Preparation and Use of a Boronic Acid Affinity Support for Separation and Quantitation of Glycosylated Hemoglobins. *Anal. Lett.* **1981**, *14* (B8), 649–661.

Martinez-Aguirre, M. A.; Villamil-Ramos, R.; Guerrero-Alvarez, J. A.; Yatsimirsky, A. K. Substituent Effects and pH Profiles for Stability Constants of Arylboronic Acid Diol Esters. *J. Org. Chem.* **2013**, *78* (10), 4674–4684.

Matsumura, T.; Iwatsuki, S.; Ishihara, K. Direct Kinetic Measurements for the Fast Interconversion Process between Trigonal Boronic Acid and Tetragonal Boronate Ion at Low Temperatures. *Inorg. Chem. Commun.* **2005**, *8* (8), 713–716.

McNulty, J.; Keskar, K.; Vemula, R. The First Well-Defined silver(I)-Complex-Catalyzed Cycloaddition of Azides onto Terminal Alkynes at Room Temperature. *Chem. Eur. J.* **2011**, *17* (52), 14727–14730.

McVey, J. K.; Shold, D. M.; Yang, N. C. Direct Observation and Characterization of Anthracene Excimer in Solution. *J. Chem. Phys.* **1976**, *65* (8), 3375–3376.

Meng, J.; Fokin, V. V.; Finn, M. G. Kinetic Resolution by Copper-Catalyzed Azide-Alkyne Cycloaddition. *Tetrahedron Lett.* **2005**, *46*, 4543–4546.

Messina, F.; Botta, M.; Corelli, F.; Schneider, M. P.; Fazio, F. Resolution of (±)-1-Aryl-2-Propynlamines via Acyl Transfer Catalyzed by Candida Antarctica Lipase. *J. Org. Chem.* **1999**, *64* (10), 3767–3769.

Metola, P.; Anslyn, E. V.; James, T. D.; Bull, S. D. Circular Dichroism of Multi-Component Assemblies for Chiral Amine Recognition and Rapid Ee Determination. *Chem. Sci.* **2012**, *3* (1), 156–161.

Mikhailov, B. M.; Ter-Sarkisyan, G. S.; Nikolaeva, N. A. Organoboron Compounds. CCXXXVI. Reactions of 1,4-Naphthoquinone with Trialkylboranes. *Zh. Obs. Khim.* **1971**, *41* (8), 1721–1725.

Miller, E. W.; Albers, A. E.; Pralle, A.; Isacoff, Ehud, Y.; Chang, C. J. Boronate-Based Fluorescent Probes for Imaging Cellular Hydrogen Peroxide. *J. Am. Chem. Soc.* **2005**, *127* (47), 16652–16659.

Mirri, G.; Bull, S. D.; Horton, P. N.; James, T. D.; Male, L.; Tucker, J. H. R. Electrochemical Method for the Determination of Enantiomeric Excess of Binol

Using Redox-Active Boronic Acids as Chiral Sensors. *J. Am. Chem. Soc.* **2010**, *132* (26), 8903–8905.

Miyaura, N.; Suzuki, A. Palladium-Catalyzed Cross-Coupling Reactions of Organoboron Compounds. *Chem. Rev.* **1995**, *95* (7), 2457–2483.

Miyaura, N.; Yamada, K.; Suzuki, A. A New Stereopecific Cross-Coupling by the Palladium-Catalyzed Reaction of 1-Alkenylboranes with 1-Alkenyl or 1-Alkynyl Halides. *Tetrahedron Lett.* **1979**, *36*, 3437–3740.

Miyazaki, Y.; Fujimori, T.; Okita, H.; Hirano, T.; Yoshimura, K. Thermodynamics of Complexation Reactions of Borate and Phenylboronate with Diol, Triol and Tetritol. *Dalt. Trans.* **2013**, *42* (29), 10473–10486.

Miyazaki, Y.; Matsuo, H.; Fujimori, T.; Takemura, H.; Matsuoka, S.; Okobira, T.; Uezu, K.; Yoshimura, K. Interaction of Boric Acid with Salicyl Derivatives as an Anchor Group of Boron-Selective Adsorbents. *Polyhedron* **2008**, *27* (13), 2785–2790.

Moulin, E.; Cormos, G.; Giuseppone, N. Dynamic Combinatorial Chemistry as a Tool for the Design of Functional Materials and Devices. *Chem. Soc. Rev.* **2012**, *41* (3), 1031–1049.

Mugridge, J. S.; Szigethy, G.; Bergman, R. G.; Raymond, K. N. Encapsulated Guest-Host Dynamics: Guest Rotational Barriers and Tumbling as a Probe of Host Interior Cavity Space. *J. Am. Chem. Soc.* **2010**, *132* (45), 16256–16264.

Musto, C. J.; Lim, S. H.; Suslick, K. S. Colorimetric Detection and Identification of Natural and Artificial Sweeteners. *Anal. Chem.* **2009**, *81* (15), 6526–6533.

Nagai, Y.; Kobayashi, K.; Toi, H.; Aoyama, Y. Stabilization of Sugar-Boronic Esters of Indolylboronic Acid in Water via Sugar-Indole Interaction: A Notable Selectivity in Oligosaccharides. *Bull. Chem. Soc. Jpn.* **1993**, *66* (10), 2965–2971.

Ni, W.; Kaur, G.; Springsteen, G.; Wang, B. Regulating the Fluorescence Intensity of an Anthracene Boronic Acid System: A B-N Bond or a Hydrolysis Mechanism? *Bioorg. Chem.* **2004**, *32* (6), 571–581.

Ni, Z.; Giordano, L.; Tenaglia, A. Cyclobutene Formation in PtCl2-Catalyzed Cycloisomerizations of Heteroatom-Tethered 1,6-Enynes. *Chem. Eur. J.* **2014**, *20* (37), 11703–11706.

Nilsson, B. M.; Hacksell, U. Base-Catalyzed Cyclization of N-Propargylamides to Oxazoles. *J. Heterocycl. Chem.* **1989**, *26* (2), 269–275.

Nilsson, B. M.; Vargas, H. M.; Ringdahl, B.; Hacksell, U. Phenyl-Substituted Analogs of Oxotremorine as Muscarinic Antagonists. *J. Med. Chem.* **1992**, *35* (2), 285–294.

Noeth, H.; Vahrenkamp, H. Nuclear Resonance Investigations on Boron Compounds. I. 11B Nuclear Resonance Spectra of Boranes with Substituents from the First Eight-Membered Period of the Periodic System. *Chem. Ber.* **1966**, *99* (3), 1049–1067.

Noeth, H.; Vahrenkamp, H. Nuclear Magnetic Resonance Spectroscopic Studies of Boron Compounds. II. Monomer-Dimer Equilibriums in Aminoboranes. *Chem. Ber.* **1967**, *100* (10), 3353–3362.

Noeth, H.; Wrackmeyer, B. *NMR Basic Principles and Progress, Vol. 14: Nuclear Magnetic Resonance Spectroscopy of Boron Compounds*; Springer-Verlag: Berlin, 1978.

O'Hara, F.; Blackmond, D. G.; Baran, P. S. Radical-Based Regioselective C-H Functionalization of Electron-Deficient Heteroarenes: Scope, Tunability, and Predictability. *J. Am. Chem. Soc.* **2013**, *135* (32), 12122–12134.

Onak, T. P.; Landesman, H.; Williams, R. E.; Shapiro, I. The B11 Nuclear Magnetic Resonance Chemical Shifts and Spin Coupling Values for Various Compounds. *J. Phys. Chem.* **1959**, *63*, 1533–1535.

Paetzold, P. I.; Hansen, H. J. Chemistry of Boron Azides. VI. Dimethylborazide and Its Amino Complexes. *Anorg. Chem.* **1966**, *345* (1-2), 79–86.

Perez-Fuentes, Y.; Kelly, A. M.; Fossey, J. S.; Powell, M. E.; Bull, S. D.; James, T. D. Simple Protocols for NMR Analysis of the Enantiomeric Purity of Chiral Primary Amines. *Nat. Protoc.* **2008**, *3* (2), 210–214.

Phillips, W. D.; Miller, H. C.; Muetterties, E. L. B11 Magnetic Resonance Study of Boron Compounds. *J. Am. Chem. Soc.* **1959**, *81*, 4496–4500.

Pizer, R.; Tihal, C. Equilibria and Reaction Mechanism of the Complexation of Methylboronic Acid with Polyols. *Inorg. Chem.* **1992**, *31* (15), 3243–3247.

Pizer, R. D.; Tihal, C. A. Mechanism of Boron Acid/polyol Complex Formation. Comments on the Trigonal/tetrahedral Interconversion on Boron. *Polyhedron* **1996**, *15* (19), 3411–3416.

Rambo, B. M.; Lavigne, J. J. Defining Self-Assembly Linear Oligo(dioxaborole)s. *Chem. Mater.* **2007**, *19* (15), 3732–3739.

Reetz, M. T.; Eipper, A.; Tielmann, P.; Mynott, R. A Practical NMR-Based High-Throughput Assay for Screening Enantioselective Catalysts and Biocatalysts. *Adv. Synth. Catal.* **2002**, *344* (9), 1008–1016.

Renney, C. M.; Fukuhara, G.; Inoue, Y.; Davis, A. P. Binding or Aggregation? Hazards of Interpretation in Studies of Molecular Recognition by Porphyrins in Water. *Chem. Commun.* **2015**, *51*, 9551–9554.

Robbins, J. S.; Schmid, K. M.; Phillips, S. T. Effects of Electronics, Aromaticity, and Solvent Polarity on the Rate of Azaquinone-Methide-Mediated Depolymerization of Aromatic Carbamate Oligomers. *J. Org. Chem.* **2013**, *78* (7), 3159–3169.

Rostovtsev, V. V; Green, L. G.; Fokin, V. V; Sharpless, K. B. A Stepwise Huisgen Cycloaddition Process: copper(I)-Catalyzed Regioselective "ligation" of Azides

and Terminal Alkynes. *Angew. Chem. Int. Ed. Engl.* **2002**, *41* (14), 2596–2599.

Rowan, S. J.; Cantrill, S. J.; Cousins Graham, R. L.; Sanders, J. K. M.; Stoddart, F. J. Dynamic Covalent Chemistry. *Angew. Chem. Int. Ed.* **2002**, *41* (6), 898–952.

Sagi, A.; Weinstain, R.; Karton, N.; Shabat, D. Self-Immolative Polymers. *J. Am. Chem. Soc.* **2008**, *130* (16), 5434–5435.

Saravanakumar, R.; Ramkumar, V.; Sankararaman, S. Synthesis and Structure of 1,4-Diphenyl-3-Methyl-1,2,3-Triazol-5-Ylidene Palladium Complexes and Application in Catalytic Hydroarylation of Alkynes. *Organometallics* **2011**, *30*, 1689–1694.

Schaeffer, R.; Todd, L. J. Boron-Nitrogen Compounds. IX. Synthesis and Properties of Some Substituted Trimethylboranes. *J. Am. Chem. Soc.* **1965**, *87* (3), 488–494.

Schiller, A.; Wessling, R. A.; Singarum, B. A Fluorescent Sensor Array for Saccharides Based on Boronic Acid Appended Bipyridinium Salts. *Angew. Chem. Int. Ed.* **2007**, *46* (34), 6457–6459.

Shabbir, S. H.; Regan, C. J.; Anslyn, E. V. A General Protocol for Creating High-Throughput Screening Assays for Reaction Yield and Enantiomeric Excess Applied to Hydrobenzoin. *Proc. Natl. Acad. Sci.* **2009**, *106* (26), 10487–10492.

Shah, J.; Khan, S.; Blumenthal, H.; Liebscher, J. 1,2,3-Triazolium-Tagged Prolines and Their Application in Asymmetric Aldol and Michael Reactions. *Synthesis (Stuttg).* **2009**, *2009* (23), 3975–3982.

Shcherbakova, E. G.; Minami, T.; Brega, V.; James, T. D.; Anzenbacher, P. J. Determination of Enantiometic Excess in Amine Derivatives with Molecular Self-Assemblies. *Angew. Chem. Int. Ed.* **2015**, *54* (24), 7130–7133.

Shore, J. *Colorants and Auxiliaries*, 2nd ed.; Shore, J., Ed.; Society of Dyers and Colourists, 1990.

Siedle, A. R. Boron-11 NMR Spectroscopy. *Annu. Rep. NMR Spectrosc.* **1982**, *12*, 177–261.

Siedle, A. R. Boron-11 NMR Spectroscopy. *Annu. Rep. NMR Spectrosc.* **1988**, *20*, 205–314.

Smith, B. M.; Owens, J. L.; Bowman, C. N.; Todd, P. Thermodynamics of Borate Ester Formation by Three Readily Grafted Carbohydrates. *Carbohydr. Res.* **1998**, *308* (1-2), 173–179.

Smith, W. L. Boron-11 NMR. *J. Chem. Ed.* **1977**, *54* (8), 469–473.

Spencer, J.; Burd, A. P.; Goodwin, C. A.; Merette, S. A. M.; Scully, M. F.; Adatia, T.; Deadman, J. J. Synthesis of Ortho-Modified Mercapto- and Piperazino-Methyl-Phenylboronic Acid Derivatives. *Tetrahedron* **2002**, *58* (8), 1551–1556.

Springsteen, G.; Wang, B. A Detailed Examination of Boronic Acid-Diol Complexation. *Tetrahedron* **2002**, *58* (26), 5291–5300.

Strynadka, N. C. J.; Adachi, H.; Jensen, S. E.; Johns, K.; Sielecki, A.; Betzel, C.; Sutoh, K.; James, M. N. G. Molecular Structure of the Acyl-Enzyme Intermediate in Beta-Lactam Hydrolysis at 1.7 A Resolution. *Nature* **1992**, *359* (6397), 700–705.

Sun, W.; Fan, J.; Hu, C.; Cao, J.; Zhang, H.; Xiong, X.; Wang, J.; Cui, S.; Sun, S.; Peng, X. A Two-Photon Fluorescent Probe with near-Infrared Emission for Hydrogen Sulfide Imaging in Biosystems. *Chem. Commun.* **2013**, *49* (37), 3890–3892.

Suzuki, A. Recent Advances in the Cross-Coupling Reactions of Organoboron Derivatives with Organic Electrophiles, 1995-1998. *Organomet. Chem.* **1999**, *576* (1-2), 147–168.

Suzuki, A.; Brown, H. C. *Organic Syntheses via Boranes. Vol. 3*; Aldrich Chemical: Milwaukee, WI, 2003.

Takaya, Y.; Ogasawara, M.; Hayashi, T.; Sakai, M.; Miyaura, N. Rhodium-Catalyzed Asymmetric 1,4-Addition of Aryl- and Alkenylboronic Acids to Enones. *J. Am. Chem. Soc.* **1998**, *120* (22), 5579–5580.

Thompson, R. J.; Davis, J. C. J. Electronegativeity Effects on 11B Chemical Shifts in Tetrahedral BX4- Ions. *Inorg. Chem.* **1965**, *4* (10), 1464–1467.

Thordarson, P. Determining Association Constants from Titration Experiments in Supramolecular Chemistry. *Chem. Soc. Rev.* **2011**, *40* (3), 1305–1323.

Tomlinson, W. J.; Chandross, E. A.; Fork, R. L.; Pryde, C. A.; Lamola, A. A. Reversible Photodimerization. New Type of Photochromism. *Appl. Opt.* **1972**, *11* (3), 533–548.

Toporcer, L. H.; Dessy, R. E.; Green, S. I. E. Preparation and Properties of Some Tetracoordinate Boron Compounds. The Pseudo-Metal Ion Concept. *Inorg. Chem.* **1965**, *4* (11), 1649–1655.

Tornøe, C. W.; Christensen, C.; Meldal, M. Peptidotriazoles on Solid Phase: [1,2,3]-Triazoles by Regiospecific Copper(i)-Catalyzed 1,3-Dipolar Cycloadditions of Terminal Alkynes to Azides. *J. Org. Chem.* **2002**, *67* (9), 3057–3064.

Uyeda, C.; Jacobsen, E. N. Transition-State Charge Stabilization through Multiple Non-Covalent Interactions in the Guanidinium-Catalyzed Enantioselective Claisen Rearrangement. *J. Am. Chem. Soc.* **2011**, *133* (13), 5062–5075.

Varki, A.; Cummings, R. D.; Esko, J. D.; Freeze, Hudson, H.; Stanley, P.; Bertozzi, C. R.; Hart, G. W.; Etzler, M. E. The Expanding World of Glycobiology: Essentials of Glycobiology, 2nd Edition. *Nat. Chem. Biol.* **2009**, *5* (6), 373.

Wang, W.; Gao, X.; Wang, B. Boronic Acid-Based Sensors. *Curr. Org. Chem.* **2002**, *6* (14), 1285–1317.

Weith, H. L.; Wiebers, J. L.; Gilham, P. T. Synthesis of Cellulose Derivatives Containing the Dihydroxyboryl Group and a Study of Their Capacity to Form Specific Complexes with Sugars and Nucleic Acid Components. *Biochem.* **1970**, *9* (22), 4396–4401.

Wiberg, K. B.; Walker, F. H. [1.1.1]Propellane. *J. Am. Chem. Soc.* **1982**, *104* (19), 5239–5240.

Wilson, M. E.; Najdi, S.; Krochta, J. M.; Hsieh, Y.-L.; Kurth, M. J. Complexation of Borate with Poly(1-(Acrylamido)-1-Deoxyactitol): Dilute Solution Viscosity, 11B NMR, and 13C NMR Studies. *Macromolecules* **1998**, *31* (14), 4486–4492.

Wiskur, S. L.; Lavigne, J. J.; Ait-Haddou, H.; Lynch, V.; Chiu, Y. H.; Canary, J. W.; Anslyn, E. V. pKa Values and Geometries of Secondary and Tertiary Amines Complexed to Boronic Acids - Implications for Sensor Design. *Org. Lett.* **2001**, *3* (9), 1311–1314.

Wrackmeyer, B. Nuclear Magnetic Resonance Spectroscopy of Boron Compounds Containing Two-, Three- and Four-Coordinate Boron. *Annu. Rep. NMR Spectrosc.* **1988**, *20*, 61–203.

Wright, A. T.; Griffin, M. J.; Zhong, Z.; McCleskey, S. C.; Anslyn, E. V; McDevitt, J. T. Differential Receptors Create Patterns That Distinguish Various Proteins. *Angew. Chem. Int. Ed. Engl.* **2005**, *44* (39), 6375–6378.

Wulff, G. Selective Binding to Polymers via Covalent Bonds. The Construction of Chiral Cavities as Specific Receptor Sites. *Pure Appl. Chem.* **1982**, *54* (11), 2093–2102.

Wulff, G.; Dederichs, W.; Grotstollen, R.; Jupe, C. On the Chemistry of Binding Sites, Part II: Specific Binding of Substances to Polymers by Fast and Reversible Covalent Interactions. In *Analytical Chemistry Symposia Series, Affinity Chromatography and Related Techniques*; Gribnau, T. C. J., Visser, J., Nivard, R. J. F., Eds.; Elsevier: Amsterdam, 1982; pp 207–216.

Wulff, G.; Lauer, M.; Boehnke, H. Chemistry of Adhesive Groups. Part 5. Rapid Proton Transfer as Cause for an Uncommonly Large Neighboring Group Effect. *Angew. Chem.* **1984**, *96* (9), 714–716.

Xing, Z.; Wang, H.-C.; Cheng, Y.; Zhu, C.; James, T. D.; Zhao, J. Selective Saccharide Recognition Using Modular Diboronic Acid Fluorescent Sensors. *Eur. J. Org. Chem.* **2012**, *2012* (6), 1223–1229.

Yang, W.; Gao, S.; Gao, X.; Karnati, V. V. R.; Ni, W.; Wang, B.; Hooks, W. B.; Carson, J.; Weston, B. Diboronic Acids as Fluorescent Probes for Cells Expressing Sialyl Lewis X. *Bioorg. Med. Chem. Lett.* **2002**, *12* (16), 2175–2177.

Yang, Y.; Seidlits, S. K.; Adams, M. M.; Lynch, V. M.; Schmidt, C. E.; Anslyn, E. V.; Shear, J. B. A Highly Selective Low-Background Fluorescent Imaging Agent for Nitric Oxide. *J. Am. Chem. Soc.* **2010**, *132* (38), 13114–13116.

Yasuda, H.; Kurokawa, T.; Fujii, Y.; Yamashita, A.; Ishibashi, S. Decreased D-Glucose Transport across Renal Brush-Border Membrane Vesicles from Streptozotocin-Induced Diabetic Rats. *Biochim. Biophys. Acta* **1990**, *1021* (2), 114–118.

Ye, L.; He, W.; Zhang, L. Gold-Catalyzed One-Step Practical Synthesis of Oxetan-3-Ones from Readily Available Propargylic Alcohols. *J. Am. Chem. Soc.* **2010**, *132* (25), 8550–8551.

Yeste, S. L.; Powell, M. E.; Bull, S. D.; James, T. D. Simple Chiral Derivatization Protocols for 1H NMR and 19F NMR Spectroscopic Analysis of the Enantiopurity of Chiral Diols. *J. Org. Chem.* **2009**, *74* (1), 427–430.

Zaubitzer, F.; Buryak, A.; Severin, K. Cp*Rh-Based Indicator-Displacement Assays for the Identification of Amino Sugars and Aminoglycosides. *Chemistry* **2006**, *12* (14), 3928–3934.

Zhai, W.; Chapin, B. M.; Yoshizawa, A.; Wang, H.-C.; Hodge, S. A.; James, T. D.; Anslyn, E. V.; Fossey, J. S. "Click-Fluors": Triazole-Linked Saccharide Sensors. *Org. Chem. Front.* **2016**, *3* (8), 918–928.

Zhang, L.; Chen, X.; Xue, P.; Sun, H. H. Y.; Williams, I. D.; Sharpless, K. B.; Fokin, V. V; Jia, G. Ruthenium-Catalyzed Cycloaddition of Alkynes and Organic Azides. *J. Am. Chem. Soc.* **2005**, *127* (46), 15998–15999.

Zhang, X.; You, L.; Anslyn, E. V.; Qian, X. Discrimination and Classification of Ginsenosides and Ginsends Using Bis-Boronic Acid Receptors in Dynamic Multicomponent Indicator Displacement Sensor Arrays. *Chem. Eur. J.* **2012**, *18* (4), 1102–1110.

Zhu, L.; Shabbir, S. H.; Gray, M.; Lynch, V.; Sorey, S.; Anslyn, E. V. A Structural Investigation of the N-B Interaction in an O-(N,N-Dialkylaminomethyl)arylboronate System. *J. Am. Chem. Soc.* **2006**, *128* (4), 1222–1232.